Modèles et indicateurs pour l'analyse des vulnérabilités des réseaux électriques aux pertes de lignes

Dinh Truc Ha

Communauté
UNIVERSITÉ Grenoble Alpes

THÈSE

Pour obtenir le grade de

DOCTEUR DE LA COMMUNAUTE UNIVERSITE GRENOBLE ALPES

Spécialité : **Génie Electrique**

Arrêté ministériel : 25 mai 2016

Présentée par

Dinh Truc HA

Thèse dirigée par **Nicolas RETIERE** et
codirigée par **Jean-Guy CAPUTO**

préparée au sein du **Laboratoire de Mathématique de L'INSA Rouen (LMI)** et du **Laboratoire de Génie Electrique de Grenoble (G2ELAB)** dans **l'École Doctorale Electronique, Electrotechnique, Automatique et Traitement du Signal (EEATS)**

Line outage vulnerabilities of power systems : Models and indicators

Thèse soutenue publiquement le **06 Mars 2018**,
devant le jury composé de :

Monsieur Nouredine HADJ-SAID
Professeur, Grenoble INP, Président
Monsieur Xavier GUILLAUD
Professeur, L'Ecole Centrale de Lille, Rapporteur
Monsieur Serge PIERFEDERICI
Professeur, Ecole Nationale Supérieure d'Electricité et de Mécanique, Rapporteur
Monsieur Nicolas RETIERE
Professeur, Université Grenoble Alpes, Directeur de thèse
Monsieur Jean-Guy CAPUTO
Maître de conférences, INSA Rouen, Co-directeur de thèse

TABLE OF CONTENTS

Acknowledgements 1

Abstract in English 2

Résumé en français 3

List of figures 4

List of tables 6

Abbreviations and acronyms 7

Chapter I. Access to electricity is a vulnerable right 8

I. The Human Right to access Electricity 9

II. A rising complexity of electrical power systems 10

III. Some previous works on power system vulnerability 13

IV. Objectives of the thesis 14

Chapter II. Contingency analysis of AC power systems 15

I. Introduction 16

II. Modeling power systems by equivalent electrical circuits 16

II.1 Transmission line modeling 16

II.2 Transformer modeling 16

II.3 Generator model 17

II.4 Load model 17

II.5 Shunt elements 17

II.6 Power flow equations 17

III. Numerical methods to solve power flow problem 19

III.1 Gauss-Seidel method 20

III.1.1 Principles 20

III.1.2 Application of Gauss-Seidel method to power-flows 21

III.2 Newton-Raphson method 23

III.2.1 Principles 23

III.2.2 Application of Newton-Raphson method to power-flow solving 26

IV. Conventional approach for analyzing power grid vulnerability 28

V. Vulnerability indicators based on AC power flow 31

V.1 AC Line outage impact metric (ACLOIM) 31

V.2 AC Network capacity reservation metric (ACNCRM) 32

VI. Line outage vulnerability analysis based on ACLOIM and ACNCRM 33

VI.1 Applying ACLOIM to quantify line vulnerability of IEEE test systems 33

VI.2 Applying ACNCRM to quantify line vulnerability of IEEE test systems 40
VII. Conclusion 43
Chapter III. Topological indicators for mapping vulnerability of power systems 44
I. Introduction 45
II. Modeling power systems 45
II.1 Basic elements of graph theory 45
II.2 Pure topological model 46
II.2.1 Definition 46
II.2.2 Shortest path calculation by dynamic programming 47
II.3 Extended topological model 48
III. Topological indicators 49
III.1 Network efficiency index 49
III.2 Line betweenness centrality 50
III.3 Net-ability index 50
IV. Assessment of system vulnerability 51
IV.1 Network efficiency based critical lines ranking 51
IV.1.1 Illustration on basic electrical circuits 51
IV.1.2 Critical lines of IEEE 30-bus test networks 52
IV.1.3 Critical lines of IEEE 39-bus, 57-bus and 118-bus test networks 55
IV.2 Line betweenness based critical lines ranking 60
IV.2.1 Star and delta circuits test cases 60
IV.2.2 IEEE test systems 60
IV.3 Net-ability based critical lines ranking 65
IV.3.1 Critical lines of a 3-node delta system 65
IV.3.2 Critical lines of IEEE 30-bus, 57-bus and 118-bus systems 65
V. Conclusion 69
Chapter IV. DC assessment of power system vulnerability 70
I. Introduction 71
II. DC approximation of power flows 71
II.1 DC power flow equations 71
II.2 Power transfer distribution factor 72
III. DC indicators of vulnerability 74
III.1 Line outage distribution factor (LODF) 74
III.2 DC line outage impact metric (DCLOIM) 76

III.3 DC network capacity reservation metric 77
IV. Application to test systems 77
IV.1 Interpretation of LODF 77
IV.2 Locating critical lines by DC line outage impact metric 78
IV.2.1 Application to basic electrical circuits 78
IV.2.2 Application to IEEE test systems 78
IV.3 Applying DC network capacity reservation metric 84
V. Conclusion 88
Chapter V. A new approach based on spectral solving of DC power flow. 89
I. Introduction 90
II. Spectral graph theory 90
II.1 Eigenvalues and eigenvectors 90
II.2 Some useful properties 91
III. Spectral solving of DC power flow 91
IV. Spectral analysis of IEEE 30-bus and 118-bus systems 97
IV.1 IEEE 30-bus network 97
IV.2 IEEE 118-bus network 106
V. Conclusion 109
Chapter VI. Conclusions and directions for future works 110
I. Conclusions 111
II. Directions for future works 111
Appendices 113
A. Data of IEEE test systems 113
I. IEEE 30-bus test system 113
II. IEEE 39-bus test system 115
III. IEEE 57-bus test system 118
IV. IEEE 118-bus test system 122
B. Algorithms 131
I. Gauss-Seidel method for power flow 131
II. Gauss-Seidel method for power flow 132
III. Dynamic programming to find shortest path 132
References 133

Acknowledgements

I would like to thank Monsieur Nicolas RETIERE and Monsieur Jean-Guy CAPUTO for their supervision, advice and invaluable encouragement during the time I have been doing this thesis. I also wish to take this opportunity to express my gratitude to Monsieur Nicolas RETIERE for his valuable comments on my thesis. All of my works in this dissertation cannot be accomplished without his correction.

I am grateful to Monsieur Xavier GUILLAUD, Monsieur Serge PIERFEDERICI, and Monsieur Nouredine HADJ-SAID spending their time to read and give the valuable comments and feedbacks to my thesis.

I wish to thank all the professors and staffs at the University of Grenoble Alpes and G2Elab for the valuable knowledge and very good services they have provided. I also thank my friends at the G2Elab for their discussion and friendship.

I would also like to thank my colleagues at Faculty of electrical engineering - Danang University of Science and Technology, especially associate Prof. NGO Van Duong for the encouragement they gave me during the time I studied at the University of Grenoble Alpes.

The last but not least, I would like to thank all members of my family, particularly my parents and my parents in law as well as my wife for their unfailing support and encouragement during more than three years I studied in Grenoble.

This work was supported by Vietnamese Ministry of Education and Training & the project FRACTAL GRID ANR-15-CE05-007-01 of the French National Research Agency (ANR).

Abstract in English

The vulnerability of electrical systems is one of the problems related to their complexity. It has received increasing attention from researchers in recent decades. Despite this, the fundamental phenomena that govern the vulnerability of the system are still not well understood.

Understanding how the vulnerability of power systems emerges from their complex organization is, therefore, the main motivation of the present work. It proposes the definition of a standard method to assess the vulnerability of power systems and identify their most critical elements. The method enables a better understanding of the links between the topology of the grid and the line outage vulnerabilities.

The first part of this research work offers a critical review of literature approaches used to assess system vulnerability. The results provided by these approaches for four IEEE test systems are confronted to a reference contingency analysis using AC power flow calculations. From these analyses, pros and cons of each approach are outlined. An improved method for assessment of system vulnerability to line outages is defined from this confrontation. It is based on DC power flow and graph theory.

The second part proposes a new approach based on spectral graph theory and solving of DC power flow to identify how system vulnerability and critical components emerge from the power network topology.

Résumé en français

La vulnérabilité des systèmes électriques est l'un des problèmes liés à leur complexité. Il a fait l'objet d'une attention croissante des chercheurs au cours des dernières décennies. Malgré cela, les phénomènes fondamentaux qui régissent la vulnérabilité du système ne sont pas encore bien compris.

Comprendre comment la vulnérabilité des réseaux électriques émerge de leur topologie est la motivation principale du présent travail. Pour cela, le présent travail de recherché propose une nouvelle méthode pour évaluer la vulnérabilité des systèmes électriques et identifier leurs éléments les plus critiques. La méthode permet d'avoir une bonne compréhension des liens entre la topologie d'un réseau et sa vulnérabilité à des pertes d'ouvrages (lignes ou transformateurs).

La première partie de ce travail consiste en une analyse critique des approches rencontrées dans la littérature, s'appuyant sur la théorie des graphes, pour analyser la vulnérabilité des réseaux électriques. Les résultats fournis par ces approches pour quatre réseaux IEEE sont comparés à ceux fournis par une analyse de contingence de référence, basée sur une résolution d'un load-flow AC. Des avantages et inconvénients de chaque approche est tirée une méthode améliorée pour l'évaluation de la vulnérabilité des réseaux électriques aux pertes d'ouvrage. Cette méthode est basée sur une approximation courant continue du power flow.

La deuxième partie propose une nouvelle approche basée sur la théorie spectrale des graphes et son utilisation pour la résolution d'un power flow DC. Elle permet de mieux comprendre comment la vulnérabilité des réseaux électriques et leurs composants critiques émergent de la topologie du graphe sous-jacent au réseau.

List of figures

Figure I.1. World electricity consumption for the last four decades [2] 9
Figure I.2. Multilayer model of power system [4]. 10
Figure I.3. Smart Grid Architecture Model [6]. 11
Figure II.1. Equivalent Π model of a transmission line between two nodes 16
Figure II.2. Equivalent circuit of a tap changing transformer 17
Figure II.3. Equivalent circuit of a generator 17
Figure II.4. Representation of a typical bus of a power system 18
Figure II.5. Graphical illustration of the Gauss-Seidel iterative method [1] 21
Figure II.6. Graphical illustration of Newton-Raphson iterative method [38]. 25
Figure II.7. Power flow of IEEE 30 bus test system in normal operation (values into brackets are the active power flow values) – Slack bus is located at bus 1. 29
Figure II.8. Line outage impact metric of IEEE 30 bus system 33
Figure II.9. Line outage impact metric of IEEE 39 bus system 35
Figure II.10. Single line diagram of IEEE 39 bus test system (red lines can separate the network into independent subsystems) – Slack bus is located at bus 39. 34
Figure II.11. Single line diagram of IEEE 57 bus test system – Slack bus is located at bus 1 36
Figure II.12. Line outage impact metric of IEEE 57 bus system without line L48 37
Figure II.13. Line outage impact metric of IEEE 118 bus system 38
Figure II.14. Single line diagram of IEEE 118 bus test system– Slack bus is located at bus 69. 39
Figure II.15. ACNCRM variation of IEEE 30 bus system 40
Figure II.16. ACNCRM variation of IEEE 118 bus system 41
Figure II.17. ACNCRM variation of IEEE 57 bus system 42
Figure III.1. A power grid (a) and its related graph (b) 46
Figure III.2. Network diagram 47
Figure III.3. Test system connected in delta 51
Figure III.4. Test system connected in star 51
Figure III.5. Network efficiency of IEEE 30 bus system 52
Figure III.6. Graphical representation of top 10 critical lines for IEEE 30 bus system according to D_E and ACLOIM 54
Figure III.7. Network efficiency of IEEE 39-bus system 55
Figure III.8. Network efficiency of IEEE 57-bus system 55
Figure III.9. Network efficiency of IEEE 118-bus system 56
Figure III.10. Comparison of top 10 critical lines of IEEE 39-bus given by D_E and ACLOIM 57
Figure III.11. Comparison of top 10 critical lines of IEEE 57-bus given by D_E and ACLOIM 58
Figure III.12. Comparison of top 10 critical lines of IEEE 118-bus given by D_E and ACLOIM 59

Figure III.13. Comparison of top 10 critical lines of IEEE 30-bus given by $CBEL$ and ACLOIM 61
Figure III.14. Comparison of top 10 critical lines of IEEE 39-bus given by $CBEL$ and ACLOIM 62
Figure III.15. Comparison of top 10 critical lines of IEEE 57-bus given by $CBEL$ and ACLOIM 63
Figure III.16. Comparison of top 10 critical lines of IEEE 118-bus given by $CBEL$ and ACLOIM 64
Figure III.17. Comparison of top 10 critical lines of IEEE 30-bus given by D_A and ACNCRM 66
Figure III.18. Comparison of top 10 critical lines of IEEE 57-bus given by D_A and ACNCRM 67
Figure III.19. Comparison of top 10 critical lines of IEEE 118-bus given by D_A and ACNCRM 68
Figure IV.1. Equivalent networks with line q outage 74
Figure IV.2. Pre-outage Thevenin equivalent circuit for modeling outage of line q 75
Figure IV.3. Top ten vulnerable lines of IEEE 30 bus system by DCLOIM and ACLOIM 80
Figure IV.4. Top ten vulnerable lines of IEEE 39-bus system by DCLOIM and ACLOIM 81
Figure IV.5. Top ten vulnerable lines of IEEE 57- bus system by DCLOIM and ACLOIM 82
Figure IV.6. Top ten vulnerable lines of IEEE 118- bus system by DCLOIM and ACLOIM 83
Figure IV.7. Top ten vulnerable lines of IEEE 30 bus system by DCNCRM and ACNCRM 85
Figure IV.8. Top ten vulnerable lines of IEEE 57- bus system by DCNCRM and ACNCRM 86
Figure IV.9. Top ten vulnerable lines of IEEE 118- bus system by DCNCRM and ACNCRIM 87
Figure V.1. The directed graph representing a power grid connected in wye. The lines are arbitrarily oriented. 94
Figure V.2. Schematic representation of eigenvector components corresponding to mode 2 95
Figure V.3. Schematic representation of eigenvector components corresponding to mode 3 95
Figure V.4. Schematic representation of eigenvector components corresponding to mode 4 96
Figure V.5. Maximal power transfer through transmission lines in every mode 97
Figure V.6. Line power flow in mode 2 98
Figure V.7. Line power distribution in IEEE 30-bus network corresponding to mode 2 99
Figure V.8. Line power flow in mode 11 100
Figure V.9. Line power distribution in IEEE 30-bus network corresponding to mode 11 101
Figure V.10. Line power flow in mode 13 102
Figure V.11. Distribution of power injection of IEEE 30-bus test system corresponding to mode 13 102
Figure V.12. Line power distribution in IEEE 30-bus network corresponding to mode 13 103
Figure V.13. Distribution of power injection of IEEE 30-bus test system corresponding to mode 29 104
Figure V.14. Line power distribution in IEEE 30-bus network corresponding to mode 29 105
Figure V.15. Maximal power transfer through transmission lines in every mode 106
Figure V.16. Nodal domains of mode 2 107
Figure V.17. Nodal domains of mode 62 108
Figure V.18. Nodal domains of mode 111 108
Figure V.19. Nodal domains of mode 118 109

List of tables

Table 2.1 Active power flow results for normal operation of IEEE 30 bus system *30*
Table 2.2 Absolute active power variations of IEEE 30 bus system when line L7 is disconnected *30*
Table 2.3 Absolute active power variations of IEEE 30 bus system when line L10 is disconnected *30*
Table 2.4 Absolute active power variations of IEEE 30 bus system when line L16 is disconnected *31*
Table 2.5 Critical lines of IEEE 30 bus system *33*
Table 2.6 Top 24 critical lines of IEEE 39 bus system *35*
Table 2.7 Power supply values before and after contingency *36*
Table 2.8 Top 24 critical lines of IEEE 57 bus system *37*
Table 2.9 Critical lines of IEEE 118 bus system *38*
Table 2.10 Top 24 critical lines of IEEE 30 bus system using ACNCRM ranking *40*
Table 2.11 Top 24 critical lines of IEEE 118 bus system using ACNCRM ranking *41*
Table 2.12 Top 24 critical lines of IEEE 57 bus system using ACNCRM ranking *41*
Table 2.13 List of critical lines leading to violations of line capacities for IEEE 39 bus system *42*
Table 3.1 Most famous matrices associated with graph *45*
Table 3.2 Effect of topology on grid vulnerability *51*
Table 3.3 Effect of line impedance on grid vulnerability *52*
Table 3.4 Critical lines of unweighted IEEE 30 bus system according to network efficiency *53*
Table 3.5 Critical lines of weighted IEEE 30 bus system according to network efficiency *53*
Table 3.6 Top 10 critical lines of IEEE 30 bus system according to DE and ACLOIM *53*
Table 3.7 Top 10 critical lines of 39- bus, 57-bus, 118-bus systems according to DE and ACLOIM *56*
Table 3.8 Effect of topology on line betweenness *60*
Table 3.9 Effect of impedance on line betweenness *60*
Table 3.10 Delta network vulnerability *65*
Table 3.11 Comparison of top ten critical lines identified by DA and ACNCRM *65*
Table 4.1 Post-contingency LODF values of the network in delta connection *77*
Table 4.2 Power flow through lines of thee-bus simple network *78*
Table 4.3 DCLOIM value for the network in delta connection shown in figure III.3 ..... *78*
Table 4.4 DC network capacity reservation of the simple network – line L12 impedance increase 3 times *78*
Table 4.5 Comparison of top ten critical lines identified by DCLOIM and ACLOIM *79*
Table 4.6 Comparison top ten critical lines identified by DCNCRM and ACNCRMM *84*

Abbreviations and acronyms

EU	:	The European Union
SGAM	:	Smart Grid Architecture Model
UCTE	:	Union for the Coordination of the Transmission of Electricity
AC	:	Alternating current
DC	:	Direct current
P-V bus	:	Voltage controlled bus
P-Q bus	:	Load bus
IEEE	:	Institute of Electrical and Electronic Engineers
ACLOIM	:	AC Line outage impact metric
ACNCRM	:	AC Network capacity reservation metric
ID	:	Identity
PTDF	:	Power transfer distribution factor
LODF	:	Line outage distribution factor
DCLOIM	:	DC Line outage impact metric
DCNCRM	:	DC Network capacity reservation metric

Chapter I.

Access to electricity is a vulnerable right

I. The Human Right to access Electricity

The issue of access to essential services is central in the debates on Human Rights. Availability of water and energy affects indeed social and economic developments. And, the Right for any Human being to access essential services, especially Electricity, is more and more recognized in international Human Rights laws [1].

According to the World Bank, the percentage of population living with access to electricity has increased by 10 points in 25 years (from 74% in 1990 to 85% in 2014). At the same time, the electric power consumption per capita has been multiplied by 1.5 [2]. Agriculture, industry, transport, personal usages and data centers are deeply depending on electrical energy. In addition, electricity is undoubtedly a key technology to have a low carbon emission future of the planet.

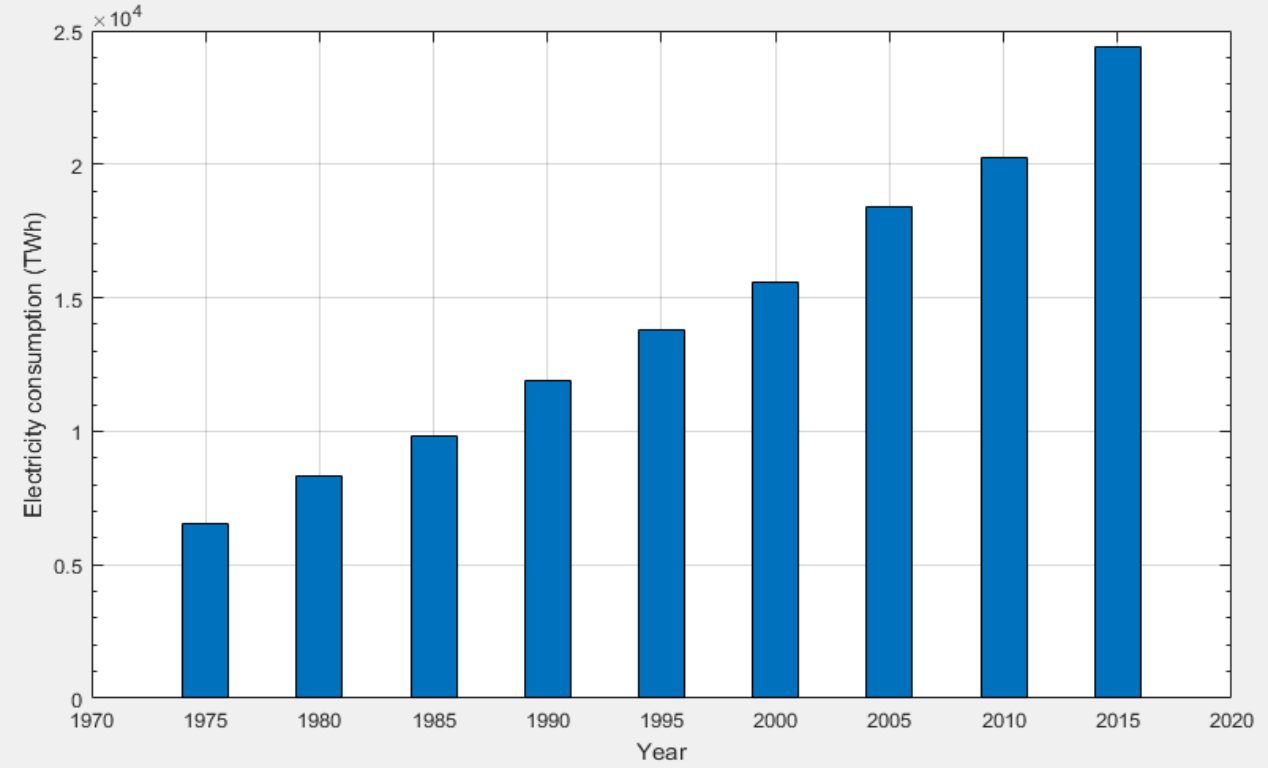

Figure I.1. World electricity consumption for the last four decades [2]

To continue progress towards accessibility, climate and environmental targets, new technologies for electric power are urgently required. They should provide even more energy efficiency in delivery, use and higher share of renewable power sources in electricity consumption. Many actions are developed to tackle with the associated fundamental, applied research and industrial issues (for instance, EU provides €3.8 billion in 2014-2020, of which €1.3 billion in 2018-2020 to help finance collaborative programs). Topics include, but are not limited to, the following: advanced materials with new functionalities and improved performances for power generation and conversion, new bio-inspired technologies and industrial processing of bio-energy for carbon mitigation, optimized devices and systems to increase availability, security and efficiency.

II. A rising complexity of electrical power systems

In order to reach electrical energy demand, bulk power systems have been built for many decades. Today, the power system is considered as one of the most complex system ever built by human being. The main factors of complexity [3] include:

- The heterogeneity of components (various types of power plants, substations, active devices, advanced components such as protections, supervisory control and data acquisition systems …).
- The multilayered and hierarchical architecture of the electrical system.
- The dynamic interactions between layers and between components.
- The possible chaotic behavior of the system which can lead to blackouts.
- The unpredictability and variability of grid operation due to the growth of renewable energy sources with a variable behavior largely dependent on weather.

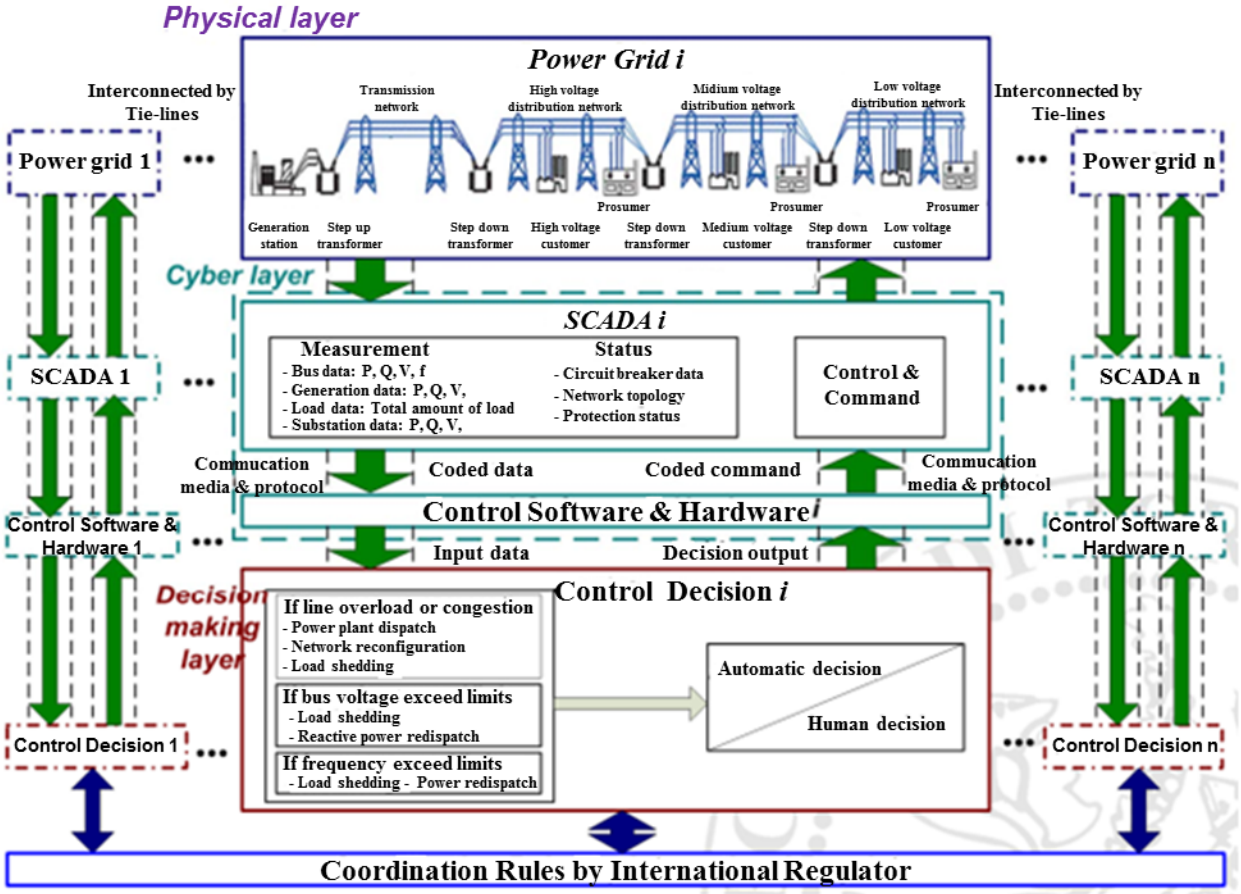

Figure I.2. Multilayer model of power system [4].

Complexity of power systems is illustrated by the multilayer model shown in figure I.2 [4]. First layer is associated with the electric grid. It is an essential layer used to generate and transmit electricity to loads. Cyber layer works as an interface between physical and decision-making layers. The latter plays a crucial role in controlling operation of power systems. Complexity of electrical

systems is not only due to their structure but also comes from the interactions with electricity markets.

With such a complex system, to achieve equilibrium in supply and demand, to maintain stability of the electrical grid under all conditions, to increase its self-healing capability, it was proposed to add more and more intelligence into the system, so that every node could respond quickly and accurately to any change or failure [5]. This gave birth to the concept of Smart Grids.

Smart Grid is a cross-technology solution that should lead to an increase of energy efficiency in order to reduce carbon emissions and the use of primary resources. It should also improve the reliability and resilience as well as limit the development of power infrastructures. Smart electrical grids connect together power systems, IT networks and energy markets in a background of a growing number of dispersed generators and active loads. New functions of analysis, control, instrumentation based on intelligent digital technologies are implemented and are used for driving the global electrical system from the utilities to the devices.

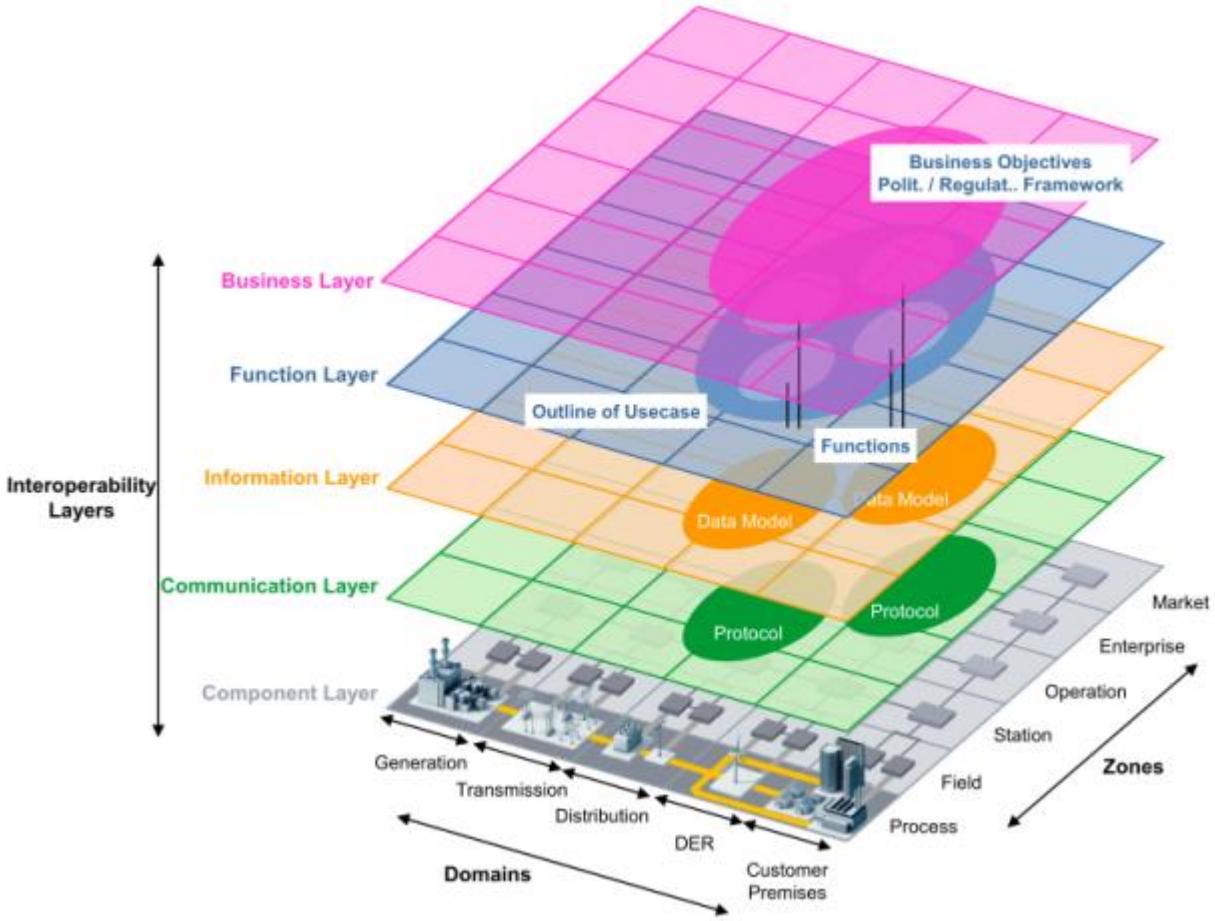

Figure I.3. Smart Grid Architecture Model [6].

The multilayered architecture of smart grids is well described by the Smart Grid Architecture Model (SGAM). This is a reference model to analyze Smart Grid use cases in a technological neutral manner [6]. The five domains (generation, transmission, distribution, Distributed Energy Resources

and customers' premises) cover the complete electrical energy conversion and transportation chain. The zones represent the hierarchical levels of the power system management. The interoperability layers give a simple presentation of the Smart Grid architecture and the different points of view that can be adopted to visualize it. The business layer describes the regulatory, economic and business structures and objectives that underlie Smart Grid operations. The function layer describes the functions and services that are required to satisfy the business and Smart Grids operation needs. The information layer describes the mechanism and protocols that are used for the exchanges between functions. The physical implementation is represented by the component layer. This includes power system equipment, protection and control devices, network infrastructure and computation centers.

The ever increasing complexity of electrical power systems raises many challenges including modeling power systems and ICT together, observability and control of the integrated system, market mechanisms for ensuring system adequacy and efficiency, distributed self-organization, self-healing, cyber-security and prevention of blackouts (due to its complexity, local unwanted variations may impact the electrical system on a very large scale and actions are required to prevent any major outages).

Massive power outages are likely to become more probable with the increasing age and load of power infrastructures and the complexity of the power system operation. Indeed, the conventional design of power network control system is hierarchically centralized and not appropriate with the vertical unbundling of electricity systems which is necessary for the implementation of competition [7]. Since the 2000s, more than ten blackouts have impacted to more than one billion people around the world [8]. They not only cost millions of US dollars [9] but also affect other important infrastructure that deliver essential services such as communication, internet, transport, water and emergency services. In 2003, on August 14th, the Great Blackout left approximately 50 million people in the dark for two days in parts of Northeast and Midwestern United States and Canada [10]. It was caused by a contact of a power line with an overgrown tree conjugated with a software bug. A similar incident occurred in 2003 when a power transmission line in Switzerland was tripped, leading to a total blackout in Italy [10]. In November 2006, a major disturbance was caused by the tripping of high voltage lines in northern Germany resulting in the split of the UCTE system into three areas. Fifteen million households were affected all over Europe. Two critical factors were the lack of coordination between the operators of the transmission and distribution systems and the lack of real time information about the dispersed generators connected to distribution grids [11]. Other major blackout happened in many places around the world including India, Brazil and, more recently, Australia in 2016 [12]. And officials now fear that major blackouts may also result from intentional attacks of electricity infrastructures.

Understanding how vulnerability of power systems emerges from their complex organization is therefore the main motivation of the present work. The literature review of power system blackouts [12] indicates that even though a power system is designed to withstand with N-1 contingencies, blackouts do occasionally happen due to failure of a single transmission component. Actually, the post-mortem analysis of past blackouts reveals that most of them result from large scale cascading

failures that are typically due to a sequence of failures and disconnections initiated by a first event that propagates through the whole network [13], [14]. This event may be natural phenomena, human actions or imbalances between generation and loads [15]. It turns that a particular attention has to be paid to single failures to evaluate the vulnerability of power systems [16] and estimate where are located the most critical components.

III. Some previous works on power system vulnerability

Although numerous research works have already focused on power systems robustness, the fundamental phenomena that mitigate or aggravate system vulnerability are still not well understood.

The first approach to assess system vulnerability is based on conventional N-1 contingency analysis based on post contingency power flow. It uses load-flow numerical simulations and physical models of components. This requires detailed data and information about system operation. For complex power system, the number of contingencies is tremendous and it becomes impossible to simulate all contingency scenarios. Thus, many works attempt on classifying contingencies and only consider the most severe ones. A typical example of this approach is given by [17]. For on-line contingency assessment, Q. Morante et al [18] propose "the employment of grid technologies to create a distributed architecture for power system contingency analysis". This work is based on data acquisition and web-based user interface to perform distributed computing and get real-time power flow solution.

It may be very challenging to perform such vulnerability analysis since AC power flow is burden load for computation and time consuming [19]. In addition, AC power flow fails to converge in severe contingencies. In these situations, the relevant security boundary cannot be monitored. Therefore, a recent study shows that analyzing and mitigating cascading failures requires a system level approach [20].

Such approach for assessment of power systems vulnerability is generally based on complex network theory [16],[21]–[36]. Literature review shows that this theory can be used to tackle vulnerability of power systems in two ways. The first one only focuses on grid's geometry (shape, size, relative position of sub-networks) and topology (relation between nodes, shortest distances …). These studies can be refined to incorporate electrical variables or Kirchhoff's laws [20], [23], [31], [24]–[29]. For instance, some works explore whether power grids are scale-free networks meaning these network follow a power law degree distribution [32] or exhibit small-world properties [33]. Through this kind of classification, researchers try to understand if power systems share some universal features and which classes of networks are more or less vulnerable. Some other works are based on centrality analysis and consider which nodes or links are the most critical for the flow of electrical power through the grid. These approaches use, for instance, edge betweenness centrality measure [25], [34] or network efficiency characterization [35], [36].

Contrary to conventional contingency analysis, the assessments of power systems vulnerability based on complex network approaches do not require time consuming computations of load-flow

solutions but we will show they may fail in capturing some important features of power grids operations. Due to these limitations, no method inspired by the theory of complex systems has been accepted now as standard [16].

IV. Objectives of the thesis

Power system vulnerability is generally defined as the measure of system weaknesses [37]. Events may be line or generator outages, malfunction of protection relay, failures of communication systems or human errors. The thesis focuses on vulnerability with respect to failures of lines or power transformer leading to unwanted consequences such as significant power redistribution, network transfer capacity reduction. As previously mentioned, only single failures will be considered.

Within this frame, the first goal of this work is to contribute to the definition of a standard method to assess vulnerability of power systems and identify their most critical elements. This method shall be easy to use by power engineers and give a global assessment of system robustness while identifying critical components for system operation. Definition of this method will start by a critical review of literature approaches based on complex system theory. The results provided by these approaches will be confronted to a reference contingency analysis using AC power flow calculations. Four IEEE test systems will be investigated. An improved method for assessment of system vulnerability to line outages will be defined from this confrontation.

The second objective of the thesis is to better understand how system vulnerability and critical components emerge from graph's topology. A new approach to solve power flow will be introduced in the thesis to help reach this goal.

The thesis report is structured as follows:

- Chapter 2 presents conventional contingency analysis of power systems using AC power flow.
- Chapter 3 reviews some topological indicators for mapping vulnerability of power systems.
- Chapter 4 considers an improved approach for DC assessment of power system vulnerability.
- Chapter 5 proposes a new approach based on spectral solving of DC power flow to identify how vulnerability emerges from network topology.
- Chapter 6 concludes the report, giving some directions for future works.

Chapter II.

Contingency analysis of AC power systems

I. Introduction

This chapter presents some conventional approaches and tools which are used for analyzing vulnerability to line outage of interconnected power systems. Power systems are assumed to be balanced and modeled by a single phase equivalent circuit. This chapter consists of five parts.

- The first part shows how to model power system as an electrical circuit. Based on this circuit, the nonlinear algebraic equations in terms of power, known as the power flow equations, are formulated.
- The second section presents methods to solve the nonlinear power flow equations.
- The following section introduces contingency analysis, a conventional approach for assessing system vulnerability to line outages.
- Then, some indicators for measuring how vulnerable is a power system are defined.
- They are finally applied to several IEEE test systems.

II. Modeling power systems by equivalent electrical circuits

A typical power grid includes a large number and variety of network components. It spans a large geographic area and contains hundreds of buses and lines. In normal operation, it is possible to assume that the power system is operating under balanced conditions and represented by a single phase diagram.

II.1 Transmission line modeling

The transmission lines are represented by their equivalent Π model. It includes series admittances y_l and total charging susceptance b_c lumped at each end of the line as shown in figure II.1.

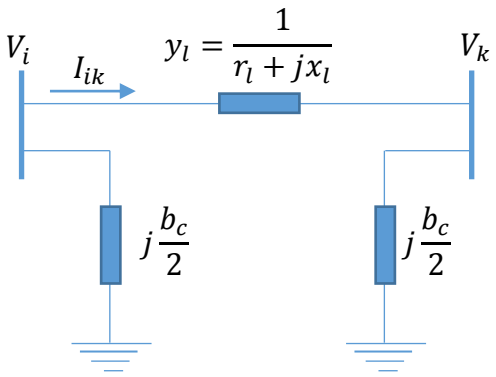

Figure II.1. Equivalent ΠΠ model of a transmission line between two nodes

II.2 Transformer modeling

Transformers and phase shifters are represented with a similar model, consisting of a series admittance y_t. Its value is obtained when the tap ratio a of the transformer is set at the nominal value. When the tap ratio is set at off-normal, the admittance must be modified to include the effect of the off-normal ratio. The resulting model is shown in figure II.2 [38]. In this model, the left side corresponds to the non-tap side and the right side corresponds to the tap side.

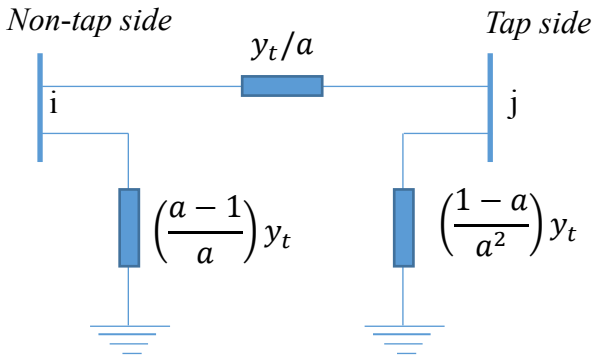

Figure II.2. Equivalent circuit of a tap changing transformer

II.3 Generator model

A generator is modeled by a complex power injection as shown in figure II.3.

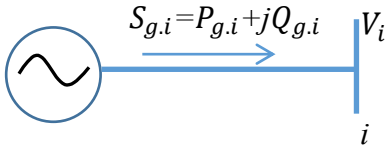

Figure II.3. Equivalent circuit of a generator

For a generator connected to bus i, $P_{g,i}$ and $Q_{g,i}$ are the active and reactive power injected at the connection node. The injection power is given by:

$$S_{g.i} = P_{g.i} + jQ_{g.i} \tag{II.1}$$

II.4 Load model

Constant power loads are modeled by:

$$S_{l.i} = P_{l.i} + jQ_{l.i} \tag{II.2}$$

Where, $P_{l,i}$ and $Q_{l,i}$ are the active and reactive power consumed at the connection node.

II.5 Shunt elements

A shunt connected element such as a capacitor or inductor is represented by a constant impedance connected to the ground at the shunt connected bus. The admittance of the shunt elements at bus i is given by:

$$y_{sh.i} = g_{sh.i} + jb_{sh.i} \tag{II.3}$$

Where, $g_{sh,i}$ and $b_{sh,i}$ are the shunt conductance and susceptance at node i.

II.6 Power flow equations

In order to formulate the power flow equations, we consider a typical bus of a power system as shown in figure II.4. The application of Kirchoff's law to bus i yields to:

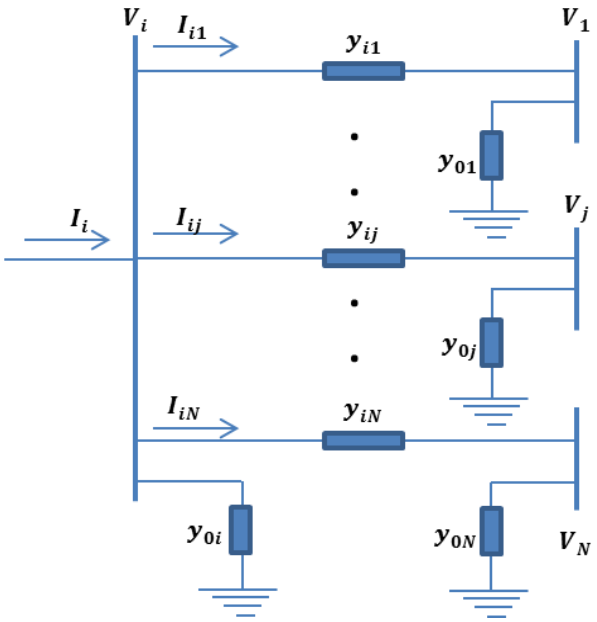

Figure II.4. Representation of a typical bus of a power system

$$I_i = y_{0i}V_i + y_{i1}(V_i - V_1) + y_{i2}(V_i - V_2) + \cdots + y_{iN}(V_i - V_N) \quad \text{(II.4)}$$

Equation (II.4) can be written as:

$$I_i = (y_{0i} + y_{i1} + \cdots + y_{iN})V_i - y_{i1}V_1 - y_{i2}V_2 - \cdots y_{iN}V_N \quad \text{(II.5)}$$

Equation (II.5) is reformulated as:

$$I_i = V_i \sum_{j=0}^{n} y_{ij} - \sum_{j=1}^{n} y_{ij}V_j \qquad (i \neq j) \quad \text{(II.6)}$$

If we now define a new variable Y called bus admittance matrix whose entry elements are defined by the relation:

$$\begin{cases} Y_{ii} = y_{0i} + y_{i1} + \cdots + y_{iN} \\ Y_{i1} = -y_{i1} \\ \cdots \\ Y_{iN} = -y_{iN} \end{cases} \quad \text{(II.7)}$$

Then equation (II.6) can be reformulated in terms of the elements of the bus admittance matrix such as:

$$I_i = Y_{ii}V_i + Y_{i1}V_1 + Y_{i2}V_2 + \cdots + Y_{iN}V_N \quad \text{(II.8)}$$

The full network equations are therefore given under a matrix form by:

$$\begin{vmatrix} I_1 \\ I_2 \\ . \\ I_N \end{vmatrix} = \begin{vmatrix} Y_{11} & Y_{12} & . & Y_{1N} \\ Y_{21} & Y_{22} & . & Y_{2N} \\ . & . & . & . \\ Y_{N1} & Y_{N2} & . & Y_{NN} \end{vmatrix} \begin{vmatrix} V_1 \\ V_2 \\ . \\ V_N \end{vmatrix} \quad \text{(II.9)}$$

The conjugate of the complex power supply at bus *i* is given by:

$$S_i^* = P_i - jQ_i = I_iV_i^* \quad \text{(II.10)}$$

Then, the current injection to bus *i* is given by:

$$I_i = \frac{P_i - jQ_i}{V_i^*} \tag{II.11}$$

Substituting I_i from equation (II.11) in (II.8), we have:

$$\frac{P_i - jQ_i}{V_i^*} = V_i Y_{ii} + \sum_{j=1}^{n} Y_{ij} V_j \qquad i \neq j \tag{II.12}$$

Multiplying equation (II.12) by V_i^*, the active power P_i and reactive power Q_i are expressed by:

$$P_i = Re\left\{V_i^*\left[V_i Y_{ii} + \sum_{j=1}^{n} Y_{ij} V_j\right]\right\} \qquad i \neq j \tag{II.13}$$

$$Q_i = -Im\left\{V_i^*\left[V_i Y_{ii} + \sum_{j=1}^{n} Y_{ij} V_j\right]\right\} \qquad i \neq j \tag{II.14}$$

Equation (II.8) can be expressed in polar form as:

$$I_i = \sum_{j=1}^{N} |Y_{ij}||V_j| \angle \delta_j + \theta_{ij} \tag{II.15}$$

Where, the complex voltage and admittance are written as:

$$V_j = |V_j| \angle \delta_j \; and \; Y_{ij} = G_{ij} + jB_{ij} = |Y_{ij}| \angle \theta_{ij} \tag{II.16}$$

Substituting I_i from equation (II.15) to equation (II.12), we get:

$$S_i = \sum_{j=1}^{N} |V_i||V_j||Y_{ij}| \angle (\theta_{ij} + \delta_j) - \delta_i \tag{II.17}$$

Then, separating the real and imaginary parts, we obtain [39]:

$$P_i = \sum_{j=1}^{N} |V_i||V_j||Y_{ij}| cos(\theta_{ij} - \delta_i + \delta_j) \tag{II.18}$$

$$Q_i = -\sum_{j=1}^{N} |V_i||V_j||Y_{ij}| sin(\theta_{ij} - \delta_i + \delta_j) \tag{II.19}$$

The group of equations (II.13) and (II.14) or (II.18) and (II.19) are the AC power flow equations. They are algebraic nonlinear equations which can be solved by using an iterative method to get the power flowing through the network.

III. Numerical methods to solve power flow problem

Solving power flow is a mandatory step of many power system analyzers. It is necessary not only for planning, economic scheduling but also for vulnerability analysis [38]. Solving power flow

problem involves determining real and reactive as well as the magnitudes and phase angle of voltages at every bus of the system. Gauss-Seidel and Newton– Raphson methods are the most common techniques used for solving the AC power flow equations [38], [40]–[43]. These methods are detailed in this section for a one dimensional equation and then applied for solving power flow problems.

III.1 Gauss-Seidel method

III.1.1 Principles

Gauss-Seidel is an iterative method used to solve linear systems of equations *AX=B*. *A* is a *n*x*n* matrix. It is decomposed into a strictly upper triangular matrix *U*, a strictly lower triangular matrix *L* and a diagonal matrix *D*. Then, the system to solve can be written as:

$$(L + D)X = B - UX \tag{II.20}$$

Using Gauss-Seidel approach, the $(k+1)^{\text{th}}$ approximation of X is given by:

$$(L + D)X^{(k+1)} = B - UX^{(k)} \tag{II.21}$$

For $i = 1, \dots, n$, the vector elements are thus expressed by:

$$x_i^{k+1} = \frac{1}{a_{ii}}\left(b_i - \sum_{j=1}^{i-1} a_{ij}x_j^{k+1} - \sum_{j=i+1}^{n} a_{ii}x_j^{k}\right) \tag{II.22}$$

The computation of x_i^{k+1} uses a combination of some $(k+1)^{\text{th}}$ approximated values and some values of the k^{th} iteration.

The convergence depends on the eigenvalues of $(L + D)^{-1}U$. In particular, the iteration process is convergent if the matrix A is either diagonally strictly dominant, or symmetrical and positive definite.

John H. Mathews [44] showed that it is possible to "Gauss-Seidelize" the solving of non-linear system of equations $F(X) = 0$ where $X = \{x_1, \dots, x_n\}$ and $F = \{f_1, \dots, f_n\}$. This proceeds from a fixed-point iteration technique using a computation process similar to Gauss-Seidel.

The system is first rewritten such as $X = G(X)$ with $G = \{g_1, \dots, g_n\}$. If it exits, the fixed point solution $X^* = \{x_1^*, \dots, x_n^*\}$ verifies $X^* = G(X^*)$.

Using a process similar to Gauss-Seidel, the computation of the $(k+1)^{\text{th}}$ approximation of X is done by:

$$\begin{cases} {x_1}^{(k+1)} = g_1\left({x_1}^{(k)}, {x_2}^{(k)}, \dots, {x_n}^{(k)}\right) \\ {x_2}^{(k+1)} = g_2\left({x_1}^{(k+1)}, {x_2}^{(k)}, \dots, {x_n}^{(k)}\right) \\ \dots\ \dots\ \dots\ \dots\ \dots\ \dots\ \dots\ \dots. \\ {x_n}^{(k+1)} = g_1\left({x_1}^{(k+1)}, {x_2}^{(k+1)}, \dots {x_{n-1}}^{(k+1)}, {x_n}^{(k)}\right) \end{cases} \tag{II.23}$$

The new values ${x_i}^{(k+1)}$ are thus used as soon as they are known. This is the main difference with a classical fixed-point iteration approach.

The procedure is started by assuming an approximate solution for each independent variable $\left({x_1}^{(0)}, {x_2}^{(0)}, \dots, {x_n}^{(0)}\right)$.

Iterations are terminated when all the variations of the variables at step *(k+1)* compared to step *k* are within the specified accuracy.

Formally, the iterative process converges if each eigenvalue *e* of $DG(X^*)$ satisfies $|e|<1$. DG is the Jacobian matrix associated to G [45].

A simple application is now shown for a nonlinear equation defined by:

$$f(x) = x^3 - 6x^2 + 9x - 3 = 0 \tag{II.24}$$

The above equation is rearranged and written as:

$$x = g(x) = -\frac{1}{9}x^3 + \frac{2}{3}x^2 + \frac{1}{3} \tag{II.25}$$

If $x^{(0)} = 2.5$ is chosen as initial value, the first iteration is formed by:

$$x^{(1)} = g\left(x^{(0)}\right) = -\frac{1}{9}(2.5)^3 + \frac{2}{3}(2.5)^2 + \frac{1}{3} = 2.7639 \tag{II.26}$$

As shown in figure II.5, the procedure is repeated until the change of value between two successive steps is less than a specified tolerance.

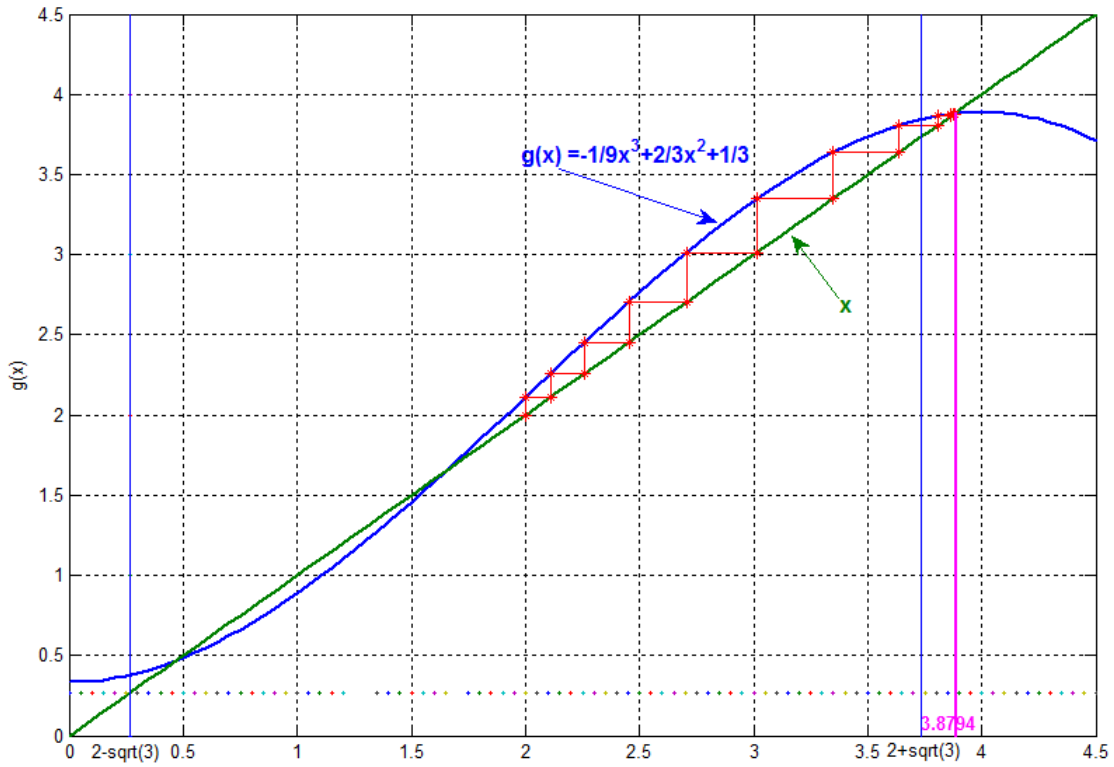

Figure II.5. Graphical illustration of the Gauss-Seidel iterative method [1]

Finally, the process converges to $x^{(f)} = 3.8794$. The convergence condition is respected to $\frac{dg(x^{(f)})}{dx} < 1$, the derivative of $g(x)$ being lower than 1 for all $x < 2 - \sqrt{3}$ *or* $x > 2 + \sqrt{3}$. The two other roots of $f(x) = 0$ did not respect this condition.

III.1.2 Application of Gauss-Seidel method to power-flows

Before solving the power flow equations, power system buses are classified into three types depending on which nodal variables are known or not.

- *Slack bus:* One bus referred as slack node is taken as reference bus where voltage magnitude and phase angle are specified.
- *Voltage controlled bus:* All generator buses except the slack bus are considered as voltage controlled buses. At these buses, the magnitude of voltage and active power are specified. The remaining variables which are reactive power and phase angle of bus voltage need to be determined.
- *Load buses:* At these buses, the active power and reactive power are specified. The magnitude and phase angle of the bus voltage are unknown, so they need to be determined.

For normal operation of power systems, the active and reactive powers at load buses and active power generation at voltage controlled buses are considered equal to the scheduled values (P_i^{sch} and Q_i^{sch}), while the voltage magnitudes of the buses are approximately equal to the rated voltage and closed to the voltage magnitude of the slack bus. The phase of the voltage controlled buses and load buses are also closed to the reference value generated. Thus, an initial estimated value of buses at $1.0\angle 0$ for unspecified voltage buses is acceptable [38]. And since the bus admittance matrix defined by equation (II.9) is symmetric and diagonally dominant, the conditions to apply Gauss-Seidel method are verified. The main steps of the iteration process are detailed now.

1. The process is initialized by assigning specified or estimated values to voltage magnitude and phase at every bus.
   a. *Slack bus:* Voltage magnitude and phase angle are specified.
   *b. Voltage controlled bus or regulated bus (P-V bus): V*oltage magnitude at these buses $|V_i|$ equal to the scheduled values, $|V_i|^{sch}$. Phase angle of bus voltages are initialized to 0 ($\delta_i = 0$).
   *c. Load buses (P-Q bus): M*agnitude and phase angle of voltage at these buses are initialized to 0 ($\delta_i = 0$) and 1.0 ($|V_i| = 1.0$), respectively.
2. At each iteration step (*k*), assuming that bus voltage ${V_i}^{(k)}$ has been calculated from the previous step, the following calculations are performed.
   a. *Slack bus:* Power injection is calculated by:

$$ {P_i}^{(k)} = Re\left\{ {V_i}^{*(k)} \left[{V_i}^{(k)} Y_{ii} - \sum_{\substack{j=1 \\ j\neq i}}^{n} Y_{ij} {V_j}^{(k)} \right] \right\} \tag{II.27} $$

$$ {Q_i}^{(k)} = -Im\left\{ {V_i}^{*(k)} \left[{V_i}^{(k)} Y_{ii} - \sum_{\substack{j=1 \\ j\neq i}}^{n} Y_{ij} {V_j}^{(k)} \right] \right\} \tag{II.28} $$

   b. Voltage controlled bus (P-V bus):
   - Reactive power ${Q_i}^{(k)}$ is computed using equation (II.28).
   - Phase angle of bus voltage is calculated from the following equations:

- Using equation (II.12) and Gauss-Seidel-like approach, voltage at bus *i* can be written as:

$$V_i^{(k+1)} = \frac{\frac{P_i^{(k)} - jQ_i^{(k)}}{V_i^{*(k)}} + \sum_{\substack{j=1 \\ b<i}}^{b} Y_{ij} V_j^{(k+1)} + \sum_{\substack{j=c \\ c>i}}^{n} Y_{ij} V_j^{(k)}}{Y_{ii}} \quad \text{(II.29)}$$

- Imaginary part of $V_i^{(k+1)}$ is then calculated. Since magnitude of voltages at P-V buses is known, the real part is obtained by:

$$\left(Re\left\{V_i^{(k+1)}\right\}\right) = \sqrt{|V_i|^2 - \left(Im\left\{V_i^{(k+1)}\right\}\right)^2} \quad \text{(II.30)}$$

Finally, voltage angle at bus *i* is given by:

$$\delta_i^{(k+1)} = arctan \frac{Im\left\{V_i^{(k+1)}\right\}}{Re\left\{V_i^{(k+1)}\right\}} \quad \text{(II.31)}$$

c. Load buses (P-Q bus):

- Equations (II.27) and (II.28) are used to compute active power and reactive power.
- $V_i^{(k+1)}$ (magnitude and phase) is calculated from equation (II.29).

3. The power residuals ($\Delta P_i^{(k)}$ and $\Delta Q_i^{(k)}$) that are the difference between the scheduled and the calculated values are given by:

$$\Delta P_i^{(k)} = P_i^{(k)} - P_i^{(k-1)} \quad \text{(II.32)}$$

$$\Delta Q_i^{(k)} = Q_i^{(k)} - Q_i^{(k-1)} \quad \text{(II.33)}$$

The convergence is finally checked. If $Max\left\{\left|\Delta P_i^{(k)}\right|, \left|\Delta Q_i^{(k)}\right|\right\} < \varepsilon$, the iterative process is stopped. Otherwise, it continues. The process can also be stopped if the user-defined maximal number of iterations if reached. In that case, it may mean that the solving is not convergent.

III.2 Newton-Raphson method

III.2.1 Principles

Newton- Raphson method is the most widely used technique to solve nonlinear algebraic set of equations [38], [42], [43]. This method is a successive approximation procedure based on an initial guessed values of the unspecified variables and the utilization of Taylor's series expansion.

For instance, let consider how to get a solution of the equation defined by:

$$f(x) = c \quad \text{(II.34)}$$

If $x^{(0)}$ is an initial estimated value of the solution, and $\Delta x^{(0)}$is the deviation from the correct solution, we should have:

$$f\left(x^{(0)} + \Delta x^{(0)}\right) = c \quad \text{(II.35)}$$

Expanding the left-hand side of equation (II.41) in Taylor's series at $x^{(0)}$, we can get:

$$f\left(x^{(0)}\right)+\left(\frac{df}{dx}\right)^{(0)}\Delta x^{(0)}+\frac{1}{2!}\left(\frac{d^2f}{dx^2}\right)^{(0)}\left(\Delta x^{(0)}\right)^2+\cdots=c \tag{II.36}$$

Assuming $\Delta x^{(0)}$ is very small, the higher-order terms can be neglected and equation (II.36) becomes:

$$f\left(x^{(0)}\right)+\left(\frac{df}{dx}\right)^{(0)}\Delta x^{(0)}=c \tag{II.37}$$

From the above equation, we can calculate $\Delta x^{(0)}$ as:

$$\Delta x^{(0)}=\frac{c-f\left(x^{(0)}\right)}{\left(\frac{df}{dx}\right)^{(0)}}=\frac{\Delta c^{(0)}}{\left(\frac{df}{dx}\right)^{(0)}} \tag{II.38}$$

Where $\Delta c^{(0)}=c-f\left(x^{(0)}\right)$

And then adding $\Delta x^{(0)}$ to the initial estimated value, we get:

$$x^{(1)}=x^{(0)}+\Delta x^{(0)}=x^{(0)}+\frac{\Delta c^{(0)}}{\left(\frac{df}{dx}\right)^{(0)}} \tag{II.39}$$

Newton-Raphson method is repeated to compute $x^{(k+1)}$ from $x^{(k)}$ as shown below:

$$x^{(k+1)}=x^{(k)}+\Delta x^{(\mathrm{k})}=x^{(k)}+\frac{\Delta c^{(k)}}{\left(\frac{df}{dx}\right)^{(k)}} \tag{II.40}$$

Where $\Delta c^{(k)}=c-f\left(x^{(k)}\right)$

We can rearrange equation (II.44) to form a new equation such as:

$$\Delta c^{(k)}=\left(\frac{df}{dx}\right)^{(k)}\Delta x^{(\mathrm{k})} \tag{II.41}$$

Equation (II.41) indicates that the nonlinear function $c-f(x)$ is approximated by a tangent line at $x^{(k)}$. The intersection of the tangent line with the x axis results in $x^{(k+1)}$. This idea is illustrated graphically in figure II.6 for $c-f(x)=3-x^3+6x^2-9x$.

Applying this method to solve the set of *n* equations given by (II.28), we obtain:

$$\begin{bmatrix}\Delta c_1^{(k)}\\ \Delta c_2^{(k)}\\ \dots\dots\\ \Delta c_2^{(k)}\end{bmatrix}=\begin{bmatrix}\left(\frac{\partial f_1}{\partial x_1}\right)^{(k)} & \left(\frac{\partial f_1}{\partial x_2}\right)^{(k)} & \dots. & \left(\frac{\partial f_1}{\partial x_n}\right)^{(k)}\\ \left(\frac{\partial f_2}{\partial x_1}\right)^{(k)} & \left(\frac{\partial f_2}{\partial x_2}\right)^{(k)} & \dots. & \left(\frac{\partial f_2}{\partial x_n}\right)^{(k)}\\ \dots\dots & \dots\dots & \dots\dots & \dots\dots\\ \left(\frac{\partial f_n}{\partial x_1}\right)^{(k)} & \left(\frac{\partial f_n}{\partial x_2}\right)^{(k)} & \dots. & \left(\frac{\partial f_n}{\partial x_n}\right)^{(k)}\end{bmatrix}\begin{bmatrix}\Delta x_1^{(k)}\\ \Delta x_2^{(k)}\\ \dots\dots\\ \Delta x_2^{(k)}\end{bmatrix} \tag{II.42}$$

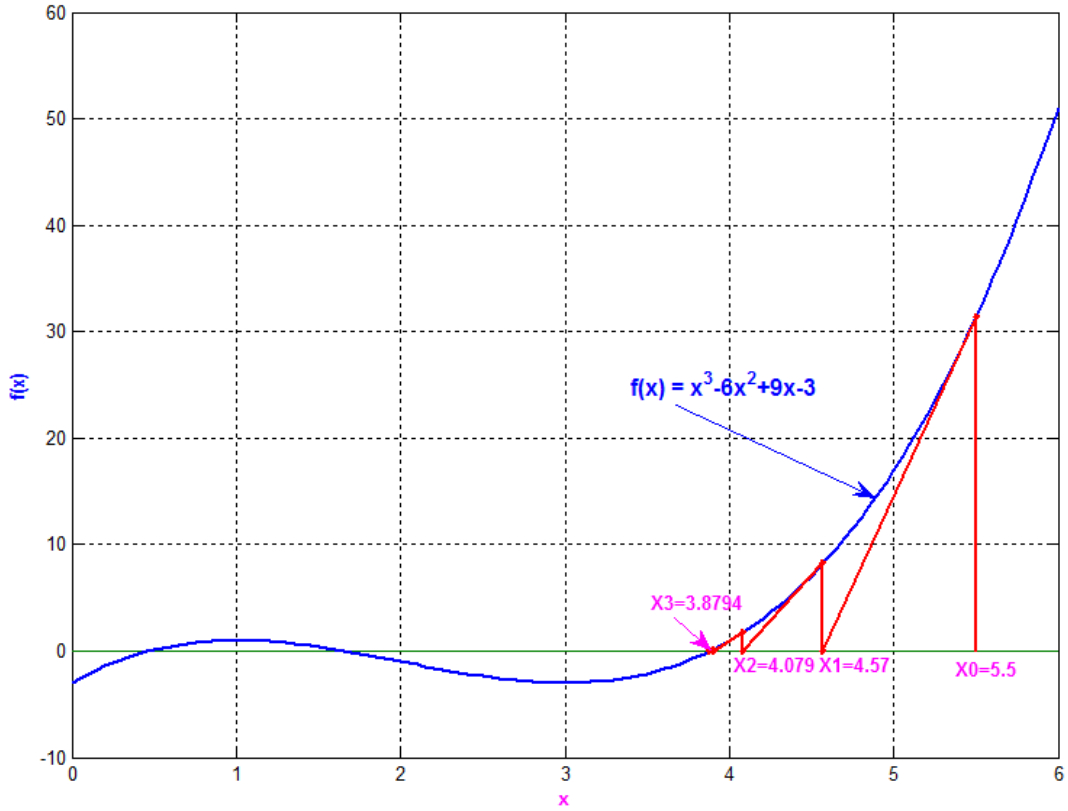

Figure II.6. Graphical illustration of Newton-Raphson iterative method [38].

The above equation can be written in matrix form such as:

$$\Delta C^{(k)} = J^{(k)} \Delta X^{(k)} \tag{II.43}$$

Where

$$\Delta C^{(k)} = \begin{bmatrix} \Delta c_1^{(k)} \\ \Delta c_2^{(k)} \\ \dots \dots \\ \Delta c_2^{(k)} \end{bmatrix} \text{ and } \quad \Delta X^{(k)} = \begin{bmatrix} \Delta x_1^{(k)} \\ \Delta x_2^{(k)} \\ \dots \dots \\ \Delta x_2^{(k)} \end{bmatrix} \tag{II.44}$$

$J^{(k)}$ is referred to the Jacobian matrix whose elements are the partial derivatives of f evaluated at $X^{(k)}$:

$$J^{(k)} = \begin{bmatrix} \left(\frac{\partial f_1}{\partial x_1}\right)^{(k)} & \left(\frac{\partial f_1}{\partial x_2}\right)^{(k)} & \dots . \left(\frac{\partial f_1}{\partial x_n}\right)^{(k)} \\ \left(\frac{\partial f_2}{\partial x_1}\right)^{(k)} & \left(\frac{\partial f_2}{\partial x_2}\right)^{(k)} & \dots . \left(\frac{\partial f_2}{\partial x_n}\right)^{(k)} \\ \dots \dots \dots \dots \dots \dots \dots \dots \dots \dots \dots \dots \\ \left(\frac{\partial f_n}{\partial x_1}\right)^{(k)} & \left(\frac{\partial f_n}{\partial x_2}\right)^{(k)} & \dots . \left(\frac{\partial f_n}{\partial x_n}\right)^{(k)} \end{bmatrix} \tag{II.45}$$

The updated values of the variables at the $(k+1)^{th}$ step are given by:

$$X^{(k+1)} = X^{(k)} + \Delta X^{(k)} \tag{II.46}$$

III.2.2 Application of Newton-Raphson method to power-flow solving

To apply Newton-Raphson, we consider a power network that consisted of slack bus and (n-1) P-Q nodes. The power is described by a set of *2(n-1)* nonlinear algebraic equations given by (II.18) and (II.19) that are necessary to compute *2(n-1)* independent variables. They correspond to magnitude and phase angle of every nodal voltage except slack node which is used as voltage reference bus. If bus 1 is assumed as slack bus, the reduced Jacobian matrix at k^{th} iteration is expressed by:

$$\begin{bmatrix} \Delta P_2^{(k)} \\ \dots \\ \Delta P_n^{(k)} \\ \Delta Q_2^{(k)} \\ \dots \\ \Delta Q_n^{(k)} \end{bmatrix} = \begin{bmatrix} \left(\frac{\partial P_2}{\partial \delta_2}\right)^{(k)} & \dots & \left(\frac{\partial P_2}{\partial \delta_n}\right)^{(k)} & \left(\frac{\partial P_2}{\partial |V_2|}\right)^{(k)} & \dots & \left(\frac{\partial P_2}{\partial |V_n|}\right)^{(k)} \\ \dots & \dots & \dots & \dots & \dots & \dots \\ \left(\frac{\partial P_n}{\partial \delta_2}\right)^{(k)} & \dots & \left(\frac{\partial P_n}{\partial \delta_n}\right)^{(k)} & \left(\frac{\partial P_n}{\partial |V_1|}\right)^{(k)} & \dots & \left(\frac{\partial P_n}{\partial |V_n|}\right)^{(k)} \\ \left(\frac{\partial Q_2}{\partial \delta_2}\right)^{(k)} & \dots & \left(\frac{\partial Q_2}{\partial \delta_n}\right)^{(k)} & \left(\frac{\partial Q_2}{\partial |V_2|}\right)^{(k)} & \dots & \left(\frac{\partial Q_2}{\partial |V_n|}\right)^{(k)} \\ \dots & \dots & \dots & \dots & \dots & \dots \\ \left(\frac{\partial Q_n}{\partial \delta_2}\right)^{(k)} & \dots & \left(\frac{\partial Q_n}{\partial \delta_n}\right)^{(k)} & \left(\frac{\partial Q_n}{\partial |V_2|}\right)^{(k)} & \dots & \left(\frac{\partial Q_n}{\partial |V_n|}\right)^{(k)} \end{bmatrix} \begin{bmatrix} \Delta \delta_2^{(k)} \\ \dots \\ \Delta \delta_n^{(k)} \\ \Delta |V_2|^{(k)} \\ \dots \\ \Delta |V_n|^{(k)} \end{bmatrix} \quad \text{(II.47)}$$

This equation can be written as:

$$\begin{bmatrix} \Delta P^{(k)} \\ \Delta Q^{(k)} \end{bmatrix} = \begin{bmatrix} J_1{}^{(k)} & J_2{}^{(k)} \\ J_3{}^{(k)} & J_4{}^{(k)} \end{bmatrix} \begin{bmatrix} \Delta \delta^{(k)} \\ \Delta |V|^{(k)} \end{bmatrix} \quad \text{(II.48)}$$

- The diagonal and off diagonal elements of J_1 are computed from:

$$\left(\frac{\partial P_i}{\partial \delta_i}\right)^{(k)} = \sum_{\substack{j=1 \\ j \neq i}}^{N} |V_i|^{(k)} \left|V_j\right|^{(k)} \left|Y_{ij}\right| sin\left(\theta_{ij} - \delta_i{}^{(k)} + \delta_j{}^{(k)}\right) \quad \text{(II.49)}$$

$$\left(\frac{\partial P_i}{\partial \delta_j}\right)^{(k)} = - |V_i|^{(k)} \left|V_j\right|^{(k)} \left|Y_{ij}\right| sin\left(\theta_{ij} - \delta_i{}^{(k)} + \delta_j{}^{(k)}\right) \quad (i \neq j) \quad \text{(II.50)}$$

- The diagonal and off diagonal elements of J_2 are given by:

$$\left(\frac{\partial P_i}{\partial |V_i|}\right)^{(k)} = 2|V_i|^{(k)} |Y_{ii}| cos\theta_{ii} + \sum_{\substack{j=1 \\ j \neq i}}^{N} \left|V_j\right|^{(k)} \left|Y_{ij}\right| cos\left(\theta_{ij} - \delta_i{}^{(k)} + \delta_j{}^{(k)}\right) \quad \text{(II.51)}$$

$$\left(\frac{\partial P_i}{\partial |V_j|}\right)^{(k)} = |V_i|^{(k)} \left|Y_{ij}\right| cos\left(\theta_{ij} - \delta_i{}^{(k)} + \delta_j{}^{(k)}\right) \quad (i \neq j) \quad \text{(II.52)}$$

- The diagonal and off diagonal elements of J_3 are expressed by:

$$\left(\frac{\partial Q_i}{\partial \delta_i}\right)^{(k)} = \sum_{\substack{j=1 \\ j \neq i}}^{N} |V_i|^{(k)} \left|V_j\right|^{(k)} \left|Y_{ij}\right| cos\left(\theta_{ij} - \delta_i{}^{(k)} + \delta_j{}^{(k)}\right) \quad \text{(II.53)}$$

$$\left(\frac{\partial Q_i}{\partial \delta_j}\right)^{(k)} = -|V_i|^{(k)}\left|V_j\right|^{(k)}\left|Y_{ij}\right|cos\left(\theta_{ij} - \delta_i{}^{(k)} + \delta_j{}^{(k)}\right) \quad (i \neq j) \tag{II.54}$$

- The diagonal and the off diagonal elements of J_4 are computed from:

$$\left(\frac{\partial Q_i}{\partial |V_i|}\right)^{(k)} = -2|V_i|^{(k)}|Y_{ii}|sin\theta_{ii} - \sum_{\substack{j=1 \\ j\neq i}}^{N}\left|V_j\right|^{(k)}\left|Y_{ij}\right|sin\left(\theta_{ij} - \delta_i{}^{(k)} + \delta_j{}^{(k)}\right) \tag{II.55}$$

$$\left(\frac{\partial Q_i}{\partial |V_j|}\right)^{(k)} = -|V_i|^{(k)}\left|Y_{ij}\right|sin\left(\theta_{ij} - \delta_i{}^{(k)} + \delta_j{}^{(k)}\right) \quad (i \neq j) \tag{II.56}$$

The procedure to compute power flow is summarized below.

1. For the initialization step, specified or estimated values are assigned to voltage magnitude and phase at every bus.
   a. *Slack bus:* Voltage magnitude and phase angle are specified.
   b. *P-Q bus:* Magnitude and phase angle of voltages are initialized to 0 and 1.0 respectively.
2. At each iteration step (*k*), assuming that bus voltage $V_i{}^{(k)}$ has been calculated from the previous step, the following calculations are performed.
   a. All buses except slack node: Power injections are estimated by equations (II.27), (II.28) and power residues are calculated from equations (II.32), (II.33).
   b. Jacobian matrix is computed from equations (II.49) to (II.56). Row and column corresponding to slack bus are removed from this matrix.
   c. Using the reduced Jacobian matrix, equation (II.48) is solved to obtain $\Delta\delta^{(k)}$ and $\Delta|V|^{(k)}$ for all P-Q nodes
   d. The updated voltage magnitudes and phase angles at bus i are then given by:

$$\delta_i{}^{(k+1)} = \delta_i{}^{(k)} + \Delta\delta_i{}^{(k)} \tag{II.57}$$

$$|V_i|^{(k+1)} = |V_i|^{(k)} + \Delta|V_i|^{(k)} \tag{II.58}$$

3. Stop criteria: If $max\left\{\left|\Delta P_i{}^{(k)}\right|, \left|\Delta Q_i{}^{(k)}\right|\right\} < \varepsilon$ or $k > k_{max}$ stop, else go to step (2)
4. Slack bus active and reactive power is calculated

The process is a bit different if the power system includes some P-V nodes. The main differences are:

- There are less variables to compute because the voltage magnitude is known and fixed at P-V nodes
- Fewer equations are required to compute the unknown variables. Usually, for power systems, the reactive power equation (II.19) associated to P-V node is not taken into

account. Thus, every P-V node needs only one equation given by (II.18). The reactive power value at these buses is computed only at the end of the process when Newton-Raphson has converged.

- Because of the former simplifications, $\frac{\partial P_i}{\partial |V_j|}$, $\frac{\partial Q_i}{\partial |V_j|}$, $\frac{\partial Q_j}{\partial |V_i|}$ and $\frac{\partial Q_j}{\partial \delta_i}$ are removed from Jacobian matrix. i refers to all the nodes except slack bus and j refers to P-V buses. If a power system consists of m voltage-controlled buses, the Jacobian matrix is of order ($2n$-2-m) x ($2n$-2-m).

Gauss-Seidel method is simple, reliable. However, Gauss-Seidel method has a slower convergence rate than Newton-Raphson approach resulting in a larger number of iterations. And it reveals convergence problems when power system is stressed by high levels of active power transfer [43].

Newton – Raphson method is therefore widely applied to solve power flow problems in many power engineering software although it requires longer computation time and more computer memory than Gauss-Seidel for each iteration. This is also the method we have decided to use for our work.

IV. Conventional approach for analyzing power grid vulnerability

Contingency analysis is the conventional approach used to determine power transfer margins or the risks inherent to a change of loading conditions. It allows to determine the preventive measures that have to be deployed to avoid such risks [46]. The analysis relies on the evaluation of post-fault power flows after one or more components fail.

Generally, when one line fails, it is isolated from the system. Two cases are then considered depending whether the whole network is split into two independent clusters or not. If there is no system separation, active power flow through the outage line is redistributed to other paths. In these conditions, we assume that the active power generated by power plants does not change. This is obviously a restricted assumption motivated by our main purpose which is not to investigate the effects of generator controls but grid topology on system vulnerability.

An example of contingency analysis is shown on IEEE 30 bus test system. The network configuration is shown in figure II.7. All the system data can be found in appendix 1. This network consists in 41 branches connecting 30 buses and a total active load of 189 MW. In normal operation, the power flow results are shown in figure II.7 and table 2.1. Now, we consider how active power is redistributed into the system when the lines L10 or L7 are disconnected.

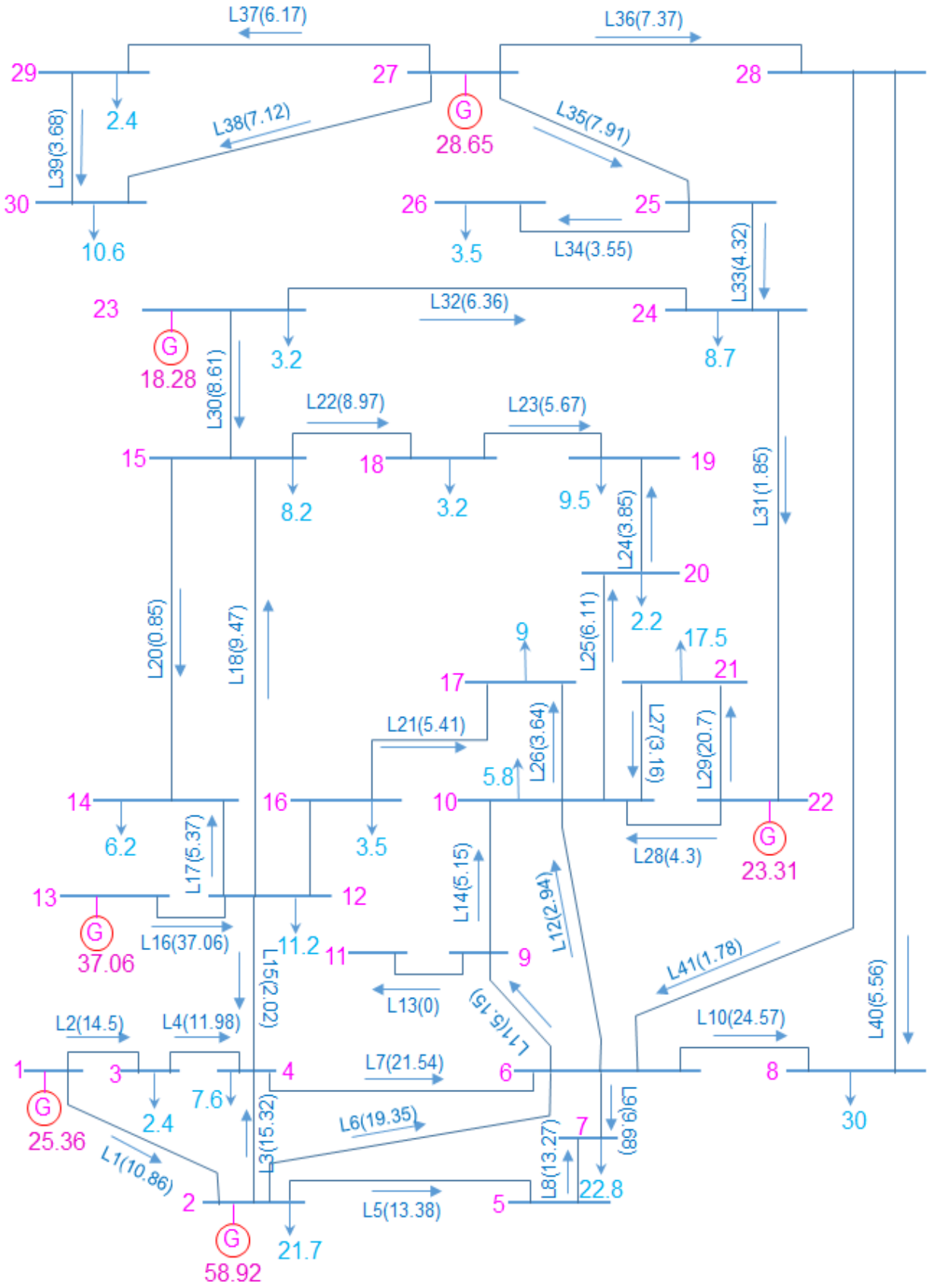

Figure II.7. Power flow of IEEE 30 bus test system in normal operation (values into brackets are the active power flow values) – Slack bus is located at bus 1.

Table 2.1 Active power flow results for normal operation of IEEE 30 bus system

Line ID	**16**	**10**	**7**	**29**	**6**	**3**	**2**	**5**	**8**	**4**	**1**	**9**	**18**	**19**
P_L	37.06	24.57	21.54	20.7	19.35	15.32	14.5	13.38	13.27	11.98	10.86	9.68	9.47	8.98
Line ID	**22**	**30**	**35**	**36**	**38**	**32**	**37**	**25**	**23**	**40**	**21**	**17**	**14**	**11**
P_L	8.97	8.61	7.91	7.37	7.12	6.36	6.17	6.11	5.67	5.56	5.41	5.39	5.15	5.15
Line ID	**33**	**28**	**24**	**39**	**26**	**34**	**27**	**12**	**15**	**31**	**41**	**20**	**13**	
P_L	4.32	4.3	3.85	3.68	3.64	3.55	3.16	2.94	2.02	1.85	1.78	0.85	0	

When one line fails, the absolute active power variations are computed and shown in table 2.2 and 2.3. If the line L7 is disconnected, power transfers through the lines L6, L3, L1, L2 … are impacted. On the other hand, when line L10 is disconnected, only the flows in lines L40 and L41 are modified. The global impact of the outage of line L7 is therefore more important than the changes caused by the disconnection of line L10. Thus, the active power redistribution not only depends on the power flow through the disconnected line before contingency but also the location of the line into the network.

Table 2.2 Absolute active power variations of IEEE 30 bus system when line L7 is disconnected

Line ID	**6**	**3**	**1**	**2**	**4**	**15**	**5**	**8**	**9**	**11**	**14**	**19**	**21**	**26**
ΔP_L	11.55	10.44	6.36	5.88	5.79	5.46	5.21	5.12	5.05	2.81	2.81	2.55	2.5	2.48
Line ID	**18**	**12**	**32**	**30**	**22**	**25**	**23**	**24**	**36**	**35**	**33**	**41**	**31**	**17**
ΔP_L	2.31	1.61	1.51	1.48	1.39	1.37	1.36	1.35	0.87	0.85	0.84	0.7	0.63	0.6
Line ID	**20**	**29**	**27**	**28**	**10**	**40**	**34**	**16**	**38**	**37**	**39**	**7**	**13**	
ΔP_L	0.6	0.37	0.34	0.23	0.16	0.16	0	0	0	0	0	0	0	

Table 2.3 Absolute active power variations of IEEE 30 bus system when line L10 is disconnected

Line ID	**41**	**40**	**1**	**36**	**35**	**33**	**7**	**2**	**4**	**31**	**6**	**3**	**15**	**27**
ΔP_L	25.32	24.44	0.97	0.72	0.71	0.69	0.53	0.51	0.5	0.44	0.43	0.33	0.29	0.28
Line ID	**29**	**11**	**14**	**32**	**30**	**5**	**18**	**8**	**9**	**28**	**12**	**19**	**21**	**26**
ΔP_L	0.28	0.25	0.25	0.25	0.24	0.2	0.19	0.19	0.19	0.16	0.14	0.05	0.05	0.05
Line ID	**17**	**20**	**22**	**25**	**23**	**24**	**34**	**16**	**38**	**39**	**37**	**10**	**13**	
ΔP_L	0.05	0.05	0	0	0	0	0	0	0	0	0	0	0	

On the other hand, if line disconnection leads to the separation of the system into two independent clusters, active power from the sending bus of the disconnected line cannot be transferred to the loads. In order to balance power demand and supply in the post-fault steady state, the primary control of generators that are not fully loaded is activated. We assume that power output of these generators is able to increase up to 10%. Every generator has the same droop value. It means that, if required, their output power will change by the same rate. If the resulting increase of the active is not enough, the power generation at slack bus is adjusted to balance power demand and supply. We consider now the outage of line L16 of IEEE 30-bus test system. When this line is

disconnected, bus 13 becomes isolated from the network. Power supplied by the generators connected to this bus cannot be transferred to the loads. In order to reach the post-fault power balance, active power from the other generators is increased by 10% of their pre-contingency value (while respecting that rated values of generators are not overcome) and the power at slack bus 1 is increased from 25.01 MW to 50.69 MW. As a result, the redistributed active power is shown in table 2.4. The global impact of L16 contingency is even worse than the effects of L7 disconnection.

Table 2.4 Absolute active power variations of IEEE 30 bus system when line L16 is disconnected

Line ID	**15**	**1**	**2**	**4**	**3**	**6**	**18**	**19**	**26**	**21**	**14**	**11**	**30**	**32**
ΔP_L	19.96	14.84	10.49	10.28	8.85	8.1	7.65	7.38	7.34	7.31	6.34	6.34	5.8	4.16
Line ID	**22**	**25**	**23**	**24**	**5**	**12**	**8**	**9**	**35**	**33**	**17**	**20**	**7**	**31**
ΔP_L	3.86	3.86	3.8	3.78	3.65	3.62	3.59	3.55	3.16	3.07	2.06	2.04	1.09	1.05
Line ID	**29**	**27**	**28**	**36**	**41**	**10**	**40**	**34**	**37**	**38**	**39**	**13**	**16**	
ΔP_L	0.78	0.76	0.47	0.37	0.29	0.08	0.08	0	0	0	0	0	0	

In conclusion, power grid vulnerability assessment should involve the analysis of many possible disturbance scenarios. The investigation of all the cases is time consuming and may become complex to be performed by electrical engineers especially for large power systems. Therefore, it is necessary to find indicators that would be able to catch the main features of the power grid vulnerability in an easier way but still accurate.

V. Vulnerability indicators based on AC power flow

V.1 AC Line outage impact metric (ACLOIM)

Vulnerability indicators useful for system planners and operators should be able to assess how line flows will be altered and redistributed in the post-fault steady-state regime. For that purpose, we first introduce a metric based on the power flow computation. The AC line outage impact metric will measure the redistribution of active power by comparing power flows at steady state before and after line *q* fails. It is defined by equation (II.59).

$$ACLOIM = \sum_{\substack{k=1 \\ k \neq q}}^{m} \left| \frac{P_{Lk} - P_{Lk,q}}{P_{demand}} \right| \qquad \text{(II.59)}$$

Where P_{demand} is the total active power load of the system.

ACLOIM measures the power grid vulnerability due to outage of line *q*, considering the pre-contingency operation state. In addition, the variation of line power is compared with the total active power load of the network to scale how important is the redistribution of power flows in the post-outage network. The higher is ACLOIM, the stronger will be the impact on the network of the disconnection of line *q*.

This indicator is computed using an AC power flow numerical simulation. It therefore gives a reference measure of grid vulnerability to line outages.

V.2 AC Network capacity reservation metric (ACNCRM)

It is also important to consider capacity reserve of lines, meaning their ability to transfer active power from sources to loads. For that purpose, we introduce a new metric, the AC network capacity reservation metric (ACNCRM). It is defined by:

$$ACNCRM = \frac{1}{m}\sum_{k=1}^{m}\frac{S_{limit_k} - |S_{Lk}|}{S_{limit_k}} \quad \text{(II.60)}$$

Where:

- S_{Lk} is the apparent power transmitted by line *k.*
- S_{limit_k} is the maximum capacity of line *k*

The capacity of a power line or transformer is defined as the maximum power that can be carried by the line or transformer. This value is provided by the thermal and stability limits of the line. The thermal limit is specified by the current-carrying capacity of the conductor and is available in the manufacturer's data. The stability limit is computed from the expression of the active power flow through a lossless line [38]:

$$P_{ij} = \frac{V_i.V_j}{X_{ij}}\, sin\delta_{ij} \quad \text{(II.61)}$$

Where, V_i, V_j, X_{ij} and δ_{ij} are the sending, receiving bus voltages, line reactance and angle difference between sending and receiving voltages, respectively. From equation (II.61), the theoretical maximum power that can be transferred under steady state condition occurs for a load angle of 90^0. To ensure an adequate margin of stability, maximum line loadability in practical operation is based on the following assumptions: $V_i/V_j \geq 0.95$ and $\delta_{ijmax}=30^0$ [38], [47]. Hence, the line capacity value for respecting the stability margin is equal to:

$$P_{limit\_ij} = \frac{(1).(0.95)}{x_{ij}}\sin(30^0) = \frac{0.475}{x_{ij}} \quad \text{(II.62)}$$

Equation (II.62) can be rewritten in matrix form for the whole network:

$$P_{limit} = 0.475 * Y_{br} \quad \text{(II.63)}$$

Where, Y_{br} is a diagonal matrix representing the *(mxm)* line admittance defined by $Y_{br} = diag\left(\frac{1}{x_{ij}}\right)$.

The vulnerability of a power grid is then determined by the AC network capacity reservation metric variation due to the outage of a line *q*. It is expressed by:

$$D_{ACNCRM} = \frac{ACNCRM_0 - ACNCRM_q}{ACNCRM_0} \quad \text{(II.64)}$$

Where, indices *0* and *q* refer to the normal operation and the post-contingency state of the network.

VI. Line outage vulnerability analysis based on ACLOIM and ACNCRM

VI.1 Applying ACLOIM to quantify line vulnerability of IEEE test systems

ACLOIM is implemented in MATLAB and used to investigate impacts of single line failure on power redistribution in test systems. ACLOIM is used as an indicator to classify the critical lines of the test systems. The assumptions about generators control are the same as in section IV for the contingency analysis.

For IEEE 30 bus system, ACLOIM results are shown in figure II.8 and table 2.5. It appears that line L16 is the most critical one with relative power redistribution equal to 90% of the total power demand. We also observe from table 2.5 that line L7 is more critical than line L10 with a relative redistributed active power equal to 49%. These results are similar to those provided by the contingency approach.

Table 2.5 Critical lines of IEEE 30 bus system

Line ID	**16**	**7**	**22**	**30**	**35**	**29**	**19**	**6**	**10**	**2**	**36**	**8**	**5**	**32**
ACLOIM	0.9	0.49	0.368	0.364	0.341	0.338	0.324	0.312	0.311	0.309	0.302	0.293	0.293	0.273
Line ID	**4**	**25**	**18**	**3**	**23**	**1**	**9**	**21**	**33**	**24**	**11**	**14**	**26**	**17**
ACLOIM	0.258	0.255	0.251	0.24	0.236	0.229	0.218	0.195	0.187	0.162	0.139	0.139	0.139	0.098
Line ID	**38**	**34**	**37**	**31**	**15**	**40**	**12**	**28**	**27**	**39**	**41**	**20**	**13**	
ACLOIM	0.095	0.082	0.079	0.077	0.077	0.067	0.061	0.059	0.055	0.045	0.026	0.015	0	

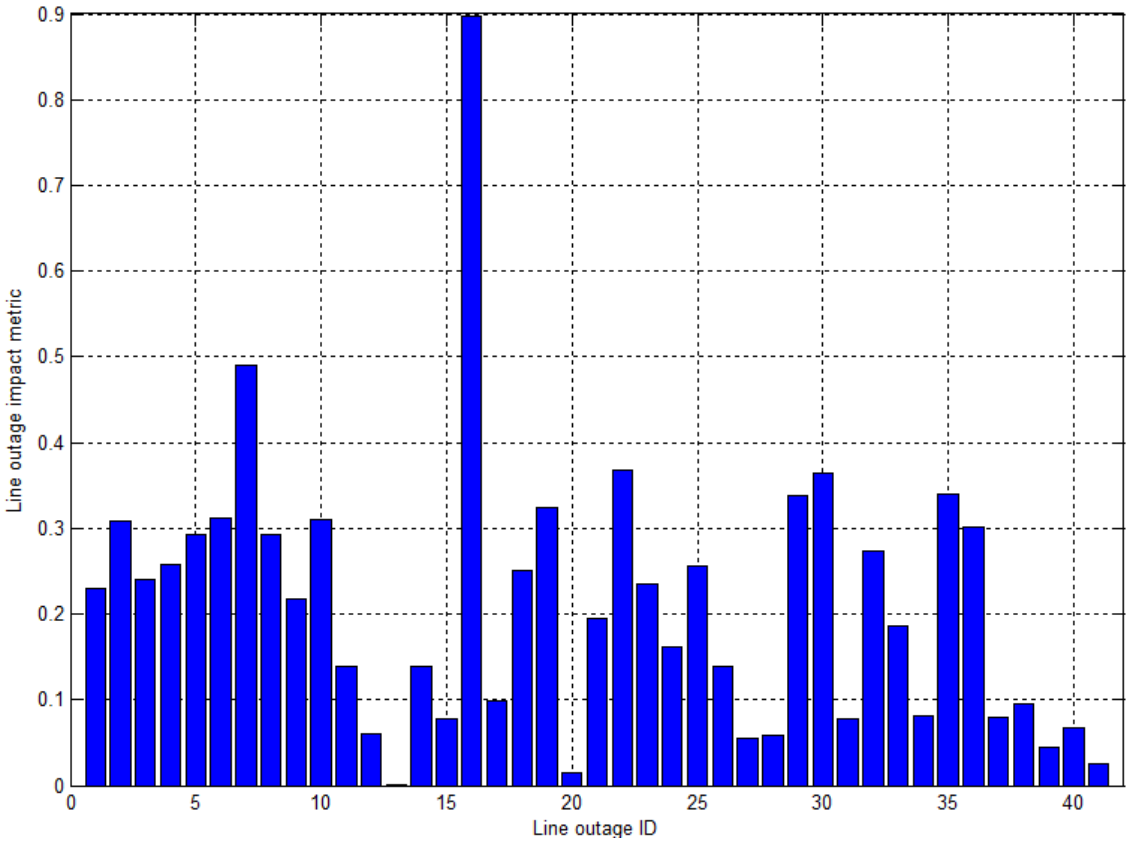

Figure II.8. Line outage impact metric of IEEE 30-bus system

For a more comprehensive analysis, ACLOIM is used to quantify critical lines of IEEE 39-bus, 57-bus and 118-bus test systems. These systems have a significantly larger amount of total load. In addition, both variances of power generation and load consumption values become greater than those of IEEE 30 bus system. The increasing complexity of these systems may pose greater challenges to application of ACLOIM to quantify critical lines as it will be discussed below.

IEEE 39 bus system, whose single line diagram is shown in figure II.9, consists in 46 branches connected to 39 buses to supply a total load of 6254 MW. The detailed data of this system can be found in appendix 1. As it can be seen from figure II.9, 11 branches can separate the network into two independent clusters when disconnected. For clarity purpose, we do not consider the power redistribution into cluster isolated from the main system.

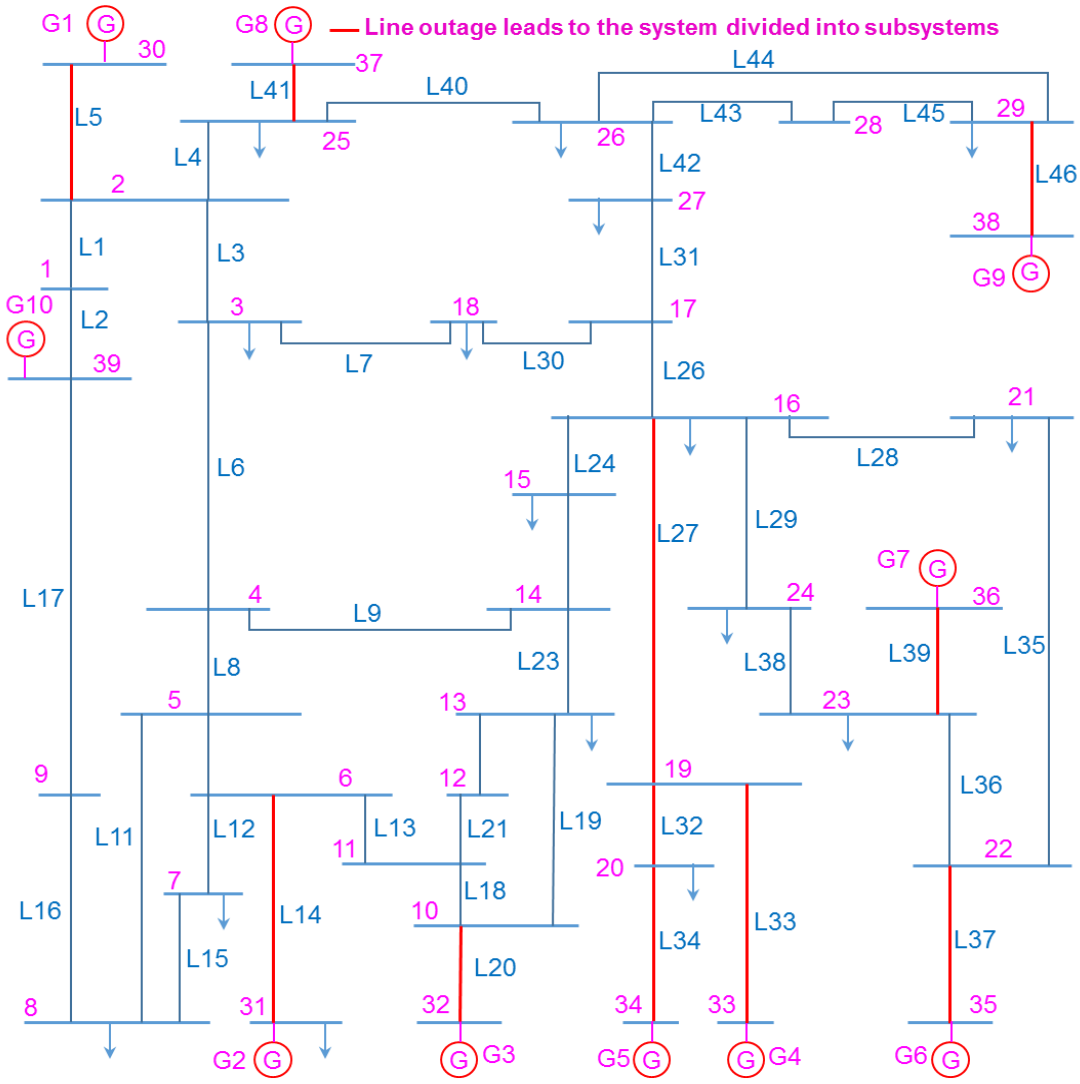

Figure II.9. Single line diagram of IEEE 39 bus test system (red lines can separate the network into independent subsystems) – Slack bus is located at bus 39.

Line outage impact values are shown in figure II.10. The top 24 critical branches are gathered in table 2.6 with their corresponding IDs.

Table 2.6 Top 24 critical lines of IEEE 39 bus system

Line ID	**37**	**46**	**39**	**33**	**20**	**27**	**34**	**1**	**14**	**3**	**5**	**41**
ACLOIM	0.96	0.856	0.817	0.788	0.758	0.7	0.688	0.589	0.571	0.51	0.495	0.449
Line ID	**13**	**2**	**35**	**25**	**18**	**10**	**23**	**26**	**12**	**19**	**9**	**42**
ACLOIM	0.448	0.436	0.42	0.412	0.362	0.353	0.329	0.315	0.303	0.274	0.27	0.243

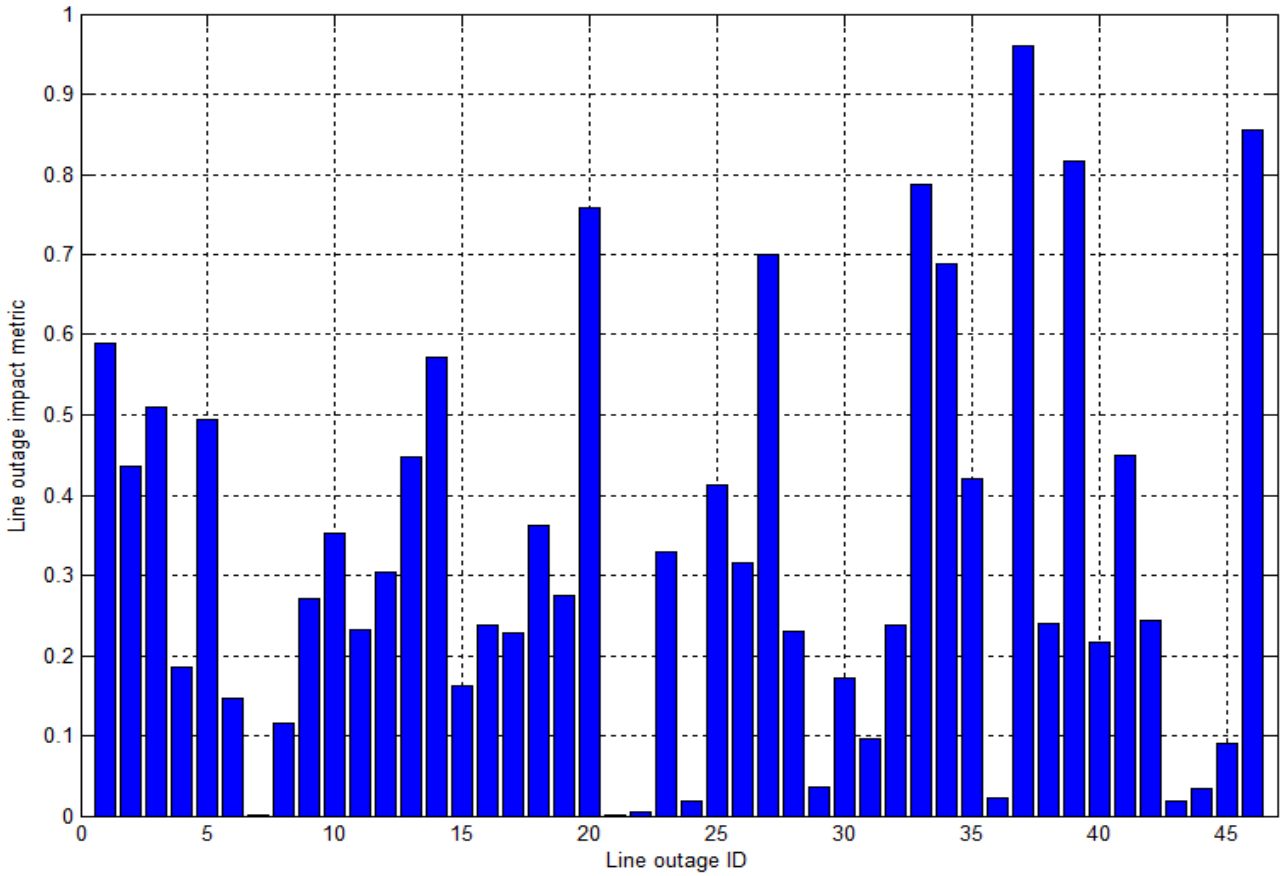

Figure II.10. Line outage impact metric of IEEE 39 bus system

Most of the red lines of figure II.9 (except L39) belongs the top 24 critical lines. For instance, after the failure of line L37, generator G6 connected to bus 35 cannot supply anymore the main system. This leads to a total power demand greater than power supply. Thus, generators control increases active power production. Since power generations from G2, G4, G5, G7 and G8 are already equal to their upper limit, these generators cannot produce more power. On the other hand, G3 increases its power output to its upper limit value (725 MW) and G9 is able to produce the required 10% supplementary power. Finally, in order to supply enough power to load, the power generation provided by the slack bus (bus 39) shall increase by 1161 MW. However, its maximum power is 1100 MW (see table 2.7). As a result, the generated power is not enough to meet the load demand and the system is operated at critical state if system operators do not take actions in time to prevent system collapse. This observation is similar to what we have already observed in contingency analysis and implementation of ACLOIM to rank critical lines of IEEE 30 bus test system.

Table 2.7 Power supply values before and after contingency

Generator	Bus	Active power limit (MW)	P (Pre-contingency)	P (After contingency)
G1	30	1040	671.59	738.75
G2	31	646	646	646
G3	32	725	671.16	725
G4	33	652	652	652
G5	34	508	508	508
G6	35	687	661	0
G7	36	580	580	580
G8	37	564	564	564
G9	38	865	654	719.4
G10	39	1100	689.59	1161

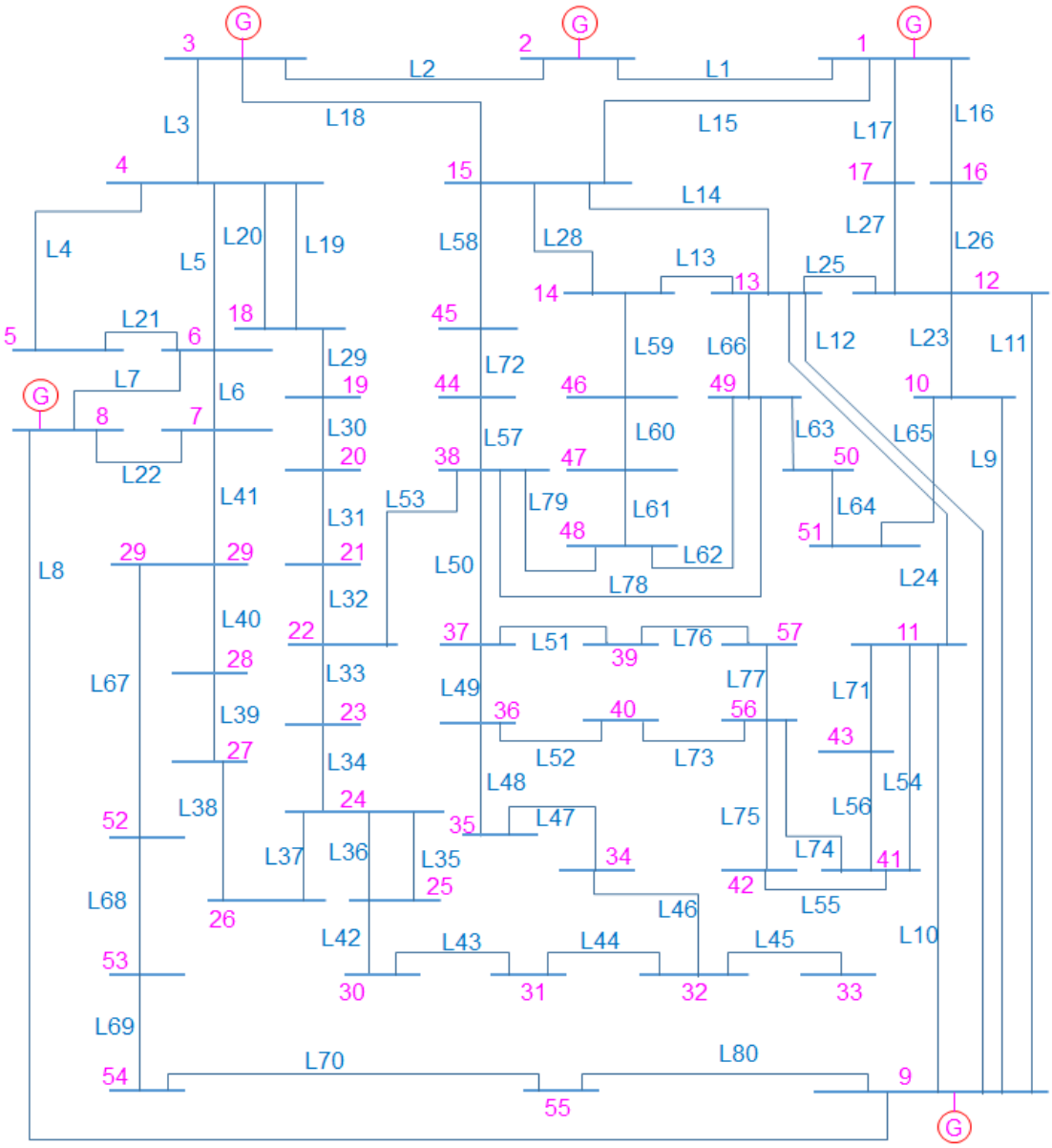

Figure II.11. Single line diagram of IEEE 57 bus test system – Slack bus is located at bus 1.

To observe further challenges, we consider the application of ACLOIM to quantify critical lines of IEEE 57 bus test system shown in figure 2.11. This system represents an approximation of the electric system in the Midwest of the United States of American in the early 1960s [48]. It includes 80 branches connected to 57 buses to supply a total load equal to 1250 MW. The detailed data of IEEE 57 bus system are found in appendix 1.

Vulnerability analysis shows that the power redistribution throughout the network is more than 60 times the total load demand when line L48 is isolated. This is very surprising. Actually, the AC power flow has failed to converge for this line outage. It means that the computation gives incorrect values of post-fault power flow leading to an incorrect ACLOIM value. Thus, the analysis of vulnerability is impossible in this case. This is one of the challenges raised by the use of the ACLOIM to rank critical lines.

If we eliminate this contingency, the remaining results are shown in figure 2.12 and the top 24 critical branches are presented in table 2.8.

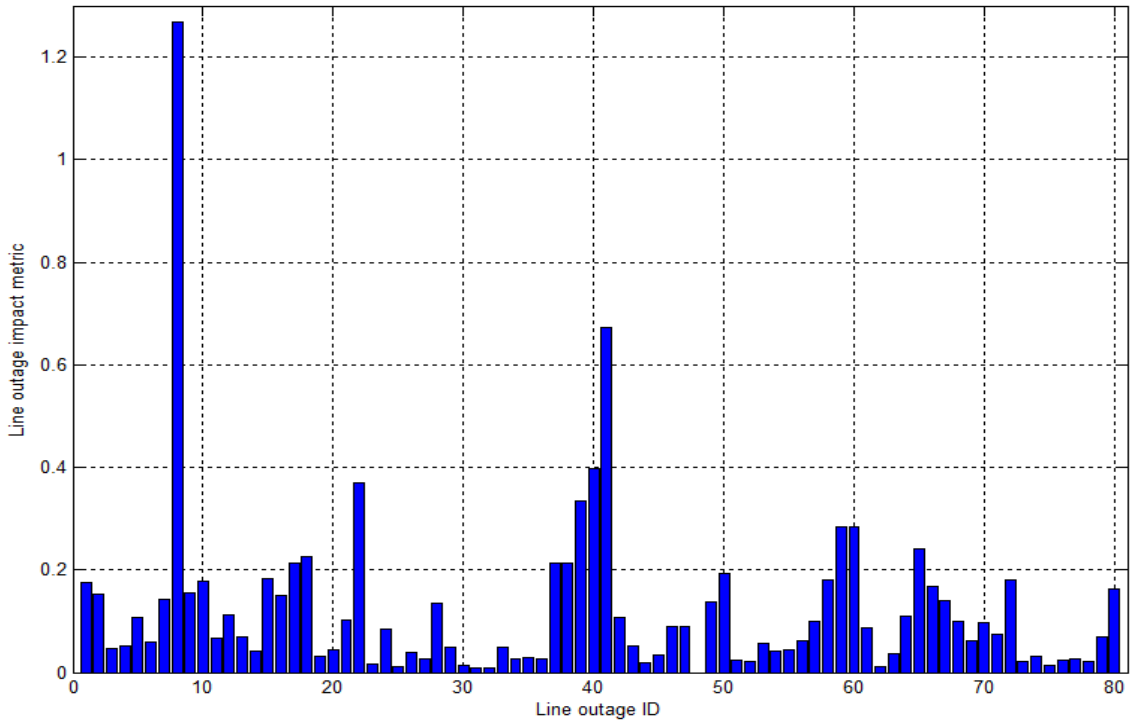

Figure II.12. Line outage impact metric of IEEE 57 bus system without line L48

Table 2.8 Top 24 critical lines of IEEE 57 bus system

Line ID	**8**	**41**	**40**	**22**	**39**	**60**	**59**	**65**	**18**	**37**	**38**	**17**
ACLOIM	1.27	0.673	0.398	0.37	0.335	0.284	0.284	0.242	0.226	0.214	0.214	0.214
Line ID	**72**	**58**	**10**	**1**	**66**	**80**	**9**	**2**	**16**	**7**	**72**	**58**
ACLOIM	0.181	0.181	0.178	0.174	0.168	0.162	0.156	0.154	0.15	0.144	0.181	0.181

Finally, the vulnerability analysis of IEEE 118 bus system is performed. This system consists of 186 branches connected to 118 buses and the total load demand is equal to 4242 MW. The single line diagram is presented in figure II.13. This system is larger and more complex than the previous ones.

The computation takes a significantly longer time to get the results. The top 24 critical lines are shown in table 2.9 and the graphical representation of ACLOIM values corresponding to line outage ID is shown in figure II.13. Lines L7 to L9 are very crucial for the system operation. Indeed, they are the only lines that connect a generator to the system without any redundancy. On the other hand, due to the complexity of the network, it is not obvious to understand why some lines such as L36, L38, L51 or L96 are so critical. This is another limitation of the ACLOIM approach that is unable to explain why some lines emerge as critical.

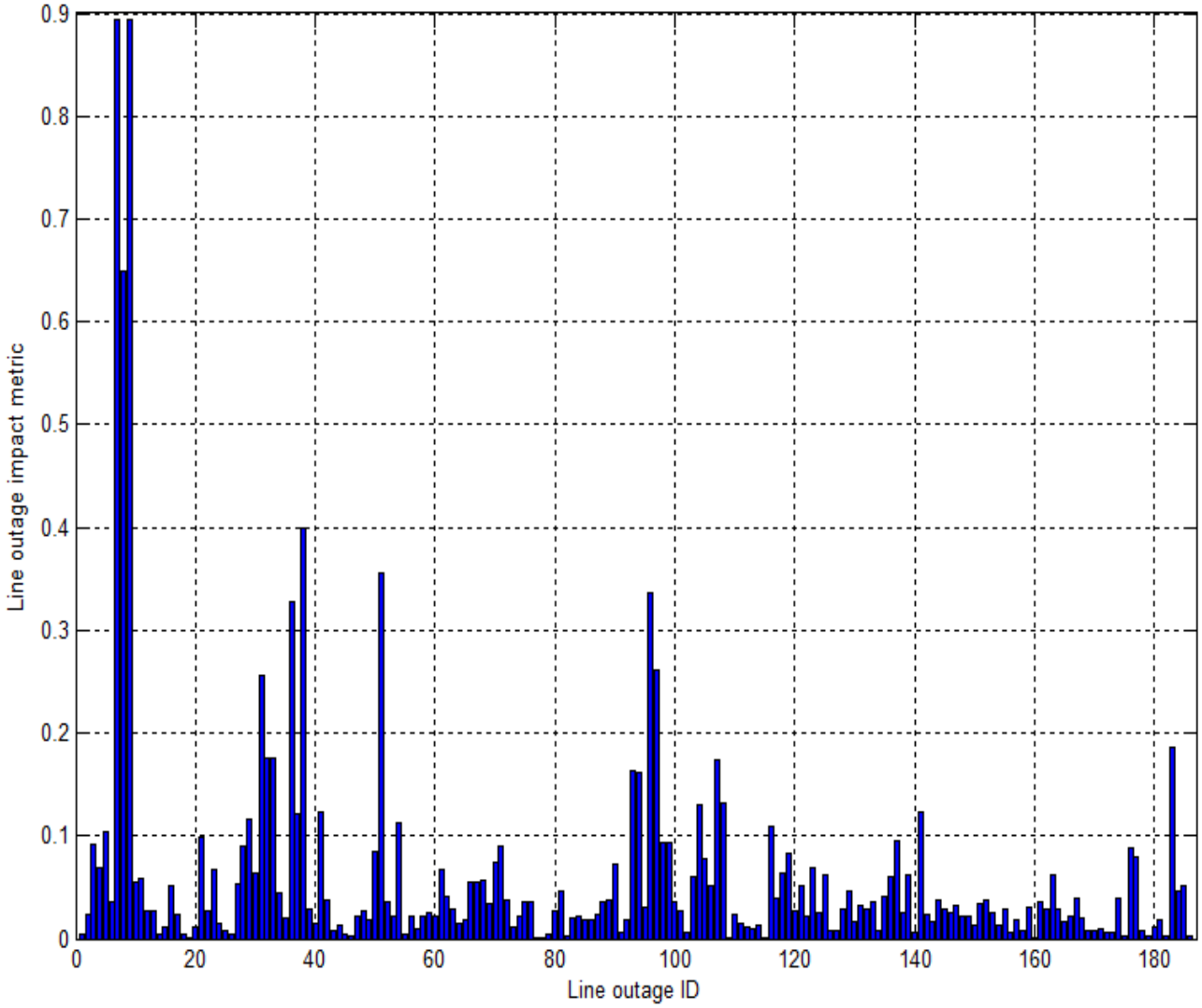

Figure II.13. Line outage impact metric of IEEE 118 bus system

Table 2.9 Critical lines of IEEE 118 bus system

Line ID	**7**	**9**	**8**	**38**	**51**	**96**	**36**	**97**	**31**	**183**	**32**	**33**
ACLOIM	0.89	0.894	0.649	0.399	0.356	0.336	0.328	0.26	0.256	0.187	0.176	0.176
Line ID	**107**	**93**	**94**	**108**	**104**	**41**	**141**	**37**	**29**	**54**	**116**	**5**
ACLOIM	0.173	0.163	0.163	0.132	0.13	0.124	0.123	0.121	0.116	0.112	0.109	0.103

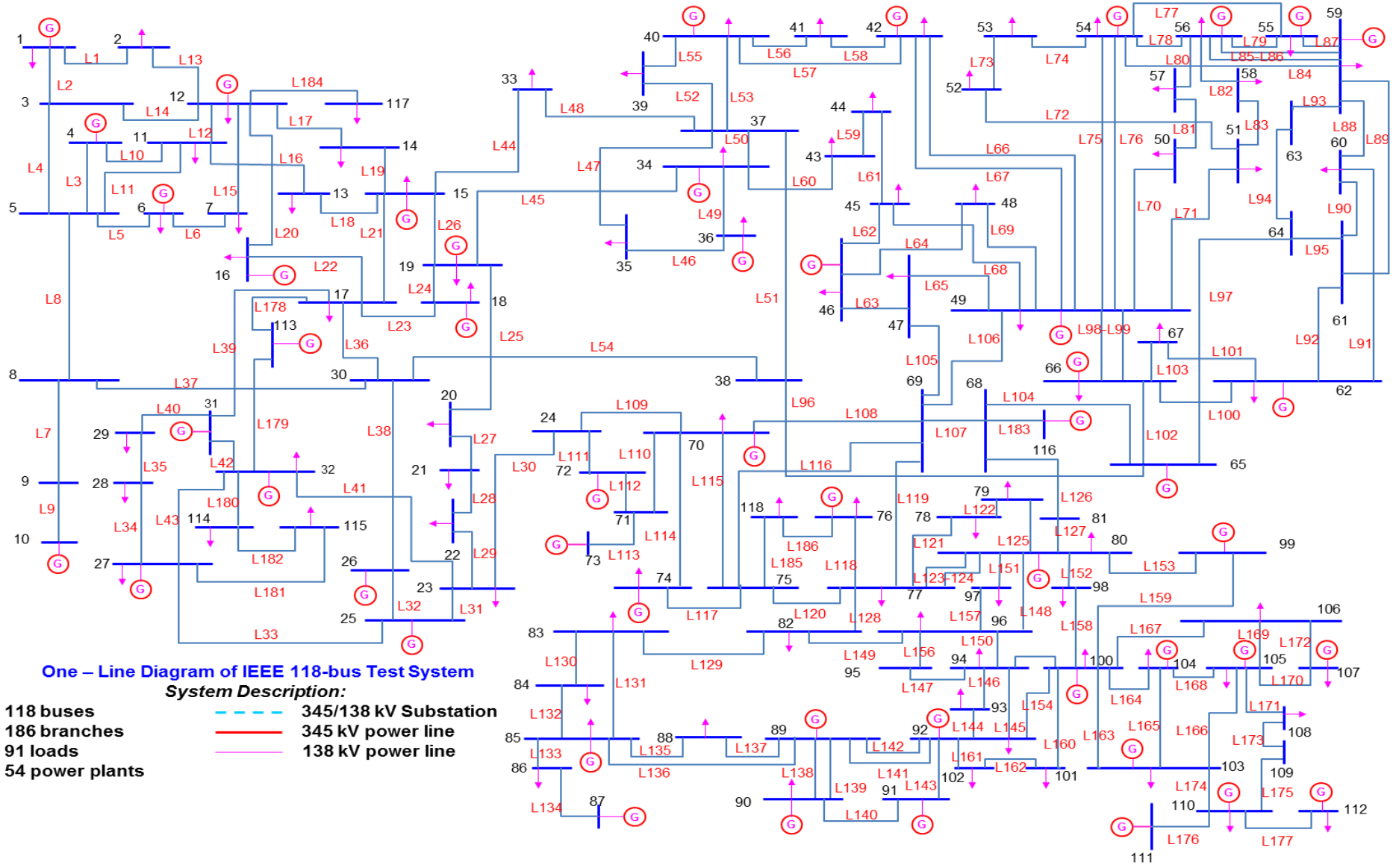

Figure II.14. Single line diagram of IEEE 118 bus test system– Slack bus is located at bus 69.

VI.2 Applying ACNCRM to quantify line vulnerability of IEEE test systems

In the previous section, ACLOIM is used as an indicator to quantify vulnerability of power systems without considering the transmission limits. However, for transmission lines and power transformers in real power grids, actual branch capacities are limited and depend on the choices made at the design stage of the network to respect the network operation requirements. Thus, in this section, we will quantify line criticality by taking into account those limited capacities.

Firstly, IEEE 30 and 118 bus test networks are investigated. The top 24 critical lines of the two test systems according to ACNCRM values are shown in table 2.10 and 2.11. The graphical representation of the variation of ACNCRM corresponding to line outage ID are illustrated in figure II.15 and II.16 for more convenient observation and analysis.

Table 2.10 Top 24 critical lines of IEEE 30 bus system using ACNCRM ranking

Line ID	**36**	**19**	**10**	**38**	**29**	**22**	**16**	**30**	**17**	**40**	**32**	**14**
ACNCRM	0.07	0.053	0.052	0.048	0.046	0.046	0.046	0.044	0.043	0.04	0.039	0.039
Line ID	**11**	**25**	**6**	**21**	**28**	**8**	**5**	**2**	**12**	**4**	**18**	**15**
ACNCRM	0.039	0.039	0.037	0.037	0.036	0.036	0.036	0.035	0.035	0.034	0.034	0.033

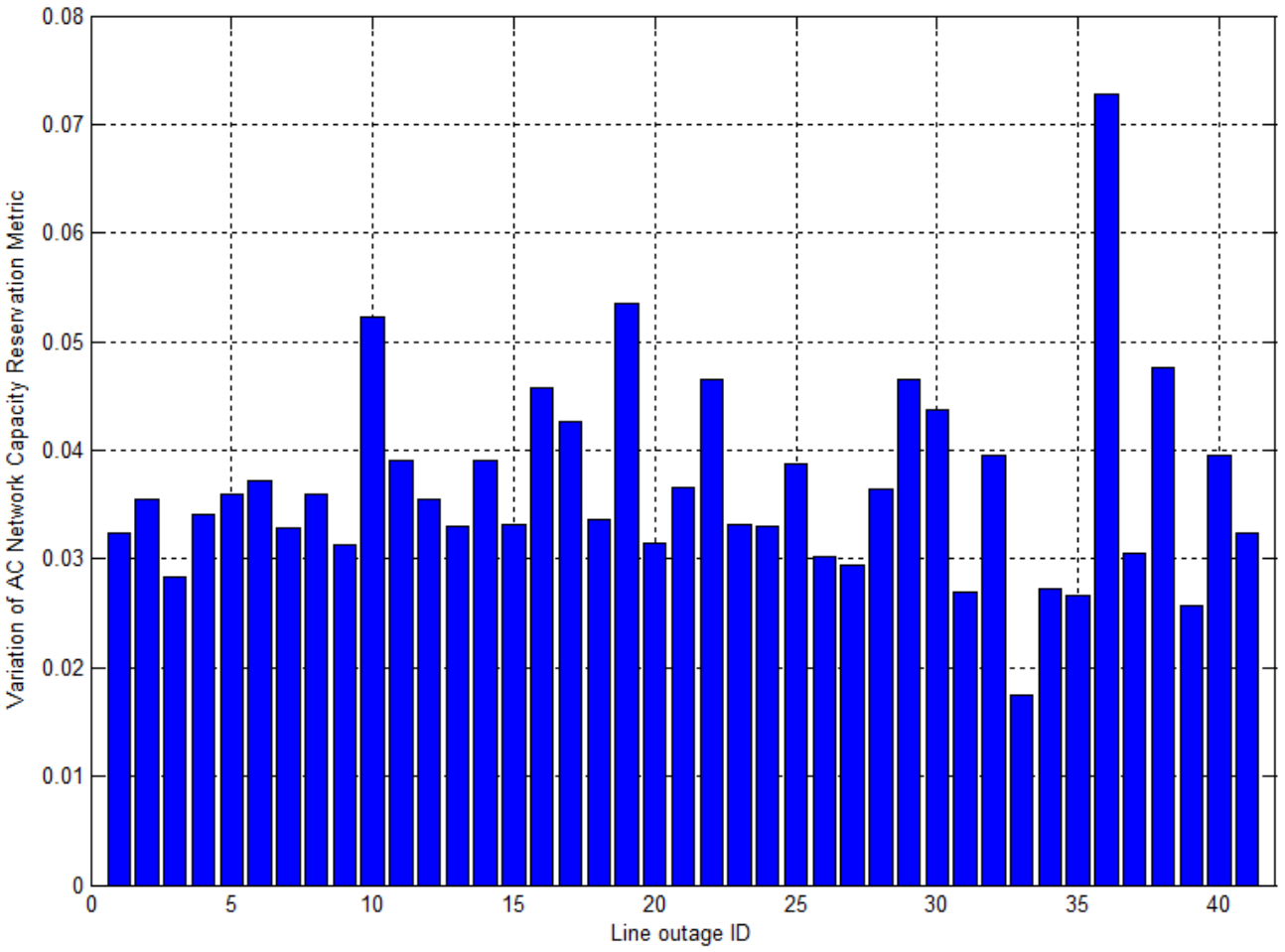

Figure II.15. ACNCRM variation of IEEE 30 bus system

Table 2.11 Top 24 critical lines of IEEE 118 bus system using ACNCRM ranking

Line ID	**8**	**7**	**9**	**51**	**38**	**36**	**96**	**33**	**97**	**21**	**133**	**50**
ACNCRM	0.04	0.031	0.025	0.024	0.022	0.022	0.019	0.016	0.015	0.013	0.013	0.013
Line ID	**37**	**108**	**5**	**4**	**93**	**94**	**116**	**71**	**90**	**174**	**137**	**29**
ACNCRM	0.012	0.012	0.012	0.011	0.011	0.011	0.011	0.01	0.01	0.01	0.01	0.01

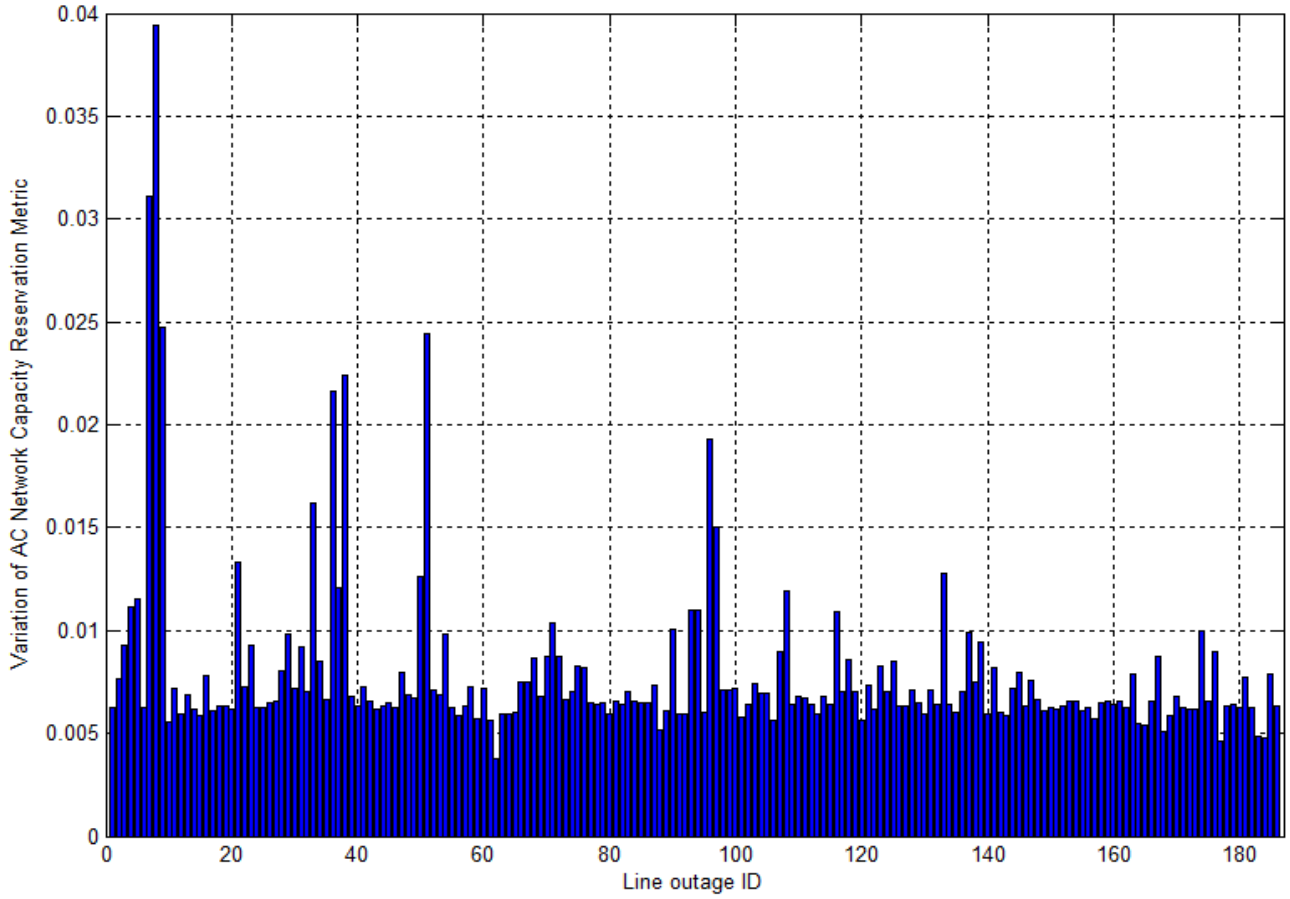

Figure II.16. ACNCRM variation of IEEE 118 bus system

It appears that, in average, the lines become more loaded after contingency. The network reservation capacity is therefore decreased, meaning that the ability to transfer power from sources to load is decreased.

For IEEE 57 bus test system, it is impossible to compute ACNCRM variation corresponding to line L48 outage. This is due to the non-convergence of the power flow calculation. If we skip this value, the other ACNCRM variation values are shown in figure II.17. The top 24 critical lines are shown in table 2.12.

Table 2.12 Top 24 critical lines of IEEE 57 bus system using ACNCRM ranking

Line ID	**8**	**41**	**50**	**49**	**40**	**65**	**39**	**47**	**46**	**17**	**10**	**60**
ACNCRM	0.04	0.027	0.02	0.02	0.019	0.017	0.017	0.017	0.017	0.016	0.016	0.016
Line ID	**59**	**42**	**22**	**9**	**67**	**71**	**55**	**72**	**58**	**15**	**56**	**80**
ACNCRM	0.016	0.016	0.016	0.015	0.015	0.015	0.015	0.014	0.014	0.014	0.014	0.014

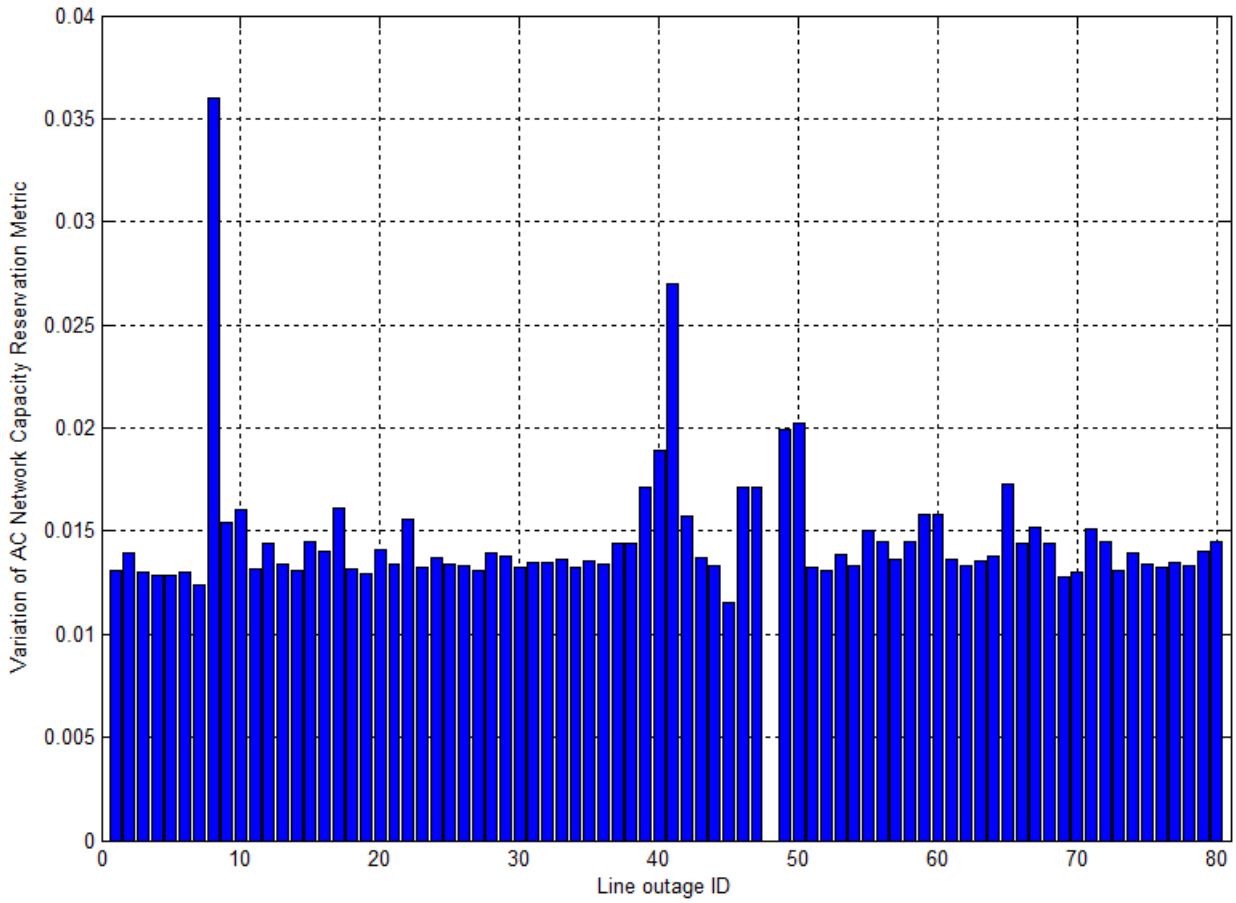

Figure II.17. ACNCRM variation of IEEE 57 bus system

Finally, IEEE 39 bus system is studied. As shown in table 2.13, there are a significant number of line outages leading to some lines overload (their maximal capacity has been overcome). The overloaded lines are tripped by overload relay protection to protect them from damage. It results a cascade of disconnections. Unfortunately, AC power flow fails to converge for these severe contingencies. As a result, ACNCRM cannot be used to quantify vulnerability of IEEE 39 bus test system. The lines, causing these severe contingencies, will obviously be considered as very critical for the system vulnerability. However, ACNCRM will not be able to assess how critical they are since the computation does not provide any useful information.

Table 2.13 List of critical lines leading to violations of line capacities for IEEE 39 bus system

Line outage ID	**1**	**2**	**9**	**13**	**14**	**18**	**19**
Overloaded line ID	L3, L13	L3	L13	L9, L19, L23	L3, L13	L19	L13, L18
Line outage ID	**20**	**23**	**27**	**28**	**30**	**32**	**33**
Overloaded line ID	L3	L13, L18	L3	L38	L3	L27	L3
Line outage ID	**34**	**35**	**37**	**38**	**39**	**40**	**42**
Overloaded line ID	L3	L29, L36, L38	L3	L28, L35	L3	L3	L3

VII. Conclusion

The application of ACLOIM and ACNCRM to compute and rank critical lines of four IEEE test system suggests that they would be useful tools to quantify power system vulnerability to line outages. However, further analysis shows that there are some shortcomings when we apply these tools to large power system. First of all, it is very challenging to perform such vulnerability analysis based on ACLOIM for complex power system, since AC power flow calculation burden may be heavy and the computation may be time consuming [19]. In addition, AC power flow fails to converge in severe contingencies. In these situations, the relevant security boundaries cannot be monitored. Furthermore, ACLOIM and ACNCRM are not able to catch the links between system vulnerability and grid topology. Therefore, it is necessary to look for other metrics that would take the advantages of these metrics and overcome their shortcomings.

Chapter III.

Topological indicators for mapping vulnerability of power systems

I. Introduction

This chapter presents recent approaches to measure vulnerability of power grids. These approaches are based on a representation of power grids as complex graphs. They should enable to better link grid topology to vulnerability while being easier to apply than conventional contingency analysis.

The chapter is organized as follows.

- First section shows how to use graph theory to represent and study power systems. In particular, an extended model is described. It enhances pure topological descriptions to better catch network's electrical properties.
- Second section introduces some indicators based on graph variables to assess power grid vulnerability to line outages.
- Final section demonstrates how these indicators can be applied for mapping vulnerability of IEEE test power systems.

II. Modeling power systems

II.1 Basic elements of graph theory

A graph G=(ϑ,*E*) is an object composed of a set of *N* vertices (ϑ) connected by a set of *m* edges *(E)*. It can be directed or not and weighted or not. A directed graph differs from an undirected one in the sense that vertices are ordered. For weighted graphs, each edge has its value [15].

Power systems are flow networks, meaning directed graphs where there are at least one source (generator) and sink (load) and power flow transmission is limited by graph edges capacities. They are sometimes represented by the corresponding unweighted graph [49], where all the vertices are equally considered as identical graph nodes.

The graph definition based on a relation between two sets is not practical for engineering studies and it is often preferred to use a matrix representation. Most famous matrices are described in the following table [50].

Table 3.1 Most famous matrices associated with graph

		Undirected graph	Directed graph
Unweighted graph	Adjacency matrix (A)	$A_{ij} = \begin{cases} 1 & if\ (i,j) \epsilon\ \vartheta\ and\ e_{ij}\ \epsilon\ E \\ 0 & otherwise \end{cases}$	$A_{ij} = \begin{cases} 1 & if\ (i,j) \epsilon\ \vartheta\ and\ e_{ij}\ \epsilon\ E \\ 0 & otherwise \end{cases}$
	Incidence matrix (K)		$K_{ij} = \begin{cases} +1 & if\ line\ i\ goes\ from\ node\ j \\ -1 & if\ line\ i\ comes\ to\ node\ j \\ 0 & if\ line\ i\ does\ not\ connect \end{cases}$
	Degree matrix (D)	$D_{ij} = \begin{cases} k_i & if\ i = j \\ 0 & otherwise \end{cases}$ Where, k_i is the degree of node *i* defined by the number of edges connected to it.	$D_{ij} = \begin{cases} k_i & if\ i = j \\ 0 & otherwise \end{cases}$ Where, k_i is the degree of node *i* defined by the number of edges connected to it.
	Laplacian matrix	$L = D - A$	$L = D - A$

Weighted graph	Adjacency matrix (A_G)	$A_G(i,j) = \begin{cases} w(i,j) & if\ (i,j) \epsilon\ E \\ 0 & otherwise \end{cases}$ Where, w(i, j) is weight of e_{ij}	$A_G(i,j) = \begin{cases} w(i,j) & if\ (i,j) \epsilon\ E \\ 0 & otherwise \end{cases}$ Where, w(i, j) is weight of e_{ij}
	Incidence matrix (K_w)		$K_{wij} = \begin{cases} +w(i,j) & if\ line\ i\ goes\ from\ node\ j \\ -w(i,j) & if\ line\ i\ comes\ to\ node\ j \\ 0 & if\ line\ i\ does\ not\ connect \end{cases}$
	Degree matrix (D_G)	$D_{ij} = \begin{cases} \sum_{\substack{j=1 \\ j \neq i}}^{N} A_G(i,j) & if\ i = j \\ 0 & otherwise \end{cases}$	$D_{ij} = \begin{cases} \sum_{\substack{j=1 \\ j \neq i}}^{N} A_G(i,j) & if\ i = j \\ 0 & otherwise \end{cases}$
	Laplacian matrix (L_G)	$L_G = D_G - A_G$	$L_G = D_G - A_G$

II.2 Pure topological model

II.2.1 Definition

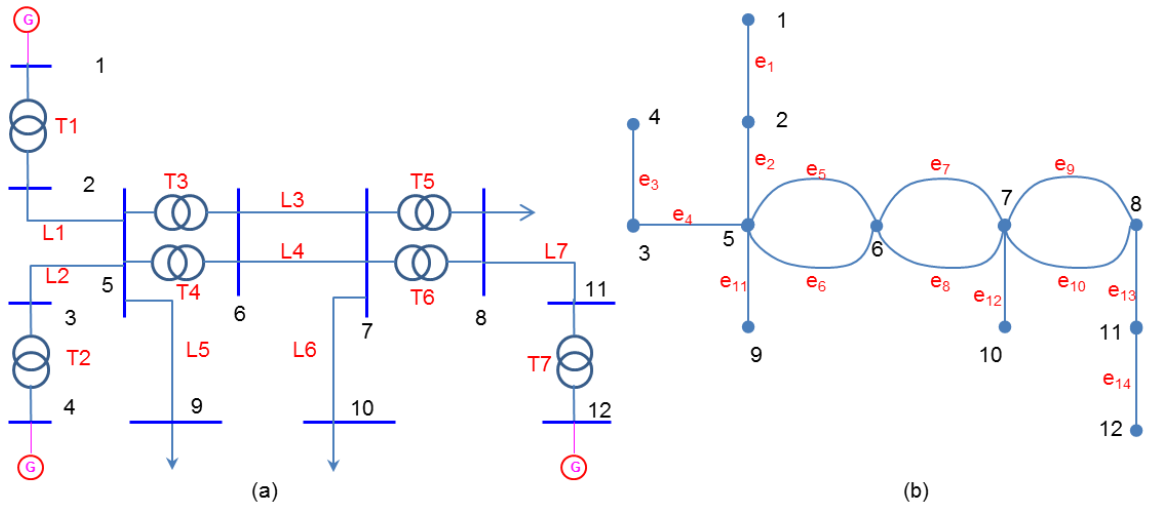

Figure III.1. A power grid (a) and its related graph (b)

The power system is considered as a graph G=(ϑ,E) as shown in figure III.1. Each bus is modeled as a node or vertex, while links or edges correspond to transmissions lines or transformers [15]. Most of works on complex network only considers graphs without duplicate connection [19], [51], [52]. In this chapter, the model takes into account of the parallel lines between two buses. Lines between nodes are represented by unweighted [19], [30], [53] or weighted links. In the latter case, weights are equal to line admittances [36], [53]–[55]. In unweighted graphs, all the links are considered identical, without differences in their quantitative features and the length of a path between two nodes i and j depends on the number of the links making the path. In a weighted network, path length depends on the weights of the links connecting the two extreme nodes of the path. This representation applies not only for high-voltage transmission grids but also for medium and low-voltage distribution network as well as smart grids made by the assemblage of power and IT networks [15].

Pure topological approaches model power networks by using topological variables only. No electrical calculation is performed. Performance of power grids is thus assessed via graph metrics such as efficiency, degree and betweenness centrality. Most of these metrics are defined considering that power is transferred between two nodes through the shortest path [19]. The shortest path length, also called shortest distance, is the minimum path length of all the possible paths connecting two nodes.

For instance, the efficiency of a power grid measures the network transmission effectiveness with the assumption that the efficiency for transmitting electricity between two nodes *s* and *t* is proportional to the reciprocal of their shortest distance [35]. In unweighted network, this distance is defined as the number of links which compose the shortest path connecting the two nodes [36]. In weighted network, it is defined as the sum of the weights.

Other topological indicators can be line and node betweenness. They are respectively defined as the number of shortest paths that pass through a given line or node [57].

II.2.2 Shortest path calculation by dynamic programming

Shortest path length is a key variable to determine the performances of electrical power grids represented by pure topological models. To determine the shortest paths between two nodes, a dynamic programing method can be used. It is an optimization method that solves a complex problem by decomposing it into simpler sub-problems in a recursive manner. A global optimal solution is then obtained by combining the solutions of sub-problems. Every sub-problem is treated sequentially with a policy decision required at each stage [58].

In order to understand this approach, we show how to find the shortest path from node 1 to node *N* (*N*=9) in the following directed and weighted graph (see figure III.2).

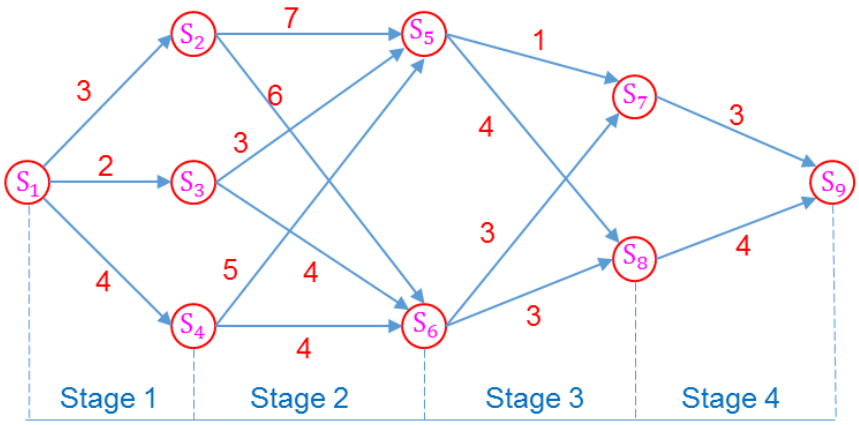

Figure III.2. Network diagram

It is obvious that this problem can be structured into a four-stage (n=4) decision process. Assuming that the shortest distance value from start node *1* to node *k* is known at the end of stage *(n-1)*, the shortest distance value from start node *1* to node *N* at stages *n* is defined by:

$$V_n(s_N) = \ min\{d_{Nk} + V_{n-1}(s_k)\} \qquad k = [1..N] \tag{III.1}$$

Where, d_{Nk} is the edge length connected vertices *k* and *N*.

The shortest path calculation follows a forward-backward procedure based on Bellman equation (III.1).

- The forward procedure is based on the following stages:
  - The shortest distance associated with the starting node is initialized to 0, i.e. $V_0(s_1) = 0$. At the end of stage 1, the values of shortest distance from start node 1 to other nodes are determined as follows:
    - From node 1 to node 2: $V_1(s_2) = \ min\{d_{12} + V_0(s_1)\} = d_{12} = 3$
    - From node 1 to node 3: $V_1(s_3) = \ min\{d_{13} + V_0(s_1)\} = d_{13} = 2$
    - From node 1 to node 4: $\mathrm{V_1(s_4)} = \ \mathrm{min\{d_{14} + V_0(s_1)\} = d_{14} = 4}$
    - From node 1 to other nodes: $\mathrm{V_1(s_j)} = \ \mathrm{min\{d_{1j} + V_0(s_1)\} = d_{1j} = +\infty}$ (j = [5 9]). This is due to these vertices not connected to vertex 1 by an edge.
  - At the end of stage 2, the values of shortest distance from start node to other nodes are determined as follows:
    - $V_2(s_5) = \ min\{d_{25} + V_1(s_2),\ d_{35} + V_1(s_3), d_{45} + V_1(s_4)\}$
      $= min\{7 + 3, 3 + 2, 5 + 4\} = 5$
    - $V_2(s_6) = \ min\{d_{26} + V_1(s_2),\ d_{36} + V_1(s_3), d_{46} + V_1(s_4)\}$
      $= min\{6 + 3, 4 + 2, 4 + 4\} = 6$
  - At the end of stage 3, the values of shortest distances may be:
    - $V_3(s_7) = \ min\{d_{57} + V_2(s_5),\ d_{67} + V_2(s_6)\} = min\{1 + 5, 3 + 6\} = 6$
    - $V_3(s_8) = \ min\{d_{58} + V_2(s_5),\ d_{68} + V_2(s_6)\} = min\{4 + 5, 3 + 6\} = 9$
  - At the end of stage 4, the system reaches the termination node:

    $$V_4(s_9) = \ min\{d_{79} + V_3(s_7),\ d_{89} + V_3(s_8)\} = min\{3 + 6, 4 + 9\} = 9$$

- The backward procedure to determine the shortest paths from the start node *1* to end node *N* follows these steps:
  - From the forward process and the calculation of $V_4(s_9)$, it is clear that in order to get a shortest distance equal to 9, the shortest path have to go through node 7.
  - Stage 3 shows that the shortest path should go via node 5.
  - Similarly, in order to reach node 5, the shortest path goes through node 3.
  - As a result, the shortest path is 1-3-5-7-9.

II.3 Extended topological model

For enhancement purposes, topological model can be extended by including some electrical variables. Such modeling approaches are presented in [30], [31], [47], [49], [52], [54], [58]–[62].

They consider power systems as flow network. Power flows across the network not via shortest paths but all posible paths according to the Kirchoff's laws. In addition, the concept of electrical distance used in this approach differs from the graph distance used in topological models [64], [65]. The distance between two nodes *i* and *j* is indeed defined as Thevenin impedance between them [20]. According to Grainger et al [42] and Arianos et al [31], Thevenin impedance between a pair of buses, also called the effective resistance in [20], [23] is determined by:

$$Z_{eq\_ij} = Z_{ii} + Z_{jj} - 2Z_{ij} \quad \text{(III.2)}$$

Z_{ij}, Z_{ii}, Z_{jj} are elements of the bus impedance matrix Z. Z_{ij} is called transfer impedance, while Z_{ii}, Z_{jj} are the driving-point impedances of buses *i* and *j*.

Finally, extended modeling takes into account the network capability (C_{ab}). It is defined as the maximum amount of power that it is possible to transmit from one generation node *a* to one load node *b* (other generators and loads are disconnected) before one power line reaches its maximum power capacity. It is determined by:

$$C_{ab} = \min_k \left\{ \frac{P_{k\_Limit}}{P_{ab,k}} \right\} = \min_k \left\{ \frac{P_{k\_Limit}}{f_{ka} - f_{kb}} \right\} \quad \text{(III.3)}$$

Where:

- $P_{ab,k}$ is the ratio of active power transfer from the generator bus *a* to the load bus *b*.

- *k* refers to the lines composing the path from *a* to *b*.

- P_{k_Limit} is line *k* capacity limit.

- f_{ka} and f_{kb} are entry elements of the power transfer distribution factor matrix. The detail process to determine this matrix is provided in the next chapter.

III. Topological indicators

III.1 Network efficiency index

An example of topological indicator is given by network efficiency in [34]–[36]. In [35], V. Latora and M. Marchiory define the efficiency as the ability of the network to transmit information flow. It measures the network transmission effectiveness with the assumption that effectiveness between two nodes is proportional to the inverse of their shortest distance [35]. The lower is the value of the shortest distance, the higher is the connectivity between two nodes and the more efficient is the network.

Based on this idea, network efficiency metric is defined as an average of the inverse of the shortest distances and expressed by (III.4).

$$E = \frac{1}{N(N-1)} \sum_{i \neq j} \frac{1}{d_{ij}} = \sum_{i \neq j} e_{ij} \quad \text{(III.4)}$$

d_{ij} stands for the shortest distance between nodes *i* and *j*.

The approach in [66] defines the vulnerability of a network as a drop in network efficiency due to the failure of an element. Similarly, in [34], [36], the influence of edges failure on the network operation is estimated by the variation of network efficiency. This variation is defined by (III.5), where E_0 is the global efficiency of the network before the disconnection of edge q, and E_q is the efficiency of the network after the failure.

$$D_{Eq} = \frac{E_0 - E_q}{E_0} \quad \text{(III.5)}$$

The larger is D_{Eq}, the more critical is edge q for the system vulnerability.

III.2 Line betweenness centrality

Line betweenness centrality is an average measure of how a link is central for the graph connectivity [34], [67]. It is given by (III.6) where A_{Zst} and $A_{Zst}(e)$ are respectively the total number of electrical shortest paths from *s* to *t* and the number of electrical shortest paths from *s* to *t* passing through link *e*.

$$C_{BEL}(e) = \frac{2}{N(N-1)} \sum_{s=1}^{N} \sum_{t=1}^{N} \frac{A_{Zst}(e)}{A_{Zst}} \quad (s \neq t) \quad \text{(III.6)}$$

Equation (III.6) indicates that higher is this value, more central is link *e* in the network. It means that a line with a high value of betweenness centrality is considered as an important line for the network operation. Indeed, if this line is removed, it disrupts the most direct route and weakens the network connectivity.

III.3 Net-ability index

Net-ability of a power grid based on the extended topological model approach is proposed by S.Arianos et al [31]. This metric is defined by:

$$A = \frac{1}{N_G N_L} \sum_{i=1}^{N_G} \sum_{j=1}^{N_L} \frac{C_{ab}}{Z_{eq\_ab}} \quad \text{(III.7)}$$

Where:

- Z_{eq_ab} is the equivalent impedance of the circuit between the pair of nodes *a* and *b*.
- N_G and N_L are the number of generation and load buses, respectively.

Net-ability is a measurement of accessibility. It measures the "potential of opportunities for interactions" [68]. Indeed, the shorter is the distance or larger is the transmission capacity, the more is potential of transmitting power from one node to another.

The vulnerability of a power grid is then determined by estimating the loss of net-ability due to the disconnection of line q:

$$D_{Aq} = \frac{A_0 - A_q}{A_0} \quad \text{(III.8)}$$

Again, critical lines for system vulnerability can be ranked according to this indicator.

IV. Assessment of system vulnerability

IV.1 Network efficiency based critical lines ranking

IV.1.1 Illustration on basic electrical circuits

Two very simple 3-node networks are first considered. They have the same number of lines but that are either star or delta connected as shown in figure III.3 and III.4.

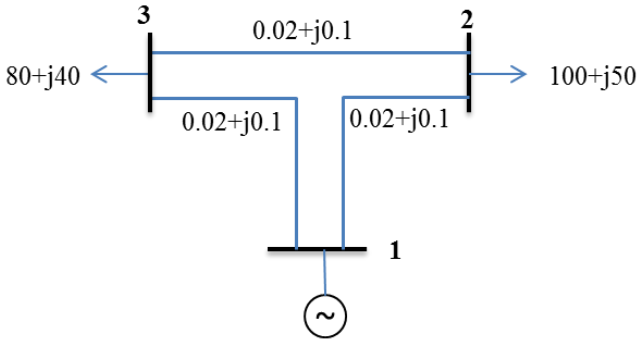

Figure III.3. Test system connected in delta

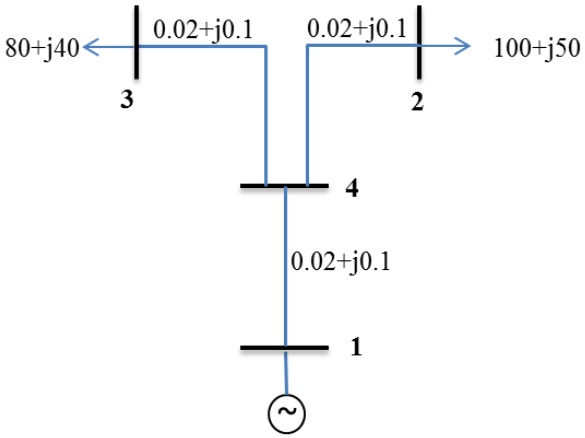

Figure III.4. Test system connected in star

Efficiency drops for the disconnection of one, two or three lines are given in table 3.1 for both topologies. Obviously delta networks are far less vulnerable than star networks. This shows how meshing grids is important to increase their robustness.

Table 3.2 Effect of topology on grid vulnerability

	D_E (%) (One Line)	D_E (%) (Two lines)	D_E (%) (Three lines)
Δ connection	16.67	66.67	100
Y connection	44.44	77.77	100

Now, the value of line impedance Z_{12} is decreased to $0.01 + j.05$ (Ω) in delta network. Table 3.3 shows that the network efficiency drop is significantly higher than before when line L_{12} is removed. It means that the loss of efficiency is higher when a good line (whose impedance is low) is disconnected. On the other hand, the drop associated to the disconnection of lines L_{13} and L_{23} is

lower. Removing "bad" lines (whose impedance values are high) is not so crucial for network efficiency.

Table 3.3 Effect of line impedance on grid vulnerability

Relative drop in network efficiency	Δ connection ($Z_{12} = 0.01 + j.05$ & $Z_{13} = Z_{23} = 0.02 + j.1$)
D_E (%) – L_{12}	37.5
D_E (%) – L_{13} or L_{23}	8.33

IV.1.2 Critical lines of IEEE 30-bus test networks

Network efficiency metric is used to determine the critical lines of IEEE 30-bus test systems. A first evaluation is provided for the unweighted graph related to the network. The top 24 most critical lines are shown in table 3.4. Then, the same evaluation is performed for the weighted graph. Because, resistive losses are small in transmission networks, weights are taken equal to the imaginary part (reactance) of transmission lines impedances [69]. Unweighted and weighted results are summarized in figure III.5. The top 24 most critical lines are given in table 3.5.

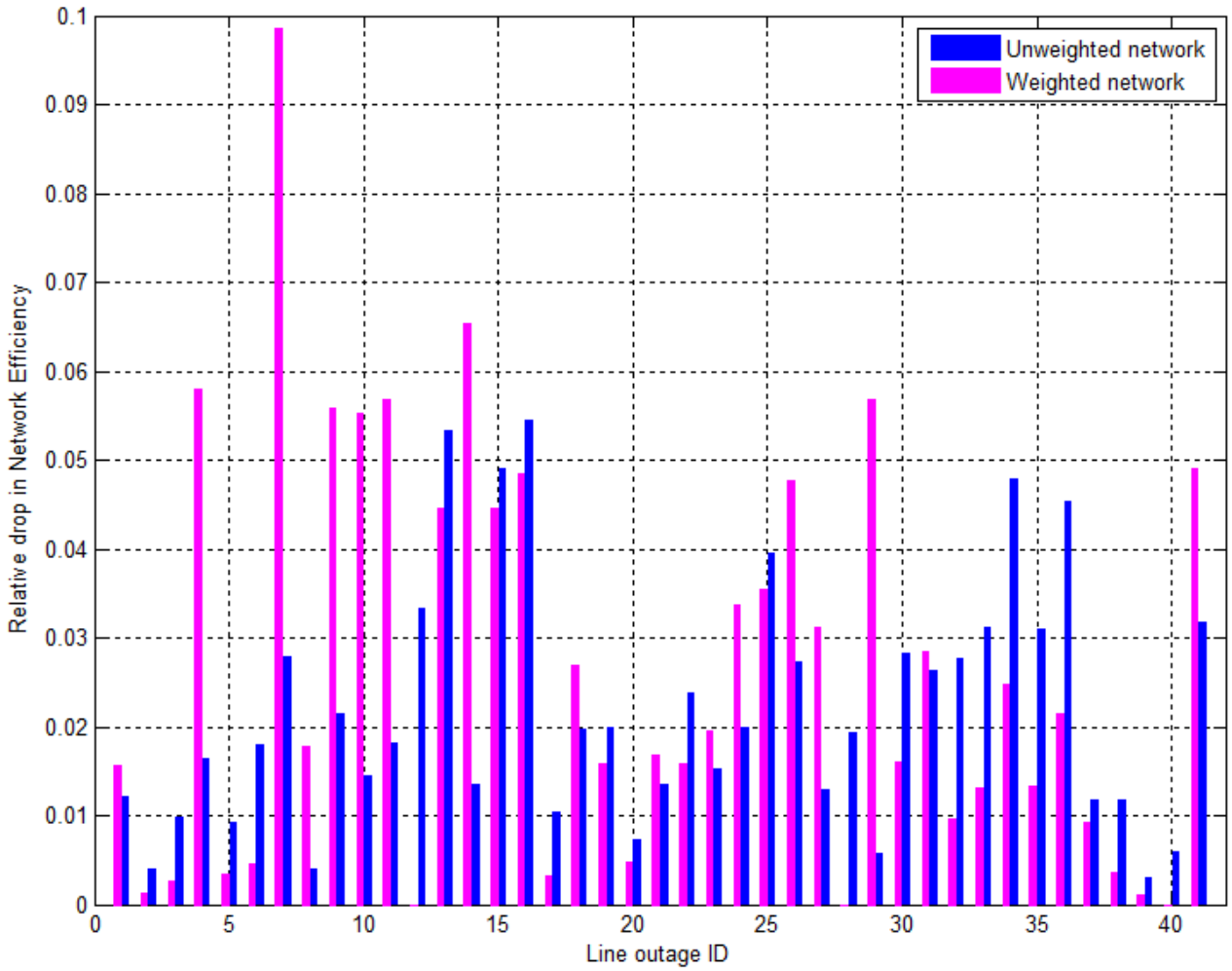

Figure III.5. Network efficiency of IEEE 30 bus system

Table 3.4 Critical lines of unweighted IEEE 30 bus system according to network efficiency

Line ID	**16**	**13**	**15**	**34**	**36**	**25**	**12**	**41**	**33**	**35**	**30**	**7**
D_E	0.054	0.053	0.049	0.048	0.045	0.04	0.033	0.032	0.031	0.031	0.028	0.028
Line ID	**32**	**26**	**31**	**22**	**9**	**19**	**24**	**18**	**28**	**11**	**6**	**4**
D_E	0.028	0.027	0.026	0.024	0.022	0.02	0.02	0.02	0.019	0.018	0.018	0.016

Table 3.5 Critical lines of weighted IEEE 30 bus system according to network efficiency

Line ID	**7**	**14**	**4**	**11**	**29**	**9**	**10**	**41**	**16**	**26**	**15**	**13**
D_E	0.098	0.065	0.058	0.057	0.057	0.056	0.055	0.049	0.048	0.048	0.045	0.045
Line ID	**25**	**24**	**27**	**31**	**18**	**34**	**36**	**23**	**8**	**21**	**30**	**19**
D_E	0.035	0.034	0.031	0.029	0.027	0.025	0.022	0.02	0.018	0.017	0.016	0.016

There are three distinct classes of lines. The first class gathers the lines with the same level of criticality regardless weights of graph edges. For instance, L13 and L16 belong to this class because their removal disconnects one generator or synchronous condenser from the network (see figure below). Also, L15 and L25 are interconnection links that belong to this class without any obvious reason. The second class gathers the lines whose criticality level has decreased a lot between unweighted and weighted cases. For instance, L34 and L36 are less critical when the weighted graph is assessed. This is due to their high value of reactance. On the other hand, some lines appear to become very critical when weights are put on edges. L7 is the most extreme case. Actually its reactance is very small making this line crucial for the network connectivity.

Finally, the results are compared with ACLOIM to validate whether network efficiency provides a meaningful metric for vulnerability assessment. For that purpose, the top ten critical lines are now ranked in table 3.6 and a graphical representation is shown in figure III.6.

Only L16 appears to be identified as critical by unweighted, weighted efficiency metrics and ACLOIM. But while it is ranked as the most critical line by ACLOIM and the unweighted indicator, it is ranked at the 9^{th} position by the weighted approach. In general, there are very few consistencies between the results provided by network efficiency and ACLOIM.

Table 3.6 Top 10 critical lines of IEEE 30 bus system according to D_E and ACLOIM

Ranking order		**1**	**2**	**3**	**4**	**5**	**6**	**7**	**8**	**9**	**10**
D_E	Unweighted	**16**	**13**	**15**	**34**	**36**	**25**	**12**	**41**	**33**	**35**
	Weighted	**7**	**14**	**4**	**11**	**29**	**9**	**10**	**41**	**16**	**26**
ACLOIM		**16**	**7**	**22**	**30**	**35**	**29**	**19**	**6**	**10**	**2**

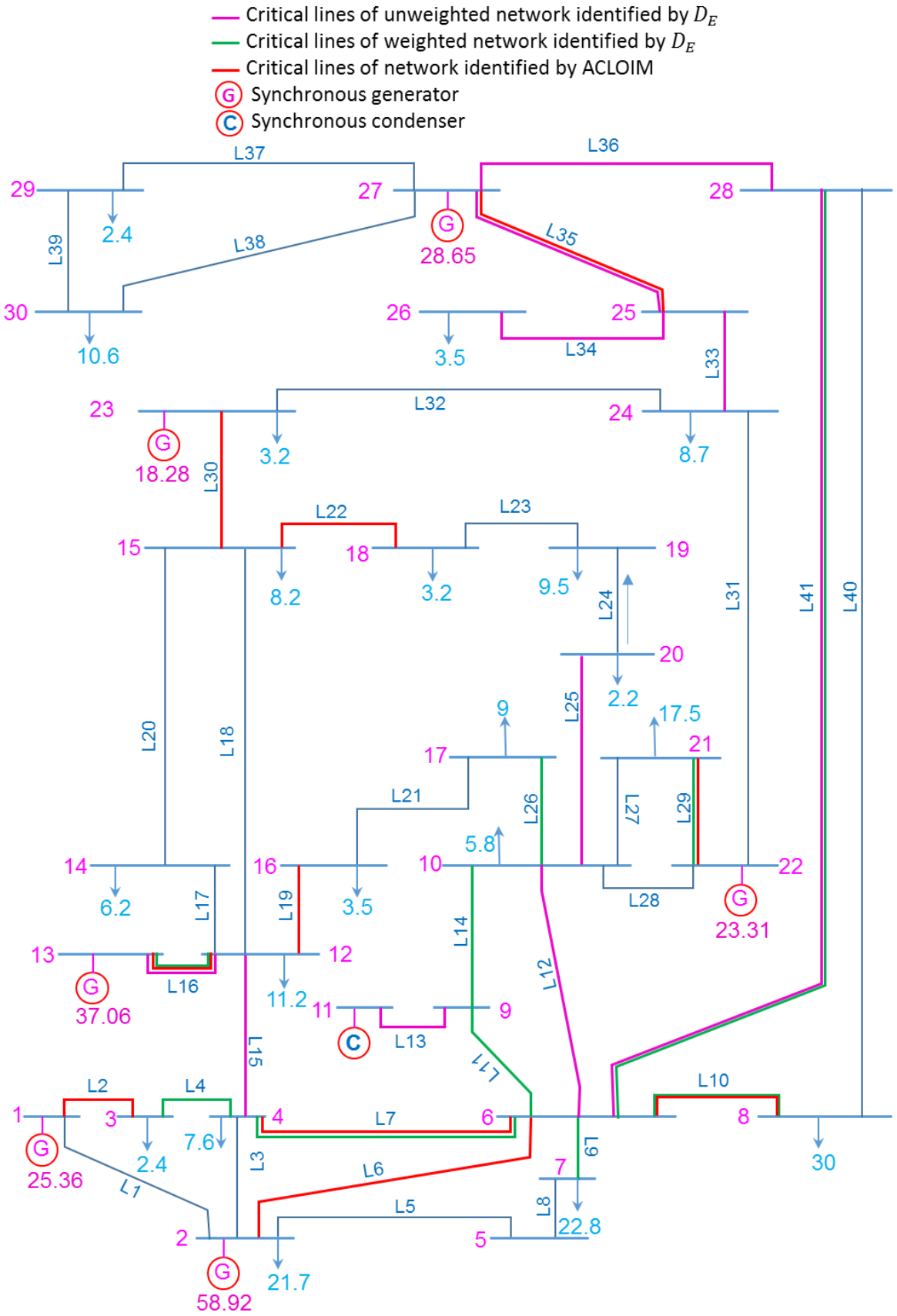

Figure III.6. Graphical representation of top 10 critical lines for IEEE 30 bus system according to D_E and ACLOIM

IV.1.3 Critical lines of IEEE 39-bus, 57-bus and 118-bus test networks

Similar results have been obtained for IEEE 39-, 57- and 118-bus test networks. They are shown in figure III.7 – III.9.

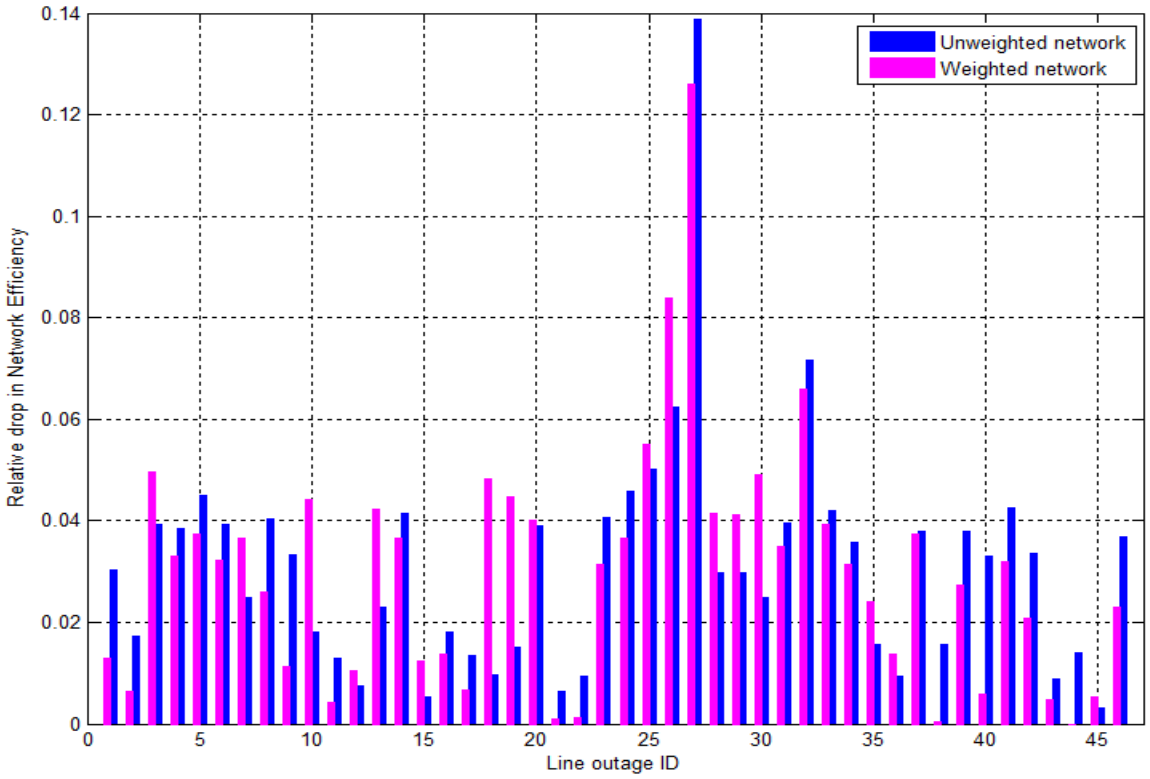

Figure III.7. Network efficiency of IEEE 39-bus system

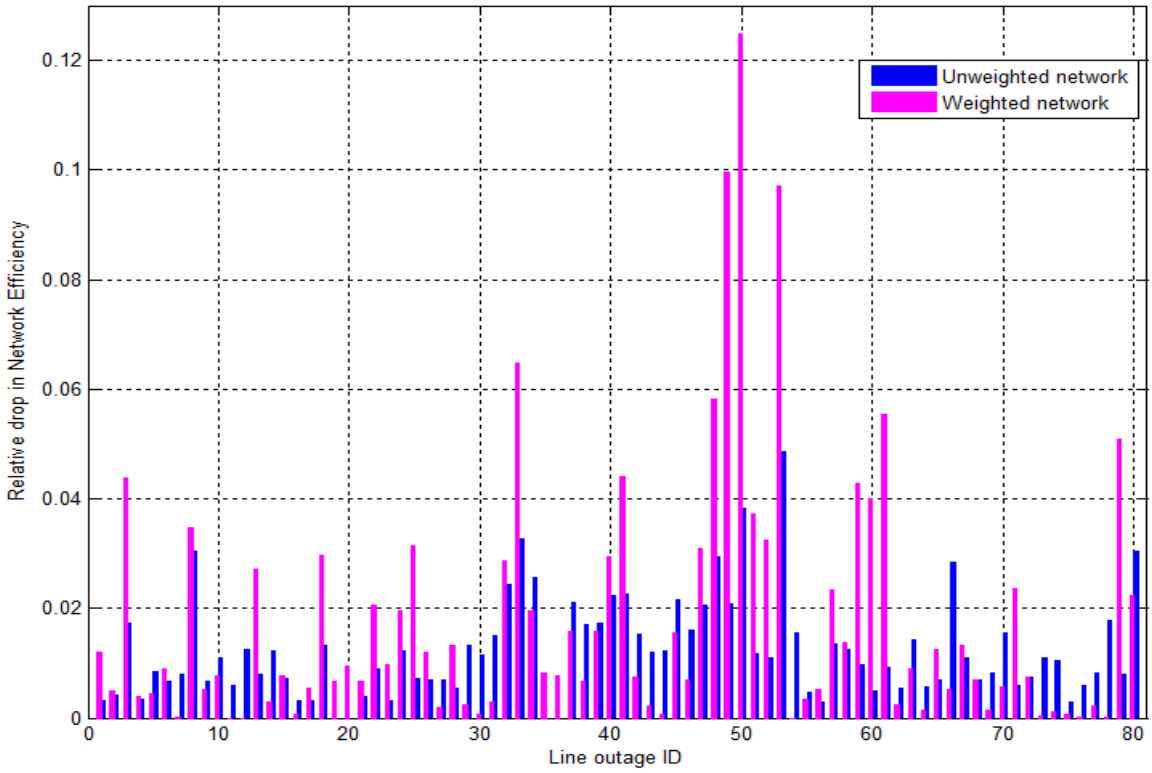

Figure III.8. Network efficiency of IEEE 57-bus system

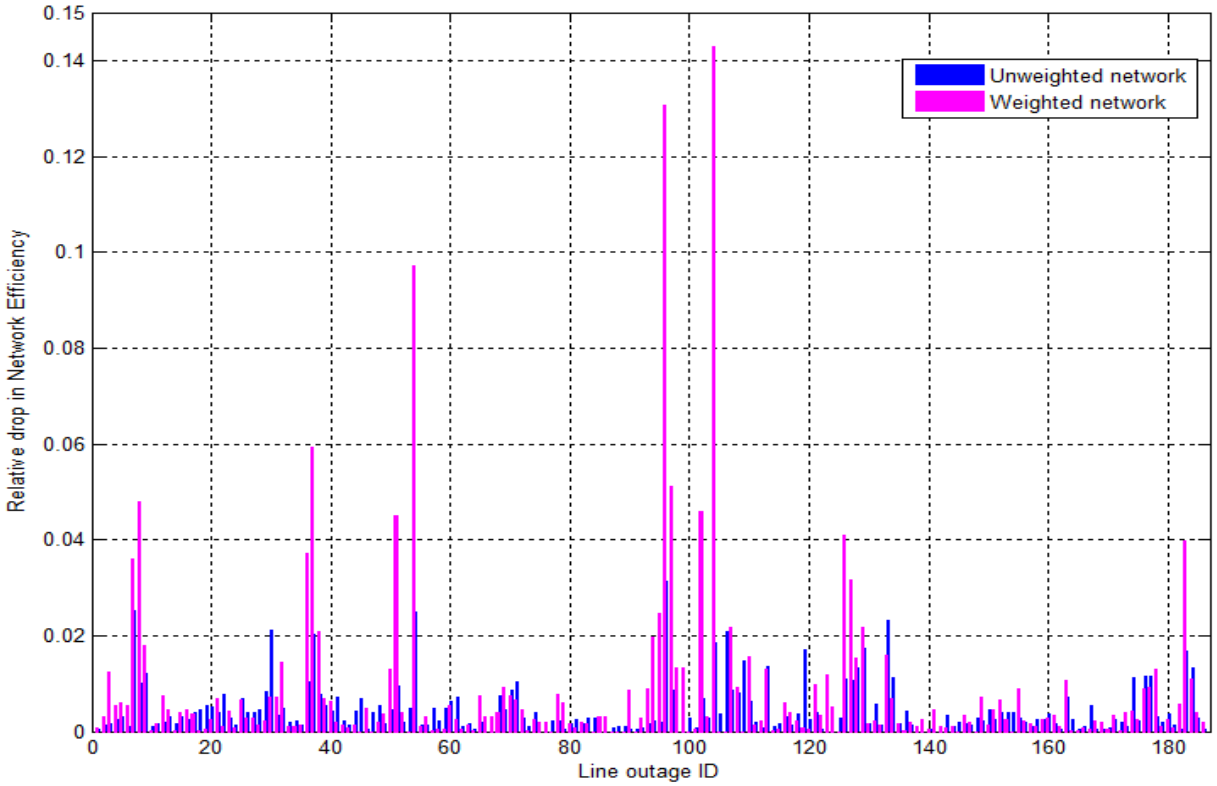

Figure III.9. Network efficiency of IEEE 118-bus system

Considering the unweighted results, IEEE 39-bus system appears to be singular. Actually, when the most critical line (L27) is removed, the drop of efficiency reaches a value close to 14%, while the disconnection of the most critical line of the three other IEEE test system leads to a value lower than 5.5%. A look at the geometrical structure of IEEE 39-bus system on figure III.11 shows that L27 is the only link that interconnects the group of nodes 19, 20, 33 and 34 to the network. Then, its removal diminishes a lot the efficiency of the network.

The top ten critical lines of the three test networks are ranked and shown in table 3.7 and figures III.10 to III.12. They are also compared to ACLOIM.

Table 3.7 Top 10 critical lines of 39- bus, 57-bus, 118-bus systems according to DE and ACLOIM

Rank order	IEEE 39-bus system			IEEE 57-bus system			IEEE 118-bus system		
	D_E		AC LOIM	D_E		AC LOIM	D_E		AC LOIM
	Un-weighted	Weighted		Un-weighted	Weighted		Un-weighted	Weighted	
1	27	27	**37**	53	50	**8**	96	104	**7**
2	32	26	**46**	50	49	**41**	7	96	**9**
3	26	32	**39**	33	53	**40**	54	54	**8**
4	25	25	**33**	80	33	**22**	133	37	**38**
5	24	3	**20**	8	48	**39**	30	97	**51**
6	5	30	**27**	48	61	**60**	106	8	**96**
7	41	18	**34**	66	79	**59**	37	102	**36**
8	33	19	**1**	34	41	**65**	104	51	**97**
9	14	10	**14**	32	3	**18**	129	126	**31**
10	23	13	**3**	41	59	**37**	119	183	**183**

Again, there is no consistency between the results provided by the unweighted and weighted approaches. And it seems that the more complex is the network, the more the efficiency of the weighted graph is dominated by some groups of lines. It may indicate a multilayer structure of bigger power systems. A first layer would correspond to the network backbone and would be crucial for system robustness. The second layer would be made of lines that would be dedicated to local connectivity between nodes. They would be thus less critical.

As previously mentioned, there is a very weak correlation between efficiency and the reference results provided by ACLOIM. Some critical lines previously identified disappear from the top 10 list of the most critical lines whereas some new lines appear to be very critical.

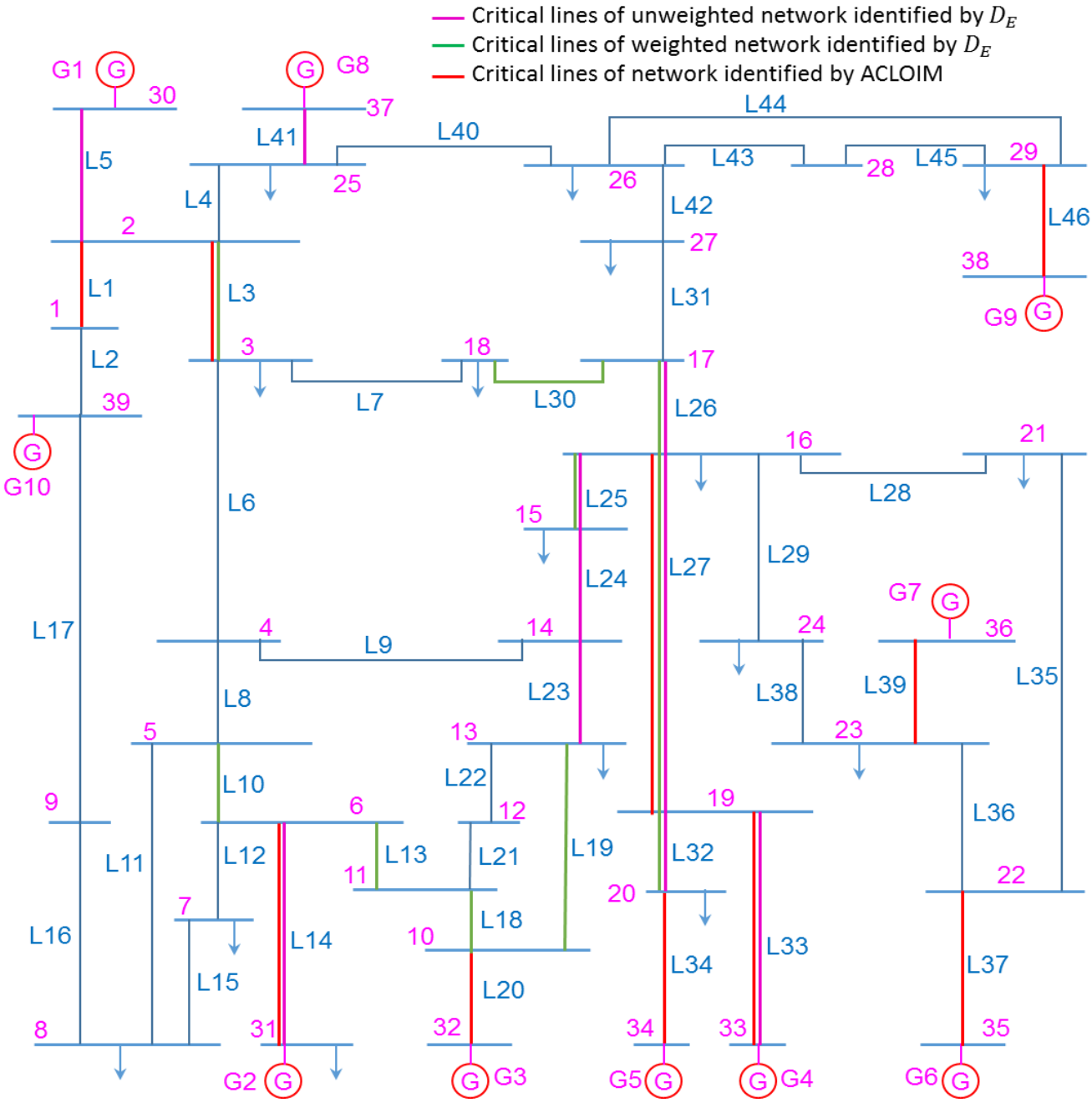

Figure III.10. Comparison of top 10 critical lines of IEEE 39-bus given by D_E and ACLOIM

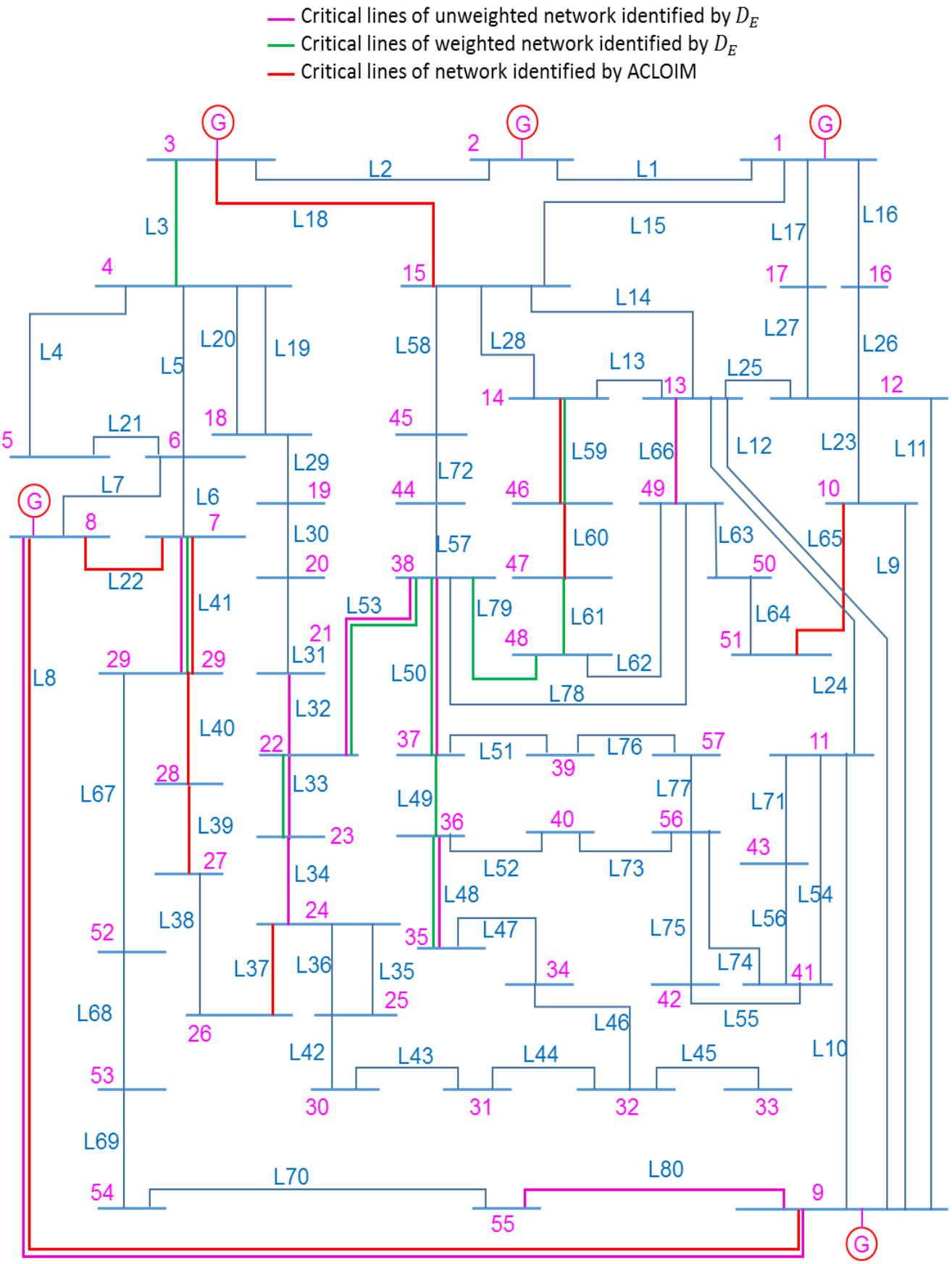

Figure III.11. Comparison of top 10 critical lines of IEEE 57-bus given by D_E and ACLOIM

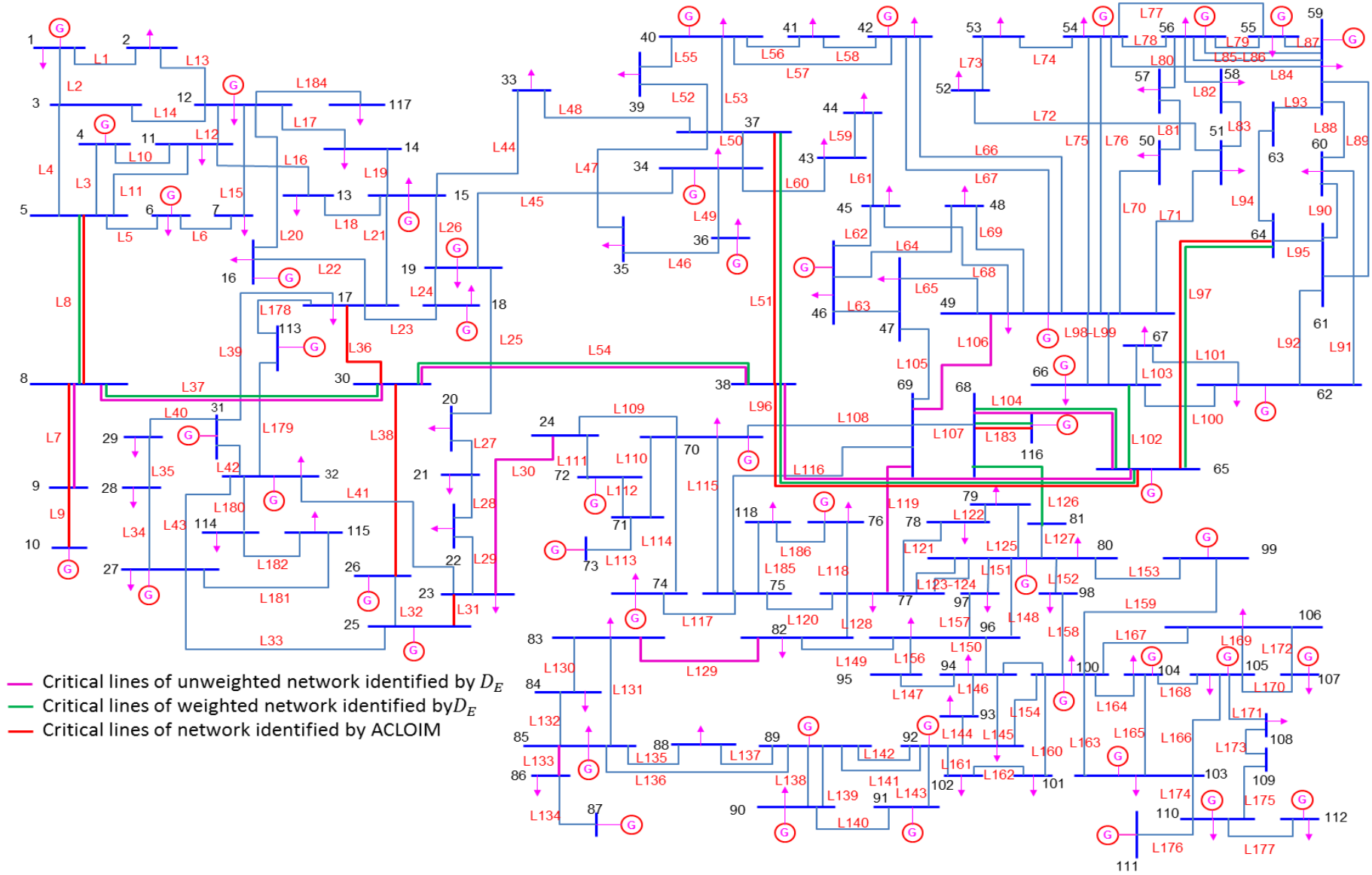

Figure III.12. Comparison of top 10 critical lines of IEEE 118-bus given by D_E and ACLOIM

IV.2 Line betweenness based critical lines ranking

IV.2.1 Star and delta circuits test cases

For 3-bus star and delta electrical circuits, the values of individual line betweenness are given in table 3.8.

Table 3.8 Effect of topology on line betweenness

$C_{BEL}(e)$	**L12**	**L13**	**L23**
Δ connection	0.3333	0.3333	0.3333
Y connection	0.5	0.5	0.5

Since the networks' structures are symmetrical, the values of line betweenness are the same for all the lines. For the delta network, the values are smaller, meaning that every line is less central. This is due to the geometrical redundancy introduced by the meshing.

According to table 3.9, centrality is more important for lines with lower impedance.

Table 3.9 Effect of impedance on line betweenness

$C_{BEL}(e)$	Δ connection ($Z_{12} = 0.02 + j.3$ & $Z_{13} = Z_{23} = 0.02 + j.1$)
L_{12}	0
L_{13} (L_{23})	0.6667

IV.2.2 IEEE test systems

All the results are shown in figures III.13 to III.16. Unlike network efficiency, all the most critical lines are interconnected links between sets of nodes. An interesting result is about IEEE 30-bus network and the group of lines L11, L12 and L14. As it can be shown in figure III.13, they form a mesh connecting nodes 6, 9 and 10. L12 criticality decreases significantly when weighted efficiency is considered while L11 and L14 criticality increases. In the unweighted case, L12 is indeed the shortest path between buses 6 and 10 but due to its high reactance (0.56 p.u.), it becomes the longest path when edges have weights (total reactance of lines L11 and L14 in series being equal to 0.33 p.u.).

In any case, line betweeness is unable to provide consistent results with ACLOIM reference. Indeed, a maximum of 30% of the top ten critical lines identified by line betweeness is matching with ACLOIM.

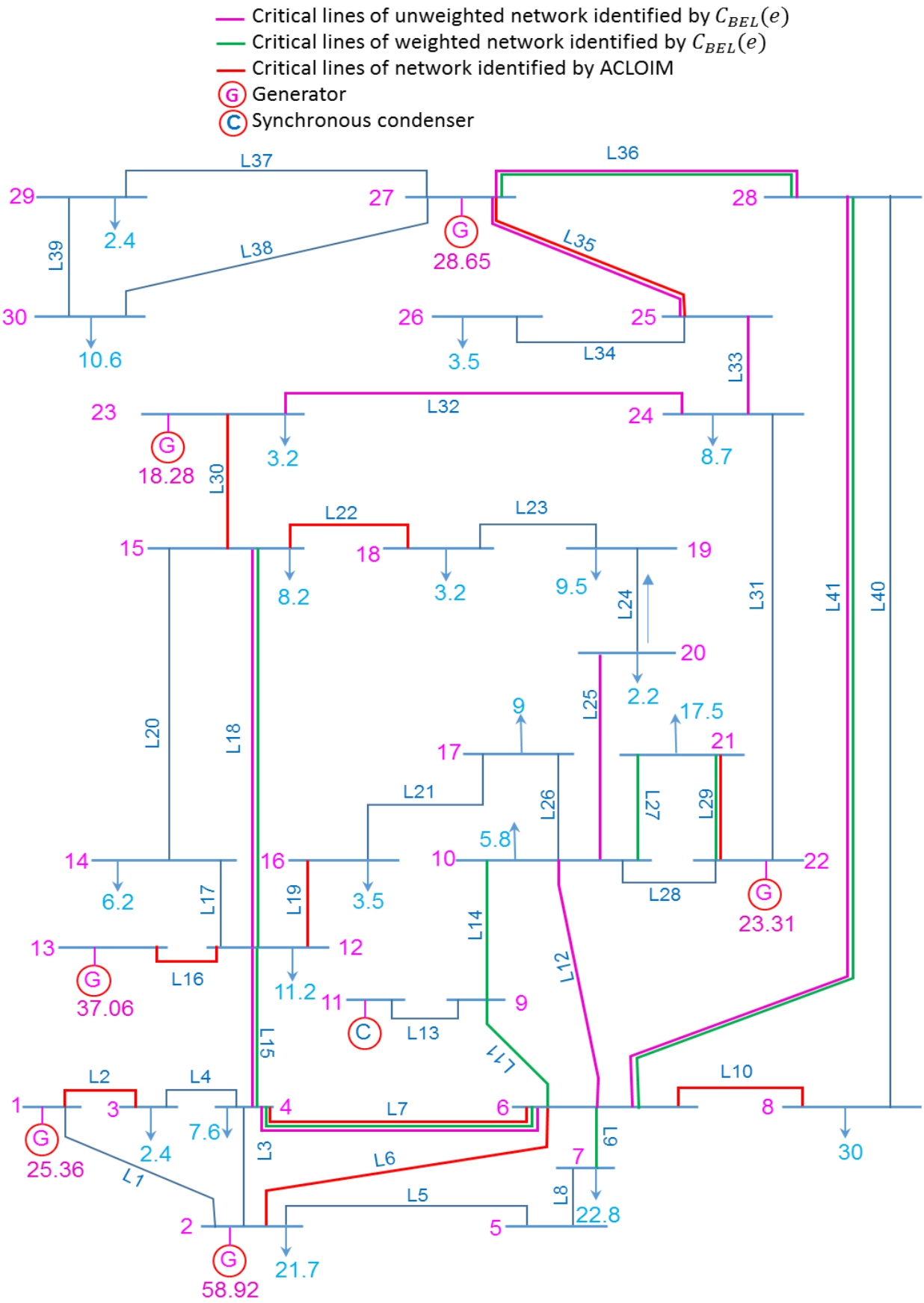

Figure III.13. Comparison of top 10 critical lines of IEEE 30-bus given by C_{BEL} and ACLOIM

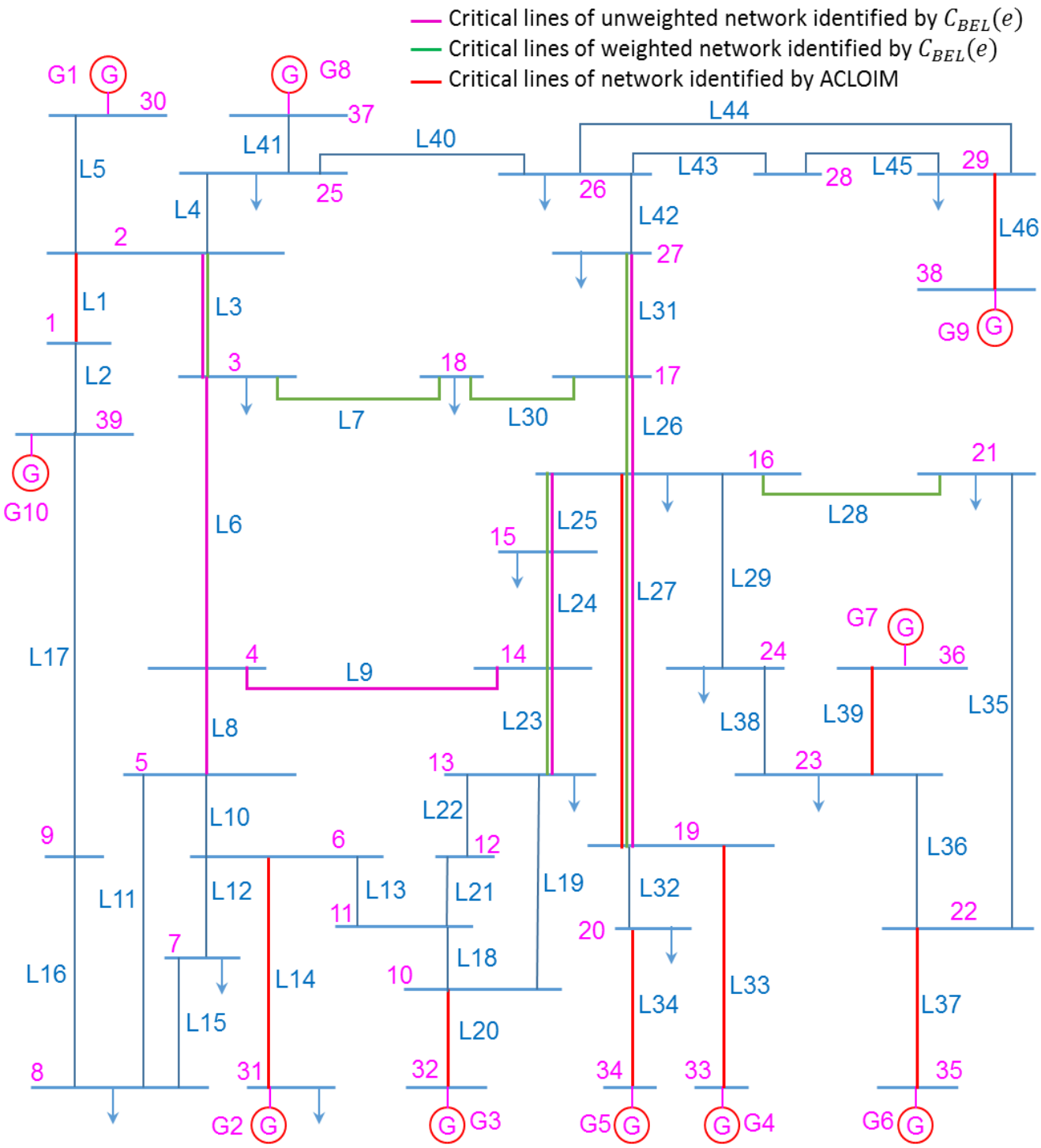

Figure III.14. Comparison of top 10 critical lines of IEEE 39-bus given by C_{BEL} and ACLOIM

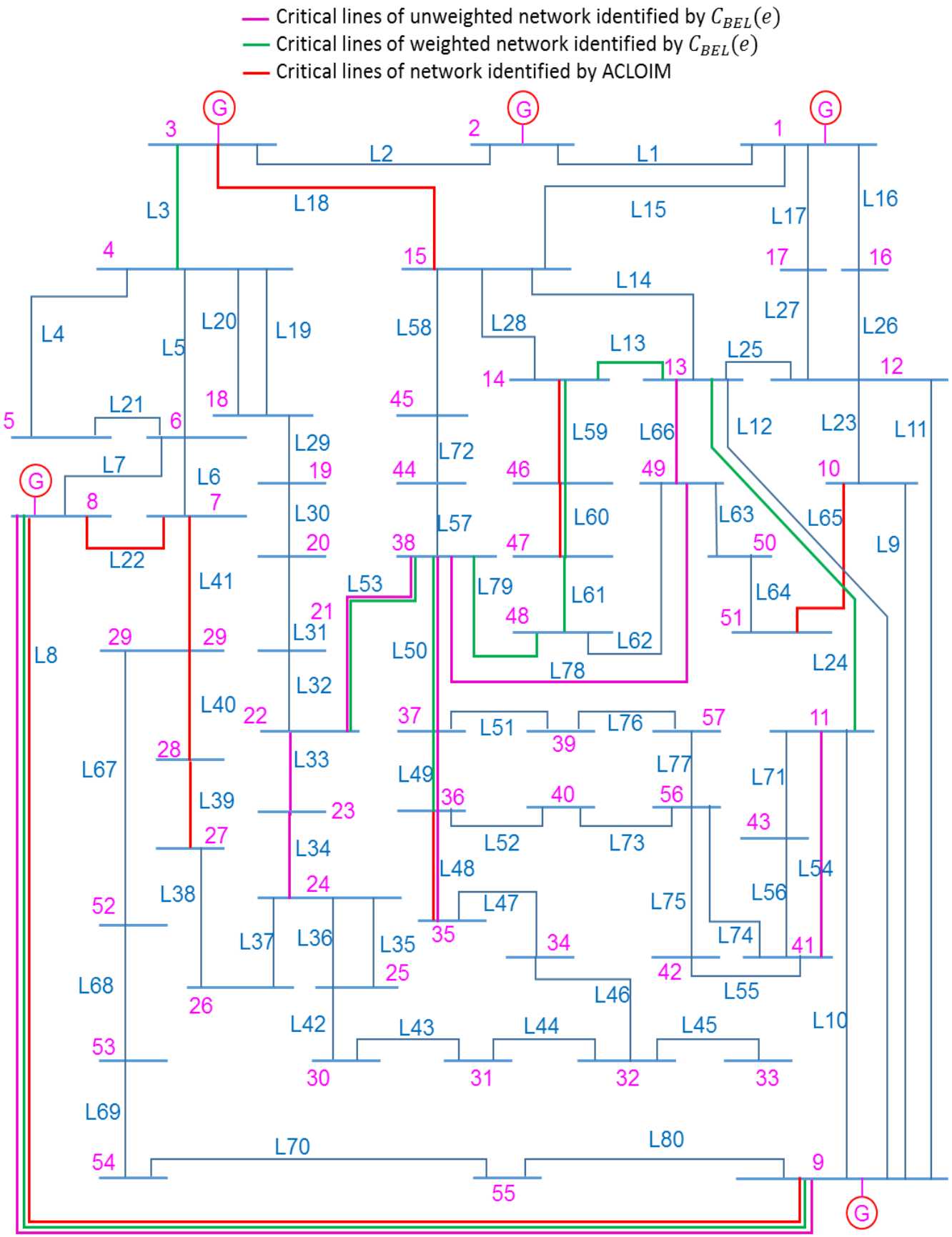

Figure III.15. Comparison of top 10 critical lines of IEEE 57-bus given by C_{BEL} and ACLOIM

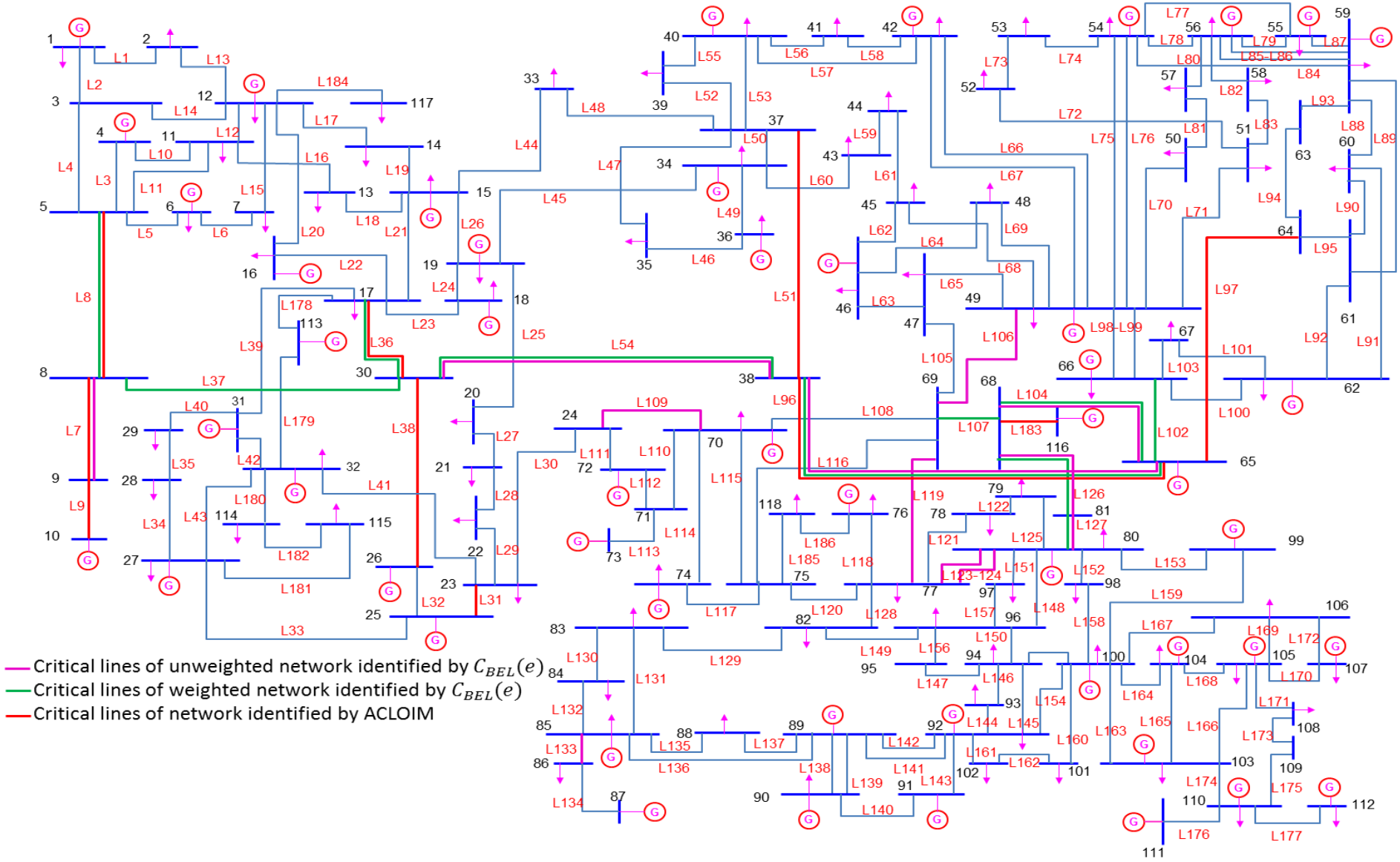

Figure III.16. Comparison of top 10 critical lines of IEEE 118-bus given by C_{BEL} and ACLOIM

IV.3 Net-ability based critical lines ranking

IV.3.1 Critical lines of a 3-node delta system

In order to illustrate the use of net-ability indicator to identify critical lines, we consider the power grid shown in figure III.3 with the assumption that the maximum capacity of power lines is equal to 500 MVA. Net-ability variations following a line outage are shown in table 3.10. They are different even though line impedances are the same. This is due to the difference of role which they play in the network. L12 and L13 connect a generation bus to a load bus, meanwhile line L23 is a connection between two load buses. This confirms that the net-ability is able to reflect the impact of the generators and loads location on system vulnerability. However, the results are the same for lines L12 and L13 although power values at nodes 2 and 3 are different.

Table 3.10 Delta network vulnerability

Line outage	*Net-ability variation (%)*
L_{12} (L_{13})	66.67
L_{23}	55.60

IV.3.2 Critical lines of IEEE 30-bus, 57-bus and 118-bus systems

Net-ability is now used to identify the most critical lines of the three IEEE test systems. The results are compared with ACNCRM reference and shown in figures III.17 to III.19.

A strange phenomenon appears on figure III.17. Most of the critical lines given by net-ability appear to be located in the lower part of the network (area 1). There is no obvious reason except that the biggest generator is located into this area. From the accessibility point of view, it may signify that the loss of one line in this area decreases a lot the "potential of opportunities for interactions", meaning the "potential of loads of being supplied". But a further analysis is difficult because net-ability combines both network capability to transmit power and Thevenin impedance between pair of nodes.

Table 3.11 shows the comparison between the ranking order provided by net-ability and ACNCRM. There is still a very weak correlation between both, meaning that even extended topological metrics are not able to evaluate correctly system vulnerability to line outages.

Table 3.11 Comparison of top ten critical lines identified by D_A and ACNCRM

IEEE 30-bus system			IEEE 57-bus system			IEEE 118-bus system		
Rank order	AC NCRM	D_A	Rank order	AC NCRM	D_A	Rank order	AC NCRM	D_A
1	**36**	**1**	1	**8**	**1**	1	**8**	**104**
2	**19**	**4**	2	**41**	**8**	2	**7**	**126**
3	**10**	**2**	3	**50**	**3**	3	**9**	**127**
4	**38**	**7**	4	**49**	**2**	4	**51**	**30**
5	**29**	**6**	5	**40**	**18**	5	**38**	**96**
6	**22**	**9**	6	**65**	**25**	6	**36**	**97**
7	**16**	**3**	7	**39**	**15**	7	**96**	**183**
8	**30**	**29**	8	**47**	**6**	8	**33**	**37**
9	**17**	**15**	9	**46**	**22**	9	**97**	**8**
10	**40**	**5**	10	**17**	**21**	10	**21**	**110**

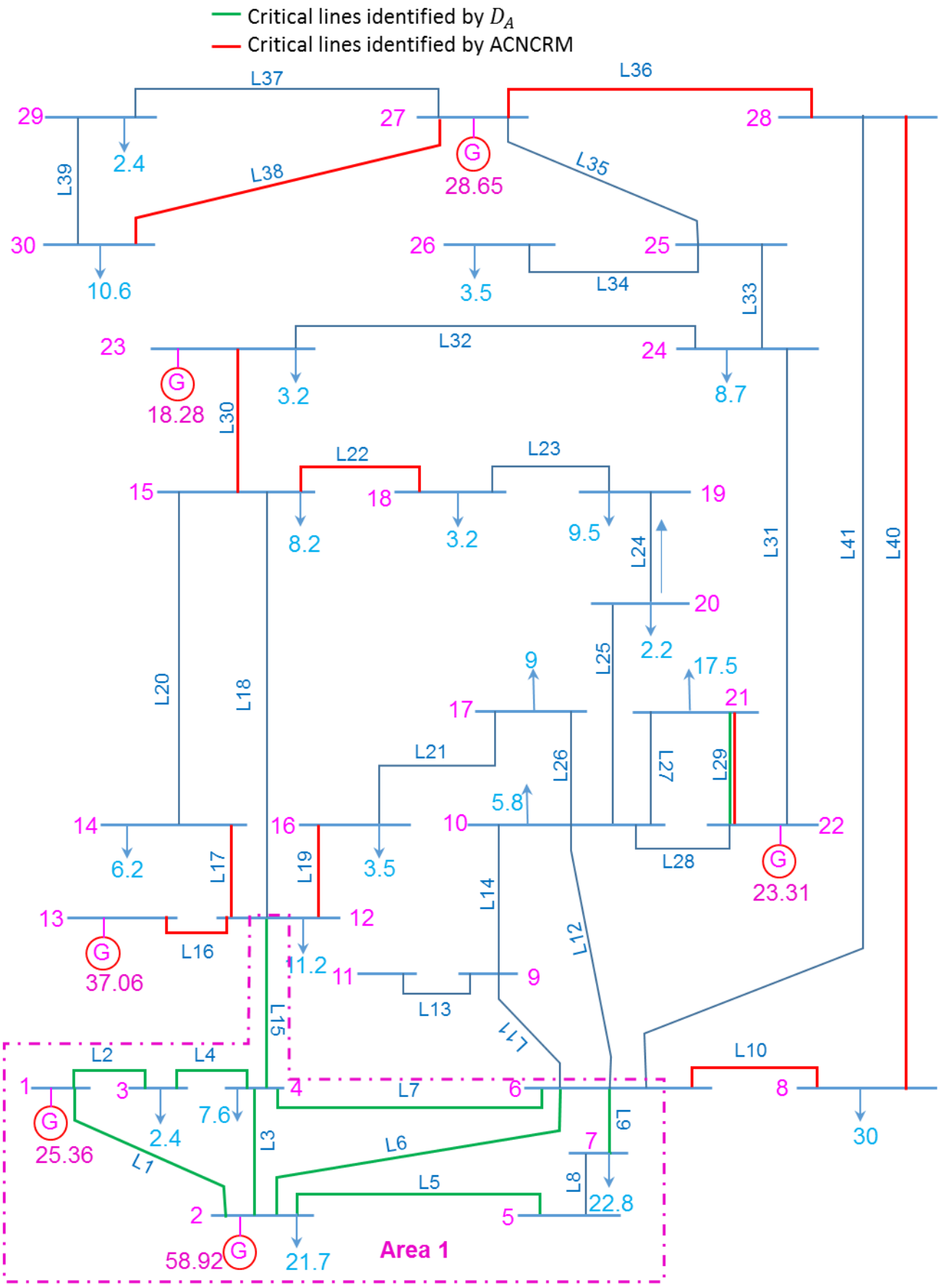

Figure III.17. Comparison of top 10 critical lines of IEEE 30-bus given by D_A and ACNCRM

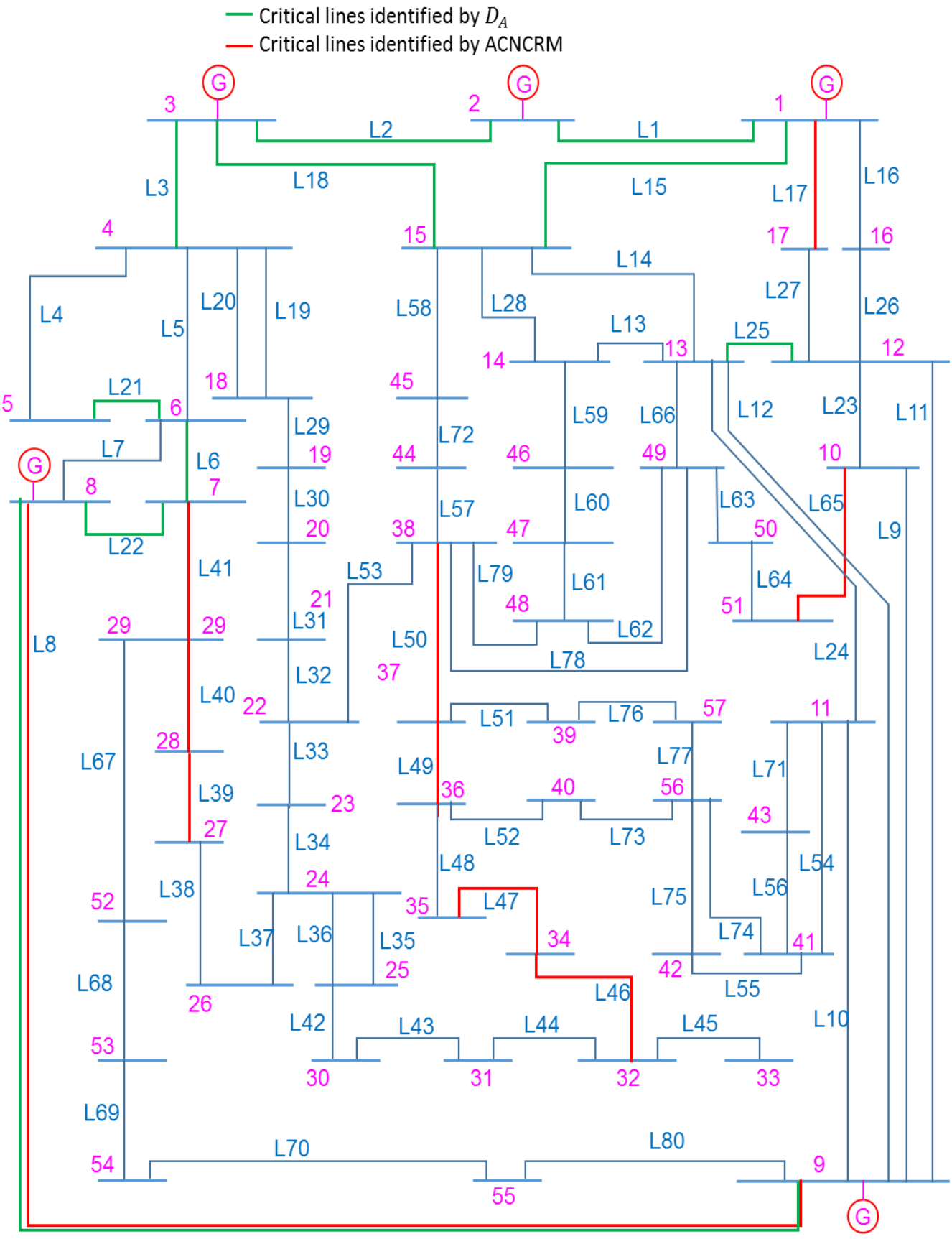

Figure III.18. Comparison of top 10 critical lines of IEEE 57-bus given by D_A and ACNCRM

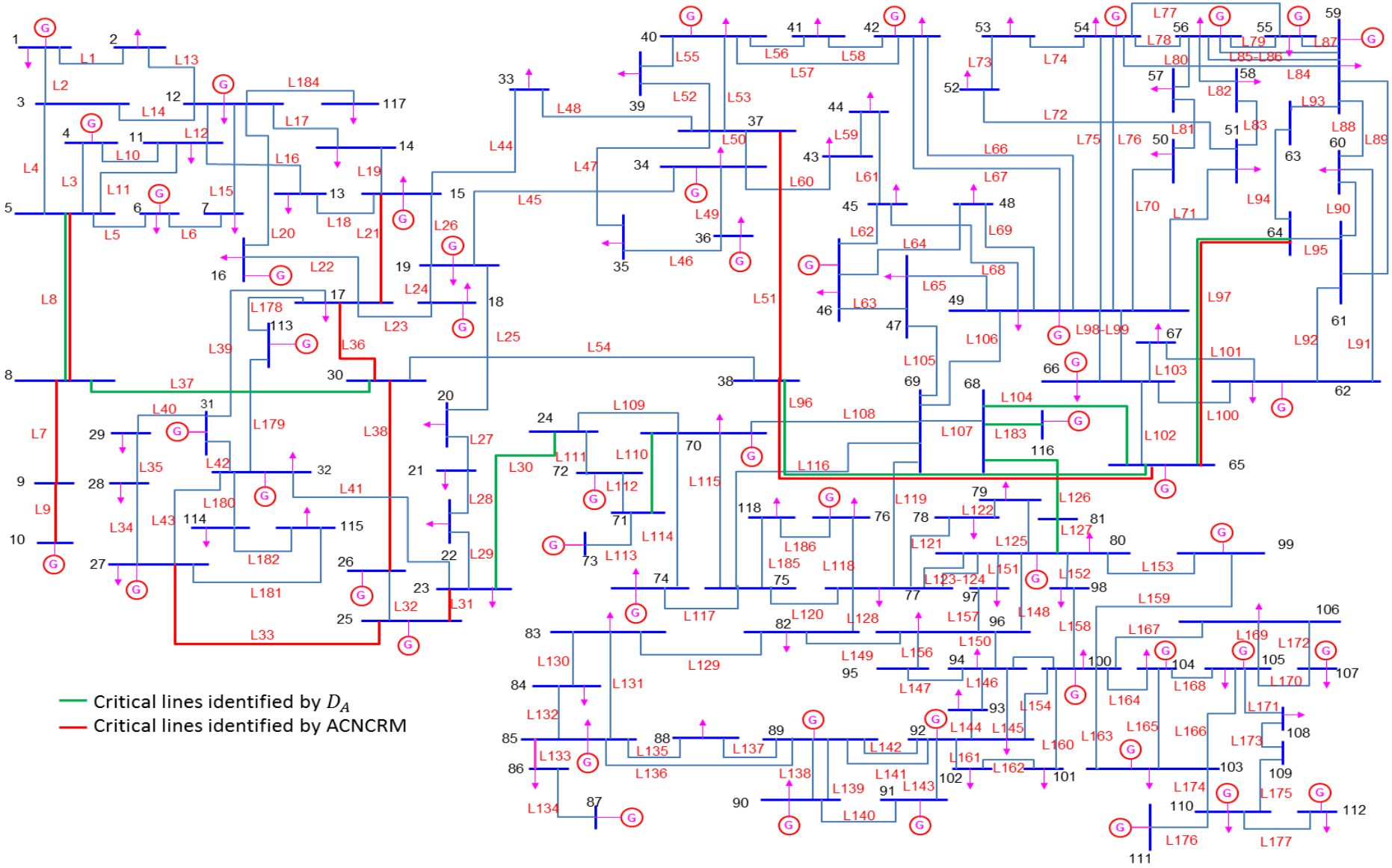

Figure III.19. Comparison of top 10 critical lines of IEEE 118-bus given by D_A and ACNCRM

V. Conclusion

Power systems are flow networks that are easily modeled and studied by graph theory-inspired methods. It can provide to power engineers a simplified view on complexity, showing how some topological features may influence system behavior. But, power engineers must be very cautious in their use of topological indicators to study system vulnerability. Indeed, our results have shown that they fail in assessing actual critical lines in the electricity infrastructure. Therefore, it would be better to propose new indices to measure vulnerability of power grids. These metrics should capture the essential electrical characteristics of power grids while keeping simple the links between system structure and its vulnerability.

Chapter IV.

DC assessment of power system vulnerability

I. Introduction

Approaches for vulnerability analysis of power grids due to line outage based on topological model fail in assessing actual failure impact on the electricity infrastructure as analyzed in previous chapter. On the other hand, full AC power flow studies fail in understanding how the organization of the network may influence its vulnerability.

In order to overcome the disadvantages of full AC models and take advantages of topological approaches, DC power flow, which is a linear approximation of power grid AC models, is proposed to be used. This approach is expected to helps power engineers to better understand the links between topology and structural vulnerabilities of power grids.

This chapter consists of three main parts.

- The first part shows how to form the DC power flow equations.
- The following section introduces DC indicators for vulnerability of power system due to line outages.
- Final section demonstrates how these indicators can be applied for assessment vulnerability of IEEE test power systems.

II. DC approximation of power flows

II.1 DC power flow equations

DC power flow equations are a simplification of AC power flow equations, considering only active power flows. Thus, AC power flow equations (II.18) and (II.19) can be linearized assuming that first reactive power flow is neglected. Only equation (II.18) is therefore taken into account. Assuming that the power grid is a lossless network ($G_{ij} = 0$), this equation becomes:

$$P_i \approx \sum_{j=1}^{N} |V_i||V_j| B_{ij} sin(\delta_i - \delta_j) = \sum_{\substack{j=1 \\ i \neq j}}^{N} P_{ij} \qquad \text{(IV.1)}$$

Where, P_{ij} is the active power flow through the line connecting buses *i* and *j*.

In normal operation, voltage angle differences across lines, which are usually less than 15 degree, are considered to be very small. Hence, $\sin(\delta_i - \delta_j) \approx (\delta_i - \delta_j)$ and P_{ij} becomes:

$$P_{ij} \approx |V_i||V_j| B_{ij}(\delta_i - \delta_j) \qquad \text{(IV.2)}$$

Finally, if magnitudes of nodal voltages are assumed to be almost closed to 1.0 per unit, meaning that every voltage is closed to its nominal value, active power at bus i is approximated by:

$$P_i \approx \sum_{j=1}^{N} B_{ij}(\delta_i - \delta_j) = \sum_{j=1}^{N} B_{ij}\theta_{ij} \qquad \text{(IV.3)}$$

This linear equation linking nodal power and voltage angles constitutes the DC approximation of AC power flow equations.

In a matrix form:

$$P \approx B.\theta \tag{IV.4}$$

Where P is the vector of active power injections, θ is the vector representing voltage phase angles at each node, referred to slack bus reference, and B is the bus susceptance matrix. It is equal to bus admittance matrix Y where the resistive terms associated to losses are neglected. It has actually the same structure as the Laplacian matrix of the underlying graph of the network.

If all active power injections are specified, voltage phase angle at each node is approximated directly from:

$$\theta \approx [B]^{-1} P = X.P \tag{IV.5}$$

Where X stands for reactance matrix and can be calculated by the Moore-Penrose pseudo-inverse of bus admittance matrix [20], [70].

Power flow through transmission lines of the grid can be rewritten as:

$$P_L = Y_{br}.K.\theta \tag{IV.6}$$

K is the link-node incidence matrix of the underlying graph of the grid and Y_{br} is a diagonal matrix representing the *(mxm)* line admittance.

Therefore:

$$P_L \approx Y_{br}.K.X.P \tag{IV.7}$$

DC approximation gives a set of linear equations that links in a simple manner electrical variables and topological properties.

II.2 Power transfer distribution factor

Power transfer distribution factor (PTDF) is a sensitivity matrix showing how power flows through lines change when nodal power injections are modified. Its entry element f_{ka} gives the ratio between the change of power flow through line k and the variation of power injection at bus a [71].

$$f_{ka} = \frac{\Delta P_k}{\Delta P_a} \tag{IV.8}$$

To keep the system balanced, power injection at node a is balanced with a modification of slack bus power.

Using DC approximation, if we neglect resistance of power lines and assume voltage magnitudes near unity value, equation (IV.9) can be written as:

$$f_{ka} = \frac{\Delta P_k}{\Delta P_a} = \frac{\Delta J_k}{\Delta I_a} \tag{IV.9}$$

J_k is the current through line k, connecting buses i and j.

Application of Kirchoff's law to a lossless power grid leads to a matrix relation between nodal currents and vectors such as:

$$\begin{vmatrix} I_1 \\ I_2 \\ . \\ I_N \end{vmatrix} = \begin{vmatrix} B_{11} & B_{12} & . & B_{1N} \\ B_{21} & B_{22} & . & B_{2N} \\ . & . & . & . \\ B_{N1} & B_{N2} & . & B_{NN} \end{vmatrix} \begin{vmatrix} V_1 \\ V_2 \\ . \\ V_N \end{vmatrix} \tag{IV.10}$$

Considering bus 1 as slack bus with voltage V_1 fixed as ${V_1}^0$ and eliminating I_1, equation (IV.10) becomes:

$$\begin{vmatrix} I_2 \\ . \\ . \\ I_N \end{vmatrix} = \begin{vmatrix} B_{11} & B_{12} & . & B_{1N} \\ B_{21} & B_{22} & . & B_{2N} \\ . & . & . & . \\ B_{N1} & B_{N2} & . & B_{NN} \end{vmatrix} \begin{vmatrix} V_2 \\ . \\ . \\ V_N \end{vmatrix} + \begin{vmatrix} B_{21} \\ . \\ . \\ B_{N1} \end{vmatrix} {V_1}^0 \tag{IV.11}$$

ΔP_a is injected at node a. Before injection, nodal voltages are given by:

$$\begin{vmatrix} {V_2}^{be} \\ . \\ . \\ {V_N}^{be} \end{vmatrix} = \begin{vmatrix} X_{22} & . & . & X_{2N} \\ . & . & . & . \\ . & . & . & . \\ X_{N2} & . & . & X_{NN} \end{vmatrix} \begin{vmatrix} {I_2}^{be} - B_{21}{V_1}^0 \\ . \\ . \\ {I_N}^{be} - B_{N1}{V_1}^0 \end{vmatrix} \tag{IV.12}$$

And line currents are expressed by:

$${J_k}^{be} = \frac{{V_i}^{be} - {V_j}^{be}}{X_{ij}} \tag{IV.13}$$

After injection, nodal voltages are determined from:

$$\begin{vmatrix} {V_2}^{af} \\ . \\ . \\ {V_N}^{af} \end{vmatrix} = \begin{vmatrix} X_{22} & . & . & X_{2N} \\ . & . & . & . \\ . & . & . & . \\ X_{N2} & . & . & X_{NN} \end{vmatrix} \begin{vmatrix} {I_2}^{af} - B_{21}{V_1}^0 \\ . \\ . \\ {I_N}^{af} - B_{N1}{V_1}^0 \end{vmatrix} \tag{IV.14}$$

And line currents become:

$${J_k}^{af} = \frac{{V_i}^{af} - {V_j}^{af}}{X_{ij}} \tag{IV.15}$$

From (IV.13) - (IV.16), the changes in bus voltages and line current after injection ΔP_a are:

$$\begin{vmatrix} \Delta V_2 \\ . \\ . \\ \Delta V_N \end{vmatrix} = \begin{vmatrix} X_{22} & . & . & X_{2N} \\ . & . & . & . \\ . & . & . & . \\ X_{N2} & . & . & X_{NN} \end{vmatrix} \begin{vmatrix} \Delta I_2 \\ . \\ . \\ \Delta I_N \end{vmatrix} \tag{IV.16}$$

$$\Delta J_k = {J_k}^{af} - {J_k}^{be} = \frac{\Delta V_i - \Delta V_j}{X_{ij}} = \sum_{\alpha=2}^{N} \left[\frac{X_{i\alpha} - X_{j\alpha}}{X_{ij}} \right] \Delta I_\alpha \tag{IV.17}$$

Where:

$$\begin{vmatrix} \Delta I_2 \\ . \\ . \\ \Delta I_N \end{vmatrix} = \begin{vmatrix} {I_2}^{be} - {I_2}^{af} \\ . \\ . \\ {I_N}^{be} - {I_N}^{af} \end{vmatrix} \tag{IV.18}$$

Since only power injection at node a changes, we have:

$$\Delta J_k = \frac{X_{ia} - X_{ja}}{X_{ij}} \Delta I_a \tag{IV.19}$$

PTDF elements can be determined from:

$$f_{ka} = \frac{X_{ia} - X_{ja}}{X_{ij}} \quad \text{(IV.20)}$$

In matrix form:

$$PTDF = Y_{br}.K.X \quad \text{(IV.21)}$$

PTDF links nodal and line powers through a very simple relation:

$$P_L = PTDF.P \quad \text{(IV.22)}$$

In the frame of DC approximation, PTDF give some crucial information on system vulnerability, giving a measure of how power flows are redistributed throughout the network when one line fails. It provides a basis variable to compute new vulnerability indicators.

III. DC indicators of vulnerability

III.1 Line outage distribution factor (LODF)

Line outage distribution factor (LODF) is commonly used during contingency analysis to screen potential line overloads when a transmission line failure occurs [69]. It is defined by the variation of power flow through line *k* due to the failure of line *q*:

$$LODF_{k,q} = \frac{P_{Lk,q} - P_{Lk}}{P_{Lq}} = \frac{\Delta P_{Lk,q}}{P_{Lq}} \quad \text{(IV.23)}$$

Where P_{Lk} and $P_{Lk,q}$ are respectively the values active power flowing through line *k* before and after line *q* outage. P_{Lq} is the power flowing through line q before its failure.

Post-contingency state shown in figure IV.1.(a) is equivalent to the superposition of pre-contingency state described in figure IV.1.(b) and a perturbation shown in figure IV.1.(c). P_{Lq} injection at node *p* and withdrawal at node *o* in [72].

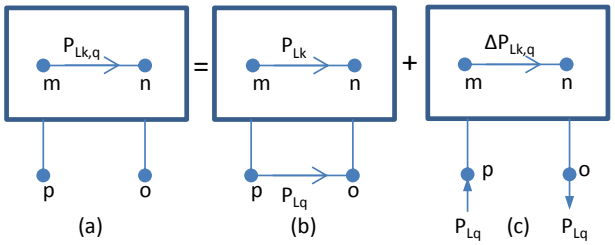

Figure IV.1. Equivalent networks with line q outage

It comes from equation (IV.23) that power flowing between nodes *m* and *n* in figure IV.1.(c) is given by:

$$\Delta P_{Lk,q} = (f'_{kp} - f'_{ko}).P_{Lq} \quad \text{(IV.24)}$$

Where f'_{kp} and f'_{ko} are entry elements of PTDF matrix (F') in the post-contingency state (line *q* being removed).

$LODF_{k,q}$ is thus expressed by:

$$LODF_{k,q} = \frac{(f'_{kp} - f'_{ko}).P_{Lq}}{P_{Lq}} = f'_{kp} - f'_{ko} \quad \text{(IV.25)}$$

Line outage distribution factor depends only on topology and parameters of post-contingency network.

The most efficient approach to calculate $LODF_{k,q}$ is based on the PTDF matrix (F) of the pre-contingency network. In the frame of DC approximation, voltage being constant, LODF can be expressed by:

$$LODF_{k,q} = \frac{\Delta J_{k,q}}{I_q} \quad \text{(IV.26)}$$

$\Delta J_{k,q}$ defines the current variation in line *k* due to line *q* disconnection.

Outage of line *q* is modeled by adding a reactance ($-x_q$) between buses *p* and *o* in the pre-contingency Thevenin equivalent circuit shown in figure IV.2 [42]. Losses being still neglected, only reactance is considered.

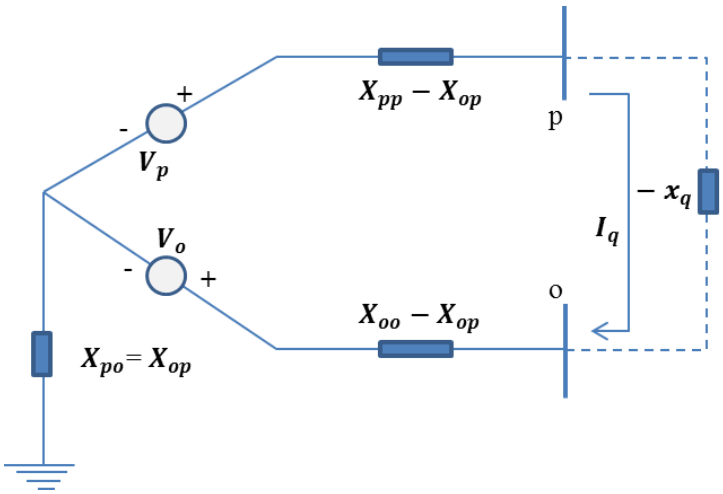

Figure IV.2. Pre-outage Thevenin equivalent circuit for modeling outage of line q

Loop current I_q can be calculated as:

$$I_q = \frac{V_p - V_o}{(X_{pp} + X_{oo} - 2X_{po}) - X_q} = \frac{V_p - V_o}{X_{eq.po} - X_q} \quad \text{(IV.27)}$$

Where V_p and V_o are pre-contingency bus voltages, and $X_{eq.po}$ is Thevenin reactance between buses *p* and *o*. The addition of ($-X_q$) cause a change of nodal current injection at nodes *p* and *q*, respectively $\Delta I_p = -I_q$ and $\Delta I_o = I_q$ injection to bus *o*. This triggers a change of line currents according to equation (IV.19):

$$\Delta J_{k,q} = f_{kp}.\Delta I_p + f_{ko}.\Delta I_o = (f_{ko} - f_{kp}).I_q \quad \text{(IV.28)}$$

Substituting I_q from (IV.27) to (IV.28) yields:

$$\Delta J_{k,q} = (f_{ko} - f_{kp}) \frac{V_p - V_o}{(X_{pp} + X_{oo} - 2X_{po}) - X_q} \quad \text{(IV.29)}$$

Loop current can also be defined in relation with nodal voltages:

$$I_q = \frac{V_p - V_o}{X_q} \quad \text{(IV.30)}$$

And we obtain:

$$\Delta J_{k,q} = \frac{I_q(f_{ko} - f_{kp})}{\frac{(X_{pp} + X_{oo} - 2X_{po})}{X_q} - 1} = \frac{I_q(f_{ko} - f_{kp})}{\frac{(X_{pp} - X_{op})}{X_q} - \frac{(X_{po} - X_{oo})}{X_q} - 1} \quad \text{(IV.31)}$$

Using PTDF elements definition (see equation IV.20), line current variation is given by:

$$\Delta J_{k,q} = \frac{I_q(f_{kp} - f_{ko})}{1 - (f_{qp} - f_{qo})} \quad \text{(IV.32)}$$

Or:

$$\frac{\Delta J_{k,q}}{I_q} = \frac{h_{k,q}}{1 - h_{q,q}} \quad \text{(IV.33)}$$

Where, $h_{k,q} = f_{kp} - f_{ko}$ and $h_{q,q} = f_{qp} - f_{qo}$.

Finally, LODF elements are given by:

$$LODF_{k,q} = \begin{cases} \frac{h_{k,q}}{1 - h_{q,q}} & \text{if } k \neq q \\ -1 & k = q \end{cases} \quad \text{(IV.34)}$$

III.2 DC line outage impact metric (DCLOIM)

DC line outage impact metric measures the redistribution of active power by comparing DC power flows at steady state before and after line q fails. It is defined by equation (IV.35).

$$DCLOIM_q = \sum_{k=1}^{m} \left| \frac{P_{Lk} - P'_{Lk,q}}{P_{demand}} \right| = \sum_{k=1}^{m} \left| \frac{\Delta P_{Lk,q}}{P_{demand}} \right| \quad \text{(IV.35)}$$

If the outage does not split the network into two parts, the calculation of DCLOIM is performed using LODF such as:

$$DCLOIM_q = \sum_{k=1}^{m} \left| \frac{LODF_{k,q} . P_{Lq}}{P_{demand}} \right| = \left| \frac{P_{Lq}}{P_{demand}} \right| \sum_{k=1}^{m} |LODF_{k,q}| \quad \text{(IV.36)}$$

Contrary to ACLOIM, the DC metric provides a direct and straightforward link between grid topology through LODF and vulnerability.

In the case of shedding one line leading to one or more buses isolated from the network, active power from the sending bus of the disconnected line cannot be transferred to the loads. In order to balance power demand and supply in the post-fault steady state, active power supplied by remain generators connected to the network is controlled as concerned in section IV of chapter 2. ACLOIM

is calculated directly from (IV.35) based on active power flow through line *k* at steady state before and after contingency.

III.3 DC network capacity reservation metric

Because reactive power flow is neglected for DC modeling, network capacity reservation metric takes into account only active powers. It is defined by:

$$DCNCRM = \frac{1}{m}\sum_{k=1}^{m}\frac{P_{limit_k} - |P_{Lk}|}{P_{limit_k}} \quad \text{(IV.37)}$$

Where:

- P_{Lk} is the active power through line k.
- P_{limit_k} is the maximum capacity of line *k*. It is defined as:

$$P_{limit_k} = \frac{P_{demand}.S_{limit_k}}{S_{demand}} \quad \text{(IV.38)}$$

If the outage does not separate the network into two parts, after contingency, power in line k being increased by $\Delta P_{Lk,q}$, DCNCRM becomes:

$$DCNCRM = \frac{1}{m}\sum_{k=1}^{m}\frac{P_{limit_k} - \left|P_{Lk} + LODF_{k,q}.P_{Lq}\right|}{P_{limit_k}} \quad \text{(IV.39)}$$

In the case of disconnecting one line resulting in one or more buses isolated from the network, DCNCRM of the network at post steady state is calculated directly from the equation (IV.37) based on DC active power flow through line *k* at steady state after contingency.

Vulnerability of a power grid is then determined by the variation of DCNCRM due to the outage of a line *q*:

$$D_{DCNCRM} = \frac{DCNCRM_0 - DCNCRM_q}{DCNCRM_0} \quad \text{(IV.40)}$$

Where, indices *0* and *q* refer to normal operation (equation IV-37) and post-contingency (equation IV-39) states of the network.

IV. Application to test systems

IV.1 Interpretation of LODF

The simple networks connected in delta given in figure III.3 are considered. Line outage distribution factors corresponding to various contingencies are computed and shown in table 4.1.

Table 4.1 Post-contingency LODF values of the network in delta connection

Contingency	$LODF_{12}$	$LODF_{13}$	$LODF_{32}$
Failure of L_{12}	-1	1	1
Failure of L_{13}	1	-1	-1
Failure of L_{32}	1	-1	-1

LODF indicates how a line outage affects the other lines of the network. For instance, when line L_{12} is disconnected, power in line L_{13} is increased by 100% of the pre-contingency power of the failed line. The absolute results are given in the table below.

Table 4.2 Power flow through lines of thee-bus simple network

Operation mode	P_{12} (MW)	P_{13}(MW)	P_{32} (MW)
Normal operation	93.3	86.7	6.7
Failure of L_{12}	0	180	100
Failure of L_{13}	180	0	- 80
Failure of L_{32}	100	80	0

LODF is not an appropriate metric for assessing system vulnerability to line outages since it only shows how individual lines are affected by contingencies. In addition, it is not possible to use LODF for systems separated into several independent clusters after contingency.

IV.2 Locating critical lines by DC line outage impact metric

IV.2.1 Application to basic electrical circuits

The same basic network as below is studied. We consider how to apply this metric to the simple network shown in figure III.3. The values of DCLOIM for the disconnection of one line are given in table 4.3.

Table 4.3 DCLOIM value for the network in delta connection shown in figure III.3

Line disconnected	L_{12}	L_{13}	L_{23}
DCLOIM	1.037	0.963	0.074

L_{12} is the most critical line since it connects directly the generator and a heavy load. On the other hand, disconnection of L23 does not impact significantly power redistribution throughout the network since it connects two load buses together. Generators and loads location is therefore a crucial parameter for system vulnerability.

Now, the value of line impedance Z_{12} is increased by a factor 3. Table 4.4 shows that the most critical line becomes L13 since the high impedance value of L12 lessens its central role in system operation.

Table 4.4 DC network capacity reservation of the simple network – line L12 impedance increase 3 times

Line disconnected	L_{12}	L_{13}	L_{23}
DCLOIM	0.6222	1.3778	0.4889

DCLOIM is therefore able to capture how the network connectivity influences its vulnerability.

IV.2.2 Application to IEEE test systems

DCLOIM is used to identify the critical lines of IEEE test systems. To check if it provides a meaningful way to assess vulnerability, the results are compared with those obtained by ACLOIM.

Table 4.5 Comparison of top ten critical lines identified by DCLOIM and ACLOIM

IEEE 30-bus system			IEEE 39-bus system			IEEE 57-bus system			IEEE 118-bus system		
Rank order	AC LOIM	DC LOIM	Rank order	AC LOIM	DC LOIM	Rank order	AC LOIM	DC LOIM	Rank order	AC LOIM	DC LOIM
1	**16**	**16**	1	**37**	**37**	1	**8**	**8**	1	**7**	**7**
2	**7**	**7**	2	**46**	**46**	2	**41**	**41**	2	**9**	**9**
3	**22**	**22**	3	**39**	**39**	3	**40**	**40**	3	**8**	**8**
4	**30**	**30**	4	**33**	**33**	4	**22**	**22**	4	**38**	**38**
5	**35**	**29**	5	**20**	**20**	5	**39**	**39**	5	**51**	**51**
6	**29**	**35**	6	**27**	**27**	6	**60**	**59**	6	**96**	**36**
7	**19**	**19**	7	**34**	**34**	7	**59**	**60**	7	**36**	**96**
8	**6**	**36**	8	**1**	**1**	8	**65**	**38**	8	**97**	**97**
9	**10**	**6**	9	**14**	**14**	9	**18**	**37**	9	**31**	**31**
10	**2**	**10**	10	**3**	**3**	10	**37**	**18**	10	**183**	**104**

According to table 4.5, DCLOIM is very consistent with the reference metric since it is able to locate the same group of critical lines. The strong correlation between DCLOIM and ACLOIM for the most critical lines is also graphically shown in figures IV.3 to IV.6. An interesting observation shows that higher is the ratio between the total active power and reactive power demand, better is the consistency of top ten critical lines identified by DCLOIM and ACLOIM. For instance, the top ten critical lines of the 39-bus network (ratio between total active power and reactive power demand equal to 4.51) are the same, while those of 118- bus, 57-bus and 30-bus test systems with lower ratio between the total active power and reactive power demand (2.96, 3.71 and 1.76, respectively) are less consistent.

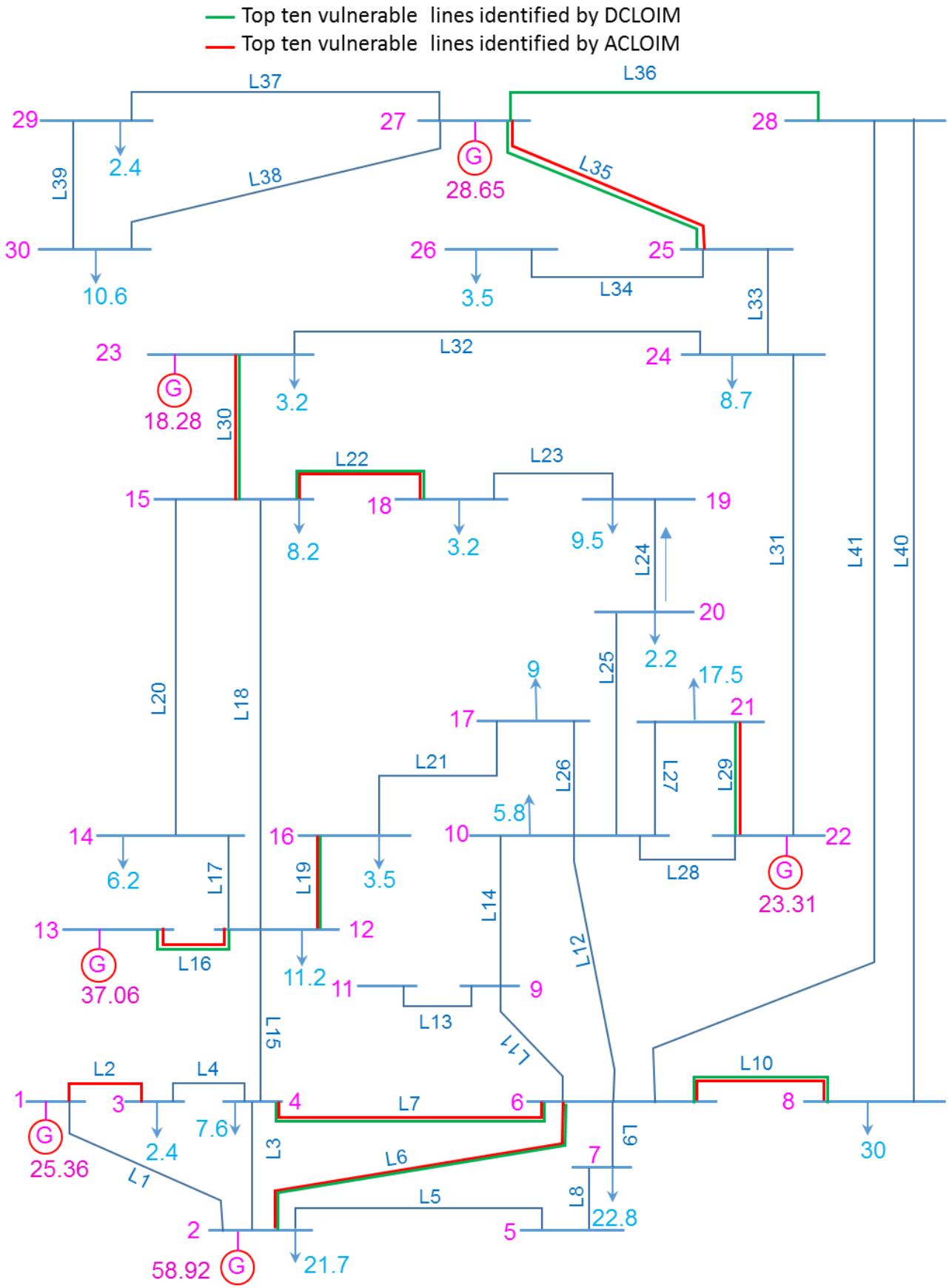

Figure IV.3. Top ten vulnerable lines of IEEE 30 bus system by DCLOIM and ACLOIM

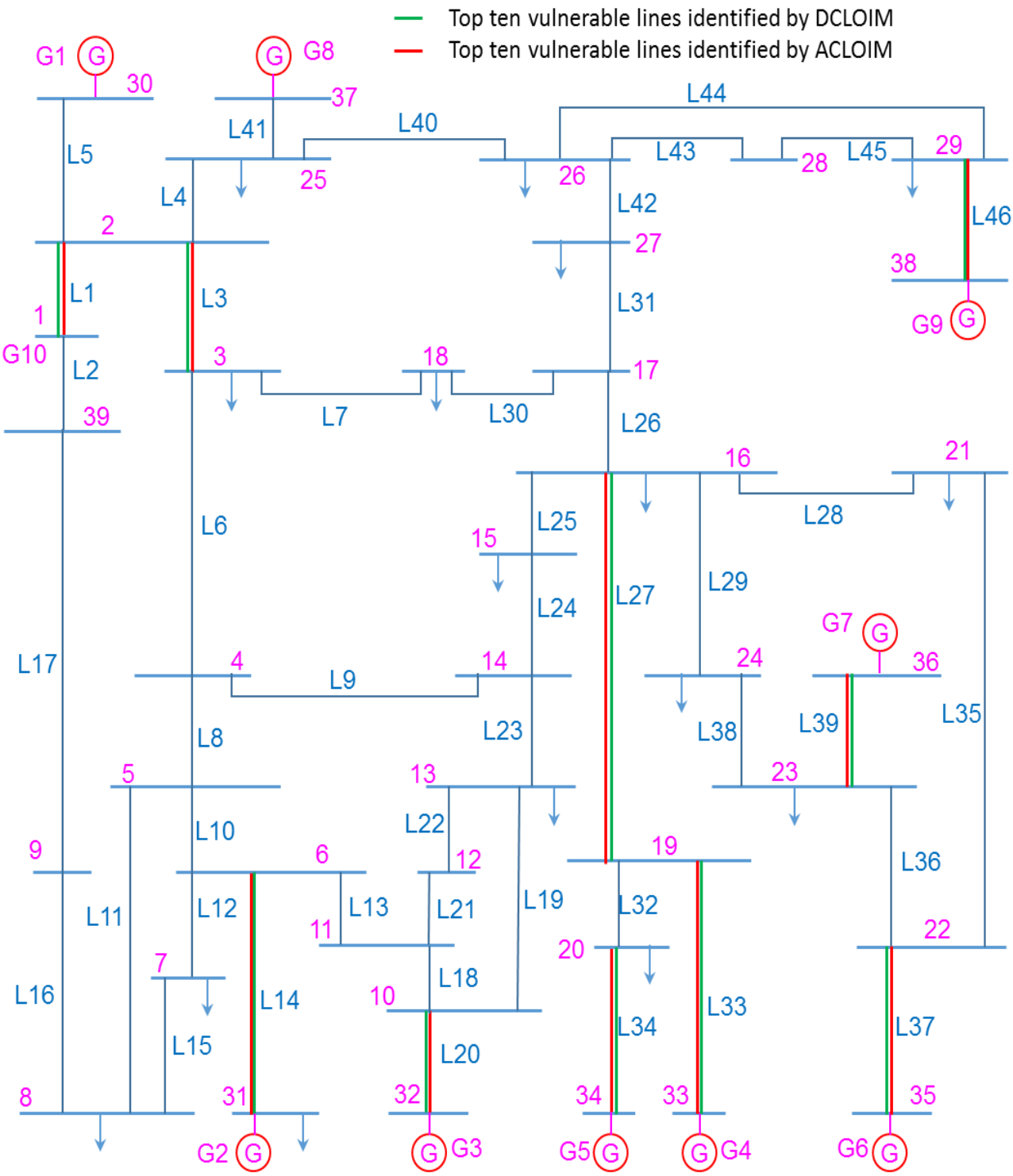

Figure IV.4. Top ten vulnerable lines of IEEE 39-bus system by DCLOIM and ACLOIM

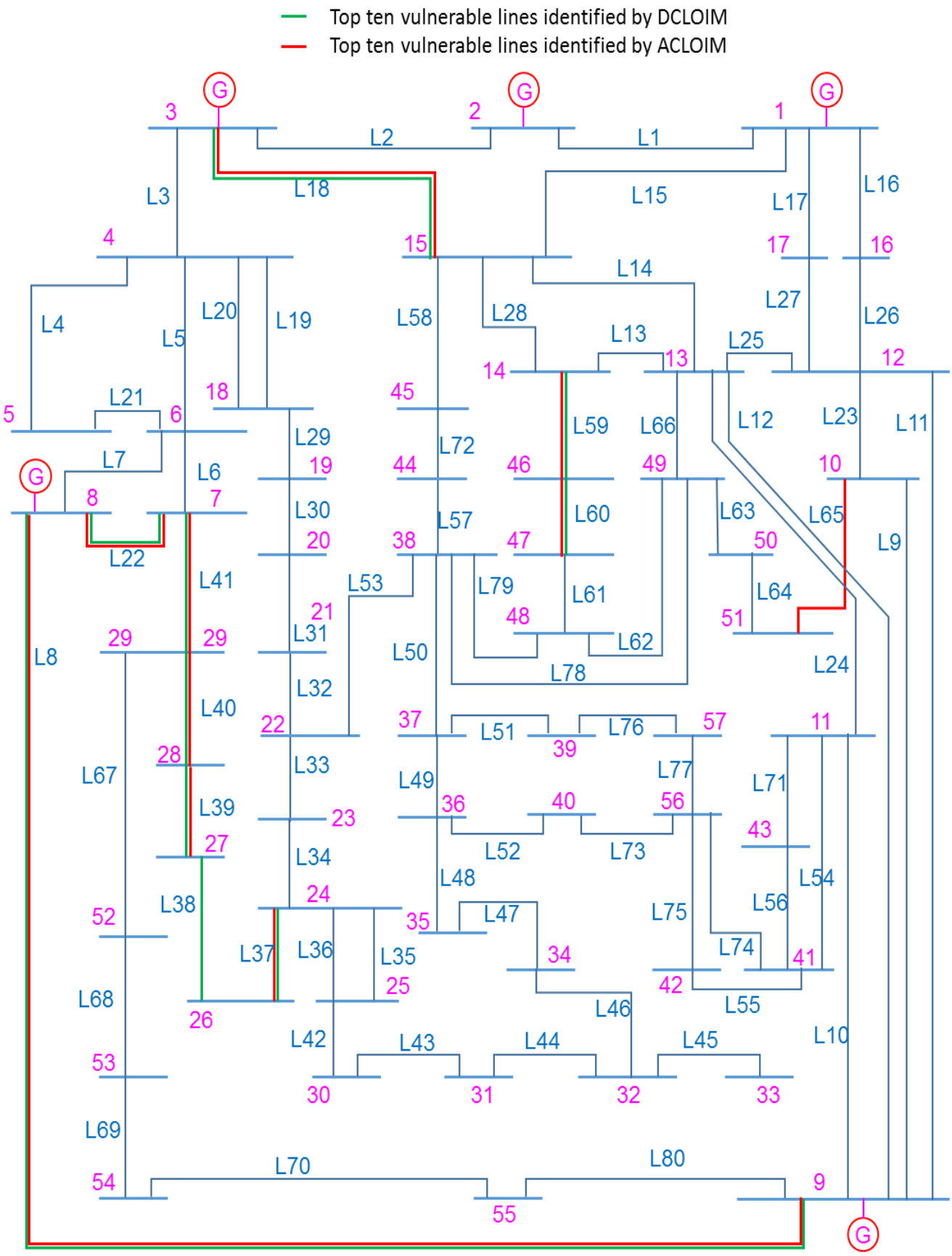

Figure IV.5. Top ten vulnerable lines of IEEE 57- bus system by DCLOIM and ACLOIM

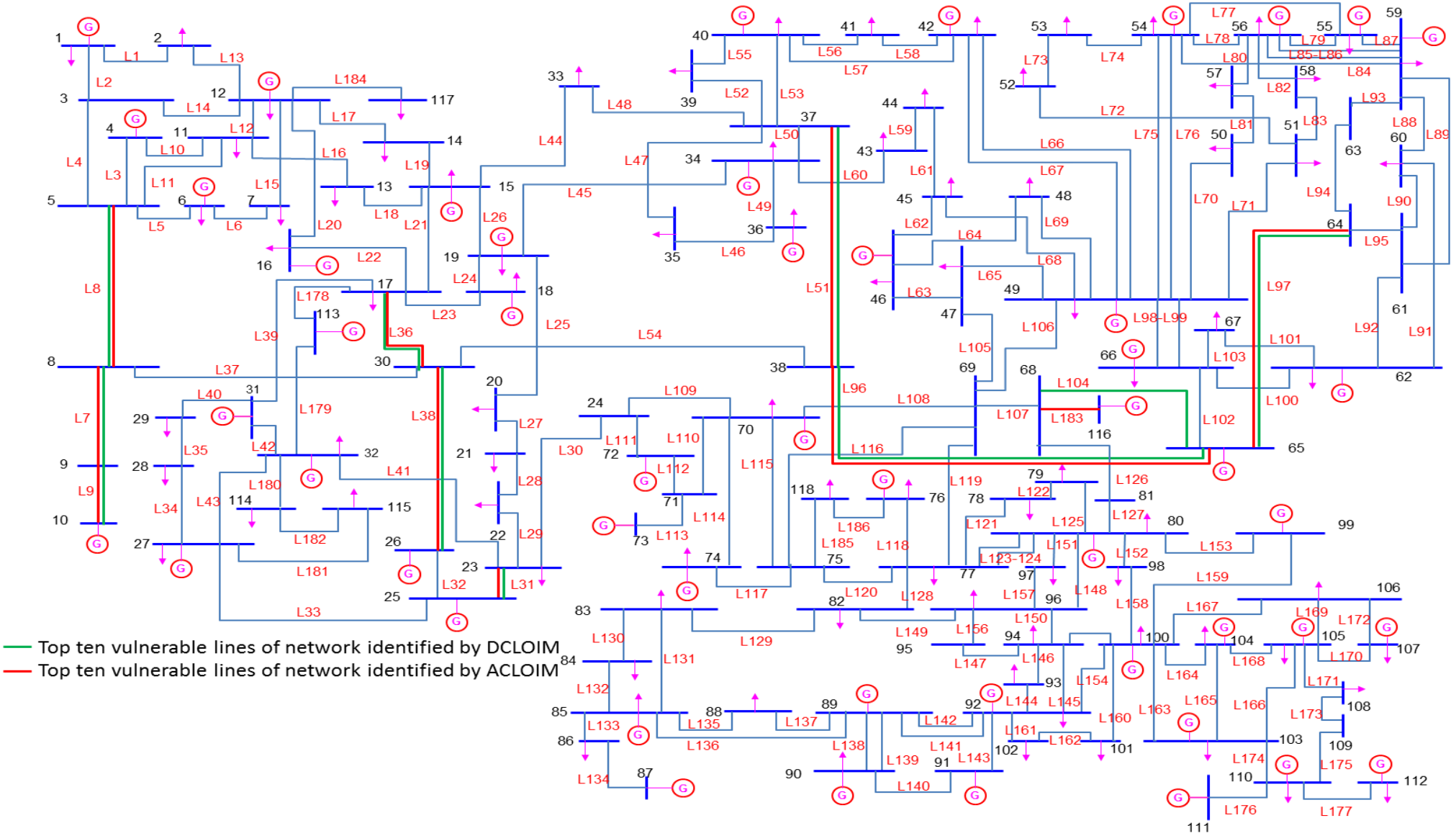

Figure IV.6. Top ten vulnerable lines of IEEE 118- bus system by DCLOIM and ACLOIM

IV.3 Applying DC network capacity reservation metric

Because, we focus only on single failures, IEEE 39-bus test is excluded from this application. Indeed, as previously mentioned in chapter 2 when applying ACNCRM to this test system, most of line outages initiate a cascade of disconnections of overloaded lines.

For the other three test systems, DC assumption provides again an ideal frame to assess with good accuracy system vulnerability as it is shown in table 4.6 and figures IV.7 to IV.9.

Unlike ACNCRM, DCNCRM is able to rank line L48 of the 57-bus test network as critical line, meaning it overcomes the disadvantages of AC power flow relative to the lack of convergence when severe contingencies are simulated.

Table 4.6 Comparison top ten critical lines identified by DCNCRM and ACNCRMM

IEEE 30-bus system			IEEE 57-bus system			IEEE 118-bus system		
Rank order	AC NCRM	DC NCRM	Rank order	AC NCRM	DC NCRM	Rank order	AC NCRM	DC NCRM
1	**36**	**36**	1	**8**	**8**	1	**8**	**8**
2	**19**	**19**	2	**41**	**41**	2	**7**	**7**
3	**10**	**38**	3	**50**	**48**	3	**9**	**38**
4	**38**	**10**	4	**49**	**49**	4	**51**	**51**
5	**29**	**16**	5	**40**	**50**	5	**38**	**9**
6	**22**	**22**	6	**65**	**40**	6	**36**	**36**
7	**16**	**30**	7	**39**	**65**	7	**96**	**33**
8	**30**	**17**	8	**47**	**39**	8	**33**	**97**
9	**17**	**29**	9	**46**	**10**	9	**97**	**37**
10	**40**	**40**	10	**17**	**17**	10	**21**	**96**

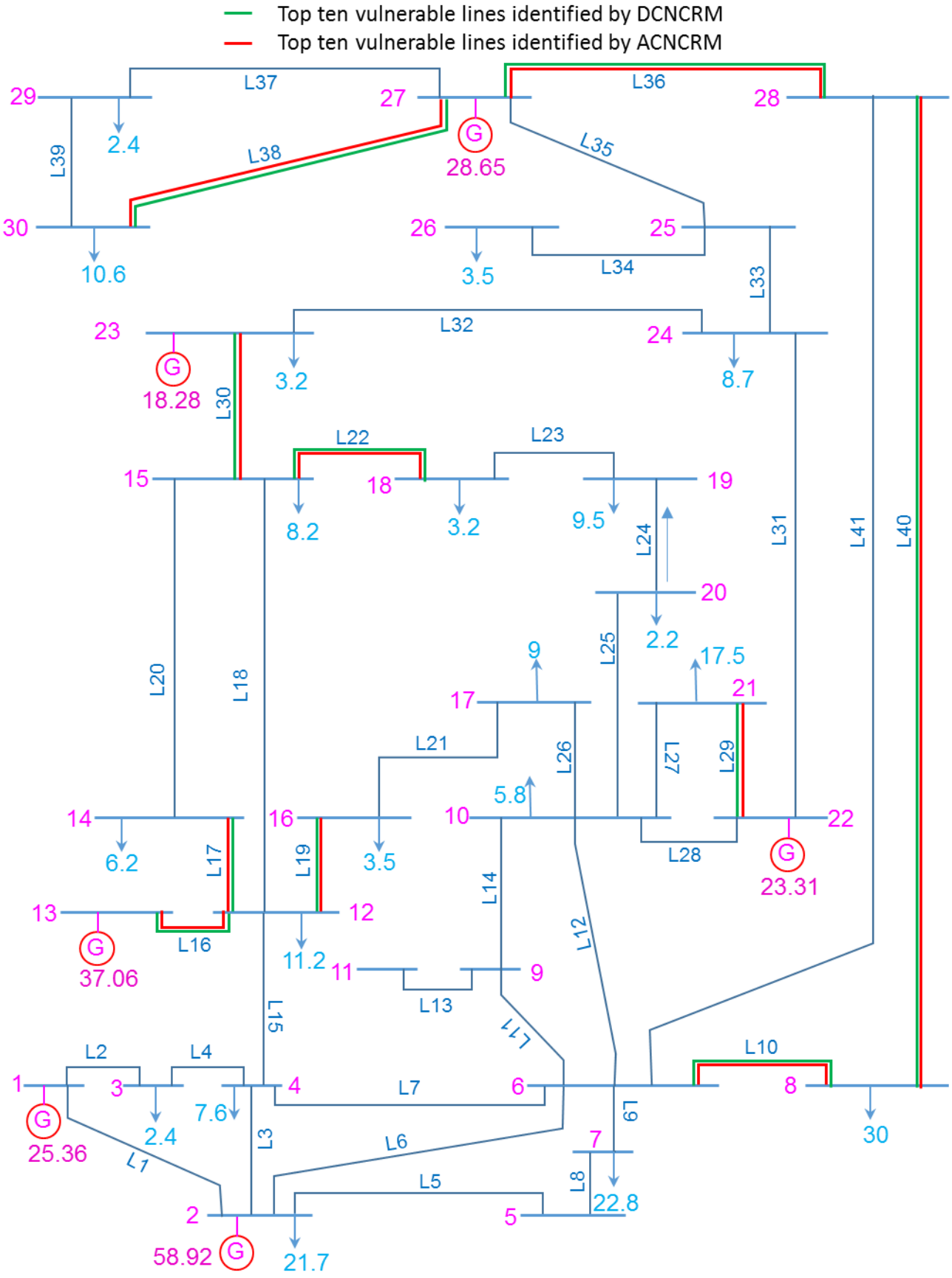

Figure IV.7. Top ten vulnerable lines of IEEE 30 bus system by DCNCRM and ACNCRM

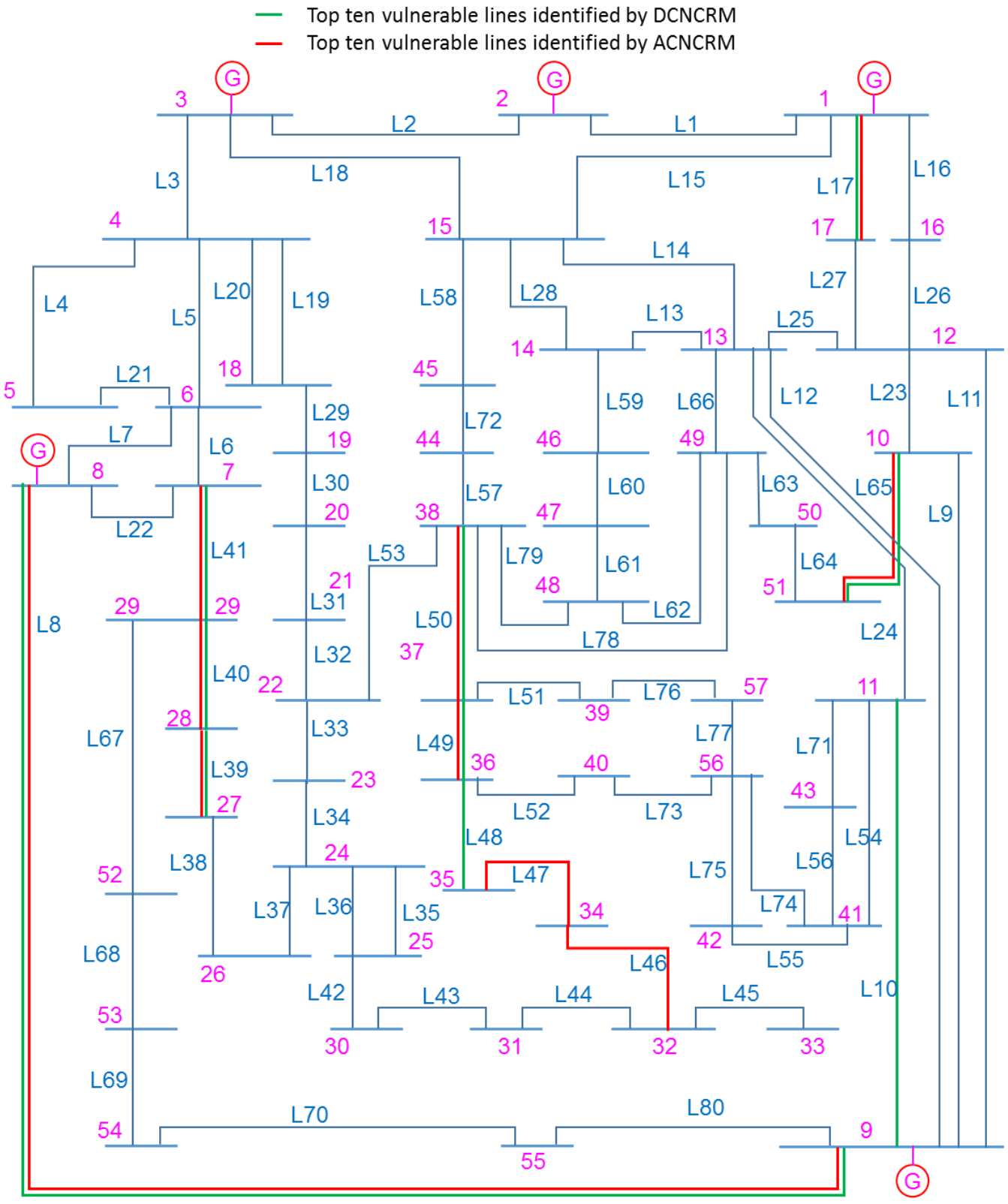

Figure IV.8. Top ten vulnerable lines of IEEE 57- bus system by DCNCRM and ACNCRM

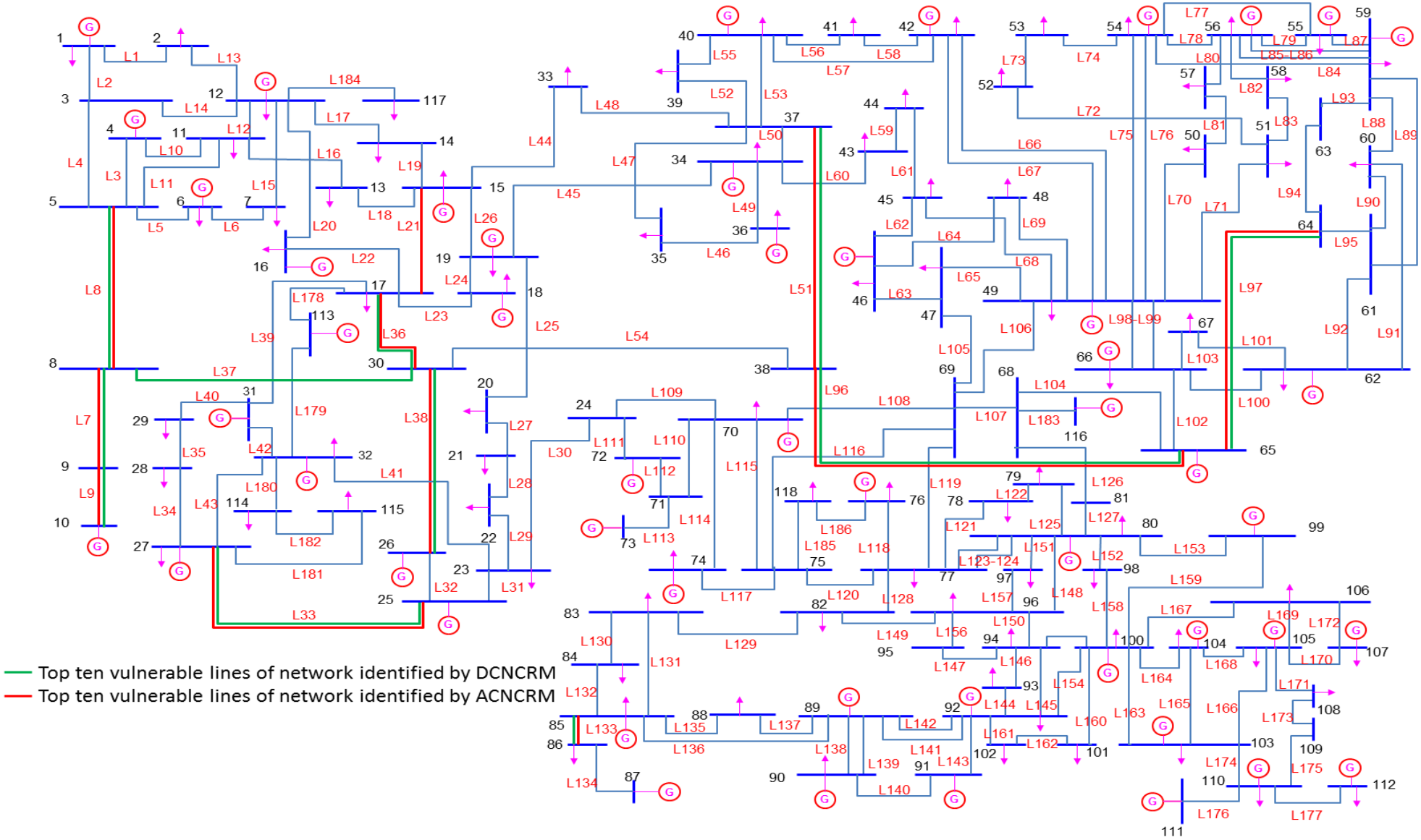

Figure IV.9. Top ten vulnerable lines of IEEE 118- bus system by DCNCRM and ACNCRIM

V. Conclusion

DCLOIM and DCNCRM are able to measure the vulnerability of power grids. These metrics are based on PTDF (Power Transfer Distribution Factor) matrix which is turn is based on Laplacian matrix of the underlying graph of the test grids. For that reason, these metrics capture electrical characteristics of power grids and give a good approximation of the set of critical lines for system vulnerability.

However, these metrics only give a global view of system vulnerability. They do not enable power engineers to easily understand how some structural choices such as the geometry of the network, the location of generators and loads affect vulnerability. A new approach based on DC modeling, which has been proved to be a convenient mathematical frame, is necessary to carry on this task.

Chapter V. A new approach based on spectral solving of DC power flow.

I. Introduction

DC approximation of power flow equations leads to a simplified frame to assess vulnerability of power systems to line outages and makes a link between steady-state properties of the network and topology of the underlying graph. In DC power flow, graph Laplacian matrix (i.e. bus admittance matrix) is a key element expressing how power is transferred from generators to loads. For obvious reasons, power systems are far from being complete (not every pair of nodes is connected by a unique edge). Laplacian matrix is therefore sparse. But, despite its sparsity, it is not straightforward to conclude about system vulnerability from Laplacian matrix structure. In this chapter, we therefore propose an alternative approach based on spectral properties of Laplacian matrix. Power flow will be solved into the spectral domain of Laplacian matrix and some preliminaries results will be provided on the impact of spectral organization of the network on its vulnerability.

The chapter is organized as follows. In a first section, the eigendecomposition of Laplacian matrix will be explained. It will be used in the second section to solve power flow into the spectral domain. Spectral analysis of IEEE 30-bus and 118-bus networks will be done using this new spectral formulation.

II. Spectral graph theory

II.1 Eigenvalues and eigenvectors

Eigenvectors u_i and eigenvalues λ_i of a (N, N) square matrix L are vectors and scalars that satisfy the following equation:

$$L.u_i = \lambda_i.u_i \tag{V.1}$$

Equation (V.1) has a non-zero vector solution if and only if determinant of $(L - \lambda.I)$ is equal to 0. I is the identity matrix. The N roots λ of the characteristic equation $\det(L - \lambda.I) = 0$ are the N eigenvalues of L. The eigenspace of L associated with an eigenvalue λ is defined by the set of vectors u that satisfies equation (V.1).

Equation (V.1) can be rewritten in matrix form such as:

$$L.U = U.\Lambda \tag{V.2}$$

Where:

- Λ is a diagonal matrix whose diagonal elements are eigenvalues λ of the matrix L
- U is a square matrix whose columns are eigenvectors associated with eigenvalues.

Matrix L can be decomposed using U, its inverse and Λ. This decomposition is known as eigendecomposition and is expressed by [73] as:

$$L = U.\Lambda.U^{-1} \tag{V.3}$$

Because L is now similar to a diagonal matrix, it is said to be diagonalizable.

If L is nonsingular then its inverse is given by [74]:

$$L^{-1} = U.\Lambda^{-1}.U^{-1} \quad \text{(V.4)}$$

II.2 Some useful properties

For Hermitian matrices L (complex square matrices that are equal to their own conjugate transpose), eigenvalues are real and eigenvectors are orthogonal for distinct eigenvalues [75].

For Hermitian positive-definite matrices L (for all non-zero column vectors x, the scalar $x^{*T}Lx$ is real and positive where x^{*T} is the conjugate transpose of x) all the eigenvalues are positive.

The eigendecomposition of a Hermitian matrix is given by:

$$L = U.\Lambda.U^{*T} \quad \text{(V.5)}$$

U is an orthogonal matrix made of orthogonal eigenvectors and U^{*T} denotes its conjugate transpose.

Laplacian matrix is a real, symmetric and semi-definite-positive matrix. It is singular. Its eigenvalues are thus real and positive and they can be sorted out such that [76]:

$$\lambda_1 = 0 < \lambda_2 \leq \lambda_3 \leq \cdots \leq \lambda_N \quad \text{(V.6)}$$

Eigenvectors are orthogonal and can be used to constitute an eigenbasis of R^N. First eigenvector associated with the zero eigenvalue is such that $L.u_1 = 0$. It comes:

$${u_1}^T L.u_1 = 0 \quad \text{(V.7)}$$

By definition of the Laplacian matrix, this can be developed as:

$$\sum_{k,l} (u_1(k) - u_1(l))^2 = 0 \quad \text{(V.8)}$$

Where k and l denote neighboring nodes and $u_1(k)$ is the k-th entry of u_1. It comes that u_1 shall be populated entirely with the same value.

Eigenvectors being orthogonal, it turns that ${u_1}^T u_i = 0$ for any i different from 1. The sum of the entries of any eigenvector u_i ($i \neq 1$) is thus equal to zero.

III. Spectral solving of DC power flow

Under DC approximation, power flow equation can be expressed by:

$$P \approx L.\theta \quad \text{(V.9)}$$

P is a N-vector associated with nodal powers. θ is a N-vector giving nodal voltage phase angles. N is the number of nodes of the grid. L is Laplacian matrix of the underlying graph.

If P_j and θ_j are power and voltage phase angle associated with node j, P and θ are defined by:

$$P = \begin{bmatrix} P_1 \\ P_2 \\ \dots \\ P_N \end{bmatrix} \tag{V.10}$$

And:

$$\theta = \begin{bmatrix} \theta_1 \\ \theta_2 \\ \dots \\ \theta_N \end{bmatrix} \tag{V.11}$$

This natural way of writing nodal variables is associated to the standard basis of the nodal space of the graph. The natural basis is defined as a set of vectors $(v_1, v_2, \dots, v_N)$ where v_j is a column vector of size N associated to node *j*. Its components are all equal to zero except the j-th entry which is equal to 1. *P* is expressed in terms of standard basis elements by:

$$P = \sum_{j=1}^{N} P_j v_j \tag{V.12}$$

It is also possible to project nodal variables *P* and θ onto the orthogonal eigenvector basis associated with the Laplacian matrix of the graph. Then:

$$P = \sum_{i=1}^{N} p_i u_i \tag{V.13}$$

And:

$$\theta = \sum_{i=1}^{N} o_i u_i \tag{V.14}$$

Developing line by line these expressions, we obtain: $P_j = \sum_{i=1}^{N} p_i u_i(j)$ and $\theta_j = \sum_{i=1}^{N} o_i u_i(j)$. It follows that the j-th entry of eigenvector u_i is associated with node *j*.

Because power systems are balanced in steady-state operation:

$$\sum_{j=1}^{N} P_j = 0 \tag{V.15}$$

It comes:

$$\sum_{j=1}^{N} \sum_{i=1}^{N} p_i u_i(j) = 0 \tag{V.16}$$

Separating the first mode from the other elements:

$$p_1 \sum_{j=1}^{N} u_1(j) + \sum_{i=2}^{N} p_i \sum_{j=1}^{N} u_i(j) = 0 \tag{V.17}$$

Because the sum of the entries of any eigenvector, except the first one, is equal to zero, then:

$$p_1 \sum_{j=1}^{N} u_1(j) = 0 \tag{V.18}$$

It comes that $p_1 = 0$ if the system is balanced.

Now, coming back to power flow equation (V.9), we obtain in terms of eigenbasis elements:

$$\sum_{i=1}^{N} p_i u_i = L \sum_{i=1}^{N} o_i u_i \tag{V.19}$$

Due to eigenvector definition, it can be expressed by:

$$\sum_{i=1}^{N} p_i u_i = \sum_{i=1}^{N} o_i \lambda_i u_i \tag{V.20}$$

Then, using orthogonality of eigenvectors (for all *i, j>0*, $i \neq j$, ${u_i}^T u_j = 0$), this is equivalent to:

$$p_i = \lambda_i o_i \tag{V.21}$$

The computation of phase angle coefficients o_i is straightforward. For all *i>1*, $\lambda_i \neq 0$ and:

$$o_i = \frac{p_i}{\lambda_i} \tag{V.22}$$

For *i=1*, o_1 is undetermined. Actually, its value refers to the choice of the reference phase angle. For simplification purpose, o_1 is chosen to be zero.

The former equation gives a simple relation between the power distribution of generators and loads described by $p_1$and the phase angles of the voltages described by o_1. It is therefore possible to simplify the analysis of power systems by evaluating N independent modal response (equation V.22) instead of considering the full (*N* x *N*) system described by *L*. This is a fundamental result due to orthogonality of eigenvectors and diagonalization of Laplacian matrix.

Power flow through transmission lines of the grid can be expressed by:

$$P_L = Y_{br}.K.\theta \tag{V.23}$$

Where, P_L is a column vector made by the assemblage of branch power flows. *K* is the link-node incidence matrix. It can be considered as the discrete gradient and is usually noted ∇ [77].

For instance, the discrete gradient of a simple graph connected in wye as shown in figure V.1. is:

$$\nabla = \begin{bmatrix} 1 & -1 & 0 & 0 \\ 0 & 1 & -1 & 0 \\ 0 & 1 & 0 & -1 \end{bmatrix} \quad \text{(V.24)}$$

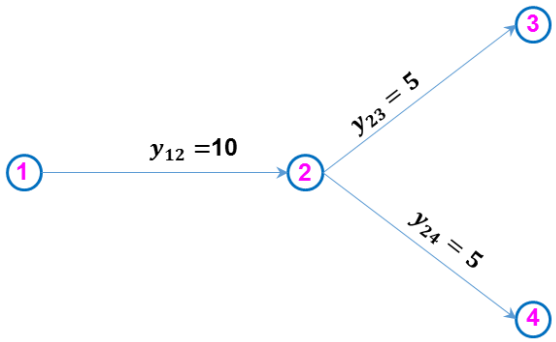

Figure V.1. The directed graph representing a power grid connected in wye. The lines are arbitrarily oriented.

Eigenvectors of this graph are:

$$U = \begin{bmatrix} 0.5000 & 0.0000 & -0.7257 & -0.4727 \\ 0.5000 & 0.0000 & -0.2037 & 0.8417 \\ 0.5000 & 0.7071 & 0.4647 & -0.1845 \\ 0.5000 & -0.7071 & 0.4647 & -0.1845 \end{bmatrix} \quad \text{(V.25)}$$

All the components of the eigenvector relative to mode 1 are equal as already mentioned. The components of the other eigenvectors are plotted in the following figures. Positive values are represented by ascending arrows while negative values are shown by descending arrows. Each corresponding discrete gradient is given just after each figure.

For each mode, there is a straightforward link between the eigenvector components and the nodal power injection. Power injection to node j in mode i is indeed determined from the following equation:

$$p_i(a) = p_i . u_i(a) \quad \text{(V.26)}$$

Now, we consider that the basic circuit in figure V.1 supplies 310 MW to loads in every mode. According to the link between eigenvector components and nodal powers, the power injections are graphically represented in figures V.2 to V.4, respectively in mode 2 to mode 4. As it can be seen from these figures, eigenvectors (and therefore nodal power injections) are organized in nodal domains. A nodal domain is defined as a connected subset of nodes where eigenvectors (nodal power injection) have the same sign. According to Courant–Fischer–Weyl theorem, the number of nodal domains of the mode k^{th} is no larger than k.

Mode 2:

$$\nabla u_2 = \begin{bmatrix} 1 & -1 & 0 & 0 \\ 0 & 1 & -1 & 0 \\ 0 & 1 & 0 & -1 \end{bmatrix} \begin{bmatrix} u_{12} \\ u_{22} \\ u_{32} \\ u_{42} \end{bmatrix} = \begin{bmatrix} u_{12} - u_{22} \\ u_{22} - u_{32} \\ u_{22} - u_{42} \end{bmatrix} = \begin{bmatrix} 0 \\ -0.7071 \\ 0.7071 \end{bmatrix} \quad \text{(V.27)}$$

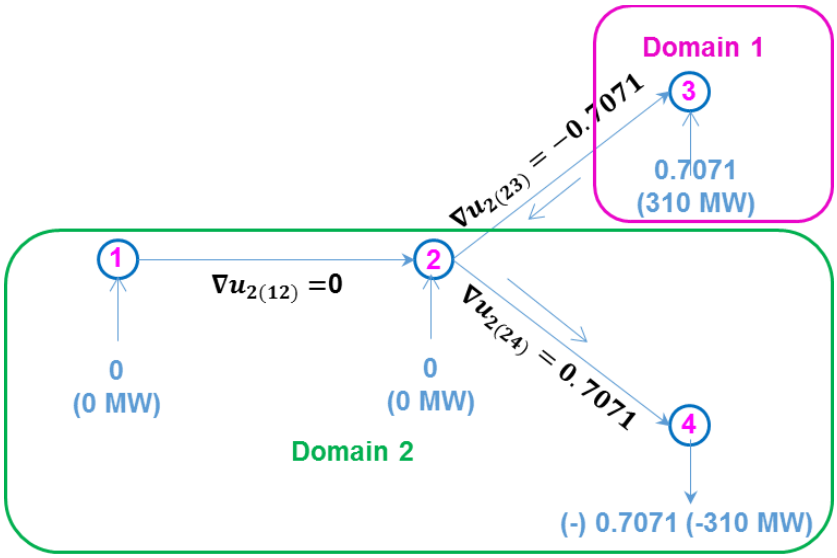

Figure V.2. Schematic representation of eigenvector components corresponding to mode 2

Mode 3:

$$\nabla u_3 = \begin{bmatrix} 1 & -1 & 0 & 0 \\ 0 & 1 & -1 & 0 \\ 0 & 1 & 0 & -1 \end{bmatrix} \begin{bmatrix} u_{13} \\ u_{23} \\ u_{33} \\ u_{43} \end{bmatrix} = \begin{bmatrix} u_{13} - u_{23} \\ u_{23} - u_{33} \\ u_{23} - u_{43} \end{bmatrix} = \begin{bmatrix} -0.5219 \\ -0.6685 \\ -0.6685 \end{bmatrix} \quad \text{(V.28)}$$

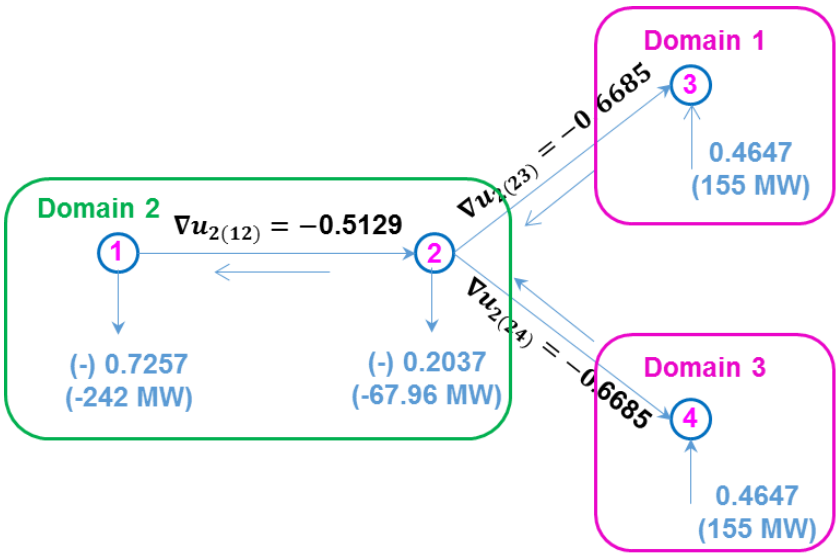

Figure V.3. Schematic representation of eigenvector components corresponding to mode 3

Mode 4:

$$\nabla u_4 = \begin{bmatrix} 1 & -1 & 0 & 0 \\ 0 & 1 & -1 & 0 \\ 0 & 1 & 0 & -1 \end{bmatrix} \begin{bmatrix} u_{14} \\ u_{24} \\ u_{34} \\ u_{44} \end{bmatrix} = \begin{bmatrix} u_{14} - u_{24} \\ u_{24} - u_{34} \\ u_{24} - u_{44} \end{bmatrix} = \begin{bmatrix} -1.3144 \\ 1.0262 \\ 1.0262 \end{bmatrix} \quad \text{(V.29)}$$

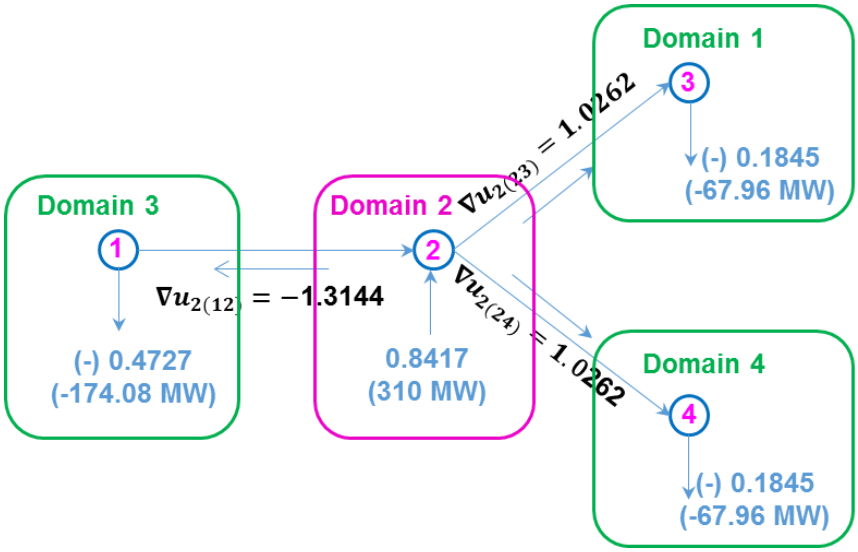

Figure V.4. Schematic representation of eigenvector components corresponding to mode 4

The nodal domains and the discrete gradients of eigenvector components have some consequences on the power flowing through the lines. Indeed, according to equations V.14, V.22 and V.23:

$$P_L = Y_{br}\left[\frac{p_2}{\lambda_2}.\nabla u_2 + \frac{p_3}{\lambda_3}.\nabla u_3 + \cdots + \frac{p_n}{\lambda_n}.\nabla u_n\right] \quad \text{(V.30)}$$

It comes that powers transmitted through the lines depend on series reactances, spectral decomposition of nodal powers, eigenvalues and discrete gradient of eigenvectors. It can be easily seen from the simple equation (V.30) that:

- Due to the sorting order of eigenvalues, lines power flow should be dominated by the lowest modes, meaning the lowest eigenvalues and their corresponding eigenvectors.
- There is more power flowing through lines connecting nodes with a large difference between their associated eigenvector components i.e. at the borders or closed to the borders between nodal domains.
- Instead of analyzing distribution of line powers in the standard basis associated with the nodes, it is possible to analyze power flows in terms of the eigenbasis elements. It is a great simplification for power engineering. Indeed, the modes are pairwise independent and line powers results from a linear combination of every modal component. Such analysis will now be carried out for two IEEE test systems.

IV. Spectral analysis of IEEE 30-bus and 118-bus systems

IV.1 IEEE 30-bus network

Using equation V.30, maximal value of transmitted power through lines for each mode is calculated and reported in Figure V.5. Obviously, there is no power transmitted on mode 1. Otherwise, it would have meant that network power is not balanced. Maximal values vary significantly and a further investigation of modal components is required. Four modes will be detailed. The 2nd and 29th ones are two extreme modes that lead to a high value of maximal transmitted power. In the intermediate range, the 11th and 13th mode will be detailed because they give two opposite results for the maximal power.

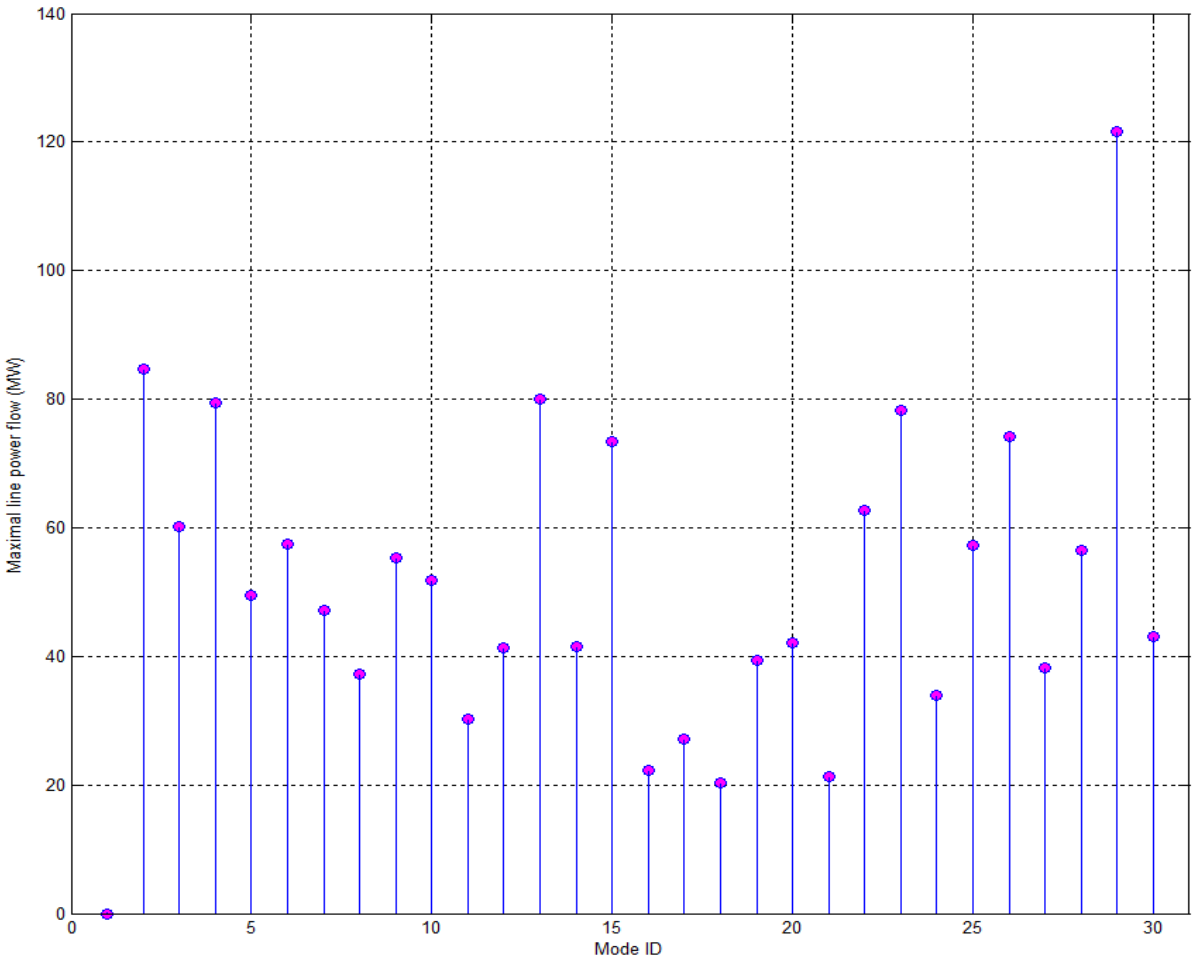

Figure V.5. Maximal power transfer through transmission lines in every mode

Mode 2

Only the second component of line power ($Y_{br}\left[\frac{p_2}{\lambda_2}.\nabla u_2\right]$) is now studied. It is a column vector. Every entry is associated to a branch of the network. Their value is plotted in Figure V.6. They are reported on the network diagram in Figure V.7. The most significant values, above 60 MW, are shown in red.

To better understand how the system is organized in this mode, the second component of nodal power ($p_2 u_2$) is also plotted in this figure. Positive values are shown by ascending pink arrows while

negative values withdrawn from the nodes are shown by descending blue arrows. It appears two nodal domains. These domains are defined as follows. Two nodes belong to the same domain if their associated eigenvector components have the same sign. It shall be noted that the number of nodal domains is predicted by Courant's theorem [77].

The highest value of line power is encountered at the border between positive and negative domains. It is situated on line L36 connecting nodes 27 and 28. Indeed, the discrete gradient of the second eigenvector between these two nodes is very high. On node 27, eigenvector component is negative and equal to -25.84 and on node 28, it is +0.57. This high value of discrete gradient explains also why L33, a line closed to the border between the domains, carries a lot of power. But, it is worth noticing that L41 (between nodes 6 and 28) is carrying a lot of power even if there is not a significant difference between the eigenvector components. Indeed, not only the spectral behavior drives power flows but also series admittance Y_{br}. In that particular case, L41 admittance (16.67 p.u) is very high with respect to average admittance (4.98 p.u).

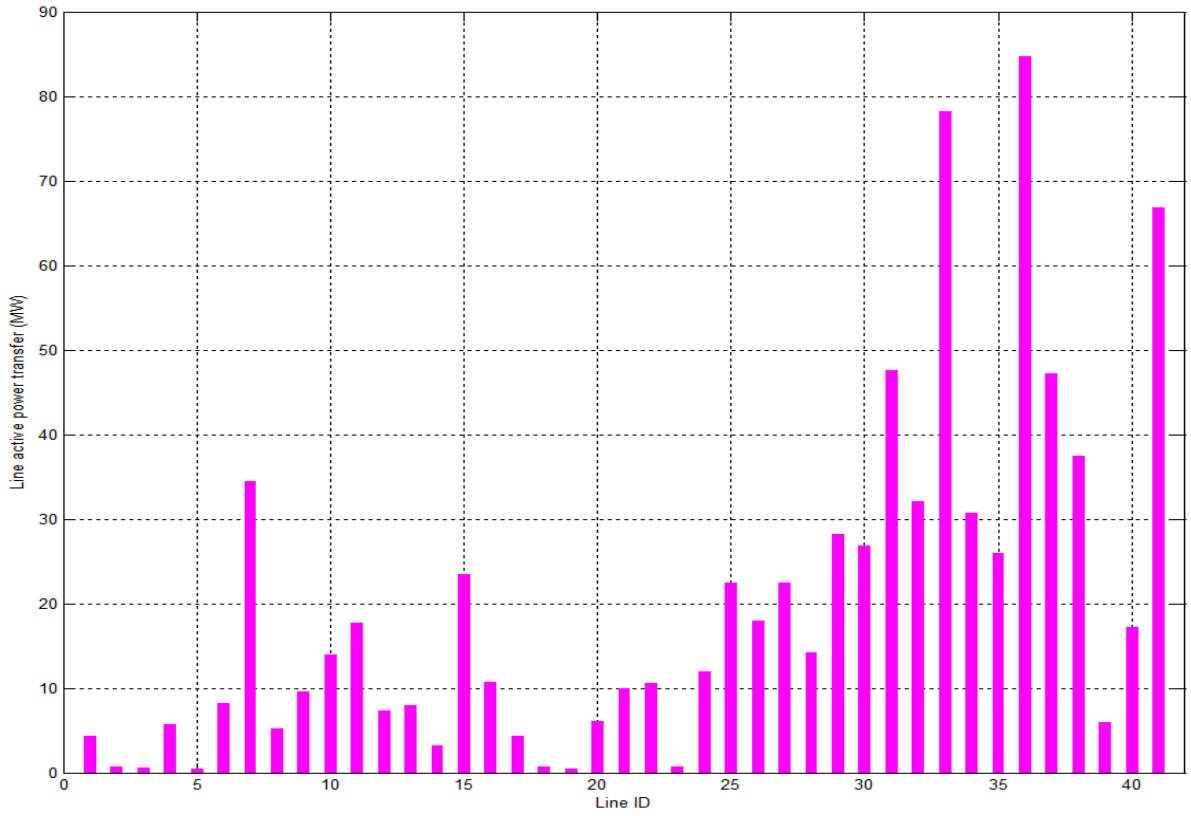

Figure V.6. Line power flow in mode 2

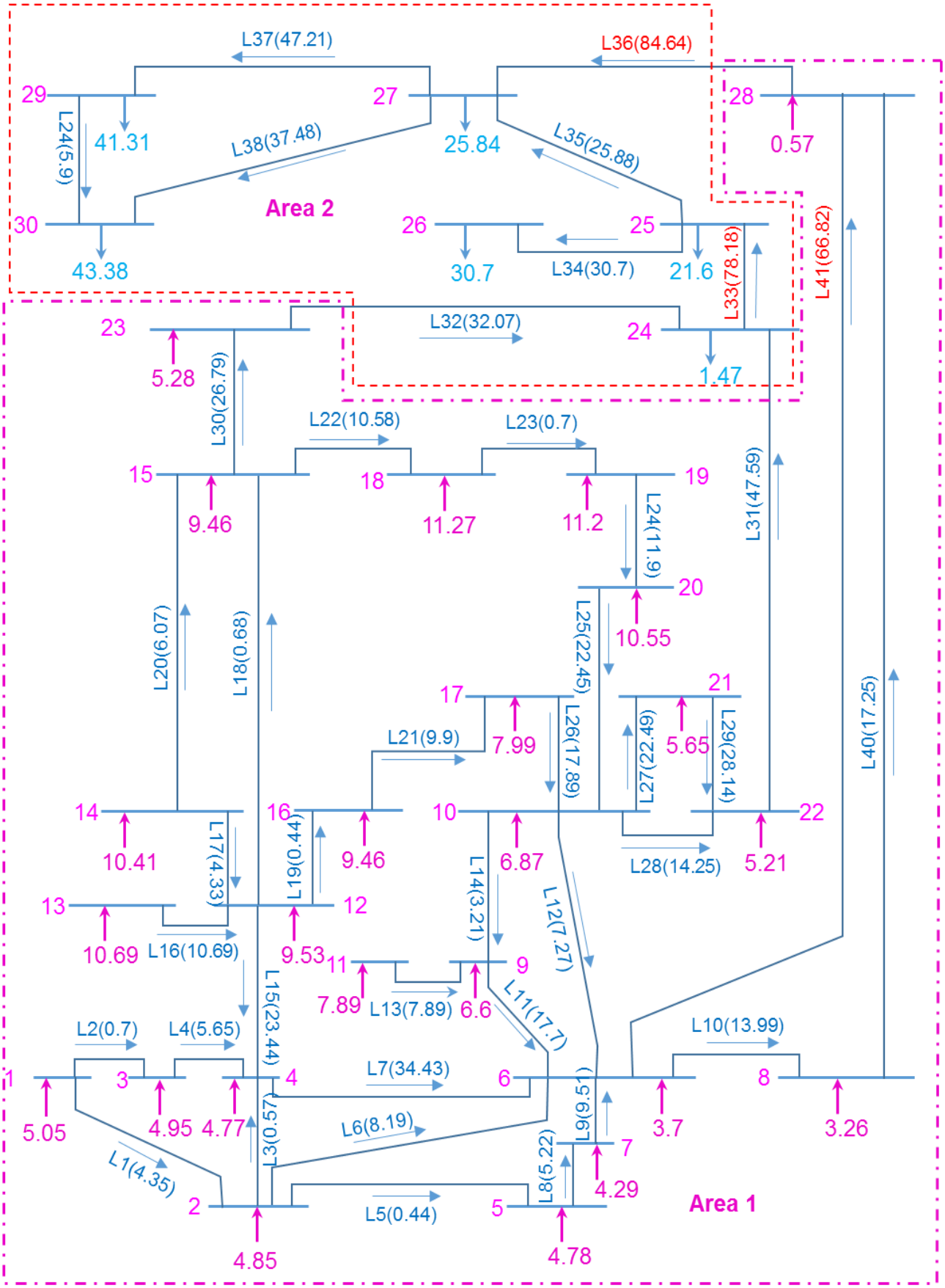

Figure V.7. Line power distribution in IEEE 30-bus network corresponding to mode 2

Mode 11

The number of nodal domains associated with $(p_{11}u_{11})$ increase while remaining below 11 as predicted by Courant's theorem. Figure V.9 shows seven domains. Because the sign of the domain indicates whether a domain is generating or consuming power, most of the power exchanges are concentrated at the borders between domains. Especially, the most loaded line (L16) is located at the border between domains 2 and 7.

But, in comparison with the second mode, due to the fragmentation of the network into several domains, in average, the lines are less loaded and the network should be less stressed and vulnerable (see Figure V.8).

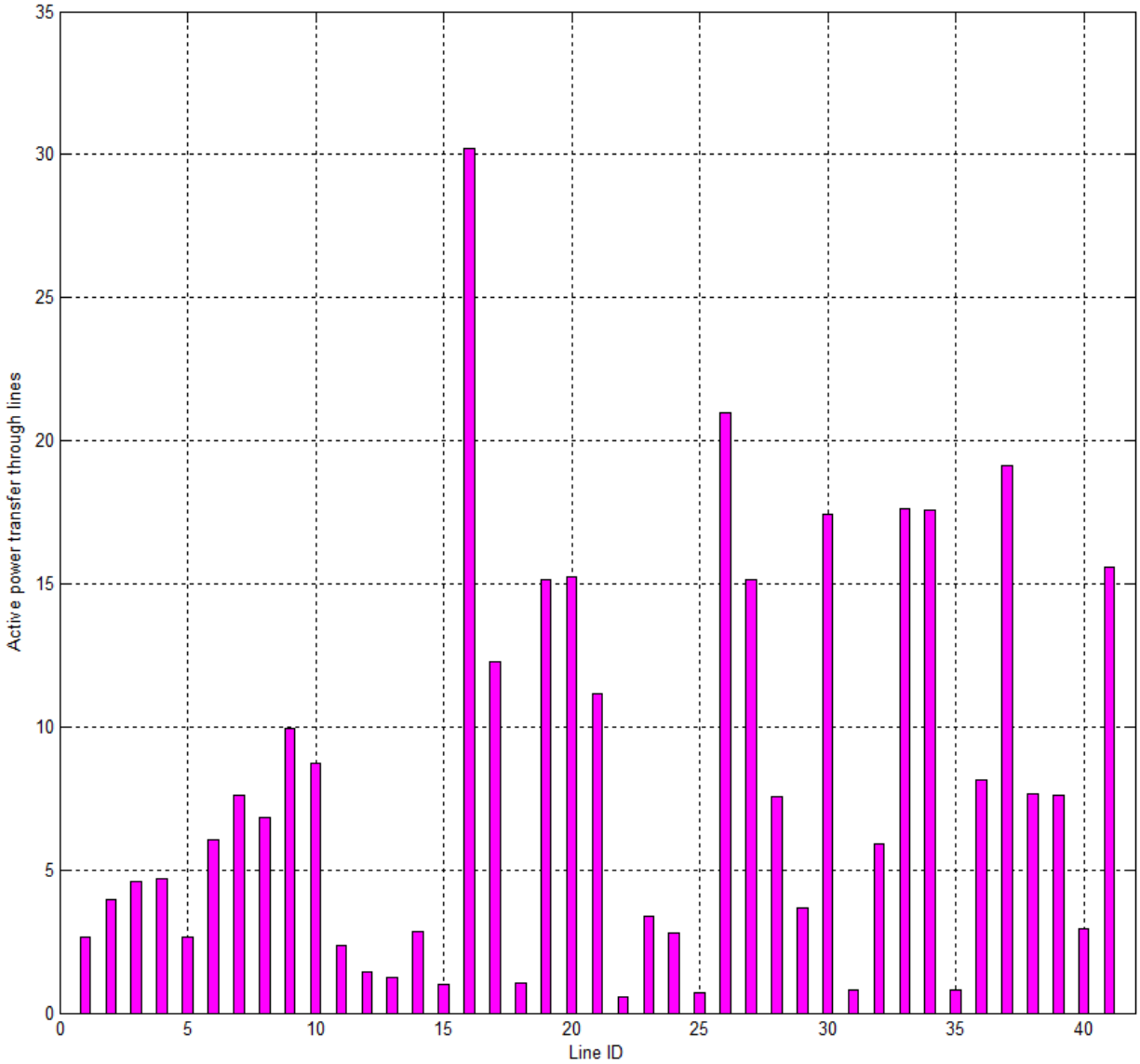

Figure V.8. Line power flow in mode 11

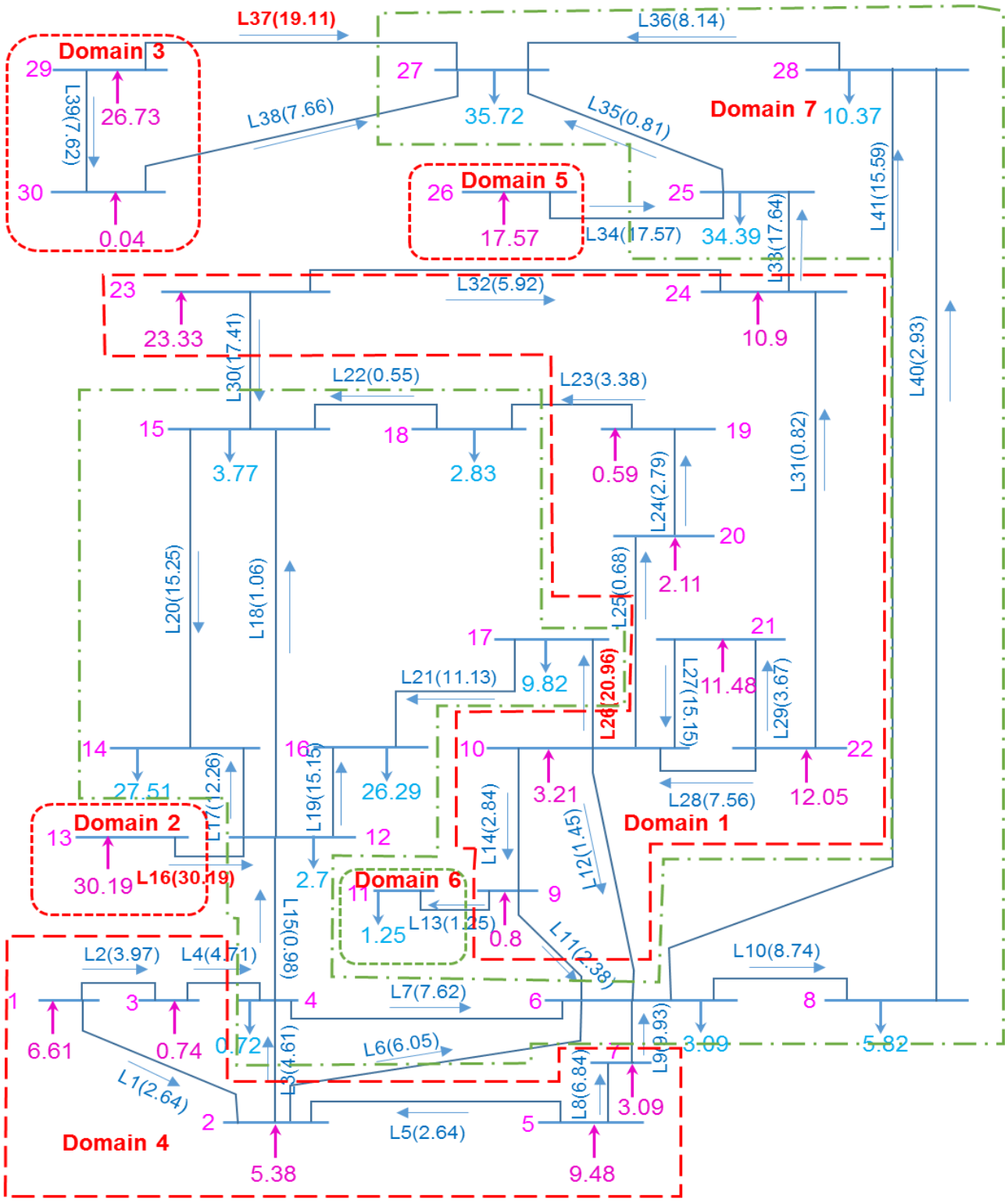

Figure V.9. Line power distribution in IEEE 30-bus network corresponding to mode 11

Mode 13

Surprisingly, this intermediate mode give opposite results to mode 11 and some lines are as stressed as in mode 2 (see Figure V.10). It appears in Figure V.11 that the nodal power is very localized on few nodes (in the range 1 to 9). As it can be shown in Figure V.12, it means that only domains 1 and 2 are active for the power transfer between generation and loads in this mode. The

other 8 domains are existing, but they embed few power. It turns that the lines interconnecting these two domains may be very loaded. This is a direct effect of the discrete gradient in equation V.24.

This is very similar to what happens for higher modes such as mode 29. Figures V.13 and V.14 show that power is much localized in domains 1 and 2 and transmitted power is concentrated on few lines.

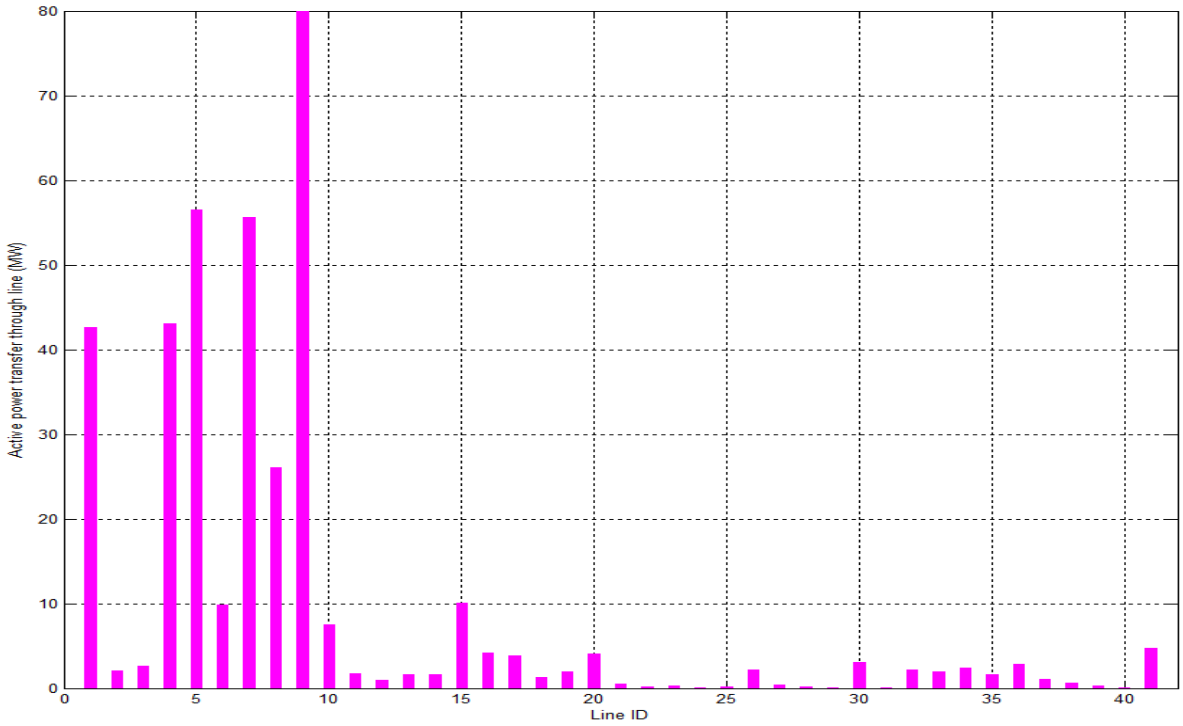

Figure V.10. Line power flow in mode 13

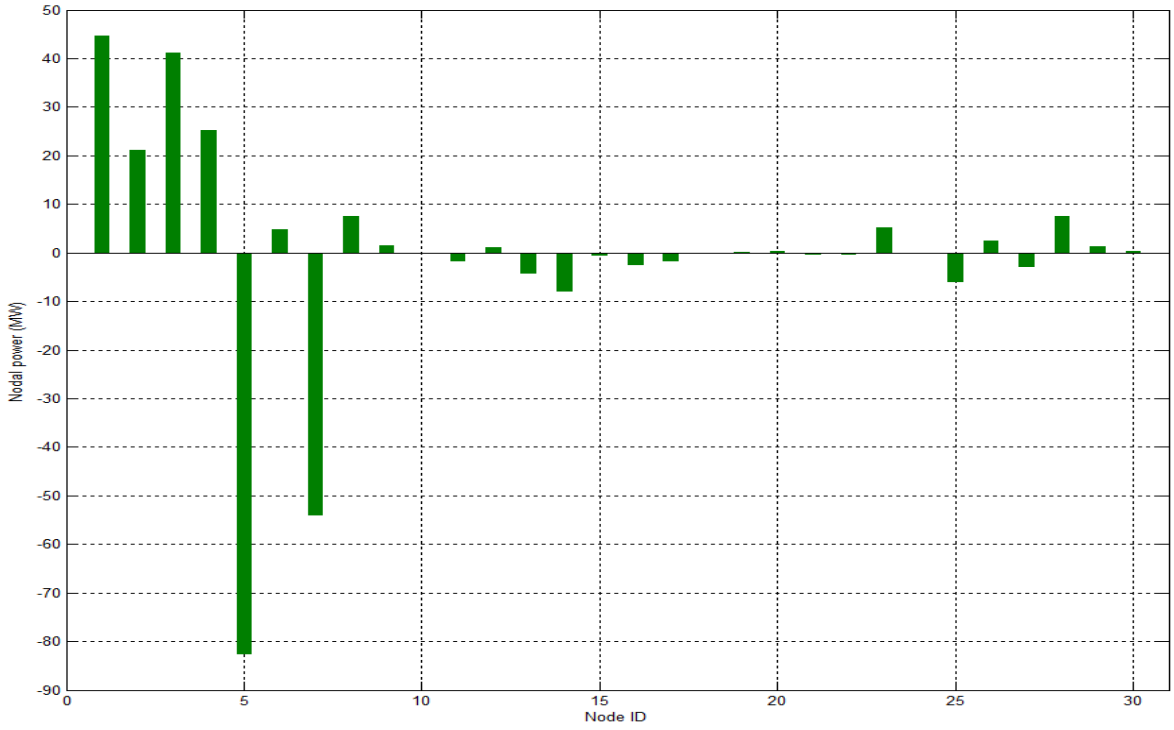

Figure V.11. Distribution of power injection of IEEE 30-bus test system corresponding to mode 13

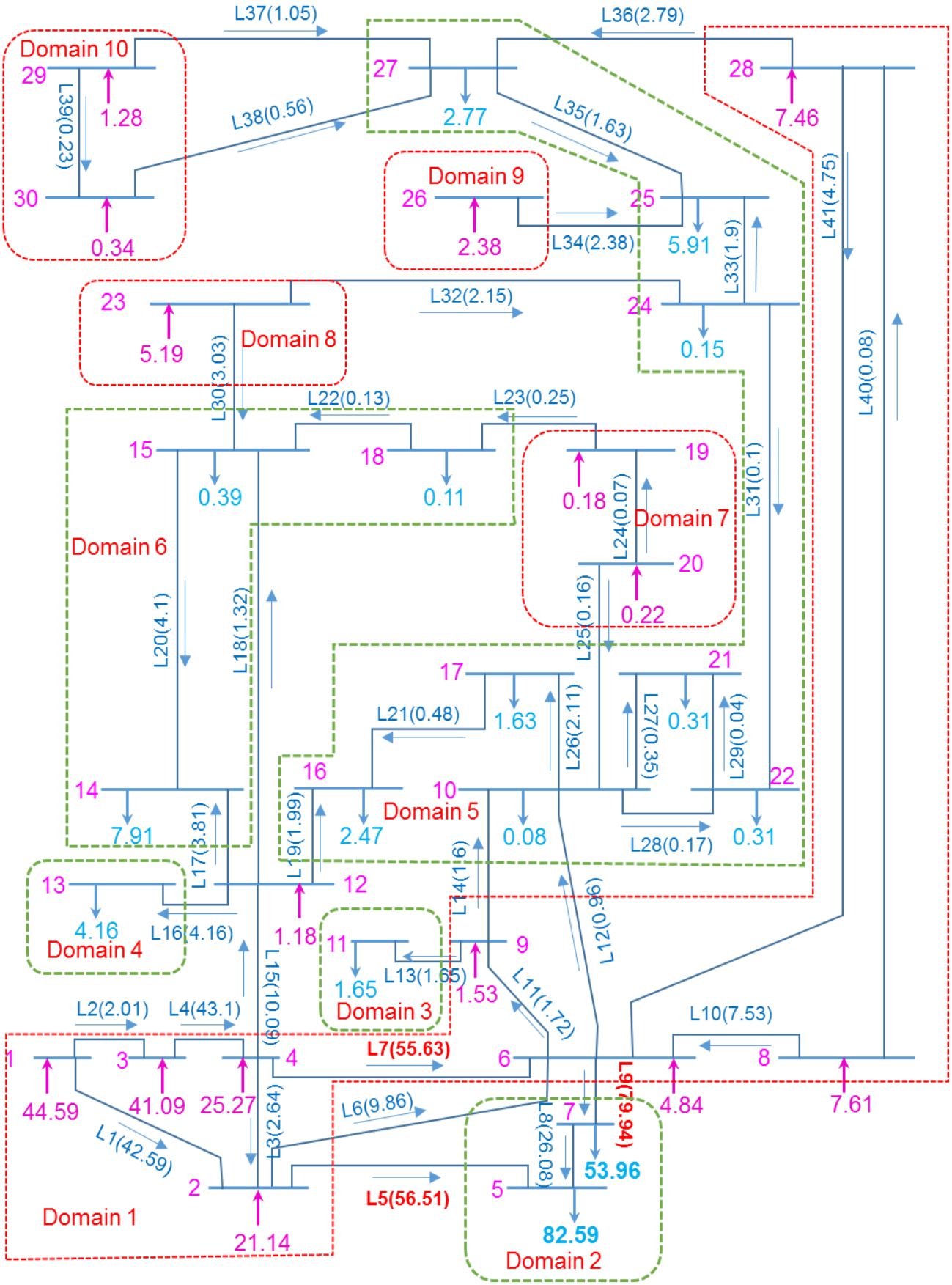

Figure V.12. Line power distribution in IEEE 30-bus network corresponding to mode 13

Mode 29

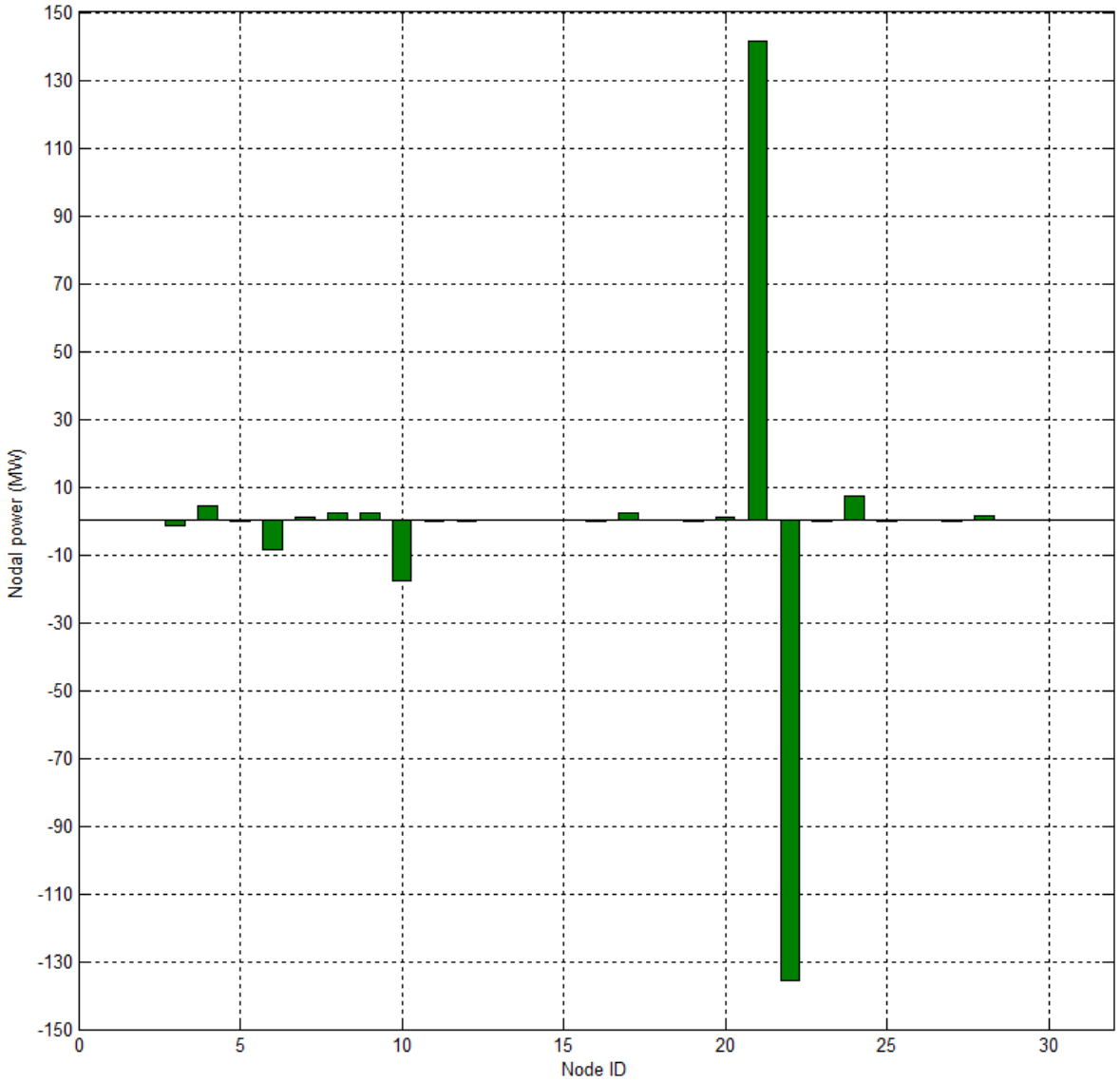

Figure V.13. Distribution of power injection of IEEE 30-bus test system corresponding to mode 29

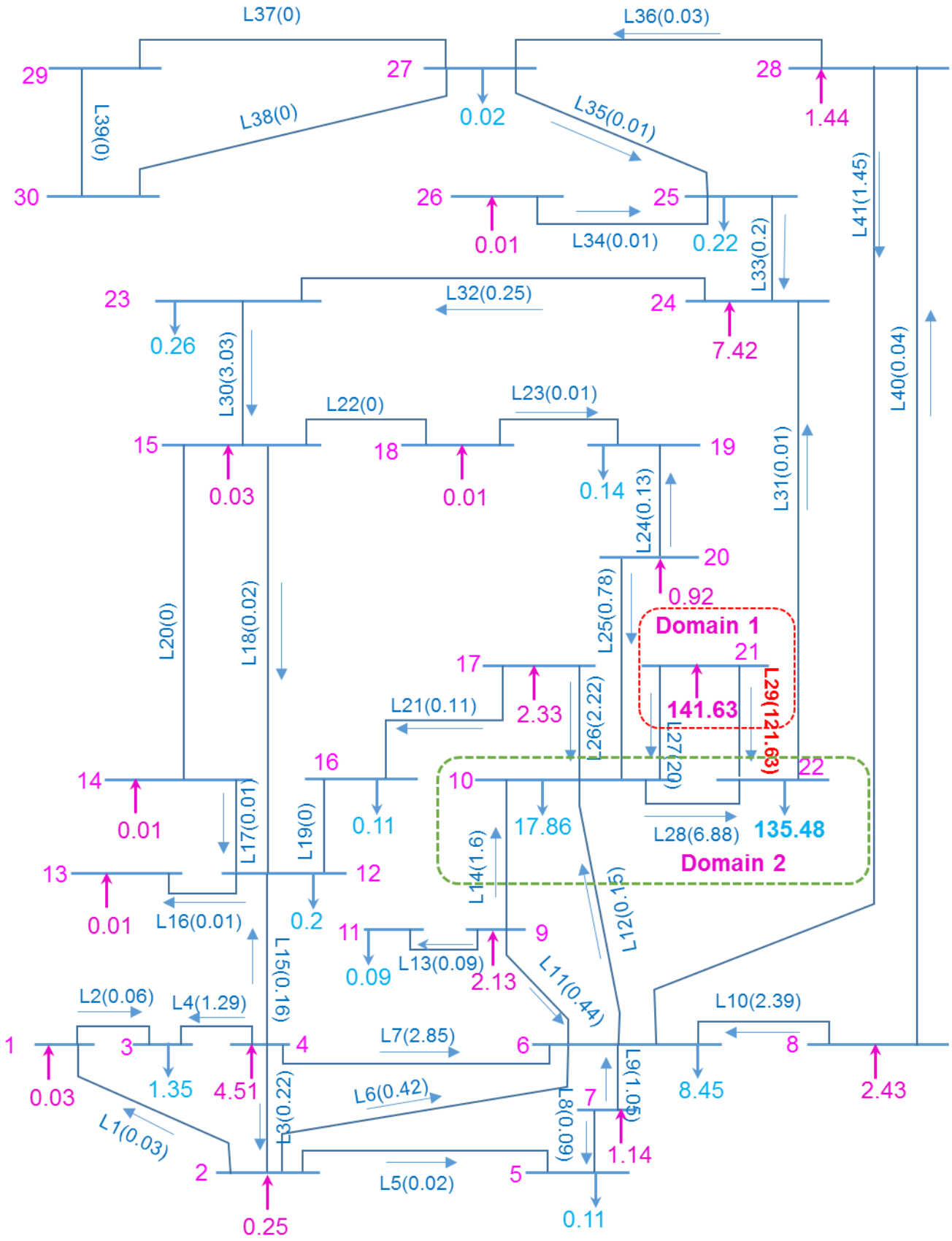

Figure V.14. Line power distribution in IEEE 30-bus network corresponding to mode 29

IV.2 IEEE 118-bus network

For a wider system, similar results are obtained. Figure V.15 shows that maximal power transfer occurs at lower modes or higher modes and at some specific intermediate modes. This can be explained by the spectral organization of the network and its nodal domains.

For lower modes, the number of nodal domains should be low as stated by Courant's theorem. It means that few large areas embed the total generation and load powers. Inter-area power flows are thus magnified and may stress the system, meaning increasing its vulnerability, the nodal domains of mode 2 in Figure V.16, for instance.

Then the number of nodal domains tends to increase with the rank of modes (see Figure V.17). Thus, generation and load powers are more and more distributed on every node. An extreme version is that every node becomes a nodal domain, being either generator or load (Courant's theorem predicts that for the IEEE-118 bus system, the maximal number of domains can be 118). Inter-domain power flows become very local and maximal power flows tend to decrease in average.

But for the highest modes, this value increases again. This sudden increase can be explained by the localization of the highest modes. It means that nodal power is concentrated on very few nodes and the lines between these nodes are very stressed (see Figure V.20). This also explains the relatively high value of maximal transmitted power for modes 62 and 111. They are localized modes as shown in Figure V.18 and Figure V.19.

The reasons why some modes are more localized than others are still to be discovered.

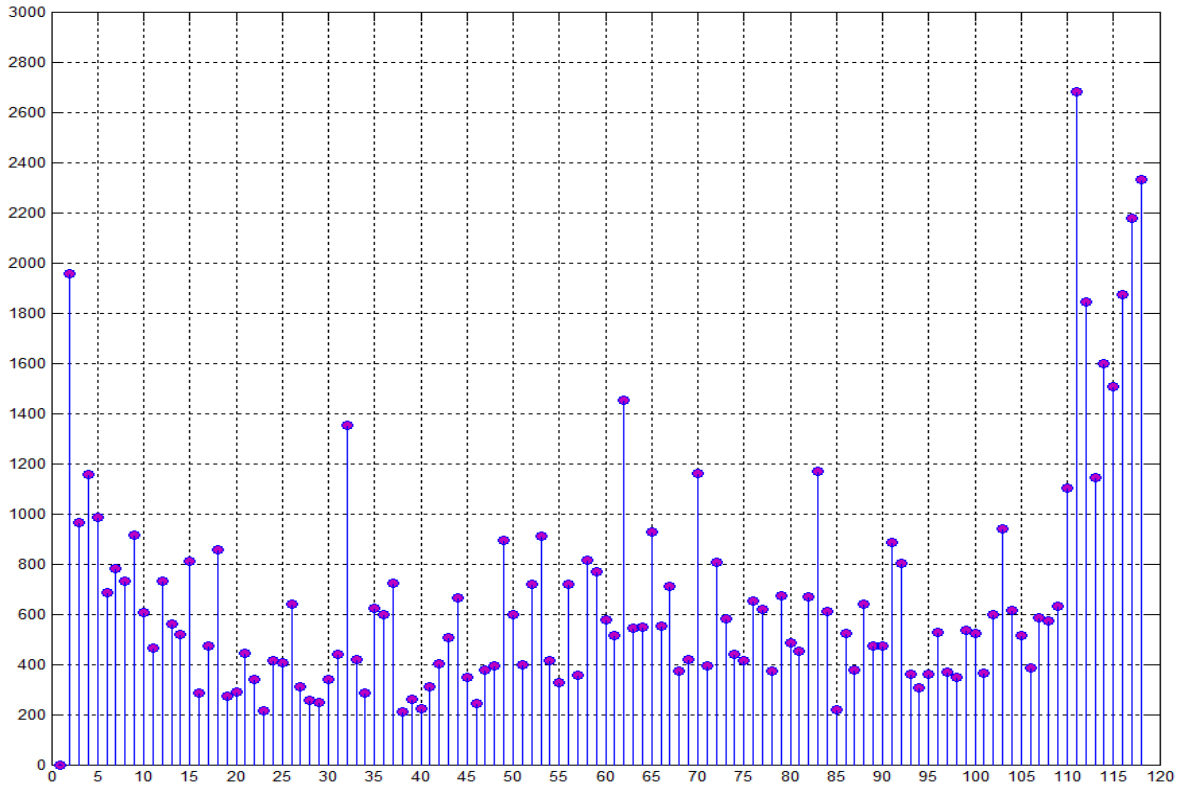

Figure V.15. Maximal power transfer through transmission lines in every mode

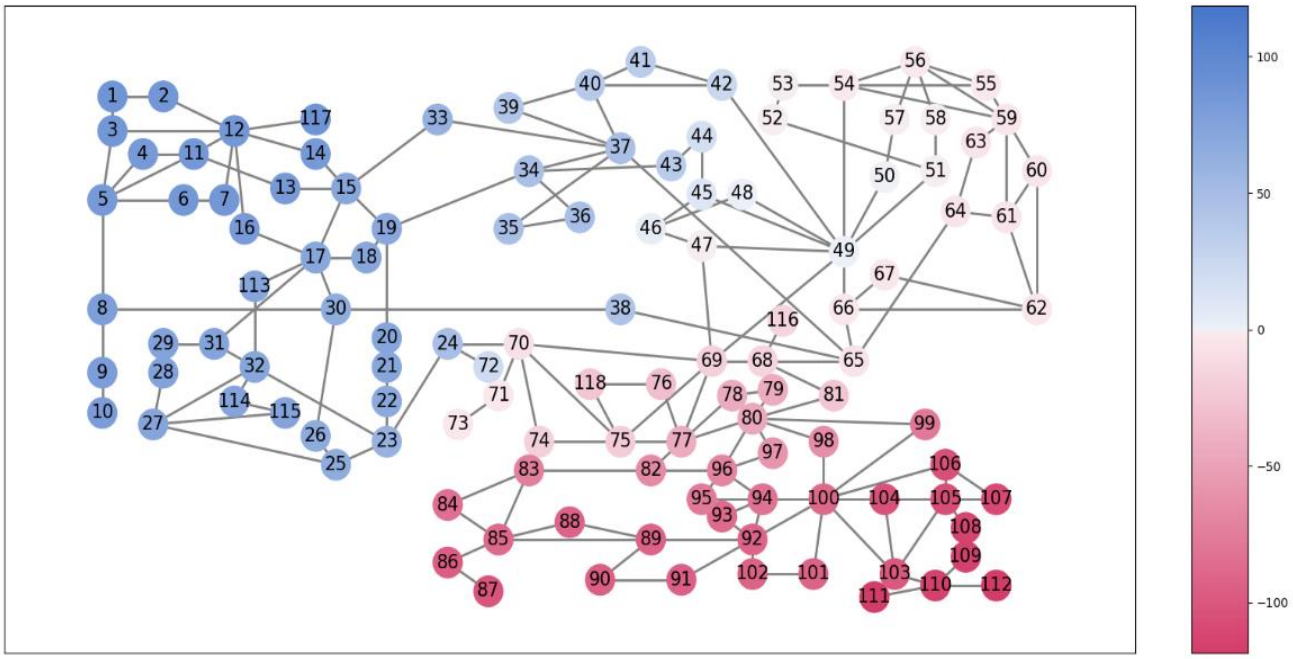

Figure V.16. Nodal domains of mode 2

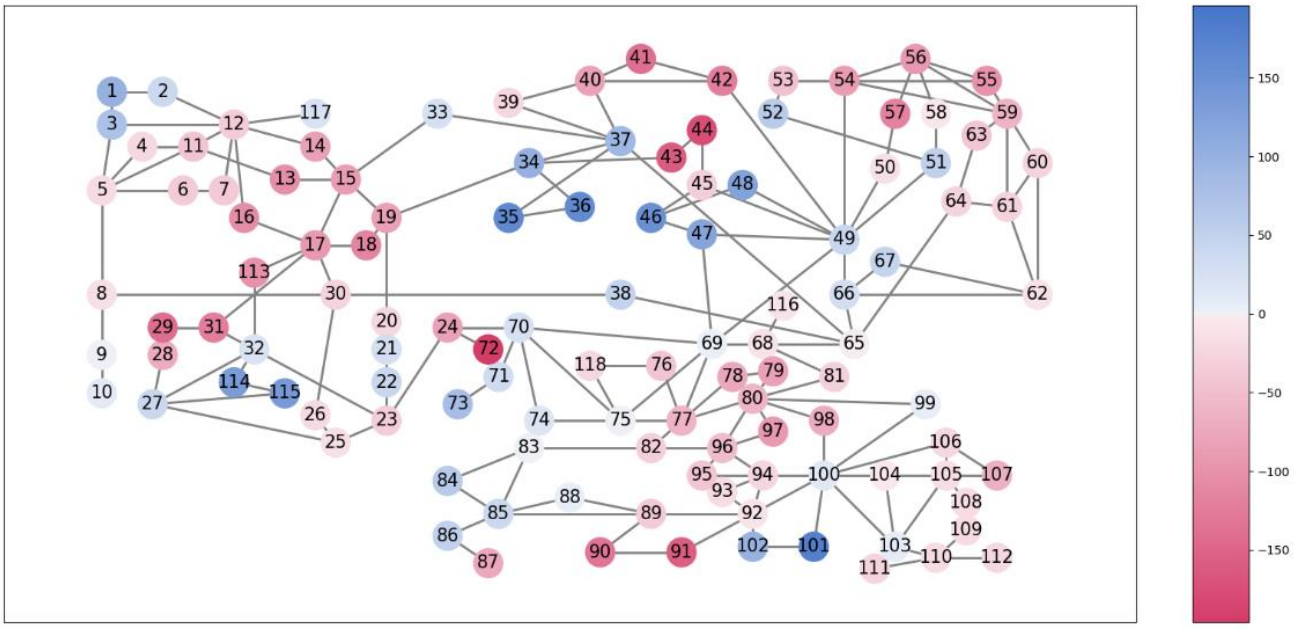

Figure V.17. Nodal domains of mode 23

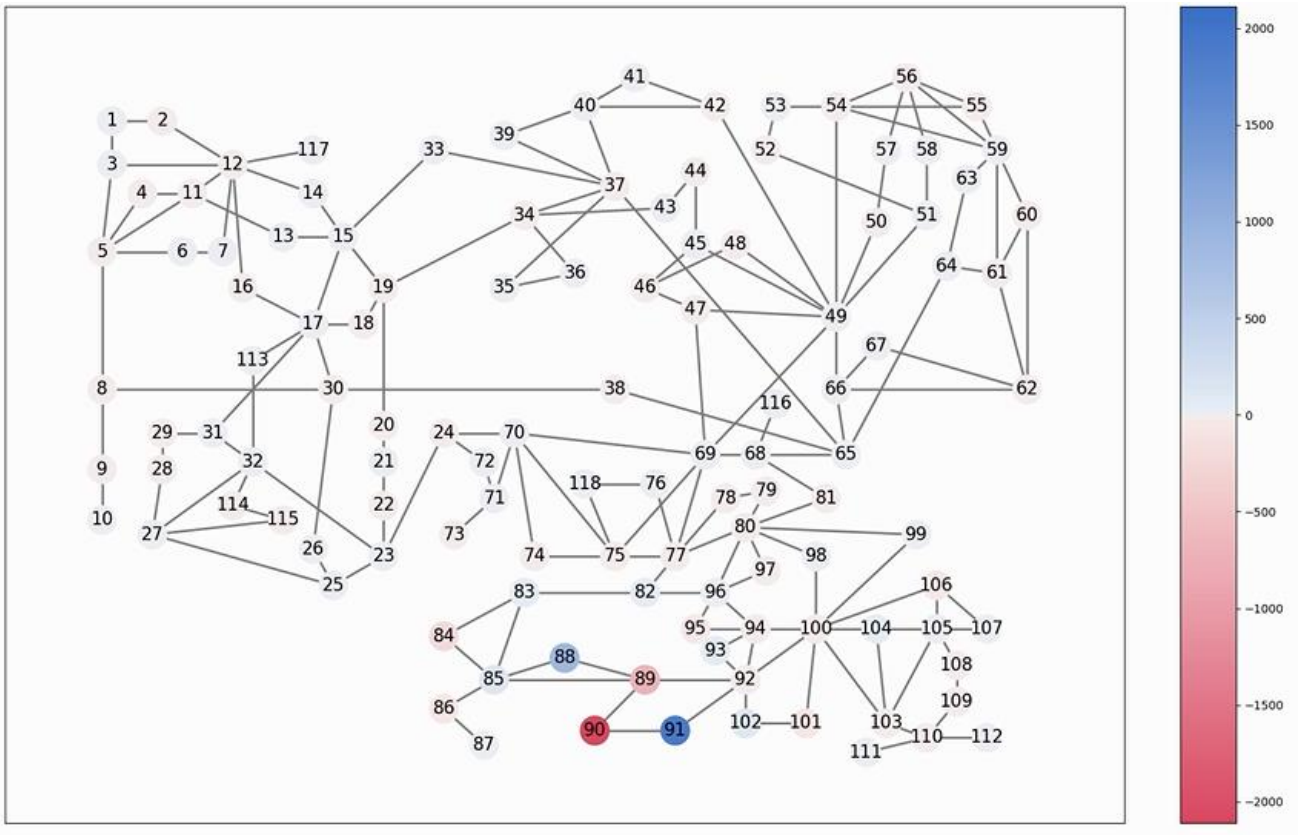

Figure V.18. Nodal domains of mode 62

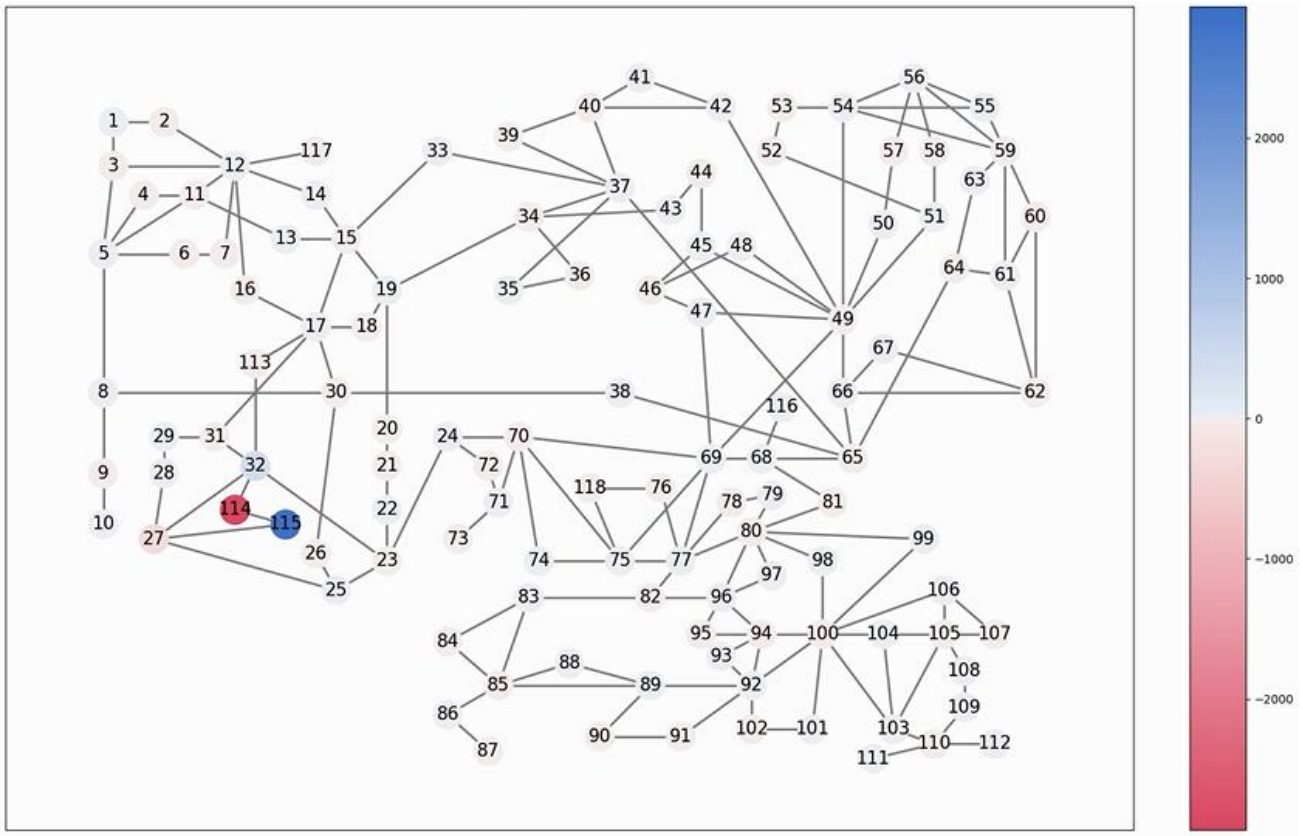

Figure V.19. Nodal domains of mode 111

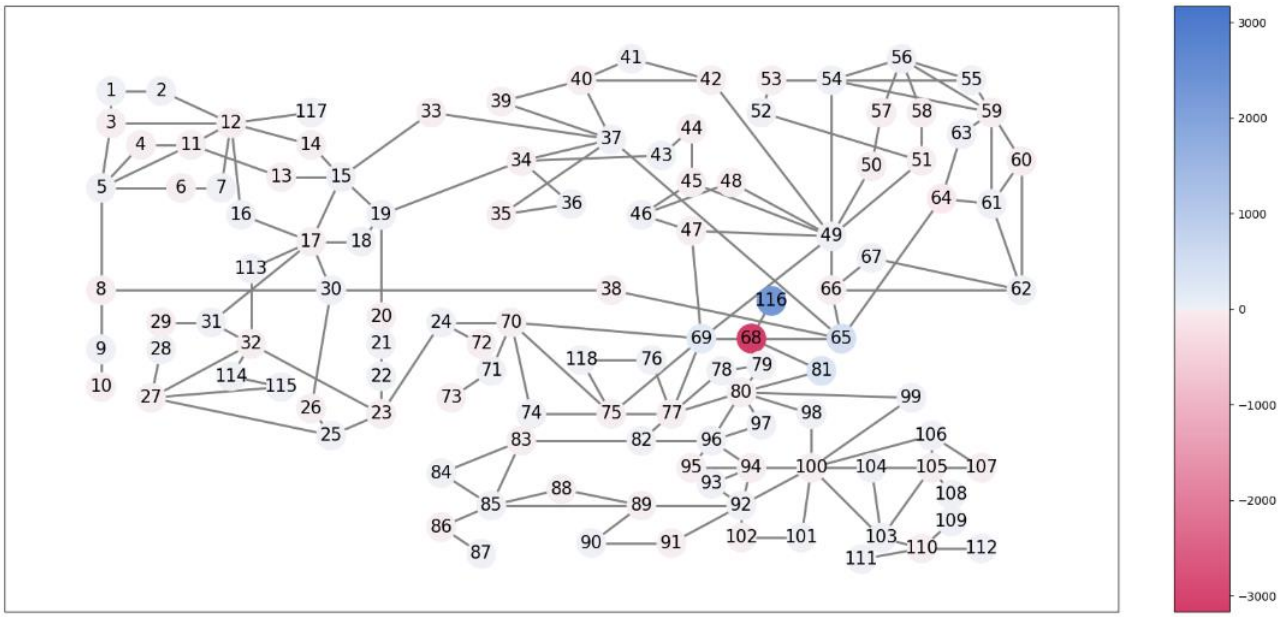

Figure V.20. Nodal domains of mode 118

V. Conclusion

Spectral solving of DC power flow is a powerful approach to obtain a comprehensive view on the links between graph topology, generators and loads location and power flows. Graph topology is translated in terms of eigenvalues and eigenvectors. Generators and loads location, node by node, is the resulting combination of power distribution mode by mode. A third parameter is brought by line series reactance Y_{br}. For a given set of spectral parameters $(p_i, \lambda_i, \mathrm{u}_i)$, it may magnify some power transfer through low impedance lines.

From the spectral point of view, power flows are mainly affected by nodal domains associated with the sign of eigenvectors components. Electrical engineer should be careful while designing power systems to not "excite" lower and higher modes to guarantee a less vulnerable system. In addition, a particular attention has to be paid to intermediate modes too. To excite a very localized intermediate mode may give some overloaded lines and a decrease in security margin.

Chapter VI.

Conclusions and directions for future works

I. Conclusions

In this work, the vulnerability of power systems, especially the vulnerability with respect to failures of lines or power transformers was investigated. The general conclusions of this thesis are summarized as:

- Power system vulnerability is generally defined as the measure of system weaknesses.
- The standard contingency analysis for assessing vulnerabilities of power systems was detailed and some metrics were defined, the so-called ACLOIM and ACNCRM. They were used to expose vulnerabilities of four IEEE test systems, proving their validity. However, the standard approach was unable to catch links between topology and vulnerability and also failed to give results for severe contingencies.
- The models for power system vulnerability analysis that are based on conventional or pure topological as well as extended topological approached were then reviewed. Some indicators relying on these models for mapping vulnerability of power systems were introduced and their results were compared with standard approach. Pros and cons of each metric were outlined. As a result, DC power flow model was considered as the best option to show the links between topology of power grids and their line outages vulnerabilities.
- Finally, this work proposed an innovative approach based on spectral solving of DC power flow to identify how vulnerabilities emerge from network topology. Spectral solving of DC power flow is a powerful approach to obtain a comprehensive view on the links between graph topology, generators and loads location and power flows. Graph topology is translated in terms of eigenvalues λ_i and eigenvectors u_i. Generators and loads (location and power) are expressed as a simple linear combination of modal components p_i. A third parameter is brought by line series reactance Y_{br}. For a given set of spectral parameters $(p_i, \lambda_i, \mathrm{u}_i)$, it may magnify some power transfer through low impedance lines. From the spectral point of view, power flows are mainly affected by nodal domains associated with the sign of eigenvectors components. The first results obtained from this work proved that it is thus necessary for power engineers to not "excite" lower modes or localized modes because they yield to severe line overloads and a decrease of system robustness.

II. Directions for future works

Because it has been proved to be a very original way to provide breakthrough analysis of power systems, main directions will concern spectral analysis of network operations:

- Further theoretical analysis of spectral solving of DC power flows should be performed to better understand the links of power system vulnerabilities with their graph topology. Open issues are: why some intermediate modes are localized, is it possible to spectrally

optimize the locations of generators and loads, is it possible to understand cascading processes in the spectral domain?

- For countries where power transmission systems are constructing such as Viet Nam, spectral analysis of DC power flow may be a useful tool to determine the suitable locations to connect major power plants in the design phase and increase system robustness.
- Spectral analysis might be applied to distribution networks. A first step will be to establish spectral solving of DC power flow equations for distribution systems. Because main objective of these networks is to ensure a high quality access to electricity for end users, a focus will be done on voltage profile. Links between nodal voltages distribution and eigen-properties of the Laplacian of the underlying graph of distribution networks should be especially done. Then, spectral graph analysis of IEEE distribution test feeders could be carried out to determine how these feeders are organized in spectral domain and what the consequences for the voltage profile are. Finally, the results could be used to determine where to locate renewable energy sources in order to optimize the voltage profile of smart grids.

Appendices

A. Data of IEEE test systems

I. IEEE 30-bus test system

Table A.1 Bus data of IEEE 30-bus test system

Bus number	Bus type	Active power demand (MW)	Reactive power demand (MVAr)	Shunt conductance (MW at V=1.0 p.u)	Shunt susceptance (MVAr at V=1.0 p.u)	Voltage magnitude (p.u)	Voltage angle (degrees)	Maximum voltage magnitude (p.u)	Minimum voltage magnitude (p.u)
1	3	0.00	0.00	0.00	0.00	1.00	0.00	1.05	0.95
2	2	21.70	12.70	0.00	0.00	1.00	0.00	1.10	0.95
3	1	2.40	1.20	0.00	0.00	1.00	0.00	1.05	0.95
4	1	7.60	1.60	0.00	0.00	1.00	0.00	1.05	0.95
5	1	0.00	0.00	0.00	0.19	1.00	0.00	1.05	0.95
6	1	0.00	0.00	0.00	0.00	1.00	0.00	1.05	0.95
7	1	22.80	10.90	0.00	0.00	1.00	0.00	1.05	0.95
8	1	30.00	30.00	0.00	0.00	1.00	0.00	1.05	0.95
9	1	0.00	0.00	0.00	0.00	1.00	0.00	1.05	0.95
10	1	5.80	2.00	0.00	0.00	1.00	0.00	1.05	0.95
11	1	0.00	0.00	0.00	0.00	1.00	0.00	1.05	0.95
12	1	11.20	7.50	0.00	0.00	1.00	0.00	1.05	0.95
13	2	0.00	0.00	0.00	0.00	1.00	0.00	1.10	0.95
14	1	6.20	1.60	0.00	0.00	1.00	0.00	1.05	0.95
15	1	8.20	2.50	0.00	0.00	1.00	0.00	1.05	0.95
16	1	3.50	1.80	0.00	0.00	1.00	0.00	1.05	0.95
17	1	9.00	5.80	0.00	0.00	1.00	0.00	1.05	0.95
18	1	3.20	0.90	0.00	0.00	1.00	0.00	1.05	0.95
19	1	9.50	3.40	0.00	0.00	1.00	0.00	1.05	0.95
20	1	2.20	0.70	0.00	0.00	1.00	0.00	1.05	0.95
21	1	17.50	11.20	0.00	0.00	1.00	0.00	1.05	0.95
22	2	0.00	0.00	0.00	0.00	1.00	0.00	1.10	0.95
23	2	3.20	1.60	0.00	0.00	1.00	0.00	1.10	0.95
24	1	8.70	6.70	0.00	0.04	1.00	0.00	1.05	0.95
25	1	0.00	0.00	0.00	0.00	1.00	0.00	1.05	0.95
26	1	3.50	2.30	0.00	0.00	1.00	0.00	1.05	0.95
27	2	0.00	0.00	0.00	0.00	1.00	0.00	1.10	0.95
28	1	0.00	0.00	0.00	0.00	1.00	0.00	1.05	0.95
29	1	2.40	0.90	0.00	0.00	1.00	0.00	1.05	0.95
30	1	10.60	1.90	0.00	0.00	1.00	0.00	1.05	0.95

Note: Bus type: Slack bus =3, P-V bus = 2, P-Q bus =1.

Table A.2 Generator data of IEEE 30-bus test system

Bus number	Active power output (MW)	Reactive power output (MVAr)	Maximum real power output (MW)	Minimum real power output (MW)	Maximum reactive power output (MVAr)	Minimum reactive power output (MVAr)
1	23.54	0.00	80.00	0.00	150.00	-20.00
2	60.97	0.00	80.00	0.00	60.00	-20.00
22	21.59	0.00	50.00	0.00	62.50	-15.00
27	26.91	0.00	55.00	0.00	48.70	-15.00
23	19.20	0.00	30.00	0.00	40.00	-10.00
13	37.00	0.00	40.00	0.00	44.70	-15.00

Table A.3 Line data of IEEE 30-bus test system

Line number	From bus number	To bus number	Resistance (p.u)	Reactance (p.u)	Total line susceptance (p.u)	Line (transformer) capacity (MVA)	Tap ratio
1	1	2	0.02	0.06	0.03	130	0.00
2	1	3	0.05	0.19	0.02	130	0.00
3	2	4	0.06	0.17	0.02	65	0.00
4	3	4	0.01	0.04	0.00	130	0.00
5	2	5	0.05	0.20	0.02	130	0.00
6	2	6	0.06	0.18	0.02	65	0.00
7	4	6	0.01	0.04	0.00	90	0.00
8	5	7	0.05	0.12	0.01	70	0.00
9	6	7	0.03	0.08	0.01	130	0.00
10	6	8	0.01	0.04	0.00	32	0.00
11	6	9	0.00	0.21	0.00	65	0.00
12	6	10	0.00	0.56	0.00	32	0.00
13	9	11	0.00	0.21	0.00	65	0.00
14	9	10	0.00	0.11	0.00	65	0.00
15	4	12	0.00	0.26	0.00	65	0.00
16	12	13	0.00	0.14	0.00	65	0.00
17	12	14	0.12	0.26	0.00	32	0.00
18	12	15	0.07	0.13	0.00	32	0.00
19	12	16	0.09	0.20	0.00	32	0.00
20	14	15	0.22	0.20	0.00	16	0.00
21	16	17	0.08	0.19	0.00	16	0.00
22	15	18	0.11	0.22	0.00	16	0.00
23	18	19	0.06	0.13	0.00	16	0.00
24	19	20	0.03	0.07	0.00	32	0.00
25	10	20	0.09	0.21	0.00	32	0.00
26	10	17	0.03	0.08	0.00	32	0.00
27	10	21	0.03	0.07	0.00	32	0.00

Line number	From bus number	To bus number	Resistance (p.u)	Reactance (p.u)	Total line susceptance (p.u)	Line (transformer) capacity (MVA)	Tap ratio
28	10	22	0.07	0.15	0.00	32	0.00
29	21	22	0.01	0.02	0.00	32	0.00
30	15	23	0.10	0.20	0.00	16	0.00
31	22	24	0.12	0.18	0.00	16	0.00
32	23	24	0.13	0.27	0.00	16	0.00
33	24	25	0.19	0.33	0.00	16	0.00
34	25	26	0.25	0.38	0.00	16	0.00
35	25	27	0.11	0.21	0.00	16	0.00
36	28	27	0.00	0.40	0.00	65	0.00
37	27	29	0.22	0.42	0.00	16	0.00
38	27	30	0.32	0.60	0.00	16	0.00
39	29	30	0.24	0.45	0.00	16	0.00
40	8	28	0.06	0.20	0.02	32	0.00
41	6	28	0.02	0.06	0.01	32	0.00

II. IEEE 39-bus test system

Table A.4 Bus data of IEEE 39-bus test system

Bus number	Bus type	Active power demand (MW)	Reactive power demand (MVAr)	Shunt conductance (MW at V=1.0 p.u)	Shunt susceptance (MVAr at V=1.0 p.u)	Voltage magnitude (p.u)	Voltage angle (degrees)	Maximum voltage magnitude (p.u)	Minimum voltage magnitude (p.u)
1	1	97.60	44.20	0.00	0.00	1.04	-13.54	1.06	0.94
2	1	0.00	0.00	0.00	0.00	1.05	-9.79	1.06	0.94
3	1	322.00	2.40	0.00	0.00	1.03	-12.28	1.06	0.94
4	1	500.00	184.00	0.00	0.00	1.00	-12.63	1.06	0.94
5	1	0.00	0.00	0.00	0.00	1.01	-11.19	1.06	0.94
6	1	0.00	0.00	0.00	0.00	1.01	-10.41	1.06	0.94
7	1	233.80	84.00	0.00	0.00	1.00	-12.76	1.06	0.94
8	1	522.00	176.60	0.00	0.00	1.00	-13.34	1.06	0.94
9	1	6.50	-66.60	0.00	0.00	1.04	-14.18	1.06	0.94
10	1	0.00	0.00	0.00	0.00	1.02	-8.17	1.06	0.94
11	1	0.00	0.00	0.00	0.00	1.01	-8.94	1.06	0.94
12	1	8.53	88.00	0.00	0.00	1.00	-9.00	1.06	0.94
13	1	0.00	0.00	0.00	0.00	1.01	-8.93	1.06	0.94
14	1	0.00	0.00	0.00	0.00	1.01	-10.72	1.06	0.94
15	1	320.00	153.00	0.00	0.00	1.02	-11.35	1.06	0.94
16	1	329.00	32.30	0.00	0.00	1.03	-10.03	1.06	0.94
17	1	0.00	0.00	0.00	0.00	1.03	-11.12	1.06	0.94
18	1	158.00	30.00	0.00	0.00	1.03	-11.99	1.06	0.94
Bus	Bus	Active	Reactive	Shunt	Shunt	Voltage	Voltage	Maximum	Minimum

number	type	power demand (MW)	power demand (MVAr)	conductance (MW at V=1.0 p.u)	susceptance (MVAr at V=1.0 p.u)	magnitude (p.u)	angle (degrees)	voltage magnitude (p.u)	voltage magnitude (p.u)
19	1	0.00	0.00	0.00	0.00	1.05	-5.41	1.06	0.94
20	1	680.00	103.00	0.00	0.00	0.99	-6.82	1.06	0.94
21	1	274.00	115.00	0.00	0.00	1.03	-7.63	1.06	0.94
22	1	0.00	0.00	0.00	0.00	1.05	-3.18	1.06	0.94
23	1	247.50	84.60	0.00	0.00	1.05	-3.38	1.06	0.94
24	1	308.60	-92.20	0.00	0.00	1.04	-9.91	1.06	0.94
25	1	224.00	47.20	0.00	0.00	1.06	-8.37	1.06	0.94
26	1	139.00	17.00	0.00	0.00	1.05	-9.44	1.06	0.94
27	1	281.00	75.50	0.00	0.00	1.04	-11.36	1.06	0.94
28	1	206.00	27.60	0.00	0.00	1.05	-5.93	1.06	0.94
29	1	283.50	26.90	0.00	0.00	1.05	-3.17	1.06	0.94
30	2	0.00	0.00	0.00	0.00	1.05	-7.37	1.06	0.94
31	2	9.20	4.60	0.00	0.00	0.98	-14.54	1.06	0.94
32	2	0.00	0.00	0.00	0.00	0.98	-0.19	1.06	0.94
33	2	0.00	0.00	0.00	0.00	1.00	-0.19	1.06	0.94
34	2	0.00	0.00	0.00	0.00	1.01	-1.63	1.06	0.94
35	2	0.00	0.00	0.00	0.00	1.05	1.78	1.06	0.94
36	2	0.00	0.00	0.00	0.00	1.06	4.47	1.06	0.94
37	2	0.00	0.00	0.00	0.00	1.03	-1.58	1.06	0.94
38	2	0.00	0.00	0.00	0.00	1.03	3.89	1.06	0.94
39	3	1104.00	250.00	0.00	0.00	1.03	0.00	1.06	0.94

Note: Bus type: Slack bus =3, P-V bus = 2, P-Q bus =1.

Table A.5 Generator data of IEEE 39-bus test system

Bus number	Active power output (MW)	Reactive power output (MVAr)	Maximum real power output (MW)	Minimum real power output (MW)	Maximum reactive power output (MVAr)	Minimum reactive power output (MVAr)
30	671.59	161.76	1040.00	0.00	400.00	140.00
31	646.00	221.57	646.00	0.00	300.00	-100.00
32	671.16	206.97	725.00	0.00	300.00	150.00
33	652.00	108.29	652.00	0.00	250.00	0.00
34	508.00	166.69	508.00	0.00	167.00	0.00
35	661.45	210.66	687.00	0.00	300.00	-100.00
36	580.00	100.17	580.00	0.00	240.00	0.00
37	564.00	-1.37	564.00	0.00	250.00	0.00
38	654.00	21.73	865.00	0.00	300.00	-150.00
39	689.59	78.47	3200.00	0.00	300.00	-100.00

Table A.6 Line data of IEEE 39-bus test system

Line number	From bus number	To bus number	Resistance (p.u)	Reactance (p.u)	Total line susceptance (p.u)	Line (transformer) capacity (MVA)	Tap ratio
1	1	2	0.0035	0.0411	0.6987	600	0.000
2	1	39	0.0010	0.0250	0.7500	1000	0.000
3	2	3	0.0013	0.0151	0.2572	500	0.000
4	2	25	0.0070	0.0086	0.1460	500	0.000
5	2	30	0.0000	0.0181	0.0000	900	1.025
6	3	4	0.0013	0.0213	0.2214	500	0.000
7	3	18	0.0011	0.0133	0.2138	500	0.000
8	4	5	0.0008	0.0128	0.1342	600	0.000
9	4	14	0.0008	0.0129	0.1382	500	0.000
10	5	6	0.0002	0.0026	0.0434	1200	0.000
11	5	8	0.0008	0.0112	0.1476	900	0.000
12	6	7	0.0006	0.0092	0.1130	900	0.000
13	6	11	0.0007	0.0082	0.1389	480	0.000
14	6	31	0.0000	0.0250	0.0000	1800	1.070
15	7	8	0.0004	0.0046	0.0780	900	0.000
16	8	9	0.0023	0.0363	0.3804	900	0.000
17	9	39	0.0010	0.0250	1.2000	900	0.000
18	10	11	0.0004	0.0043	0.0729	600	0.000
19	10	13	0.0004	0.0043	0.0729	600	0.000
20	10	32	0.0000	0.0200	0.0000	900	1.070
21	12	11	0.0016	0.0435	0.0000	500	1.006
22	12	13	0.0016	0.0435	0.0000	500	1.006
23	13	14	0.0009	0.0101	0.1723	600	0.000
24	14	15	0.0018	0.0217	0.3660	600	0.000
25	15	16	0.0009	0.0094	0.1710	600	0.000
26	16	17	0.0007	0.0089	0.1342	600	0.000
27	16	19	0.0016	0.0195	0.3040	600	0.000
28	16	21	0.0008	0.0135	0.2548	600	0.000
29	16	24	0.0003	0.0059	0.0680	600	0.000
30	17	18	0.0007	0.0082	0.1319	600	0.000
31	17	27	0.0013	0.0173	0.3216	600	0.000
32	19	20	0.0007	0.0138	0.0000	900	1.060
33	19	33	0.0007	0.0142	0.0000	900	1.070
34	20	34	0.0009	0.0180	0.0000	900	1.009
35	21	22	0.0008	0.0140	0.2565	900	0.000
36	22	23	0.0006	0.0096	0.1846	600	0.000
37	22	35	0.0000	0.0143	0.0000	900	1.025
38	23	24	0.0022	0.0350	0.3610	600	0.000

Line number	From bus number	To bus number	Resistance (p.u)	Reactance (p.u)	Total line susceptance (p.u)	Line (transformer) capacity (MVA)	Tap ratio
39	23	36	0.0005	0.0272	0.0000	900	1.000
40	25	26	0.0032	0.0323	0.5310	600	0.000
41	25	37	0.0006	0.0232	0.0000	900	1.025
42	26	27	0.0014	0.0147	0.2396	600	0.000
43	26	28	0.0043	0.0474	0.7802	600	0.000
44	26	29	0.0057	0.0625	1.0290	600	0.000
45	28	29	0.0014	0.0151	0.2490	600	0.000
46	29	38	0.0008	0.0156	0.0000	1200	1.025

III. IEEE 57-bus test system

Table A.7 Bus data of IEEE 57-bus test system

Bus number	Bus type	Active power demand (MW)	Reactive power demand (MVAr)	Shunt conductance (MW at V=1.0 p.u)	Shunt susceptance (MVAr at V=1.0 p.u)	Voltage magnitude (p.u)	Voltage angle (degrees)	Maximum voltage magnitude (p.u)	Minimum voltage magnitude (p.u)
1	3	55.00	17.00	0.00	0.00	1.04	0.00	1.06	0.94
2	2	3.00	88.00	0.00	0.00	1.01	-1.18	1.06	0.94
3	2	41.00	21.00	0.00	0.00	0.99	-5.97	1.06	0.94
4	1	0.00	0.00	0.00	0.00	0.98	-7.32	1.06	0.94
5	1	13.00	4.00	0.00	0.00	0.98	-8.52	1.06	0.94
6	2	75.00	2.00	0.00	0.00	0.98	-8.65	1.06	0.94
7	1	0.00	0.00	0.00	0.00	0.98	-7.58	1.06	0.94
8	2	150.00	22.00	0.00	0.00	1.01	-4.45	1.06	0.94
9	2	121.00	26.00	0.00	0.00	0.98	-9.56	1.06	0.94
10	1	5.00	2.00	0.00	0.00	0.99	-11.43	1.06	0.94
11	1	0.00	0.00	0.00	0.00	0.97	-10.17	1.06	0.94
12	2	377.00	24.00	0.00	0.00	1.02	-10.46	1.06	0.94
13	1	18.00	2.30	0.00	0.00	0.98	-9.79	1.06	0.94
14	1	10.50	5.30	0.00	0.00	0.97	-9.33	1.06	0.94
15	1	22.00	5.00	0.00	0.00	0.99	-7.18	1.06	0.94
16	1	43.00	3.00	0.00	0.00	1.01	-8.85	1.06	0.94
17	1	42.00	8.00	0.00	0.00	1.02	-5.39	1.06	0.94
18	1	27.20	9.80	0.00	10.00	1.00	-11.71	1.06	0.94
19	1	3.30	0.60	0.00	0.00	0.97	-13.20	1.06	0.94
20	1	2.30	1.00	0.00	0.00	0.96	-13.41	1.06	0.94
21	1	0.00	0.00	0.00	0.00	1.01	-12.89	1.06	0.94
22	1	0.00	0.00	0.00	0.00	1.01	-12.84	1.06	0.94

Bus number	Bus type	Active power demand (MW)	Reactive power demand (MVAr)	Shunt conductance (MW at V=1.0 p.u)	Shunt susceptance (MVAr at V=1.0 p.u)	Voltage magnitude (p.u)	Voltage angle (degrees)	Maximum voltage magnitude (p.u)	Minimum voltage magnitude (p.u)
23	1	6.30	2.10	0.00	0.00	1.01	-12.91	1.06	0.94
24	1	0.00	0.00	0.00	0.00	1.00	-13.25	1.06	0.94
25	1	6.30	3.20	0.00	5.90	0.98	-18.13	1.06	0.94
26	1	0.00	0.00	0.00	0.00	0.96	-12.95	1.06	0.94
27	1	9.30	0.50	0.00	0.00	0.98	-11.48	1.06	0.94
28	1	4.60	2.30	0.00	0.00	1.00	-10.45	1.06	0.94
29	1	17.00	2.60	0.00	0.00	1.01	-9.75	1.06	0.94
30	1	3.60	1.80	0.00	0.00	0.96	-18.68	1.06	0.94
31	1	5.80	2.90	0.00	0.00	0.94	-19.34	1.06	0.94
32	1	1.60	0.80	0.00	0.00	0.95	-18.46	1.06	0.94
33	1	3.80	1.90	0.00	0.00	0.95	-18.50	1.06	0.94
34	1	0.00	0.00	0.00	0.00	0.96	-14.10	1.06	0.94
35	1	6.00	3.00	0.00	0.00	0.97	-13.86	1.06	0.94
36	1	0.00	0.00	0.00	0.00	0.98	-13.59	1.06	0.94
37	1	0.00	0.00	0.00	0.00	0.99	-13.41	1.06	0.94
38	1	14.00	7.00	0.00	0.00	1.01	-12.71	1.06	0.94
39	1	0.00	0.00	0.00	0.00	0.98	-13.46	1.06	0.94
40	1	0.00	0.00	0.00	0.00	0.97	-13.62	1.06	0.94
41	1	6.30	3.00	0.00	0.00	1.00	-14.05	1.06	0.94
42	1	7.10	4.40	0.00	0.00	0.97	-15.50	1.06	0.94
43	1	2.00	1.00	0.00	0.00	1.01	-11.33	1.06	0.94
44	1	12.00	1.80	0.00	0.00	1.02	-11.86	1.06	0.94
45	1	0.00	0.00	0.00	0.00	1.04	-9.25	1.06	0.94
46	1	0.00	0.00	0.00	0.00	1.05	-11.89	1.06	0.94
47	1	29.70	11.60	0.00	0.00	1.03	-12.49	1.06	0.94
48	1	0.00	0.00	0.00	0.00	1.03	-12.59	1.06	0.94
49	1	18.00	8.50	0.00	0.00	1.04	-12.92	1.06	0.94
50	1	21.00	10.50	0.00	0.00	1.02	-13.39	1.06	0.94
51	1	18.00	5.30	0.00	0.00	1.05	-12.52	1.06	0.94
52	1	4.90	2.20	0.00	0.00	0.98	-11.47	1.06	0.94
53	1	20.00	10.00	0.00	6.30	0.97	-12.23	1.06	0.94
54	1	4.10	1.40	0.00	0.00	1.00	-11.69	1.06	0.94
55	1	6.80	3.40	0.00	0.00	1.03	-10.78	1.06	0.94
56	1	7.60	2.20	0.00	0.00	0.97	-16.04	1.06	0.94
57	1	6.70	2.00	0.00	0.00	0.97	-16.56	1.06	0.94

Note: Bus type: Slack bus =3, P-V bus = 2, P-Q bus =1.

Table A.8 Generator data of IEEE 57-bus test system

Bus number	Active power output (MW)	Reactive power output (MVAr)	Maximum real power output (MW)	Minimum real power output (MW)	Maximum reactive power output (MVAr)	Minimum reactive power output (MVAr)
1	142.63	-16.10	575.88	0.00	200.00	-140.00
2	87.80	-0.80	100.00	0.00	50.00	-17.00
3	45.07	-1.00	140.00	0.00	60.00	-10.00
6	72.87	0.80	100.00	0.00	25.00	-8.00
8	459.81	62.10	550.00	0.00	200.00	-140.00
9	97.60	2.20	100.00	0.00	9.00	-3.00
12	361.53	128.50	410.00	0.00	155.00	-150.00

Table A.9 Line data of IEEE 57-bus test system

Line number	From bus number	To bus number	Resistance (p.u)	Reactance (p.u)	Total line susceptance (p.u)	Line (transformer) capacity (MVA)	Tap ratio
1	1	2	0.0083	0.0280	0.1290	1696	0.000
2	2	3	0.0298	0.0850	0.0818	559	0.000
3	3	4	0.0112	0.0366	0.0380	1298	0.000
4	4	5	0.0625	0.1320	0.0258	360	0.000
5	4	6	0.0430	0.1480	0.0348	321	0.000
6	6	7	0.0200	0.1020	0.0276	466	0.000
7	6	8	0.0339	0.1730	0.0470	275	0.000
8	8	9	0.0099	0.0505	0.0548	941	0.000
9	9	10	0.0369	0.1679	0.0440	283	0.000
10	9	11	0.0258	0.0848	0.0218	560	0.000
11	9	12	0.0648	0.2950	0.0772	161	0.000
12	9	13	0.0481	0.1580	0.0406	301	0.000
13	13	14	0.0132	0.0434	0.0110	1094	0.000
14	13	15	0.0269	0.0869	0.0230	547	0.000
15	1	15	0.0178	0.0910	0.0988	522	0.000
16	1	16	0.0454	0.2060	0.0546	231	0.000
17	1	17	0.0238	0.1080	0.0286	440	0.000
18	3	15	0.0162	0.0530	0.0544	896	0.000
19	4	18	0.0000	0.5550	0.0000	86	0.970
20	4	18	0.0000	0.4300	0.0000	110	0.978
21	5	6	0.0302	0.0641	0.0124	741	0.000
22	7	8	0.0139	0.0712	0.0194	667	0.000
23	10	12	0.0277	0.1262	0.0328	376	0.000
24	11	13	0.0223	0.0732	0.0188	649	0.000
25	12	13	0.0178	0.0580	0.0604	819	0.000
26	12	16	0.0180	0.0813	0.0216	584	0.000
27	12	17	0.0397	0.1790	0.0476	265	0.000
28	14	15	0.0171	0.0547	0.0148	868	0.000
29	18	19	0.4610	0.6850	0.0000	69	0.000
30	19	20	0.2830	0.4340	0.0000	109	0.000
31	21	20	0.0000	0.7767	0.0000	61	1.043
32	21	22	0.0736	0.1170	0.0000	406	0.000

Line number	From bus number	To bus number	Resistance (p.u)	Reactance (p.u)	Total line susceptance (p.u)	Line (transformer) capacity (MVA)	Tap ratio
33	22	23	0.0099	0.0152	0.0000	3125	0.000
34	23	24	0.1660	0.2560	0.0084	186	0.000
35	24	25	0.0000	1.1820	0.0000	40	1.000
36	24	25	0.0000	1.2300	0.0000	39	1.000
37	24	26	0.0000	0.0473	0.0000	1004	1.043
38	26	27	0.1650	0.2540	0.0000	187	0.000
39	27	28	0.0618	0.0954	0.0000	498	0.000
40	28	29	0.0418	0.0587	0.0000	809	0.000
41	7	29	0.0000	0.0648	0.0000	733	0.967
42	25	30	0.1350	0.2020	0.0000	235	0.000
43	30	31	0.3260	0.4970	0.0000	96	0.000
44	31	32	0.5070	0.7550	0.0000	63	0.000
45	32	33	0.0392	0.0360	0.0000	1319	0.000
46	34	32	0.0000	0.9530	0.0000	50	0.975
47	34	35	0.0520	0.0780	0.0032	609	0.000
48	35	36	0.0430	0.0537	0.0016	885	0.000
49	36	37	0.0290	0.0366	0.0000	1298	0.000
50	37	38	0.0651	0.1009	0.0020	471	0.000
51	37	39	0.0239	0.0379	0.0000	1253	0.000
52	36	40	0.0300	0.0466	0.0000	1019	0.000
53	22	38	0.0192	0.0295	0.0000	1610	0.000
54	11	41	0.0000	0.7490	0.0000	63	0.955
55	41	42	0.2070	0.3520	0.0000	135	0.000
56	41	43	0.0000	0.4120	0.0000	115	0.000
57	38	44	0.0289	0.0585	0.0020	812	0.000
58	15	45	0.0000	0.1042	0.0000	456	0.955
59	14	46	0.0000	0.0735	0.0000	646	0.900
60	46	47	0.0230	0.0680	0.0032	699	0.000
61	47	48	0.0182	0.0233	0.0000	2039	0.000
62	48	49	0.0834	0.1290	0.0048	368	0.000
63	49	50	0.0801	0.1280	0.0000	371	0.000
64	50	51	0.1386	0.2200	0.0000	216	0.000
65	10	51	0.0000	0.0712	0.0000	667	0.930
66	13	49	0.0000	0.1910	0.0000	249	0.895
67	29	52	0.1442	0.1870	0.0000	254	0.000
68	52	53	0.0762	0.0984	0.0000	483	0.000
69	53	54	0.1878	0.2320	0.0000	205	0.000
70	54	55	0.1732	0.2265	0.0000	210	0.000
71	11	43	0.0000	0.1530	0.0000	310	0.958
72	44	45	0.0624	0.1242	0.0040	382	0.000
73	40	56	0.0000	1.1950	0.0000	40	0.958
74	56	41	0.5530	0.5490	0.0000	87	0.000
75	56	42	0.2125	0.3540	0.0000	134	0.000
76	39	57	0.0000	1.3550	0.0000	35	0.980
77	57	56	0.1740	0.2600	0.0000	183	0.000
78	38	49	0.1150	0.1770	0.0030	268	0.000
79	38	48	0.0312	0.0482	0.0000	985	0.000
80	9	55	0.0000	0.1205	0.0000	394	0.940

IV. IEEE 118-bus test system

Table A.10 Bus data of IEEE 118-bus test system

Bus number	Bus type	Active power demand (MW)	Reactive power demand (MVAr)	Shunt conductance (MW at V=1.0 p.u)	Shunt susceptance (MVAr at V=1.0 p.u)	Voltage magnitude (p.u)	Voltage angle (degrees)	Maximum voltage magnitude (p.u)	Minimum voltage magnitude (p.u)
1	2	51.00	27.00	0.00	0.00	0.96	10.67	1.06	0.94
2	1	20.00	9.00	0.00	0.00	0.97	11.22	1.06	0.94
3	1	39.00	10.00	0.00	0.00	0.97	11.56	1.06	0.94
4	2	39.00	12.00	0.00	0.00	1.00	15.28	1.06	0.94
5	1	0.00	0.00	0.00	-40.00	1.00	15.73	1.06	0.94
6	2	52.00	22.00	0.00	0.00	0.99	13.00	1.06	0.94
7	1	19.00	2.00	0.00	0.00	0.99	12.56	1.06	0.94
8	2	28.00	0.00	0.00	0.00	1.02	20.77	1.06	0.94
9	1	0.00	0.00	0.00	0.00	1.04	28.02	1.06	0.94
10	2	0.00	0.00	0.00	0.00	1.05	35.61	1.06	0.94
11	1	70.00	23.00	0.00	0.00	0.99	12.72	1.06	0.94
12	2	47.00	10.00	0.00	0.00	0.99	12.20	1.06	0.94
13	1	34.00	16.00	0.00	0.00	0.97	11.35	1.06	0.94
14	1	14.00	1.00	0.00	0.00	0.98	11.50	1.06	0.94
15	2	90.00	30.00	0.00	0.00	0.97	11.23	1.06	0.94
16	1	25.00	10.00	0.00	0.00	0.98	11.91	1.06	0.94
17	1	11.00	3.00	0.00	0.00	1.00	13.74	1.06	0.94
18	2	60.00	34.00	0.00	0.00	0.97	11.53	1.06	0.94
19	2	45.00	25.00	0.00	0.00	0.96	11.05	1.06	0.94
20	1	18.00	3.00	0.00	0.00	0.96	11.93	1.06	0.94
21	1	14.00	8.00	0.00	0.00	0.96	13.52	1.06	0.94
22	1	10.00	5.00	0.00	0.00	0.97	16.08	1.06	0.94
23	1	7.00	3.00	0.00	0.00	1.00	21.00	1.06	0.94
24	2	13.00	0.00	0.00	0.00	0.99	20.89	1.06	0.94
25	2	0.00	0.00	0.00	0.00	1.05	27.93	1.06	0.94
26	2	0.00	0.00	0.00	0.00	1.02	29.71	1.06	0.94
27	2	71.00	13.00	0.00	0.00	0.97	15.35	1.06	0.94
28	1	17.00	7.00	0.00	0.00	0.96	13.62	1.06	0.94
29	1	24.00	4.00	0.00	0.00	0.96	12.63	1.06	0.94
30	1	0.00	0.00	0.00	0.00	0.97	18.79	1.06	0.94
31	2	43.00	27.00	0.00	0.00	0.97	12.75	1.06	0.94
32	2	59.00	23.00	0.00	0.00	0.96	14.80	1.06	0.94
33	1	23.00	9.00	0.00	0.00	0.97	10.63	1.06	0.94
34	2	59.00	26.00	0.00	14.00	0.99	11.30	1.06	0.94

Bus number	Bus type	Active power demand (MW)	Reactive power demand (MVAr)	Shunt conductance (MW at V=1.0 p.u)	Shunt susceptance (MVAr at V=1.0 p.u)	Voltage magnitude (p.u)	Voltage angle (degrees)	Maximum voltage magnitude (p.u)	Minimum voltage magnitude (p.u)
35	1	33.00	9.00	0.00	0.00	0.98	10.87	1.06	0.94
36	2	31.00	17.00	0.00	0.00	0.98	10.87	1.06	0.94
37	1	0.00	0.00	0.00	-25.00	0.99	11.77	1.06	0.94
38	1	0.00	0.00	0.00	0.00	0.96	16.91	1.06	0.94
39	1	27.00	11.00	0.00	0.00	0.97	8.41	1.06	0.94
40	2	66.00	23.00	0.00	0.00	0.97	7.35	1.06	0.94
41	1	37.00	10.00	0.00	0.00	0.97	6.92	1.06	0.94
42	2	96.00	23.00	0.00	0.00	0.99	8.53	1.06	0.94
43	1	18.00	7.00	0.00	0.00	0.98	11.28	1.06	0.94
44	1	16.00	8.00	0.00	10.00	0.99	13.82	1.06	0.94
45	1	53.00	22.00	0.00	10.00	0.99	15.67	1.06	0.94
46	2	28.00	10.00	0.00	10.00	1.01	18.49	1.06	0.94
47	1	34.00	0.00	0.00	0.00	1.02	20.73	1.06	0.94
48	1	20.00	11.00	0.00	15.00	1.02	19.93	1.06	0.94
49	2	87.00	30.00	0.00	0.00	1.03	20.94	1.06	0.94
50	1	17.00	4.00	0.00	0.00	1.00	18.90	1.06	0.94
51	1	17.00	8.00	0.00	0.00	0.97	16.28	1.06	0.94
52	1	18.00	5.00	0.00	0.00	0.96	15.32	1.06	0.94
53	1	23.00	11.00	0.00	0.00	0.95	14.35	1.06	0.94
54	2	113.00	32.00	0.00	0.00	0.96	15.26	1.06	0.94
55	2	63.00	22.00	0.00	0.00	0.95	14.97	1.06	0.94
56	2	84.00	18.00	0.00	0.00	0.95	15.16	1.06	0.94
57	1	12.00	3.00	0.00	0.00	0.97	16.36	1.06	0.94
58	1	12.00	3.00	0.00	0.00	0.96	15.51	1.06	0.94
59	2	277.00	113.00	0.00	0.00	0.99	19.37	1.06	0.94
60	1	78.00	3.00	0.00	0.00	0.99	23.15	1.06	0.94
61	2	0.00	0.00	0.00	0.00	1.00	24.04	1.06	0.94
62	2	77.00	14.00	0.00	0.00	1.00	23.43	1.06	0.94
63	1	0.00	0.00	0.00	0.00	0.97	22.75	1.06	0.94
64	1	0.00	0.00	0.00	0.00	0.98	24.52	1.06	0.94
65	2	0.00	0.00	0.00	0.00	1.01	27.65	1.06	0.94
66	2	39.00	18.00	0.00	0.00	1.05	27.48	1.06	0.94
67	1	28.00	7.00	0.00	0.00	1.02	24.84	1.06	0.94
68	1	0.00	0.00	0.00	0.00	1.00	27.55	1.06	0.94
69	3	0.00	0.00	0.00	0.00	1.04	30.00	1.06	0.94
70	2	66.00	20.00	0.00	0.00	0.98	22.58	1.06	0.94

Bus number	Bus type	Active power demand (MW)	Reactive power demand (MVAr)	Shunt conductance (MW at V=1.0 p.u)	Shunt susceptance (MVAr at V=1.0 p.u)	Voltage magnitude (p.u)	Voltage angle (degrees)	Maximum voltage magnitude (p.u)	Minimum voltage magnitude (p.u)
71	1	0.00	0.00	0.00	0.00	0.99	22.15	1.06	0.94
72	2	12.00	0.00	0.00	0.00	0.98	20.98	1.06	0.94
73	2	6.00	0.00	0.00	0.00	0.99	21.94	1.06	0.94
74	2	68.00	27.00	0.00	12.00	0.96	21.64	1.06	0.94
75	1	47.00	11.00	0.00	0.00	0.97	22.91	1.06	0.94
76	2	68.00	36.00	0.00	0.00	0.94	21.77	1.06	0.94
77	2	61.00	28.00	0.00	0.00	1.01	26.72	1.06	0.94
78	1	71.00	26.00	0.00	0.00	1.00	26.42	1.06	0.94
79	1	39.00	32.00	0.00	20.00	1.01	26.72	1.06	0.94
80	2	130.00	26.00	0.00	0.00	1.04	28.96	1.06	0.94
81	1	0.00	0.00	0.00	0.00	1.00	28.10	1.06	0.94
82	1	54.00	27.00	0.00	20.00	0.99	27.24	1.06	0.94
83	1	20.00	10.00	0.00	10.00	0.99	28.42	1.06	0.94
84	1	11.00	7.00	0.00	0.00	0.98	30.95	1.06	0.94
85	2	24.00	15.00	0.00	0.00	0.99	32.51	1.06	0.94
86	1	21.00	10.00	0.00	0.00	0.99	31.14	1.06	0.94
87	2	0.00	0.00	0.00	0.00	1.02	31.40	1.06	0.94
88	1	48.00	10.00	0.00	0.00	0.99	35.64	1.06	0.94
89	2	0.00	0.00	0.00	0.00	1.01	39.69	1.06	0.94
90	2	163.00	42.00	0.00	0.00	0.99	33.29	1.06	0.94
91	2	10.00	0.00	0.00	0.00	0.98	33.31	1.06	0.94
92	2	65.00	10.00	0.00	0.00	0.99	33.80	1.06	0.94
93	1	12.00	7.00	0.00	0.00	0.99	30.79	1.06	0.94
94	1	30.00	16.00	0.00	0.00	0.99	28.64	1.06	0.94
95	1	42.00	31.00	0.00	0.00	0.98	27.67	1.06	0.94
96	1	38.00	15.00	0.00	0.00	0.99	27.51	1.06	0.94
97	1	15.00	9.00	0.00	0.00	1.01	27.88	1.06	0.94
98	1	34.00	8.00	0.00	0.00	1.02	27.40	1.06	0.94
99	2	42.00	0.00	0.00	0.00	1.01	27.04	1.06	0.94
100	2	37.00	18.00	0.00	0.00	1.02	28.03	1.06	0.94
101	1	22.00	15.00	0.00	0.00	0.99	29.61	1.06	0.94
102	1	5.00	3.00	0.00	0.00	0.99	32.30	1.06	0.94
103	2	23.00	16.00	0.00	0.00	1.00	24.44	1.06	0.94
104	2	38.00	25.00	0.00	0.00	0.97	21.69	1.06	0.94
105	2	31.00	26.00	0.00	20.00	0.97	20.57	1.06	0.94
106	1	43.00	16.00	0.00	0.00	0.96	20.32	1.06	0.94

Bus number	Bus type	Active power demand (MW)	Reactive power demand (MVAr)	Shunt conductance (MW at V=1.0 p.u)	Shunt susceptance (MVAr at V=1.0 p.u)	Voltage magnitude (p.u)	Voltage angle (degrees)	Maximum voltage magnitude (p.u)	Minimum voltage magnitude (p.u)
107	2	50.00	12.00	0.00	6.00	0.95	17.53	1.06	0.94
108	1	2.00	1.00	0.00	0.00	0.97	19.38	1.06	0.94
109	1	8.00	3.00	0.00	0.00	0.97	18.93	1.06	0.94
110	2	39.00	30.00	0.00	6.00	0.97	18.09	1.06	0.94
111	2	0.00	0.00	0.00	0.00	0.98	19.74	1.06	0.94
112	2	68.00	13.00	0.00	0.00	0.98	14.99	1.06	0.94
113	2	6.00	0.00	0.00	0.00	0.99	13.74	1.06	0.94
114	1	8.00	3.00	0.00	0.00	0.96	14.46	1.06	0.94
115	1	22.00	7.00	0.00	0.00	0.96	14.46	1.06	0.94
116	2	184.00	0.00	0.00	0.00	1.01	27.12	1.06	0.94
117	1	20.00	8.00	0.00	0.00	0.97	10.67	1.06	0.94
118	1	33.00	15.00	0.00	0.00	0.95	21.92	1.06	0.94

Note: Bus type: Slack bus =3, P-V bus = 2, P-Q bus =1.

Table A.11 Generator data of IEEE 118-bus test system

Bus number	Active power output (MW)	Reactive power output (MVAr)	Maximum real power output (MW)	Minimum real power output (MW)	Maximum reactive power output (MVAr)	Minimum reactive power output (MVAr)
1	26.49	0.00	100.00	0.00	15.00	-5.00
4	0.00	0.00	100.00	0.00	300.00	-300.00
6	0.20	0.00	100.00	0.00	50.00	-13.00
8	0.00	0.00	100.00	0.00	300.00	-300.00
10	401.87	0.00	550.00	0.00	200.00	-147.00
12	85.79	0.00	185.00	0.00	120.00	-35.00
15	20.88	0.00	100.00	0.00	30.00	-10.00
18	13.22	0.00	100.00	0.00	50.00	-16.00
19	21.58	0.00	100.00	0.00	24.00	-8.00
24	0.00	0.00	100.00	0.00	300.00	-300.00
25	193.81	0.00	320.00	0.00	140.00	-47.00
26	279.76	0.00	414.00	0.00	1000.00	-1000.00
27	9.92	0.00	100.00	0.00	300.00	-300.00
31	7.25	0.00	107.00	0.00	300.00	-300.00
32	14.86	0.00	100.00	0.00	42.00	-14.00
34	4.89	0.00	100.00	0.00	24.00	-8.00
36	10.66	0.00	100.00	0.00	24.00	-8.00
40	49.32	0.00	100.00	0.00	300.00	-300.00

Bus number	Active power output (MW)	Reactive power output (MVAr)	Maximum real power output (MW)	Minimum real power output (MW)	Maximum reactive power output (MVAr)	Minimum reactive power output (MVAr)
42	40.99	0.00	100.00	0.00	300.00	-300.00
46	19.04	0.00	119.00	0.00	100.00	-100.00
49	193.33	0.00	304.00	0.00	210.00	-85.00
54	49.54	0.00	148.00	0.00	300.00	-300.00
55	32.13	0.00	100.00	0.00	23.00	-8.00
56	32.56	0.00	100.00	0.00	15.00	-8.00
59	149.70	0.00	255.00	0.00	180.00	-60.00
61	148.41	0.00	260.00	0.00	300.00	-100.00
62	0.00	0.00	100.00	0.00	20.00	-20.00
65	352.24	0.00	491.00	0.00	200.00	-67.00
66	348.86	0.00	492.00	0.00	200.00	-67.00
69	453.67	0.00	805.20	0.00	300.00	-300.00
70	0.00	0.00	100.00	0.00	32.00	-10.00
72	0.00	0.00	100.00	0.00	100.00	-100.00
73	0.00	0.00	100.00	0.00	100.00	-100.00
74	16.93	0.00	100.00	0.00	9.00	-6.00
76	22.85	0.00	100.00	0.00	23.00	-8.00
77	0.00	0.00	100.00	0.00	70.00	-20.00
80	430.84	0.00	577.00	0.00	280.00	-165.00
85	0.00	0.00	100.00	0.00	23.00	-8.00
87	3.63	0.00	104.00	0.00	1000.00	-100.00
89	501.84	0.00	707.00	0.00	300.00	-210.00
90	0.00	0.00	100.00	0.00	300.00	-300.00
91	0.00	0.00	100.00	0.00	100.00	-100.00
92	0.00	0.00	100.00	0.00	9.00	-3.00
99	0.00	0.00	100.00	0.00	100.00	-100.00
100	231.59	0.00	352.00	0.00	155.00	-50.00
103	38.25	0.00	140.00	0.00	40.00	-15.00
104	0.00	0.00	100.00	0.00	23.00	-8.00
105	5.16	0.00	100.00	0.00	23.00	-8.00
107	29.03	0.00	100.00	0.00	200.00	-200.00
110	7.03	0.00	100.00	0.00	23.00	-8.00
111	35.24	0.00	136.00	0.00	1000.00	-100.00
112	36.48	0.00	100.00	0.00	1000.00	-100.00
113	0.00	0.00	100.00	0.00	200.00	-100.00
116	0.00	0.00	100.00	0.00	1000.00	-1000.00

Table A.12 Line data of IEEE118-bus test system

Line number	From bus number	To bus number	Resistance (p.u)	Reactance (p.u)	Total line susceptance (p.u)	Line (transformer) capacity (MVA)	Tap ratio
1	1	2	0.0303	0.0999	0.0254	175	0.000
2	1	3	0.0129	0.0424	0.0108	175	0.000
3	4	5	0.0018	0.0080	0.0021	500	0.000
4	3	5	0.0241	0.1080	0.0284	175	0.000
5	5	6	0.0119	0.0540	0.0143	175	0.000
6	6	7	0.0046	0.0208	0.0055	175	0.000
7	8	9	0.0024	0.0305	1.1620	500	0.000
8	8	5	0.0000	0.0267	0.0000	500	0.985
9	9	10	0.0026	0.0322	1.2300	500	0.000
10	4	11	0.0209	0.0688	0.0175	175	0.000
11	5	11	0.0203	0.0682	0.0174	175	0.000
12	11	12	0.0060	0.0196	0.0050	175	0.000
13	2	12	0.0187	0.0616	0.0157	175	0.000
14	3	12	0.0484	0.1600	0.0406	175	0.000
15	7	12	0.0086	0.0340	0.0087	175	0.000
16	11	13	0.0223	0.0731	0.0188	175	0.000
17	12	14	0.0215	0.0707	0.0182	175	0.000
18	13	15	0.0744	0.2444	0.0627	175	0.000
19	14	15	0.0595	0.1950	0.0502	175	0.000
20	12	16	0.0212	0.0834	0.0214	175	0.000
21	15	17	0.0132	0.0437	0.0444	500	0.000
22	16	17	0.0454	0.1801	0.0466	175	0.000
23	17	18	0.0123	0.0505	0.0130	175	0.000
24	18	19	0.0112	0.0493	0.0114	175	0.000
25	19	20	0.0252	0.1170	0.0298	175	0.000
26	15	19	0.0120	0.0394	0.0101	175	0.000
27	20	21	0.0183	0.0849	0.0216	175	0.000
28	21	22	0.0209	0.0970	0.0246	175	0.000
29	22	23	0.0342	0.1590	0.0404	175	0.000
30	23	24	0.0135	0.0492	0.0498	175	0.000
31	23	25	0.0156	0.0800	0.0864	500	0.000
32	26	25	0.0000	0.0382	0.0000	500	0.960
33	25	27	0.0318	0.1630	0.1764	500	0.000
34	27	28	0.0191	0.0855	0.0216	175	0.000
35	28	29	0.0237	0.0943	0.0238	175	0.000
36	30	17	0.0000	0.0388	0.0000	500	0.960
37	8	30	0.0043	0.0504	0.5140	500	0.000
38	26	30	0.0080	0.0860	0.9080	500	0.000

Line number	From bus number	To bus number	Resistance (p.u)	Reactance (p.u)	Total line susceptance (p.u)	Line (transformer) capacity (MVA)	Tap ratio
39	17	31	0.0474	0.1563	0.0399	175	0.000
40	29	31	0.0108	0.0331	0.0083	175	0.000
41	23	32	0.0317	0.1153	0.1173	140	0.000
42	31	32	0.0298	0.0985	0.0251	175	0.000
43	27	32	0.0229	0.0755	0.0193	175	0.000
44	15	33	0.0380	0.1244	0.0319	175	0.000
45	19	34	0.0752	0.2470	0.0632	175	0.000
46	35	36	0.0022	0.0102	0.0027	175	0.000
47	35	37	0.0110	0.0497	0.0132	175	0.000
48	33	37	0.0415	0.1420	0.0366	175	0.000
49	34	36	0.0087	0.0268	0.0057	175	0.000
50	34	37	0.0026	0.0094	0.0098	500	0.000
51	38	37	0.0000	0.0375	0.0000	500	0.935
52	37	39	0.0321	0.1060	0.0270	175	0.000
53	37	40	0.0593	0.1680	0.0420	175	0.000
54	30	38	0.0046	0.0540	0.4220	500	0.000
55	39	40	0.0184	0.0605	0.0155	175	0.000
56	40	41	0.0145	0.0487	0.0122	175	0.000
57	40	42	0.0555	0.1830	0.0466	175	0.000
58	41	42	0.0410	0.1350	0.0344	175	0.000
59	43	44	0.0608	0.2454	0.0607	175	0.000
60	34	43	0.0413	0.1681	0.0423	175	0.000
61	44	45	0.0224	0.0901	0.0224	175	0.000
62	45	46	0.0400	0.1356	0.0332	175	0.000
63	46	47	0.0380	0.1270	0.0316	175	0.000
64	46	48	0.0601	0.1890	0.0472	175	0.000
65	47	49	0.0191	0.0625	0.0160	175	0.000
66	42	49	0.0715	0.3230	0.0860	175	0.000
67	42	49	0.0715	0.3230	0.0860	175	0.000
68	45	49	0.0684	0.1860	0.0444	175	0.000
69	48	49	0.0179	0.0505	0.0126	175	0.000
70	49	50	0.0267	0.0752	0.0187	175	0.000
71	49	51	0.0486	0.1370	0.0342	175	0.000
72	51	52	0.0203	0.0588	0.0140	175	0.000
73	52	53	0.0405	0.1635	0.0406	175	0.000
74	53	54	0.0263	0.1220	0.0310	175	0.000
75	49	54	0.0730	0.2890	0.0738	175	0.000
76	49	54	0.0869	0.2910	0.0730	175	0.000
77	54	55	0.0169	0.0707	0.0202	175	0.000
78	54	56	0.0028	0.0096	0.0073	175	0.000

Line number	From bus number	To bus number	Resistance (p.u)	Reactance (p.u)	Total line susceptance (p.u)	Line (transformer) capacity (MVA)	Tap ratio
79	55	56	0.0049	0.0151	0.0037	175	0.000
80	56	57	0.0343	0.0966	0.0242	175	0.000
81	50	57	0.0474	0.1340	0.0332	175	0.000
82	56	58	0.0343	0.0966	0.0242	175	0.000
83	51	58	0.0255	0.0719	0.0179	175	0.000
84	54	59	0.0503	0.2293	0.0598	175	0.000
85	56	59	0.0825	0.2510	0.0569	175	0.000
86	56	59	0.0803	0.2390	0.0536	175	0.000
87	55	59	0.0474	0.2158	0.0565	175	0.000
88	59	60	0.0317	0.1450	0.0376	175	0.000
89	59	61	0.0328	0.1500	0.0388	175	0.000
90	60	61	0.0026	0.0135	0.0146	500	0.000
91	60	62	0.0123	0.0561	0.0147	175	0.000
92	61	62	0.0082	0.0376	0.0098	175	0.000
93	63	59	0.0000	0.0386	0.0000	500	0.960
94	63	64	0.0017	0.0200	0.2160	500	0.000
95	64	61	0.0000	0.0268	0.0000	500	0.985
96	38	65	0.0090	0.0986	1.0460	500	0.000
97	64	65	0.0027	0.0302	0.3800	500	0.000
98	49	66	0.0180	0.0919	0.0248	500	0.000
99	49	66	0.0180	0.0919	0.0248	500	0.000
100	62	66	0.0482	0.2180	0.0578	175	0.000
101	62	67	0.0258	0.1170	0.0310	175	0.000
102	65	66	0.0000	0.0370	0.0000	500	0.935
103	66	67	0.0224	0.1015	0.0268	175	0.000
104	65	68	0.0014	0.0160	0.6380	500	0.000
105	47	69	0.0844	0.2778	0.0709	175	0.000
106	49	69	0.0985	0.3240	0.0828	175	0.000
107	68	69	0.0000	0.0370	0.0000	500	0.935
108	69	70	0.0300	0.1270	0.1220	500	0.000
109	24	70	0.0022	0.4115	0.1020	175	0.000
110	70	71	0.0088	0.0355	0.0088	175	0.000
111	24	72	0.0488	0.1960	0.0488	175	0.000
112	71	72	0.0446	0.1800	0.0444	175	0.000
113	71	73	0.0087	0.0454	0.0118	175	0.000
114	70	74	0.0401	0.1323	0.0337	175	0.000
115	70	75	0.0428	0.1410	0.0360	175	0.000
116	69	75	0.0405	0.1220	0.1240	500	0.000
117	74	75	0.0123	0.0406	0.0103	175	0.000
118	76	77	0.0444	0.1480	0.0368	175	0.000

Line number	From bus number	To bus number	Resistance (p.u)	Reactance (p.u)	Total line susceptance (p.u)	Line (transformer) capacity (MVA)	Tap ratio
119	69	77	0.0309	0.1010	0.1038	175	0.000
120	75	77	0.0601	0.1999	0.0498	175	0.000
121	77	78	0.0038	0.0124	0.0126	175	0.000
122	78	79	0.0055	0.0244	0.0065	175	0.000
123	77	80	0.0170	0.0485	0.0472	500	0.000
124	77	80	0.0294	0.1050	0.0228	500	0.000
125	79	80	0.0156	0.0704	0.0187	175	0.000
126	68	81	0.0018	0.0202	0.8080	500	0.000
127	81	80	0.0000	0.0370	0.0000	500	0.935
128	77	82	0.0298	0.0853	0.0817	200	0.000
129	82	83	0.0112	0.0367	0.0380	200	0.000
130	83	84	0.0625	0.1320	0.0258	175	0.000
131	83	85	0.0430	0.1480	0.0348	175	0.000
132	84	85	0.0302	0.0641	0.0123	175	0.000
133	85	86	0.0350	0.1230	0.0276	500	0.000
134	86	87	0.0283	0.2074	0.0445	500	0.000
135	85	88	0.0200	0.1020	0.0276	175	0.000
136	85	89	0.0239	0.1730	0.0470	175	0.000
137	88	89	0.0139	0.0712	0.0193	500	0.000
138	89	90	0.0518	0.1880	0.0528	500	0.000
139	89	90	0.0238	0.0997	0.1060	500	0.000
140	90	91	0.0254	0.0836	0.0214	175	0.000
141	89	92	0.0099	0.0505	0.0548	500	0.000
142	89	92	0.0393	0.1581	0.0414	500	0.000
143	91	92	0.0387	0.1272	0.0327	175	0.000
144	92	93	0.0258	0.0848	0.0218	175	0.000
145	92	94	0.0481	0.1580	0.0406	175	0.000
146	93	94	0.0223	0.0732	0.0188	175	0.000
147	94	95	0.0132	0.0434	0.0111	175	0.000
148	80	96	0.0356	0.1820	0.0494	175	0.000
149	82	96	0.0162	0.0530	0.0544	175	0.000
150	94	96	0.0269	0.0869	0.0230	175	0.000
151	80	97	0.0183	0.0934	0.0254	175	0.000
152	80	98	0.0238	0.1080	0.0286	175	0.000
153	80	99	0.0454	0.2060	0.0546	200	0.000
154	92	100	0.0648	0.2950	0.0472	175	0.000
155	94	100	0.0178	0.0580	0.0604	175	0.000
156	95	96	0.0171	0.0547	0.0147	175	0.000
157	96	97	0.0173	0.0885	0.0240	175	0.000
158	98	100	0.0397	0.1790	0.0476	175	0.000

Line number	From bus number	To bus number	Resistance (p.u)	Reactance (p.u)	Total line susceptance (p.u)	Line (transformer) capacity (MVA)	Tap ratio
159	99	100	0.0180	0.0813	0.0216	175	0.000
160	100	101	0.0277	0.1262	0.0328	175	0.000
161	92	102	0.0123	0.0559	0.0146	175	0.000
162	101	102	0.0246	0.1120	0.0294	175	0.000
163	100	103	0.0160	0.0525	0.0536	500	0.000
164	100	104	0.0451	0.2040	0.0541	175	0.000
165	103	104	0.0466	0.1584	0.0407	175	0.000
166	103	105	0.0535	0.1625	0.0408	175	0.000
167	100	106	0.0605	0.2290	0.0620	175	0.000
168	104	105	0.0099	0.0378	0.0099	175	0.000
169	105	106	0.0140	0.0547	0.0143	175	0.000
170	105	107	0.0530	0.1830	0.0472	175	0.000
171	105	108	0.0261	0.0703	0.0184	175	0.000
172	106	107	0.0530	0.1830	0.0472	175	0.000
173	108	109	0.0105	0.0288	0.0076	175	0.000
174	103	110	0.0391	0.1813	0.0461	175	0.000
175	109	110	0.0278	0.0762	0.0202	175	0.000
176	110	111	0.0220	0.0755	0.0200	175	0.000
177	110	112	0.0247	0.0640	0.0620	175	0.000
178	17	113	0.0091	0.0301	0.0077	175	0.000
179	32	113	0.0615	0.2030	0.0518	500	0.000
180	32	114	0.0135	0.0612	0.0163	175	0.000
181	27	115	0.0164	0.0741	0.0197	175	0.000
182	114	115	0.0023	0.0104	0.0028	175	0.000
183	68	116	0.0003	0.0041	0.1640	500	0.000
184	12	117	0.0329	0.1400	0.0358	175	0.000
185	75	118	0.0145	0.0481	0.0120	175	0.000
186	76	118	0.0164	0.0544	0.0136	175	0.000

B. Algorithms

I. Gauss-Seidel method for power flow

(i) **Initialization:** Assign voltage magnitude $|V_i|$ and phase angle δ_i:

a. *Slack bus:* $|V_{slack}| = |V|^{sch}$ and $\delta_{slack} = \delta^{sch}$

b. P-V buses: $|V_i| = |V_i|^{sch}$ and $\delta_i{}^{(0)} = 0$

c. P-Q buses: $|V_i|^{(0)} = 1$ and $\delta_i{}^{(0)} = 0$

(ii) **Iterarion:** Compute $P_i{}^{(k)}$ and $Q_i{}^{(k)}$ from (II.27), (II.28) and $\Delta P_i{}^{(k)}$, $\Delta Q_i{}^{(k)}$ from (II.32), (II.33). Update voltage at bus i:

a. *Slack bus:* $|V_{slack}|^{(k+1)} = |V|^{sch}$ and $\delta_{slack}{}^{(k+1)} = \delta^{sch}$

b. P-V buses: If $Q_i^{(k)} > Q_i^{max}$, then $Q_i^{(k)} = Q_i^{max}$, or if $Q_i^{(k)} < Q_i^{min}$, then $Q_i^{(k)} = Q_i^{min}$. $|V_i|^{(k+1)} = |V_i|^{sch}$ and obtain $\delta_i^{(k+1)}$ from (II.31).

c. P-Q buses: $|V_i|^{(k+1)}$ and $\delta_i^{(k+1)}$ from (II.29).

(iii) **Stop iterative criteria:** *If* $max\{|\Delta P_i^{(k)}|, |\Delta Q_i^{(k)}|\} < \varepsilon$ *or* $k > k_{max}$ *stop else go to step (ii)*

II. Gauss-Seidel method for power flow

(i) **Initialization:** Assigning voltage magnitude $|V_i|$ and its phase angle δ_i is similar to the initialization of the Gausse-Seidel method.

(ii) **Iterarion:** Compute $P_i^{(k)}$ and $Q_i^{(k)}$ from (II.27), (II.28). Update voltage at step (k+1)[th]:

a. P-V buses: If $Q_i^{(k)} > Q_i^{max}$, then $Q_i^{(k)} = Q_i^{max}$, or if $Q_i^{(k)} < Q_i^{min}$, then $Q_i^{(k)} = Q_i^{min}$.

b. Compute $\Delta P_i^{(k)}$ and $\Delta Q_i^{(k)}$ from (II.32) and (II.33).

c. Compute the Jacobian matrix from group of equations (II.49) – (II.56).

d. Solve equation (II.48) to obtain $\Delta\delta^{(k)}$ and $\Delta|V|^{(k)}$.

e. The updated voltage magnitudes and phase angles at bus *i* are then given by (II.57), (II.58) :

(iii) **Stop iterative criteria:** *If* $max\{|\Delta P_i^{(k)}|, |\Delta Q_i^{(k)}|\} < \varepsilon$ *or* $k > k_{max}$ *stop else go to step (ii)*

III. Dynamic programming to find shortest path

(i) Input: Length of the edge matrix L ($l_{ij} = +\infty$ if the pairs of vertices *i* and *j* are not adjacent, other way l_{ij} is length of the edge *i-j*), shortest distance from node s to node s: $V_0(s) = 0$, $k = 1$

(ii) Compute state matrix S_k, $V_k(j)$ from Bellman equation (III.1) and following equations, then save S_k, $V_k(j)$ to stage{k}

$$V_k(j) = min\{d_{ij} + V_{k-1}(i)\} \qquad i, j = [1..N] \; and \; k = [1 \dots (N-1)] \tag{B.1}$$

$$V_k(j) = min\{S_{ij}\} \tag{B.2}$$

(iii) $D = V_k(j)$, $k = k + 1$, $V_{k-1}(i) = D$, update state matrix S_k, $V_k(j)$ from (B.1) and (B.2), then save S_k, $V_k(j)$ to stage{k}.

(iv) Check conditions: $(k < N - 1)$ and $V_k \neq V_{k-1}(j)$, return to (iii). Otherwise, go to step (v).

(v) $D_{node}(k, t) = t$ {D_{node} is a (k x N) matrix whose nonzero elements indicates node numbers composed shortest path}

(vi) Stage *k*: For each node *j* {*j* from 1 to N}, if $D_{node}(k, j) \neq 0$, meaning that node *j* belong to shortest paths from start node *s* to terminal node *t*, find all possible nodes *i* connected to node *j* satisfied condition:

$$V_k(j) = d_{ij} + V_{k-1}(i) \qquad \{i = 1{:}N\} \tag{B.3}$$

Add node *i* to shortest paths containing node *j* and set up $D_{node}(k - 1, i) = i$.

(vii) Check condition: *if k>1 then* $k = k - 1$ *and return step* (vi) *else stop*.

References

[1] S. Tully, “The Human Right to Access Electricity”, the Electricity Journal, vol. 19, no. 3, pp. 30–39, April 2006.

[2] International Energy Agency, “Electricity”, viewed 18 December 2017, [Online]. Available: https://www.iea.org/topics/electricity/.

[3] E. Kuznetsova, K. Culver, and E. Zio, “Complexity and vulnerability of Smartgrid systems”, presented at the ESREL 2011, 2011, pp. 2474–2482.

[4] E. Bompard, E. Pons, L. Luo, and M. Rosas Casals, “A Perspective overview of topological approaches for vulnerability analysis of power transmission grids”, presented at the International Conference on Critical Information Infrastructure Security, 2012, pp. 477–485.

[5] S. M. Amin and B. F. Wollenberg, “Toward a smart grid: power delivery for the 21st century”, IEEE Power Energy Magazine, vol. 3, no. 5, pp. 34–41, September 2005.

[6] CEN-CENELEC-ETSI Smart Grid Coordination Group, “SG-CG/ M490/F_ Overview of SG-CG Methodologies”, http://www.energynetworks.org/assets/files/electricity/engineering/Standards/SGCG%20Reports%20071014/SGCG_WGMethod_Sec0076_INF_ReportforComments(incl_annexes).pdf.

[7] N. Hadjsaïd and J.C. Sabonnadière (Ed.), *Smart Grids*, first edition, Wiley-ISTE, London : Hoboken, Newyork, 2012.

[8] Wikipedia, “List of major power outages”, viewed 08 June 2016, [Online]. Available: https://en.wikipedia.org/wiki/List_of_major_power_outages.

[9] J. R. Minkel, “The 2003 Northeast Blackout--Five Years Later”, Scientific American, viewed 24 May 2016, [Online]. Available: http://www.scientificamerican.com/article/2003-blackout-five-years-later/.

[10] G. Andersson et al, “Causes of the 2003 major grid blackouts in North America and Europe, and recommended means to improve system dynamic performance”, IEEE Transaction on Power System, vol. 20, no. 4, pp. 1922–1928, Nov. 2005.

[11] European Network of Transmission System Operators for Electricity, “Final Report System Disturbance on 4 November 2006”, viewed 19 December 2017, [Online]. Available: https://www.entsoe.eu/news-events/former-associations/ucte/other-reports/Pages/default.aspx.

[12] A. Atputharajah and T. K. Saha, “Power system blackouts - literature review”, International Conference on Industrial and Information Systems (ICIIS), pp. 460–465, 2009.

[13] J. Yan, Y. Tang, H. He, and Y. Sun, “Cascading Failure Analysis with DC Power Flow Model and Transient Stability Analysis”, IEEE Transaction on Power System, vol. 30, no. 1, pp. 285–297, Jan. 2015.

[14] J. Qi, K. Sun, and S. Mei, “An Interaction Model for Simulation and Mitigation of Cascading Failures”, IEEE Transaction on Power System, vol. 30, no. 2, pp. 804–819, March 2015.

[15] L. Cuadra, S. Salcedo-Sanz, J. Del Ser, S. Jiménez-Fernández, and Z. W. Geem, “A Critical Review of Robustness in Power Grids Using Complex Networks Concepts”, Energies, vol. 8, no. 9, pp. 9211–9265, Aug. 2015.

[16] R. Baldick et al., "Vulnerability assessment for cascading failures in electric power systems", in Power Systems Conference and Exposition, 2009. PSCE '09. IEEE/PES, 2009, pp. 1–9.

[17] R. H. Chen, J. Gao, O. P. Malik, S.-Y. Wang, and N.-D. Xiang, "Automatic contingency analysis and classification", the Fourth International Conference on Power System Control and Management (Conf. Publ. No. 421), 1996, pp. 82–86.

[18] Q. Morante, N. Ranaldo, A. Vaccaro, and E. Zimeo, "Pervasive grid for large-scale power systems contingency analysis", IEEE Transactions on Industrial Informatics, vol. 2, no. 3, pp. 165–175, Aug. 2006.

[19] E. Bompard, R. Napoli, and F. Xue, "Analysis of structural vulnerabilities in power transmission grids", International Journal of Critical Infrastructure Protection, vol. 2, no. 1–2, pp. 5–12, Mai 2009.

[20] Y. Koç, M. Warnier, P. V. Mieghem, R. E. Kooij, and F. M. T. Brazier, "The impact of the topology on cascading failures in a power grid model", Physica A: Statistical Mechanics and its Applications, vol. 402, pp. 169–179, Mai 2014.

[21] L. Luo, G. A. Pagani, and M. Rosas-Casals, "Spatial and Performance Optimality in Power Distribution Networks", IEEE Systems Journal, vol. PP, no. 99, pp. 1–9, 2016.

[22] E. I. Bilis, W. Kröger, and C. Nan, "Performance of Electric Power Systems Under Physical Malicious Attacks", IEEE Systems Journal, vol. 7, no. 4, pp. 854–865, December2013.

[23] E. Cotilla-Sanchez, P. D. H. Hines, C. Barrows, and S. Blumsack, "Comparing the Topological and Electrical Structure of the North American Electric Power Infrastructure", IEEE Systems Journal, vol. 6, no. 4, pp. 616–626, December 2012.

[24] J. Yan, H. He, and Y. Sun, "Integrated Security Analysis on Cascading Failure in Complex Networks", IEEE Transactions on Information Forensics and Security, vol. 9, no. 3, pp. 451–463, March 2014.

[25] Z. Wang, A. Scaglione, and R. J. Thomas, "Electrical centrality measures for electric power grid vulnerability analysis", in 49th IEEE Conference on Decision and Control (CDC), 2010, pp. 5792–5797.

[26] Y. Zhu, J. Yan, Y. Sun, and H. He, "Revealing Cascading Failure Vulnerability in Power Grids Using Risk-Graph", IEEE Transactions on Parallel and Distributed Systems, vol. 25, no. 12, pp. 3274–3284, December 2014.

[27] E. Bompard, E. Pons, and D. Wu, "Extended Topological Metrics for the Analysis of Power Grid Vulnerability", IEEE Systems Journal, vol. 6, no. 3, pp. 481–487, September 2012.

[28] A. Dwivedi, X. Yu, and P. Sokolowski, "Analyzing power network vulnerability with maximum flow based centrality approach", in 2010 8th IEEE International Conference on Industrial Informatics, pp. 336–341, 2010.

[29] S. Pahwa, A. Hodges, C. Scoglio, and S. Wood, "Topological analysis of the power grid and mitigation strategies against cascading failures", in 2010 4th Annual IEEE Systems Conference, pp. 272–276, 2010.

[30] R. Albert, I. Albert, and G. L. Nakarado, "Structural vulnerability of the North American power grid", Physical Review E, vol. 69, no.2, p. 025103, February 2004.

[31] S. Arianos, E. Bompard, A. Carbone, and F. Xue, "Power grid vulnerability: A complex network approach", Chaos: An Interdisciplinary Journal of Nonlinear Science, vol. 19, no. 1, p. 013119, March 2009.

[32] D. Chassin and C. Posse, “Evaluating North American Electric Grid Reliability Using the Barabasi-Albert Network Model”, Physica A: Statistical Mechanics and its Applications, vol. 355, pp. 667–677, Sep. 2005.

[33] D. J. Watts and S. H. Strogatz, “Collective dynamics of ‘small-world’ networks”, Nature, vol. 393, no. 6684, p. 440, June 1998.

[34] A. Dwivedi, X. Yu, and P. Sokolowski, “Identifying vulnerable lines in a power network using complex network theory”, in 2009 IEEE International Symposium on Industrial Electronics, pp. 18–23, 2009.

[35] V. Latora and M. Marchiori, “Efficient Behavior of Small-World Networks”, Physical Review Letters, vol. 87, no. 19, p. 198701, Oct. 2001.

[36] K. Sun, “Complex Networks Theory: A New Method of Research in Power Grid”, in Transmission and Distribution Conference and Exhibition: Asia and Pacific, 2005 IEEE/PES, pp. 1–6, 2005.

[37] S. Einarsson and M. Rausand, “An Approach to Vulnerability Analysis of Complex Industrial Systems”, Risk Analysis, vol. 18, pp. 535–546, October 1998.

[38] H. Saadat, *Power system Analysis*, 3rd edition, The McGraw-Hill Companies, Singapore, 2002.

[39] J. Machowski, J. Bialek, and J. R. Bumby, *Power System Dynamics and Stability*, John Wiley & Sons, 1997.

[40] DIgSILENT, “Power Factory: User manual”, viewed 10 July 2017, http://www.digsilent.de/index.php/fr-products-powerfactory.html.

[41] R. D. Zimmerman, C. E. Murillo-Sanchez, and R. J. Thomas, “MATPOWER: Steady-State Operations, Planning, and Analysis Tools for Power Systems Research and Education”, IEEE Transactions on Power Systems, vol. 26, no. 1, pp. 12–19, February 2011.

[42] J. J. Grainger and W. D. Stevenson, *Power system analysis*, McGraw-Hill, 1994.

[43] P. Kundur and N. J. Balu, *Power system stability and control*, McGraw-Hill, New York, 1994.

[44] J. H. Mathews, *Numerical Methods for Mathematics, Science and Engineering*, Pearson Education, Englewood Cliffs, New York, 1992.

[45] J. Guckenheimer and P. Holmes, *Nonlinear Oscillations, Dynamical Systems, and Bifurcations of Vector Fields*, Springer Science & Business Media, 2013.

[46] A. J. Wood and B. F. Wollenberg, *Power Generation, Operation, and Control*, John Wiley & Sons, 2012.

[47] D. L. Pepyne, “Topology and cascading line outages in power grids”, Journal of Systems Science and Systems Engineering, vol. 16, no. 2, pp. 202–221, June 2007.

[48] Illinois Center for a Smarter Electric Grid (ICSEG), “IEEE 57-Bus System”, viewed 08 June 2016, [Online]. Available: http://icseg.iti.illinois.edu/ieee-57-bus-system/.

[49] G. A. Pagani and M. Aiello, “The Power Grid as a complex network: A survey”, Physica A: Statistical Mechanics and its Applications, vol. 392, no. 11, pp. 2688–2700, June 2013.

[50] K. Sun, “Complex Networks Theory: A New Method of Research in Power Grid”, in Transmission and Distribution Conference and Exhibition: Asia and Pacific, 2005 IEEE/PES, pp. 1–6, 2005.

[51] L. da F. Costa, F. A. Rodrigues, G. Travieso, and P. R. V. Boas, “Characterization of complex networks: A survey of measurements”, Advances in Physics, vol. 56, no. 1, pp. 167–242, January 2007.

[52] P. Hines, S. Blumsack, E. C. Sanchez, and C. Barrows, "The Topological and Electrical Structure of Power Grids", in 2010 43rd Hawaii International Conference on System Sciences (HICSS), pp. 1–10, 2010.

[53] P. Crucitti, V. Latora, and M. Marchiori, "Model for cascading failures in complex networks", Physical Review E, vol. 69, no. 4, pp.1-4, Avril 2004.

[54] P. Crucitti, V. Latora, and M. Marchiori, "A topological analysis of the Italian electric power grid", Physica A: Statistical Mechanics and its Applications, vol. 338, no. 1–2, pp. 92–97, July 2004.

[55] Y. Guo, J. Cao, R. Duan, and S. Li, "Power Grid Vulnerability Identifying Based on Complex Network Theory", in 2012 Second International Conference on Instrumentation, Measurement, Computer, Communication and Control (IMCCC), pp. 474–477, 2012.

[56] Z. Guohua, W. Ce, Z. Jianhua, Y. Jingyan, Z. Yin, and D. Manyin, "Vulnerability assessment of bulk power grid based on complex network theory", in Third International Conference on Electric Utility Deregulation and Restructuring and Power Technologies, 2008. DRPT 2008, pp. 1554–1558, 2008.

[57] Massachusetts Institute of Technology, "AMP dynamic programming", viewed 15 June 2015, [Online]. Available: http://web.mit.edu/15.053/www/AMP-Chapter-11.pdf.

[58] M. Ouyang, Z. Pan, L. Hong, and L. Zhao, "Correlation analysis of different vulnerability metrics on power grids", Physica A: Statistical Mechanics and its Applications, vol. 396, pp. 204–211, February 2014.

[59] K. Wang, B. Zhang, Z. Zhang, X. Yin, and B. Wang, "An electrical betweenness approach for vulnerability assessment of power grids considering the capacity of generators and load", Physica A: Statistical Mechanics and its Applications, vol. 390, no. 23–24, pp. 4692–4701, November 2011.

[60] E. Bompard, L. Luo, and E. Pons, "A perspective overview of topological approaches for vulnerability analysis of power transmission grids", International Journal of Critical Infrastructures, vol. 11, no. 1, pp. 15–26, January 2015.

[61] E. Bompard, R. Napoli, and F. Xue, "Extended topological approach for the assessment of structural vulnerability in transmission networks", IET Generation, Transmission & Distribution, vol. 4, no. 6, pp. 716–724, June 2010.

[62] A. B. M. Nasiruzzaman, H. R. Pota, and A. Anwar, "Comparative study of power grid centrality measures using complex network framework", in Power Engineering and Optimization Conference (PEDCO) Melaka, Malaysia, 2012 IEEE International, pp. 176–181, 2012.

[63] S. Blumsack, P. Hines, M. Patel, C. Barrows, and E. C. Sanchez, "Defining power network zones from measures of electrical distance", IEEE Power Energy Society General Meeting, 2009. PES '09, pp. 1–8, 2009.

[64] Y. Wang, J. Zhao, F. Zhang, and B. Lei, "Study on structural vulnerabilities of power grids based on the electrical distance", IEEE PES Innovative Smart Grid Technologies, pp. 1–5, 2012.

[65] V. Latora and M. Marchiori, "Vulnerability and protection of infrastructure networks", Physical Review E, vol. 71, no. 1, pp.1-4, January 2005.

[66] Z. Wang, A. Scaglione, R. Thomas, "Electrical Centrality Measures for Electric Power Grid Vulnerability Analysis", 49th IEEE Conference on Decision and Control, pp.5792-5797, Hilton Atlanta Hotel, Atlanta, GA, USA, December, 2010.

[67] W. G. Hansen, “How Accessibility Shapes Land Use”, Journal of the American Institute of Planners, vol. 25, no. 2, pp. 73–76, May 1959.

[68] T. A. Ernster and A. K. Srivastava, “Power system vulnerability analysis - towards validation of centrality measures”, Transmission and Distribution Conference and Exposition (T&D), 2012 IEEE PES, pp. 1–6, 2012.

[69] F. Dorfler and F. Bullo, “Kron Reduction of Graphs with Applications to Electrical Networks”, IEEE Transactions on Circuits and Systems I: Regular Papers, vol. 60, no. 1, pp. 150–163, Jan. 2013.

[70] P. W. Sauer, K. E. Reinhard, and T. J. Overbye, “Extended factors for linear contingency analysis”, Proceedings of the 34th Annual Hawaii International Conference on System Sciences, pp. 697–703, 2001.

[71] J. Guo, Y. Fu, Z. Li, and M. Shahidehpour, “Direct Calculation of Line Outage Distribution Factors”, IEEE Transactions on Power Systems, vol. 24, no. 3, pp. 1633–1634, Aug. 2009.

[72] B. Stott, J. Jardim, and O. Alsac, “DC Power Flow Revisited”, IEEE Transactions on Power Systems, vol. 24, no. 3, pp. 1290–1300, Aug. 2009.

[74] L. Lov´asz, “Eigenvalues of graphs”, viewed 11 December 2017 [Online]. Available: http://web.cs.elte.hu/~lovasz/eigenvals-x.pdf.

[75] F. R. K. Chung, *Spectral Graph Theory*, American Mathematical Soc, 1997.

[76] J.-G. Caputo, A. Knippel, and E. Simo, “Oscillations of networks: the role of soft nodes”, Journal of Physics A: Mathematical and Theoretical, vol. 46, no. 3, p. 035101, 2013.

[77] Y. Dekel, J. R. Lee, and N. Linial, “Eigenvectors of random graphs: Nodal Domains”, Random Structures & Algorithms, vol. 39, no. 1, pp. 39–58, Aug. 2011.